DISSERTATION

SUSTAINABILITY TRADEOFFS WITHIN PHOTOAUTOTROPHIC CULTIVATION SYSTEMS: INTEGRATING PHYSICAL AND LIFECYCLE MODELING FOR DESIGN AND OPTIMIZATION

Submitted by

Carlos Enrique Quiroz Arita

Department of Mechanical Engineering

In partial fulfillment of the requirements

For the Degree of Doctor of Philosophy

Colorado State University

Fort Collins, Colorado

Summer 2018

Doctoral Committee:

Advisor: Thomas H. Bradley

David Bark
Myra Blaylock
Anthony Marchese
Sybil Sharvelle
Bryan Willson

ABSTRACT

SUSTAINABILITY TRADEOFFS WITHIN PHOTOAUTOTROPHIC CULTIVATION SYSTEMS: INTEGRATING PHYSICAL AND LIFECYCLE MODELING FOR DESIGN AND OPTIMIZATION

Photoautotroph-based biofuels are considered one of the most promising renewable resources to meet the global energy requirements for transportation systems. Long-term research and development has resulted in demonstrations of microalgae areal oil productivities that are higher than crop-based biofuels, about 10 times that of palm oil and about 130 times that of soybean. Cyanobacteria is reported to have ~4 times the areal productivity of microalgae on an equivalent energy basis. Downstream of this cultivation process, the cyanobacteria biomass and bioproducts can be supplied to biorefineries producing feed, biomaterials, biosynthetic chemicals, and biofuels. As such, cyanobacteria, and microalgae-based systems can be a significant contributor to more sustainable energy and production systems. This research presents novel means to be able to analyze, integrate, assess, and design sustainable photoautotrophic biofuel and bioproduct systems, as defined using lifecycle assessment methods (LCA).

As part of a broad collaboration between industry, academia, and the national laboratories, I have developed models and experiments to quantify tradeoffs among the scalability, sustainability, and technical feasibility of cyanobacteria biorefineries and microalgae cultivation systems. A central hypothesis to this research is that the lifecycle energy costs and benefits, the cultivation productivity, and the scalability of any given organism or technology is

governed by the fluid mechanics of the photobioreactor systems. The fluid characteristics of both open raceway ponds and flat photobioreactors, are characterized through industrial-scale experiment and modeling. Turbulent mixing is studied by applying Acoustic Doppler Velocimetry (ADV), Particle Image Velocimetry (PIV), and computational fluid dynamics (CFD) characterization tools. The implications of these fluid conditions on photoautotrophic organisms are studied through cultivation and modeling of the cyanobacteria, *Synechocystis* sp. PCC6803. Growth-stage models of this cyanobacteria include functions dependent on incident radiation, temperature, nutrient availability, dark and photo-respiration.

By developing an integrated approach to laboratory experimentation and industrial-scale growth experiments, we have validated models to quantify the scalability and sustainability of these novel biosystems. These capabilities are utilized to perform long-term and industrially-relevant assessments of the costs and benefits of these promising technologies, and will serve to inform the biological engineering research and development of new organisms.

ACKNOWLEDGMENTS

First, I would like to acknowledge my PhD advisor, Dr. Thomas H. Bradley. Thank you for giving me the opportunity to pursue a career in science and academia, for enhancing my strengths and expanding my research interests, for helping me overcome my weaknesses beyond my limitations, and for being such a great mentor on this road. I could not make this possible without your guidance. I am honored to be your student and mentee.

I thank my doctoral committee; Dr. David Bark, Dr. Myra Blaylock, Dr. Anthony Marchese, Dr. Sybil Sharvelle, and Dr. Bryan Willson. Thank you for your insights and constructive feedback throughout this process. I feel privileged to be surrounded by this group of scientists with expertise in multidisciplinary topics that enriched my dissertation.

I would like to acknowledge the sponsors and institutions that made my career in science and academia possible. First, I thank the Fulbright Latin American Scholarship Program of American Universities (LASPAU), who sponsored my intensive English program and masters' degree at Colorado State University. Thank you Colorado State University and the network of staff and faculty that welcomed me to be part of this prestigious university. Lastly, I thank National Science Foundation and Sandia National Laboratories who made possible my research and dissertation through their financial support. You contributed to make this dream possible.

I thank the large and multidisciplinary group of collaborators with whom I had the opportunity to work. I thank the principal investigators of the EFRI team (Integrated design of cyanobacterial biorefineries): Dr. Kenneth Reardon, Dr. Christie Peebles, Dr. David Dandy, and Dr. Graham Peers. Your insights and feedback contributed to my growth as a scientist. I thank other faculty members of Colorado State University with whom I had the honor to collaborate;

Dr. Jason C. Quinn, Dr. John J. Sheehan, Dr. Kimberly B. Catton, and Dr. Lakshmi Prasad Dasi. I thank the large group of post-doctoral researchers, graduate students, and undergraduate students with whom we collaborated during my masters and doctoral studies. Thank you to Lincoln H. Mueller, Jr. from Drake water reclamation Facility and the City of Fort Collins with whom we collaborated. I would like to thank Dr. John McGowen from the Algae-Testbed Public-Private Partnership and Arizona State University for the opportunity to collaborate with you. Lastly, I would like to thank the staff of Sandia National Laboratories (SNL); Dr. Patricia E. Gharagozloo, Dr. Myra L. Blaylock, Dr. Ryan Davis, and Dr. Ben Wu. I appreciate the opportunity I was given to be a graduate intern in your prestigious laboratory, and the continued research relationship with ongoing funding through Colorado State University. It has been an honor to work with the staff of SNL and incorporate our research efforts in this dissertation.

I would like to acknowledge the people I love and truly love me, you know who you are. I'm grateful for my parents, Saris Arita-Valdiviezo and Carlos Enrique Quiroz. Thank you for giving the best gifts a son can receive: your love, principles, and guidance. I will always love you Mom and Dad. I'm thankful for my first mentor, Rafael Dominguez Munoz, not only for sharing your knowledge with me in engineering, but your life experience. I'm honored I met you in life and that I became your mentee, your friend, and your godson.

Last but not least, I acknowledge my wife, Juanita Izaguirre-Paredes, and my first son, Leonardo Quiroz-Izaguirre. This is our effort and our accomplishment. Thank you for being with me throughout this journey. Only you know how we struggled together. You will learn our story when you grow up, my son. Thank you Juanita and Leo for cheering me up in the most difficult times of my life. Thank you for being my family. You are my inspiration and my reason to do better every day. I love you.

DEDICATION

to my mother, Saris Josefina Arita-Valdiviezo, for your unconditional love, patience, and dedication. You will always live in my heart.

TABLE OF CONTENTS

ABSTRACT ii
ACKNOWLEDGMENTS iv
DEDICATION vi
CHAPTER 1: Introduction 1
1.1 Background 1
1.2 Research statement 2
1.3 Life Cycle Assessments of Cyanobacterial Biorefinery 3
1.3.2 State of the Field 3
1.3.3 Research Question 1.1 5
1.3.4 Hypothesis 1.1 5
1.4 Wastewater Treatment Facility & Cyanobacterial Biorefinery Integration 5
1.4.1 State of the Field 5
1.4.2 Research Questions 2.1 7
1.4.3 Hypothesis 2.1 7
1.5 Turbulent Mixing/Thermal and Growth as it influences LCA metrics 8
1.5.1 State of the Field 8
1.5.2 Research Question 3.1 and 3.2 9
1.5.3 Hypothesis 3.1 10
1.6 Dissertation Outline 10
CHAPTER 2: Life Cycle Net Energy and Greenhouse Gas Emissions of Photosynthetic Cyanobacterial Biorefineries: Challenges for Industrial Production of Biofuels 13
2.1 Introduction 13
2.2 Methods 14
2.2.1 Goals and Scope 14
2.2.2 Impacts considered 15
2.2.3 Functional unit 16
2.2.4 System boundary 16
2.2.5 LCA Tools 18
2.2.6 Cyanobacteria Cultivation and Biofuel Concentration Systems 18
2.2.7 Sensitivity Analysis Description 19

2.3 Results and Discussion 22
2.3.1 The energy efficiency of cyanobacteria-based biofuels production systems 23
2.3.2 The carbon footprint of cyanobacteria -based biofuels production systems 24
2.3.3 The drivers to enhance the environmental benefits are identified by a sensitivity analysis.... 25
2.3.4 Challenges and future perspectives 26
2.3.4.1 Photoinhibition and low carbon partitioning into biofuels constraints the environmental benefits of photosynthetic biorefineries 26
2.3.4.2 Replacement of Industrial Fertilizers 28
2.3.4.3 Optimized bioprocess technologies will maximize the benefits in PSBR systems 28
2.4 Conclusions 31
2.5 Answer to Research Question 1.1 31
CHAPTER 3: A Geographical Assessment of Vegetation Carbon Stocks and Greenhouse Gas Emissions on Potential Microalgae-based Biofuel Facilities in The United States 32
3.1 Introduction 32
3.2 Materials and Methods 34
3.2.1 Spatial Inputs to Life Cycle Assessment and Direct Land Use Change Modeling 35
3.2.2 Spatial Analysis of Direct Land Use Change and Related Emissions 36
3.2.3 Total GHG emissions 37
3.3 Results and Discussion 38
3.3.1 AGB and SOC disturbed by microalgae-based biofuel facilities 38
3.3.2 Carbon stocks limit the locations available for sustainable microalgae-based biofuel cultivation 39
3.3.3 Including DLUC reduces GHG benefit of microalgae biofuel 43
3.4 Conclusions 44
3.5 Answer to Research Question 1.1 44
CHAPTER 4: Scalability of Combining Microalgae-based Biofuels with Wastewater Facilities: A Review 46
4.1 Introduction 46
4.2 Microalgae-based biofuels grown in wastewater 48
4.2.1 Microalgae genera and strains able to grow in wastewater 48
4.2.2 Limiting nutrients' growth-rate in wastewater for microalgae 49
4.2.3 Microalgae growth and lipid productivity in wastewater 50
4.3 The role of municipal wastewater treatment facilities in microalgae growth 57
4.3.1 Overview of the treatment process 57

4.3.2 Biological nutrient removal (BNR) process 58
4.3.3 Sludge dewatering and centrate production 62
4.3.4 The impact of the wastewater discharge permits and their relationship with microalgae-based biofuels 62
4.3.5 Potential contaminants that could inhibit the growth of microalgae 63
4.4 Computational methods to predict the growth of microalgae in wastewater 64
4.4.1 Overview 64
4.4.2 Growth kinetics of microalgae 65
4.4.3 Modeling microalgae bioreactors 68
4.4.3.1 Challenges in modeling the scalability of microalgae grown in wastewater 68
4.4.3.2 Scaled-up microalgae growth and neutral lipid synthesis model 69
4.4.3.3 Modeling and scale-up of computational fluid dynamics (CFD) for microalgae-bioreactors 72
4.4.3.4 Validation of mathematical and computational models 74
4.5 Conclusions 75
4.6 Answer to Research Question 2.1 76
CHAPTER 5: A Cyanobacterial Sidestream Nutrient Removal Process and its Life Cycle Implications 77
5.1 Introduction 77
5.2 Materials and Methods 79
5.2.1 Goals and scope 79
5.2.2 System boundary 80
5.2.3 Functional unit 81
5.2.4 Impacts assessment 82
5.2.5 LCA model development 83
5.2.6 Synechocystis sp. PCC 6803 cultivation in sludge centrate 84
5.2.7 Cyanobacterial Nutrient Removal Process 84
5.2.8 Sidestream wastewater treatment by cyanobacterial photobioreactors 85
5.2.9 Kinetics of struvite precipitation from sludge centrate 87
5.2.10 Modelling of Synechocystis sp. PCC 6803 thin layer growth with sludge centrate inhibition 88
5.2.11 Modelling of anaerobic co-digestion of activated sludge and cyanobacterial biomass 90
5.2.12 Sensitivity Analysis of Centrate Dilution Scenarios 92
5.3 Results and Discussion 93

5.3.1 Struvite precipitation rates are increased in combined cyanobacterial cultivation and sidestream wastewater treatment 93
5.3.2 Growth of Synechocystis sp. PCC 6803 including sludge centrate inhibition 94
5.3.3 Nitrogen uptake by Synechocystis sp. PCC 6803 96
5.3.4 Co-digestion of cyanobacterial biomass with activated sludge 99
5.3.5 Life cycle Net Energy and Greenhouse Gas Emissions 100
5.4 Conclusions 101
5.5 Answer to Research Question 2.1 102
CHAPTER 6: Sustainability Implications of Mixing Energy for the Industrial Scale Design of Cyanobacterial Cultivation in Open Raceway Ponds and Flat-Panel Photobioreactors 104
6.1 Introduction 104
6.2 Materials and Methods 108
6.2.1 Scale-up and Acclimation of Cyanobacterial Cultures 108
6.2.2 Configuration for Industrially Scale Experimental Analysis of flat-Panel Photobioreactors and Open Raceway Ponds 109
6.2.3 Flat-panel photobioreactors and open raceway pond monitoring 112
6.2.4 Life cycle Energy Implications of Mixing Energy Inputs 113
6.2.4.1 System boundary and Functional Unit 113
6.2.4.2 Impacts considered 114
6.2.4.3 LCA tools 115
6.3 Results and Discussion 115
6.3.1 Industrially relevant mixing energy inputs control physiological responses of Synechocystis sp. PCC 6803 116
6.3.2 Synechocystis sp. PCC 6803 grows limited by carbon at low mixing energy inputs 120
6.3.3 Low mixing energy inputs for cultivation in open raceway ponds and flat-panel photobioreactors reduce the life cycle energy of cyanobacterial biofuels 122
6.4 Conclusions 124
6.5 Answer to Research Question 3.1 125
CHAPTER 7: Pilot scale open raceway ponds and flat-panel photobioreactors maintain well-mixed conditions under wide range of mixing energy inputs 127
7.1 Introduction 127
7.2 Materials and Methods 132
7.2.1 Flat-Panel Photobioreactors Configuration 133
7.2.2 Open Raceway Pond Configuration 134
7.2.3 Experimental Fluid Mechanics Methods 135

7.2.3.1 Flat-panel photobioreactors fluid characterization by PIV 135
7.2.3.2 Open raceway pond fluid characterization by ADV 136
7.2.3.3 Characterizing cell motion by CFD 136
7.3 Results and Discussion 138
7.3.1 Flat-panel photobioreactor flow characterization 138
7.3.2 Pilot scale open raceway pond flow characterization 139
7.3.3 Frequency of cells motion are not significantly impacted due to differences in mixing energy 142
7.4 Conclusions 144
7.5 Answer to Research Question 3.2 145
CHAPTER 8: A Dynamic Lumped Thermal and Well-Mixed Algal Growth Model for Pilot Scale Open Raceway Ponds 146
8.1 Introduction 146
8.2 Dynamic modelling, uncertainty quantification, and parameter estimation methods 148
8.2.1 Pilot Scale Open Raceway Ponds Configuration and Monitoring at ATP[3] 149
8.2.2 Dynamic Thermal Model 150
8.2.2.1 Light Absorption 151
8.2.2.2 Radiation Heat Transfer with Sky 152
8.2.2.3 Convective Heat Transfer 152
8.2.2.4 Conductive Heat Transfer 153
8.2.2.5 Evaporation and Water Control Practices 154
8.2.2.6 Capacitance, Energy Balance, and Dynamic Water Temperature Simulation 154
8.2.3 Dynamic Algae Growth Modelling 155
8.2.3.1 Temperature Function 155
8.2.3.2 Light Function 155
8.2.3.3 Nutrients Function 156
8.2.3.4 Basal metabolism Function 156
8.2.3.5 Dynamic Algae Growth Simulation 157
8.2.4 Uncertainty Quantification 157
8.2.5 Calibration Procedure 158
8.3 Results and Discussion 159
8.3.1 The uncertainty of the thermal model is driven by thermal capacitance, evaporation, and heat transfer coefficients 159

8.3.2 The uncertainty of algae growth modelling is driven by dark- and photo-respiration effects 163

8.3.3 Propagated uncertainty in algae cultivation systems embedding thermal models increase the error for summer conditions 167

8.4 Conclusions 169

8.5 Answer to Research Question 3.2 169

CHAPTER 9: Cyanobacterial biomass productivity in pilot scale open raceway ponds and flat-panel photobioreactors is predicted by well-mixed growth modelling under a wide range of mixing energy inputs 170

9.1 Introduction 170

9.2 Materials and Methods 175

9.2.1 Flat-Panel Photobioreactors Cultivation Methods 175

9.2.2 Open Raceway Pond Cultivation Methods 177

9.2.3 Predictive capability of well-mixed growth models 178

9.2.3.1 Scale-up and Acclimation of Cyanobacterial Cultures 178

9.2.3.2 Well-mixed Growth Modelling and Validation 179

9.3 Results and Discussion 182

9.3.1 The predictive capability of well-mixed growth model is demonstrated under mixing energy input variability 182

9.3.2 Light attenuation in Synechocystis sp. PCC 6803 cultures is not impacted by mixing energy inputs and reactor configuration 186

9.4 Conclusions 188

9.5 Answer to Research Question 3.2 188

CHAPTER 10: Conclusions 190

10.1 Contributions to the Field 190

10.2 Summary of Answers to Research Questions 191

10.3 Future work 193

References 195

APPENDIX A: Cyanobacterial Growth in Baseline LCA 233

APPENDIX B: Geographical Assessment of DLUC in Microalgae Facilities 234

APPENDIX C: Combined Wastewater Treatment Facility and Cyanobacterial Biorefinery 252

APPENDIX D: Cyanobacteria Growth Under Wide Range of Mixing Energy Inputs 259

APPENDIX E: Applied CFD of Flat-panel Photobioreactors and Open Raceway Ponds 266

APPENDIX F: Temperature Function, Light Function, and Basal Metabolism 269

APPENDIX G: Well-mixed Cyanobacterial Growth Model Parameters 272

CHAPTER 1: Introduction

1.1 Background

Life on earth can be divided into three domains: Archaea, Eukarya, and Bacteria. Photoautotrophic microorganisms, which are present in the Eukarya and Bacteria domains, are those capable of photosynthesis [1]. Microalgae are capable of photosynthesis because the presence of organelles known as chloroplasts [2], which strong evidence suggest were inherited from the original symbiosis between a cyanobacterium and a nonphotosynthetic eukaryote [3, 4]. Microalgae, as a result, are believed to be descendants of cyanobacteria. For decades microalgae has been extensively researched for biofuel production. Microalgae's areal oil productivities reported from laboratory experimentation are about 10 times that of palm oil and about 131 times that of soybean [5]. More recently, the bioenergy industry and research community have measured cyanobacterial areal equivalent energy productivities of about four times that of microalgae, based on laboratory experimentation [6].

Photoautotrophic microorganisms are cultivated in photobioreactors (PBR), the most prevalent being the open raceway ponds, and flat panel PBR [7]. Open raceway ponds are constructed in a configuration with channels, using paddlewheel mixers that promote a low shear environment [8]. Flat panel PBR are vertically translucent flat plates, illuminated on both sides and stirred by aeration [9]. Unlike outdoor raceways and outdoor PBR, laboratory-scale experiments are most commonly grown under ideal conditions including ideal mixing rates, optimum light intensities, and optimized media. The results of these experiments indicate biomass and biofuels productivities that are generally overestimated when compared to industrial-scale systems. For instance, the light saturation of *Synechocystis sp.* PCC6803 is reported at about 200 μmol photons.s^{-1}.m^{-2} [10], whereas photoautotrophic microorganisms will

face incident radiations of about 2000 μmol photons.s^{-1}.m^{-2} at noon in locations such as Colorado [11], resulting in light inhibition of the culture when grown in the field. For the case of algae, considering that 46% of the spectrum is in the photosynthetic active radiation (PAR) range of 400 to 700 nm, there are losses due to photon transmissions efficiency of 95%, photon utilization efficiency ranging from 10% to 30%, biomass accumulation efficiency of 50%, and biomass energy content of 21.9 kJ·g^{-1}, resulting in a total photo conversion efficiency from 2.6% (at high light) to 6.3% (at reduced light) [12].

Algal and cyanobacterial biomass can be converted via hydrothermal liquefaction to produce bio-oil [13], and by fermentation to produce ethanol [14], among other technologies. More recently, researchers have developed metabolic engineering tools to promote the direct biosynthesis of biofuels by manipulating cellular pathways and enhance the product yields [15], but these systems are yet to be rigorously considered using a lifecycle assessment (LCA) framework. An LCA is a framework for evaluating the energy use, emissions and impacts of direct, indirect, and supply chain processes [16]. LCA has been used to evaluate metabolically engineered cyanobacteria biofuels [17], but these previous efforts to assess the life cycle implications at the system level from laboratory experimentation are characterized by high uncertainty due to the lack of industrially-scaled cultivation data available for validation.

1.2 Research statement

Biosynthetic co-products excreted from engineered cyanobacteria is a novel and developing technology whose objective is the development of scalable, sustainable, resource conserving bio-product systems. There is a need for analyses and evaluation techniques that will allow for the inclusion of these system-level metrics of performance in the evaluation of

laboratory-level technologies. This can be accomplished by developing a bridge and feedback loop approach between lab and industrial scale research (Figure 1.1).

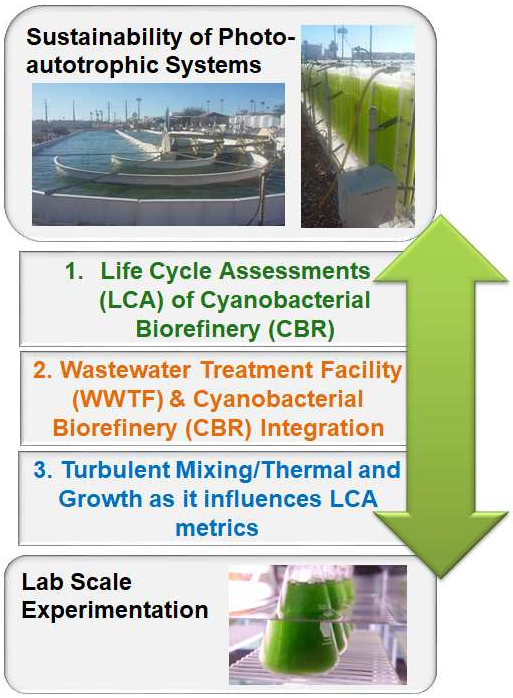

Figure 1.1 Feedback loop approach between lab and industrial scale research.

The state of the field, research questions, and hypothesis for each topic that were developed for this research proposal are elaborated in detail in the following sections.

1.3 Life Cycle Assessments of Cyanobacterial Biorefinery

1.3.2 State of the Field

Biofuel technologies, especially microalgae, have been extensively researched to model their environmental impacts, techno-economics, net energies and greenhouse gas (GHG) emissions. There is a high degree of uncertainty in these studies, for instance, from optimistic scenarios of GHG emissions of -95.7 g CO_2eq.MJ^{-1} to pessimistic scenarios of 534 g CO_2eq.MJ^{-1} [18-27].

One source of this uncertainty is disagreement regarding the boundaries of the LCA. The photoautotrophic biofuel LCA present in the literature have excluded the effects of direct land

use change (DLUC) from facility construction under the assumption that DLUC effects are negligible in barren land areas of the U.S. Previous studies that consider forested, or pasture lands as suitable for microalgae production will disturb above ground biomass (AGB) and soil organic carbon (SOC) at higher rates per unit of land area [7, 28]. There is a need to integrate available carbon stock data, including above and below ground biomass, with photoautotrophic based LCA to have a more holistic understanding of the environmental impact associated with biofuels production.

Another example, is that novel products and systems are not well characterized for LCA. For cyanobacteria-based biofuels, previous research using ethanol as a bioproduct reports net energy ratios (NER) ranging from 0.20 to 0.55 MJ consumed.(MJ produced)$^{-1}$ and GHG emissions ranging from 12.3 to 19.8 g CO_2eq.MJ^{-1} [17]. None of the studies to date have evaluated the novel biofuels bisabolene and heptadecane produced by cyanobacteria. Although this previous research presents an in-depth review of the processes involved in the proposed technology, productivities of ethanol were based on a cost-effective range established by the authors, as opposed to near-term or physically realizable productivities. Additionally, this previous effort to study the life cycle energy and GHG emissions of cyanobacterial ethanol production ignored the commonly accepted cultivation technologies of raceway ponds and flat photobioreactors. Based on this understanding, we can define a need for a baseline LCA of *Synechocystis sp.* PCC6803 that can consider the current data regarding biofuel production including biomass productivities in industrial cultivation systems, new biofuel productivities from biosynthesis, and process energy consumption.

1.3.3 Research Question 1.1

Based on the challenges described above in performing LCA of photoautotrophic biofuels, the first research challenge is:

What are the baseline life cycle characteristics of a cyanobacteria-based bio-product/bio-fuel technology, in terms of sustainability goals?

1.3.4 Hypothesis 1.1

Cyanobacterial derived biofuels, being an emerging technology, requires further research to reduce the uncertainties in biomass productivities, mixing energy requirements, and energy conversion. DLUC due to construction of photosynthetic-derived biofuel plants in barren land areas of the U.S. plays a major role in the sustainability of this technology.

1.4 Wastewater Treatment Facility & Cyanobacterial Biorefinery Integration

1.4.1 State of the Field

The U.S. goal of producing 40 billion gallons of biofuel per year from microalgae will be limited by the very large scale of the required water and nutrients. For instance, water equivalent to 27 % of the Colorado River annual flow, 1900 % of the total urea production of U.S., and potential excess of non-fuel carbon co-products equivalent to 7500 % of the North American glycerin production are required to produce 40 billion gallons of biofuel per year from microalgae [29]. These water and nutrients requirements limit the scalability of microalgae-based biorefineries and could reduce the anticipated economic feasibility and environmental sustainability of photosynthetic-based biofuel production technologies.

At the same time, municipal wastewater treatment facilities around the globe including U.S. are facing new challenges to meet the water quality criteria, in terms of nitrogen (annual median of 7 $mg.l^{-1}$) and phosphorous (annual median of 0.7 $mg.l^{-1}$), established by States water

regulations and the Environmental Protection Agency (EPA). The major concern for these facilities is the sidestream wastewater treatment for sludge centrate due to eutrophication in surface waters by nitrogen and phosphorous [30]. Several technologies have been developed for the sidestream wastewater treatment including modified Bardenpho process [31], sludge centrate recycling [32], anaerobic ammonium oxidation (Anammox) [33], adsorption [34], electrodialysis [32], ammonia stripping [32], and struvite precipitation [35, 36]. Among these processes, Biological Nutrient Removal (BNR) processes, such as modified Bardenpho, have revealed the total nitrogen (TN) and total phosphorous effluents to about 3 and 1 $mg.l^{-1}$, respectively (EPA 2007). However, these BNR technologies require a high capital cost in the range of 150 to 1,840 $\$. m^{-3}$- [37] and energy consumption of 0.09 $kwh.m^{-3}$-wastewater [38] relative to the conventional wastewater treatment facility. While struvite precipitation from sludge centrate is recovered in the form of fertilizer [35, 36], the treated effluents reported in the literature [39] with 128 ± 5 mg NH_4-$N.l^{-1}$ and 12.3 ± 6.2 mg PO_4-$P.l^{-1}$ do not meet the water quality expectations for nitrogen and phosphorous.

The environmental impacts of photosynthetic biorefineries and wastewater treatment facilities may be reduced by integrating these technologies to accomplish both 1) providing resources to enable the large scale cultivation of cyanobacteria for energy production, and 2) the large-scale remediation of nitrogen and phosphorous from wastewater [30, 37]. Several past studies [40-46] have extensively investigated the growth of photosynthetic microorganisms in wastewater. Some recent studies [37, 47, 48] have shown the potential growth of photoautotrophic microorganisms in the sludge centrate obtained from the dewatering processes of a wastewater treatment facility. These studies suggest that the sludge centrate itself could be supplied as the main source of nutrients due to the high concentrations of nitrogen and

phosphorous. However, ammonia, the nitrogen compound present in the sludge centrate, inhibits the growth of cyanobacteria, including the strain selected in this study-*Synechocystis sp.* PCC6803 [49, 50]. For instance, the biomass productivity of this cyanobacteria strain is inhibited at high intracellular concentrations of ammonia of 63 mg $NH_4.l^{-1}$ [51] due to damage to photosystem II [52]. These efforts suggest that photoautotrophic microorganisms, such as cyanobacteria, could potentially solve the challenges associated with the sidestream wastewater treatment system once centrate inhibition can be mitigated or controlled.

Past LCA studies have focused on biofuel and bioproducts production, and none of the previous studies have investigated the synergistic benefits of combining photosynthetic biorefineries, based on *Synechocystis sp.* PCC6803, and wastewater treatment facilities. These synergistic benefits include improvement in the quality of water from the wastewater treatment facilities, energy recovery, and greenhouse gas (GHG) emissions reduction due to fossil fuels and commercial fertilizers displacements with biofuels and co-products, respectively.

1.4.2 Research Questions 2.1

By considering the challenges in the integration of wastewater treatment facilities and cyanobacterial biorefineries, I propose a second research question:

To what extent are the joint achievement of sustainability, scalability, and water quality goals assisted by the integration of cyanobacterial biorefinery (CBR) and wastewater treatment facility (WWTF)?

1.4.3 Hypothesis 2.1

Integration of CBR and WWTF provides synergistic lifecycle benefits including the displacement of fertilizers for cyanobacteria cultivation by wastewater nutrients, reduction of

energy consumption to remove nutrients from the treated wastewater, and improvement of water quality from wastewater facilities.

1.5 Turbulent Mixing/Thermal and Growth as it influences LCA metrics

1.5.1 State of the Field

Photoautotrophic productivity in terms of biomass and biofuel are well-understood to be overestimated by laboratory scale experiments, relative to industrial scale systems. For instance, the light saturation of *Synechocystis sp.* PCC6803 is reported at about 200 μmol photons.s^{-1}.m^{-2} [10], whereas photoautotrophic microorganisms will face incident radiations of about 2000 μmol photons.s^{-1}.m^{-2} in their natural environments [11]. For example, the photo-conversion efficiency of microalgae ranges from 2.6% at high incident radiations, to 6.3% at reduced incident radiations [12].

Previous studies have investigated the effects of mixing rates on photoautotroph biomass productivities [11, 15, 62, 63]. Some of these efforts have identified optimum volumes of air flow rates per unit volume (VVM) of photobioreactors that might be industrially relevant for microalgae [11]. Many others have considered mixing energy inputs that are far outside the energy consumption that can be considered economic, or industrially relevant, ranging from 8 to 633 W.m^{-3} [53]. For raceway ponds, for instance, energy inputs from 1 to 2 W.m^{-3} are utilized in the algae cultivation demonstrations performed to date [7, 54]. None of this previous research on culture mixing has evaluated the implications of turbulent mixing on the NER (and other lifecycle sustainability metrics) of the system as whole.

There are several ongoing efforts in the literature to understand the connections between photoautotrophic microorganism's bioprocesses, and mixing in raceway ponds and photobioreactors. Yet most of the literature relies on light distribution in photobioreactors based

on Beer-Lambert law [55, 56]. Although previous efforts measured the light absorption coefficient of *Nannochloropsis sp.* in photobioreactors [56], the derived model can only be used to describe light distribution for particular validated conditions. The only predictive work concerning radiative transfer in aqueous suspensions was developed by Incropera [57, 58], consisting of a discrete ordinate method for modeling heat transfer in scattering fluids. None of previous efforts in the literature have integrated Incropera's work in raceway ponds and photobioreactors modeling, due to its computational complicatedness relative to Beer-Lambert.

Similarly, some studies have attempted to predict the fluid mechanics of raceway ponds and photobioreactors via Computational Fluid Dynamics (CFD) approaches [59-70]. The conclusion of many of the raceway pond CFD models that have been applied to investigate velocity, heat transfer, are weakened because they use average velocities as boundary conditions [54, 71], missing the dynamics of these systems downstream of the paddlewheel. Other studies utilized Acoustic Doppler Velocimetry (ADV) to describe the velocity field of raceway ponds [72] but, ignore the time scales and turbulence that describe the physics of this reactors. Lastly, there is previous research concerning particle tracking with neutrally buoyant particles in photobioreactors [73], but the statistical and temporal nature of turbulence modeling was not considered. In general, previous studies have failed in analyzing the flow characteristics at industrially relevant mixing energy inputs.

1.5.2 Research Question 3.1 and 3.2

From this understanding of the research in turbulent mixing in photoautotrophic microorganisms and life cycle metrics at the system level, we have developed the following research questions:

Research question 3.1:

What are the implications of mixing rates in the life cycle metrics of flat photobioreactors and raceways ponds?

Research question 3.2:

What is the incident radiation and thermal environment experienced by single cyanobacteria cells. How is the bulk thermal system impacted by turbulent mixing?

1.5.3 Hypothesis 3.1

Differences in mixing energy change metrics of growth and sustainability for photoautotrophic-derived biofuel systems. Fluid flow and mixing in open raceway ponds is hypothesized to strongly influence algae growth. Pilot scale open raceway ponds and flat-panel photobioreactors maintain well-mixed conditions under a variety of operating conditions, and their cyanobacterial growth performance is described by well-mixed models.

1.6 Dissertation Outline

This research presents novel means to be able to analyze, integrate, assess, and design photoautotrophic biofuel and bioproduct systems, as defined using LCA. To understand the connections between the physical environment and the biological responses of cyanobacteria and microalgae, we used experimental and computational fluid mechanics, and models of the cultivation system and growth (Figure 1.2). The research effort is composed of a set of research tasks that contribute to this overall objective. To answer the research questions this dissertation is organized into 10 chapters.

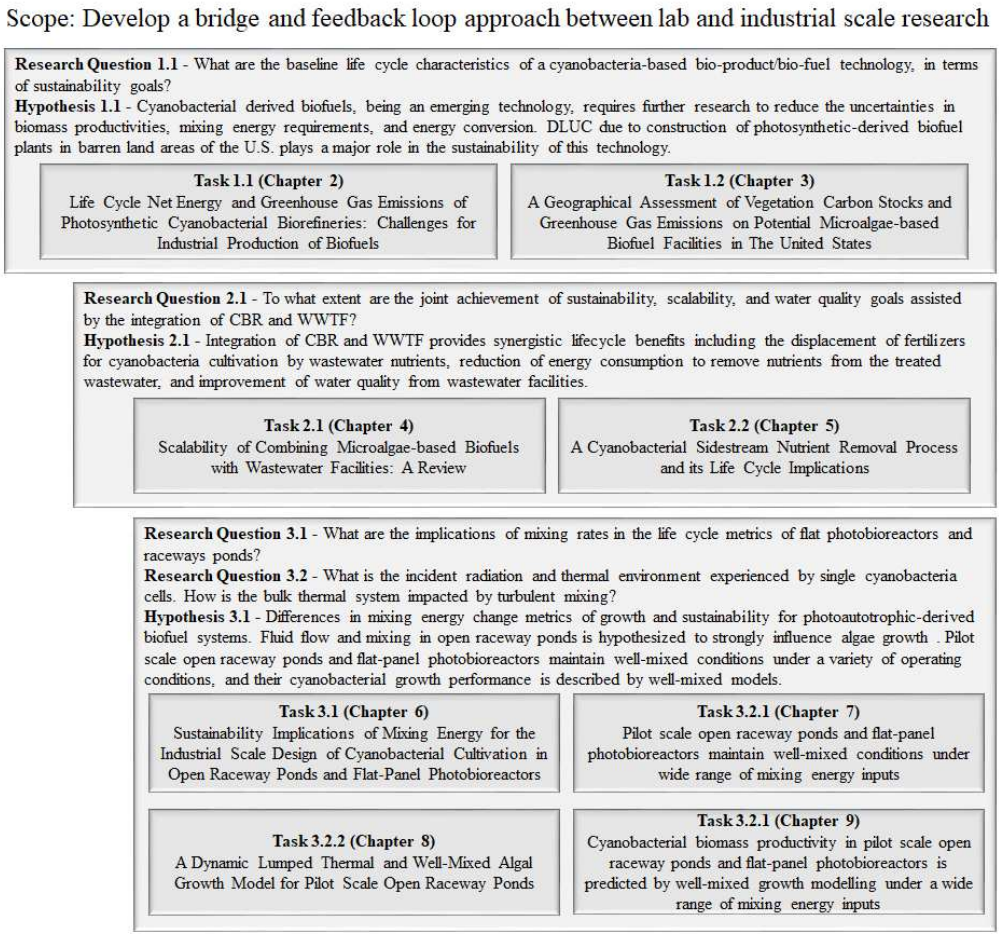

Figure 1.2 Summary of research questions, hypothesis, and tasks associated with this dissertation.

The first research question (1.1) is answered in Chapters 2 and 3. Chapter 2 develops naïve models of laboratory scale data, including cyanobacterial biomass productivities, carbon partitioning (biofuel yield), and extrapolated mixing and conversion energy requirements. From this chapter, an analysis and quantification of baseline sustainability metrics is performed using an LCA of cyanobacterial biorefinery to national relevant scale. Chapter 3 develops an inclusive geographical assessment of microalgae facilities in the U.S. to evaluate the impact of DLUC on life cycle GHG emissions by constructing refineries in barren land areas. The second research question (2.1) is answered in Chapters 4 and 5. Chapter 4 reviews the growth and productivity of

photoautotrophic microorganisms grown in wastewater resources, including raw, primary and secondary treated, and sludge centrate. Chapter 5 integrates cultivation of cyanobacteria in sludge centrate, evaluating the biological and sustainability tradeoffs of centrate dilution.

The third research question (3.1) is answered in Chapter 6. In this chapter we integrated cyanobacterial cultivation at high radiations experienced by photoautotrophic microorganisms and biological and sustainability tradeoffs with mixing energy inputs in flat-panel photobioreactors and open raceway ponds, with metrics that are relevant for the industry. The drivers of growth and biomass productivity are identified in this chapter. Because fluid mechanics is hypothesized to influence photoautotrophic growth and productivity, the last research question (3.2) of this dissertation in answered in Chapters 7, 8, and 9. Chapter 7 seeks to understand the flow characteristics of flat-panel photobioreactors and open raceway ponds, and the role that flow characteristics have in the motion and light experienced by photoautotrophic microorganisms (Figure 1.2). Chapter 8 evaluates the predictive capability of a dynamic lumped-thermal model based on open raceway ponds operated in outdoor conditions as part of a collaboration with Sandia National Laboratories. The propagated uncertainty of the lumped-thermal system embedded into an algae growth model is quantified and the epistemic and aleatory uncertainty parameters are identified. Chapter 9 seeks to understand biological epistemic parameters in well-mixed cyanobacterial growth models by integrating growth as a function of mixing energy input in a photo-inhibiting environment. Lastly, Chapter 10 concludes by synthesizing the contributions, main findings, and future directions of this dissertation.

CHAPTER 2: Life Cycle Net Energy and Greenhouse Gas Emissions of Photosynthetic Cyanobacterial Biorefineries: Challenges for Industrial Production of Biofuels[1]

2.1 Introduction

Photoautotroph-based biofuels are considered one of the most promising renewable resources to meet the global energy requirements for the transportation system [5]. Long-term research and development has resulted in demonstrations of microalgae areal oil productivities that are higher than crop-based biofuels, about 10 times that of palm oil and about 131 times that of soybean [5, 74-76]. Cyanobacteria is reported to have ~4 times the areal productivity of microalgae on an equivalent energy basis [6]. Downstream of the cultivation process, the cyanobacteria biomass and bioproducts are supplied to biorefineries producing feed, biomaterials, biosynthetic chemicals, and biofuels [77].

Biofuel technologies, especially microalgae, have been extensively researched to model their environmental impacts, techno-economics, net energies and greenhouse gas (GHG) emissions [18-24, 26, 27, 78]. None of these studies have evaluated the biofuels bisabolene and heptadecane produced by cyanobacteria. For cyanobacteria-based ethanol, previous research reports net energy ratios (NER) ranging from 0.20 to 0.55 MJ consumed·(MJ produced)$^{-1}$ and GHG emissions ranging from 12.3 to 19.8 g CO_{2eq}.MJ^{-1} [17]. Although this previous research report presents an in-depth review of the processes involved in the proposed technology, productivities of ethanol were based on a cost-effective range established by the authors rather than being based on near-term or physically realizable productivities. In this LCA, we consider the current data regarding biofuel production including biomass productivities, biofuel

[1] **This chapter is adapted from a published refereed journal article:** Quiroz-Arita, Carlos, John J. Sheehan, and Thomas H. Bradley. "Life cycle net energy and greenhouse gas emissions of photosynthetic cyanobacterial biorefineries: Challenges for industrial production of biofuels." Algal Research 26 (2017): 445-452.

productivities and process energy consumptions. This LCA is novel in that the lifecycle impacts of the two biofuels investigated in this study, bisabolene and heptadecane, from genetically modified cyanobacteria will be evaluated in comparison to more conventional ethanol production schemes.

This research seeks to model the NER and GHG emissions for photosynthetic biorefineries growing cyanobacteria, where bisabolane and heptadecane biofuels are compared to ethanol so as to understand the biological and process engineering challenges for industrial scale production.

2.2 Methods

2.2.1 Goals and Scope

Life Cycle Assessment (LCA) is a framework for evaluating the energy use, emissions and impacts of direct, indirect, and supply chain processes [16]. A LCA model was developed in this study to assess these aspects of a cyanobacteria-based biofuel facility. In developing the goals and scope of this project, we seek to compare a bisabolane or heptadecane production to cyanobacteria-based ethanol production, a near-term and commercially promising technology. Cyanobacteria-based ethanol is chosen as the baseline for comparison because these organisms display the highest productivities and rates of carbon partitioning [79], and could potentially meet the environmental goals as for renewable fuels in the U.S. [80].

The primary audience for this LCA includes cyanobacteria researchers, policy makers, and process engineers. The outputs of this study are direct lifecycle comparisons of the environmental and energy impacts of these cyanobacteria based biofuel systems.

This LCA considers biomass productivities and biofuel yields of *Synechocystis* sp. PCC6803. Current biofuel yields of biosynthetic bisabolane and heptadecane reported in the

literature serve as the baseline in a sensitivity analysis at the system level. The biosynthetic bisabolane and heptadecane biofuels secreted by *Synechocystis* sp. PCC6803 are compared to state-of-the-art cyanobacteria-based biofuel, ethanol. Cyanobacteria-based ethanol is the cyanobacteria-based biofuel which reaches the highest carbon partitioning assimilated, 63%, during cultivation of *Synechocystis* sp. PCC6803 [79], and therefore has the highest commercialization potential.

This study considers a cyanobacteria production system located in Fort Collins, CO USA. Weather conditions, including temperature and incident radiation, are used to model real-world biomass productivities.

2.2.2 Impacts considered

The two sustainability metrics and impacts considered in this study are net energy ratio (NER) and lifecycle GHGs, and were elicited from a set of surveyed stakeholders.

The production of biofuel as an energy carrier is the primary goal of any potential biofuel technology. Therefore, net energy ratios (Equation 1) were the first metric of interest for this LCA.

$$\text{NER} = \frac{\text{E}_{\text{consumed}}}{\text{E}_{\text{produced}}} \quad \text{Eq. 1}$$

NER are defined in this study by normalizing the energy consumed ($E_{consumed}$) in the cyanobacteria growth, fuel extraction, and conversion processes by the energy produced ($E_{produced}$) by this system as embedded in the lower heating value of the biofuel.

Various economic and policy incentives have been developed to incent the production of fuels with low net GHG emissions [80]. Therefore, the second metric of interest is lifecycle greenhouse gas (GHG) emissions (Equation 2).

$$\text{GHG emissions}_{\text{fuel/energy}} = FC * EF_{\text{fuel}} * P_{\text{technology}} \quad \text{Eq. 2}$$

Lifecycle GHG emissions (GHG emissions $_{fuel/energy}$) are defined by the Intergovernmental Panel on Climate Change (IPCC) as the direct or indirect amount of fuel or energy consumed (*FC*) by the emission factor based on the type of fuel or energy technology (*EF* $_{fuel}$), and the penetration ($P_{technology}$) or fraction of the energy source of a given energy technology [81].

2.2.3 Functional unit

The functional units for this study is the energy produced from biofuels to displace petroleum fuels, in MJ (Figure 2.1).

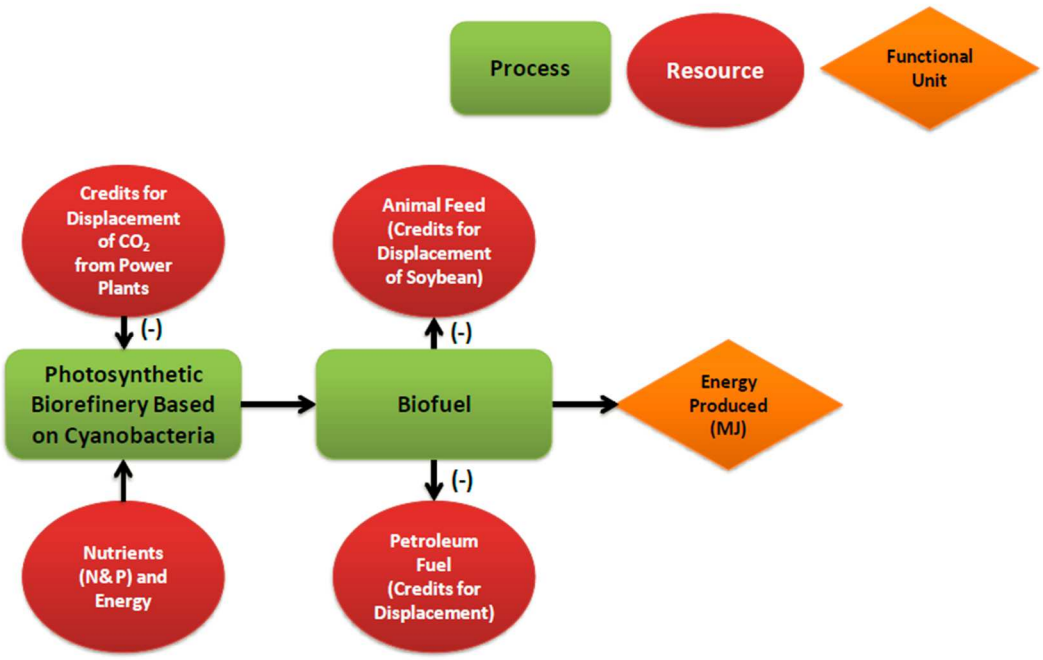

Figure 2.1 Functional unit of Photosynthetic Biorefinery (PBR) System.

2.2.4 System boundary

The boundaries of the combined growth, extraction and conversion systems to be researched in this LCA are illustrated and summarized in Figure 2.1. The processes considered for this study start with the growth stage of the cyanobacteria, and end at the point of conversion

of the bioproducts to a biofuel which can displace conventional fuels. The system includes the direct energy requirements of the facility. The embedded GHG emissions for each of the energy sources are included. The water and nutrient requirements will be supplied by recycled commercial water and commercial/industrial fertilizers. Carbon dioxide is assumed to be obtained from waste streams from local industrial CO_2 facilities including power plants, amine natural gas treatment plants, and fermentation plants.

Three novel cyanobacteria-based biofuel production systems will be evaluated as independent systems. The impacts of these biofuels will be compared to those of the conventional fuels they would displace. Bisabolane will replace conventional jet fuel from crude oil, heptadecane will replace low-sulfur diesel from crude oil, and ethanol will replace gasoline blendstock from crude oil. The distribution of biofuels and the end use (combustion of these biofuels) will not be taken into account to avoid misinterpretations when comparing different cyanobacteria-based biofuel systems.

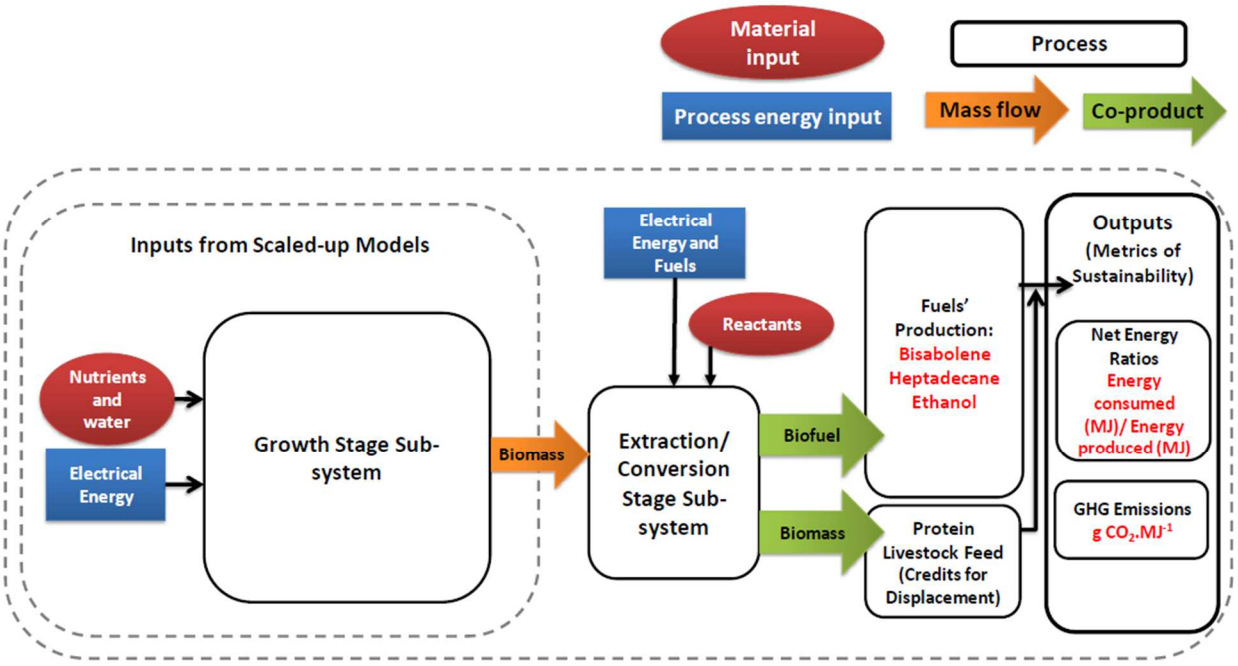

Figure 2.2 Boundaries and inputs of Photosynthetic Biorefinery (PSBR) System.

2.2.5 LCA Tools

The PSBR systems were modeled in the GaBi 6 software by constructing three comparable models to describe the function of these three cyanobacteria-based biofuels. GaBi is a tool that allows for the estimation of the lifecycle energy and emissions output of a process as a function of the energy, material consumed for that process. The GaBi model was used to calculate the lifecycle, material consumption, net energy use, and GHG emissions for the lifecycle of the cyanobacteria-to-biofuel process.

In evaluating the life cycle energy consumption of the cyanobacteria-to-biofuel process, the biomass that is not converted to fuel can be considered as a co-product. For this study, the cyanobacteria co-product credits are allocated using the displacement method. The displacement method assumes that the co-product displaces a preexisting conventional product. The displacement co-product credits represent the lifecycle energy and GHG emissions that would be required to produce the displaced product. Co-product credits are subtracted from the overall energy and GHG emissions of the cyanobacteria-to-biofuel process.

2.2.6 Cyanobacteria Cultivation and Biofuel Concentration Systems

The genetically engineered cyanobacteria, *Synechocystis* sp. PCC6803, that are the subject of this study, are cultivated in enclosed photobioreactors to protect them from contamination and to enable the collection of the biofuel from the photobioreactor media and headspace. The batch bioprocess is carried out in flat photobioreactors providing a total culture volume of 126,000 m^3. For validation purposes of the growth stage subsystem of this LCA, we performed experimental work in a bench scale flat photobioreactor with surface to volume ratio of 112 $m^2.m^{-3}$. Cultures were mixed by sparged air at the bottom of the photobioreactor at 0.5 m^3 of air per minute per cubic meter (VVM) (+/- 0.3). Photobioreactors were inoculated with *Synechocystis* sp. PCC6803

cells at 0.107 $g.l^{-1}$ (+/- 0.061). The cultures were grown using a high-pressure sodium (HPS) lighting system with a spectrum ranging from 400 to 700 nm at extreme conditions, sunny day at noon or a Photosynthetic Active Radiation (PAR) over 1,600 μmol $Photons.m^{-2}.s^{-1}$. Cyanobacterium biomass was harvested upon quasi-steady state conditions, reaching a productivity of 0.128 $g.l^{-1}.d^{-1}$ (+/- 0.033) (Appendix A).

The cyanobacteria were grown in BG11 media. CO_2 enriched air (2% CO_2) is sparged through the bioreactor to provide carbon and active mixing of the culture. Mixing by sparge is performed during periods of photosynthetically active growth and when bioavailable nitrogen is present in the media. Industrial forms used in our bioprocess modelling include sodium nitrate and monopotassium phosphate [29]. Thermal regulation of the photobioreactors is performed by a temperature controlled heat exchanger coil, set at 29 □C, supplying tap water. US average grid electricity is used to power pumping and sparging of the cultivation process.

During cultivation of these genetically engineered cyanobacteria strains, the metabolism of the organism produces a carbon flux that generates the biofuel products within the cell. Diffusion and secretion transfers the biofuel to the growth media. When grown in batch culture, the biofuel becomes concentrated in the media, and carried via sparged air into the headspace of the photobioreactor. The biofuel is removed from the headspace by vapor compression and distillation of the exhaust air.

2.2.7 Sensitivity Analysis Description

Because a high degree of uncertainty must be associated with modeling of these novel organisms and bioproducts, sensitivity analysis will allow for the consideration of various characteristics of growth, extraction and conversion for these cyanobacteria-based biofuel

systems. The source of these uncertainties, including productivities and resource requirements, will be discussed in more detail in the results section.

Sensitivity analysis of the growth stage of the system will consider ranges of growth system energy consumption, of nutrient uptake rates, and of biomass productivities. A primary source of energy consumption in the growth stage is due to the energy required to mix culture by air/CO_2 sparging or paddlewheels. Various studies [82] [83] report air flow rates per volume of reactors ranging from 0.2 m^3 to 1.2 m^3 of air per minute per cubic meter (VVM). Mixing energy consumptions ranging from 0.5 $W.m^{-3}$ to 5.0 $W.m^{-3}$ will be evaluated in this LCA. Previous research based on a cyanobacteria strain, *Synechocystis* sp. PCC6803, reported nitrogen and phosphorus uptakes ranging from 0.05 to 0.098 $g.l^{-1}.d^{-1}$ and 0.0024 to 0.0114 $g.l^{-1}.d^{-1}$, respectively [10, 84]. These studies report biomass productivities for *Synechocystis sp.* PCC6803 ranging from 0.12 to 0.76 $g.l^{-1}.d^{-1}$. Ranges of productivities and concentrations will be evaluated for bisabolene, heptadecane, and ethanol. Bisabolene production will be evaluated in a range from 3.6E-05 $g.l^{-1}.d^{-1}$ to 2.3E-04 $g.l^{-1}.d^{-1}$ as computed from biomass productivities and yields reported in the literature [6, 79, 85]. Heptadecane production, will be evaluated from 0.00132 $g.l^{-1}.d^{-1}$ to 0.008 $g.l^{-1}.d^{-1}$ as reported in the literature for other cyanobacteria strains [86]. Ethanol, as reported by the state-of-the-art biofuel production from cyanobacteria, will be evaluated between 0.024 $g.l^{-1}.d^{-1}$ to 0.24 $g.l^{-1}.d^{-1}$ [79]. These ranges of inputs define the ranges of the sensitivity analysis for the growth stage.

The energy requirements in the extraction and conversion stage processes will depend upon the biofuel to be assessed in this study: bisabolane, heptadecane, or ethanol (Figure 2.3). For these cyanobacteria-excreted biofuels, a dilute water solution of biomass and biosynthetic biofuel is obtained from the growth stage [6], bisabolane is then converted to bisabolene, a

biosynthetic substitute of D2 diesel, by vapor compression and distillation followed by chemical hydrogenation. Chemical hydrogenation requires 4.07 $MJ.g_{biomass}^{-1}$ due to the consumption of electricity, natural gas, and hydrogen during the process [87]. Heptadecane is assumed to require vapor compression and distillation, whereas ethanol extraction and conversion will include an additional filtration by molecular sieve [17, 88]. The separation technology, for heptadecane and ethanol, has an energy consumption range of 0.108 to 0.159 $MJ.MJ_{fuel}^{-1}$ and 190 to 280 $MJ.MJ_{fuel}^{-1}$, respectively [17]. These ranges of inputs define the ranges of the sensitivity analysis for the extraction and conversion stages.

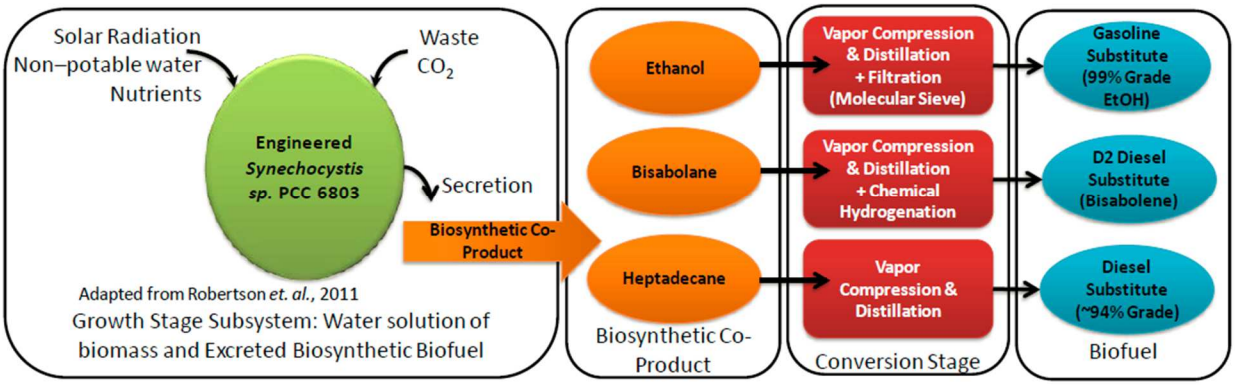

Figure 2.3 Biosynthetic co-products excreted from engineered cyanobacteria and biofuel's conversion processes.

Microalgae biomass has been previously researched for its potential to replace corn and soybean meals in animal feed [89]. Although there is no previous research evaluating the displacement of these meals by cyanobacteria, we assumed that the cyanobacteria biomass co-product will be able to displace the GHG and energy emissions associated with the cultivation and processing of these feeds. The range of inputs to be used in the sensitivity analysis concerning nutrient uptake, biomass productivities, separation, and biofuel productivities are illustrated in Table 2.1. The baseline values in Table 2.1 are used as inputs of the baseline LCA for bisabolene, heptadecane, and ethanol productions, respectively. The low and high input

values are utilized to compute the uncertainty of the results when evaluating the three biofuel processes. For the case of cyanobacteria-based ethanol production, the sensitivity analysis is performed by evaluating the NER and GHG emissions response due to input variation by +/- 20% with respect to the baseline.

Table 2.1 Inputs for sensitivity analysis

Process stage	Low	Baseline	High
Biomass Productivity ($g.L_{media}^{-1}.d^{-1}$)	0.12	0.44	0.76
Bisabolene Productivity ($g.L_{media}^{-1}.d^{-1}$)	0.000036	0.00013	0.00023
Heptadecane Productivity ($g.L_{media}^{-1}.d^{-1}$)	0.0013	0.005	0.008
Ethanol Productivity ($g.L_{media}^{-1}.d^{-1}$)	0.04	0.14	0.24
Mixing Energy ($W.m_{media}^{-3}$)	0.50	2.00	5.00
Nitrogen uptake ($g.L_{media}^{-1}.d^{-1}$)	0.05	0.07	0.098
Phosphorous uptake ($g.L_{media}^{-1}.d^{-1}$)	0.0024	0.0069	0.011
Vapor compression/distillation ($MJ.MJ_{biofuel}^{-1}$)	0.108	0.194	0.280

2.3 Results and Discussion

The research results are divided into four components. First, we compared the NER for photosynthetic cyanobacterial biorefineries producing bisabolane and heptadecane, respectively, with a cyanobacteria-based ethanol production system. Second, the GHG emissions of these three biosynthetic biofuel production pathways were compared. By contrasting the NER and GHG of these three biofuel pathways, we have identified that cyanobacteria-based ethanol production has the lowest environmental cost. The uncertainty of the NER and GHG emissions results due to input data variability are included in these sections. Third, we present a sensitivity

analysis of the cyanobacteria-based ethanol production system, identifying the major process that impact in the system response in terms of NER and GHG emissions. Lastly, we discuss the challenges and future perspectives for the most sensitive processes, establishing the potential improvements by metabolic engineering of cyanobacteria, displacement of fertilizers, and optimization of bioprocess technologies that would maximize the environmental benefits of photosynthetic cyanobacterial refineries.

2.3.1 The energy efficiency of cyanobacteria-based biofuels production systems

The most efficient pathway identified in this research is the state-of-the-art cyanobacteria-based ethanol production system, which has the lowest NER compared to bisabolane and heptadecane production. Across the sensitivities considered, the NER of the ethanol production pathway ranges from 2.64 to 1.16 $MJ.MJ^{-1}$, where the lowest value represents the best case scenario.

When compared to cyanobacteria-based ethanol production systems proposed in literature, these results are more conservative than the results reported by Luo *et. al.* [17], which ranged from NERs of 0.55 and 0.20 $MJ.MJ^{-1}$. These differences may be attributed to the 1) higher energy requirements in this proposed process due to higher rates of mixing, and 2) the energy associated with water consumption despite modeling that 90% of water is recycled in the process. Cyanobacteria-derived bisabolane and cyanobacteria-derived heptadecane had worse NER than the ethanol technologies considered in this study. Under best case scenarios, the production of bisabolene resulted in a relative increase of 240% for NER compared to cyanobacteria-derived ethanol. Under best case scenarios, the production of heptadecane resulted in a relative increase of 673% for NER with respect to cyanobacteria-derived ethanol (Figure 2.4a and 2.5a). These results are summarized in Table 2.2.

The NER of bisabolane and heptadecane production systems identified in this research can serve as a baseline to pursue more efficient bioprocesses. These biosynthetic biofuels should target in the mid-term similar NER identified in the ethanol production system to justify their manufacture by the industry. All the cyanobacteria-based biofuels production systems evaluated in this research; however, should accomplish in the long-term more sustainable NER, less than one, contributing to the energy efficiency and cost-effectiveness of this bioenergy technology.

2.3.2 The carbon footprint of cyanobacteria -based biofuels production systems

The lowest environmental impacts were observed in the cyanobacteria-based ethanol production system. The GHG emissions for the cyanobacteria-derived ethanol ranged from 233.5 to 89.6 g $CO_{2eq}.MJ^{-1}$. The GHG emissions results found here are more conservative than was reported by Luo *et. al.* [17] for ethanol production, 29.8 to 12.3 g $CO_{2eq}.MJ^{-1}$. The GHG emissions obtained by our model are within the range of the values reported by Passell *et. al.* [90], Sills *et. al.* [91], Vasudevan *et. al.* [27], Grierson *et. al.* [92], and Brentner *et. al.* [93] for open raceway ponds and photobioreactors.

Cyanobacteria-derived bisabolane and cyanobacteria-derived heptadecane had higher GHG emissions than the ethanol technologies considered in this study. Under best case scenarios, the production of bisabolene resulted in a relative increase of 30,610% for GHG emissions compared to cyanobacteria-derived ethanol. Under best case scenarios, the production of heptadecane resulted in a relative increase of 1,096% for GHG emissions with respect to cyanobacteria-derived ethanol (Figure 2.4a and 2.5a). These results are summarized in Table 2Table.2.

The cyanobacteria-based biofuels pathways evaluated in this research have proven to have high carbon footprints, particularly for bisabolane and heptadecane production systems. In the

following sections we discuss the drivers and challenges to enhance the environmental benefits of photosynthetic cyanobacterial refineries.

2.3.3 The drivers to enhance the environmental benefits are identified by a sensitivity analysis

In general, these results demonstrate that the environmental performance of these biofuel producing cyanobacteria and their associated processes are worse than the performance of the ethanol system, despite their reported high areal biofuel productivities [6, 94].

So as to understand the drivers of the environmental costs for these systems, we performed a sensitivity analysis of the ethanol biofuel production system, as it represents the most well-developed of the cyanobacteria production systems modeled in this study. For this ethanol biofuel production system, Figures 4b and 5b present tornado plots of the percent change in lifecycle NER and GHG emissions due to a ± 20% change in each of the sensitivity inputs from Table 2.1. These plots demonstrate that the environmental impacts are particularly sensitive to the parameters of ethanol productivity, the energy consumption associated with the biofuel vapor compression and distillation processes, the energy consumption associated with culture mixing, and the embedded energy in nutrients.

Table 2.2 Net Energy Ratios (NER) and GHG emissions of PSBR based on cyanobacteria

Biofuel	Scenario		
	Low	Middle	High
Ethanol (baseline)			
NER ($MJ_{consumed}$. $MJ_{produced}^{-1}$)	2.64	1.18	1.16
GHG (gCO_{2eq}. $MJ_{produced}^{-1}$)	233.5	105.9	89.6
Bisabolene			
NER ($MJ_{consumed}$. $MJ_{produced}^{-1}$)	1306.85	411.53	279.24

Biofuel	Scenario		
	Low	Middle	High
GHG (gCO_{2eq}. $MJ_{produced}^{-1}$)	123,757.4	42,013.3	27,516.1
Heptadecane			
NER ($MJ_{consumed}$. $MJ_{produced}^{-1}$)	33.99	9.75	7.96
GHG (gCO_{2eq}. $MJ_{produced}^{-1}$)	3,245	1,039	845.5

2.3.4 Challenges and future perspectives

2.3.4.1 Photoinhibition and low carbon partitioning into biofuels constraints the environmental benefits of photosynthetic biorefineries

One means to address the environmental costs of these biofuel production systems is through biological and metabolic engineering of the cyanobacteria to improve biofuels productivity.

Metabolic engineering of cyanobacteria has been utilized to engineer pathways for production of carbon-based co-products, including biofuels, from carbon dioxide, incident radiation, water, and nutrients [79]. Theoretical ethanol productivities computed from the literature have a range of uncertainty of between 0.04 to 0.24 g $EtOH.L_{media}^{-1}.d^{-1}$. (assuming *Synechocystis* sp. *PCC6803* biomass productivities range from 0.12 to 0.76 $g.L_{media}^{-1}.d^{-1}$ in photobioreactors subjected to incident radiation above 1000 μmol photons. $s^{-1}.m^{-2}$ [10, 84], and 50% of carbon content and 63% of carbon partitioning into ethanol [79]). On the other hand, the theoretical bisabolene and heptadecane biofuel yields are 0.09% and 3.5% of ethanol yields, respectively. These low yields compared to ethanol, particularly in bisabolene, are due to reduced carbon partitioning of 0.06% and 0.55% (1.1% of cell dry weight and assuming 50% of carbon content) as reported in the literature for bisabolene by Davies *et. al.*[85] and for

heptadecane by Wang *et. al* [86], respectively. As illustrated in the sensitivity analysis, the carbon partitioning assimilated as bioproduct in cyanobacteria leads to low ethanol productivity, which is a significant factor in the life cycle NER and GHG emissions of these biofuels.

Based on the theoretical yields, bisabolene and heptadecane productivities will not be as high as ethanol unless the carbon partitioning is enhanced by metabolic engineering approaches. This means that low biofuel yields contribute to low energy produced in the system, worsening metrics of sustainability such as NER and GHG emissions when normalized by our functional unit. As the engineering of these bisabolene and heptadecane producing pathways improves, the environmental benefits of their associated biofuels will correspondingly improve.

Another means for improving the environmental and energetic performance of these organisms is through genetic engineering or optical engineering of their response to outdoor lighting conditions. Although incident solar radiation seems as an ideal resource to grow microalgae and cyanobacteria, the photosynthetic active radiation fraction is about 46% of the spectrum and the photon utilization efficiency range from 10% to 30% under high incident light conditions [12]. The light saturation of *Synechocystis* sp. *PCC6803*, for instance, is reported at about 200 μmol photons. $s^{-1}.m^{-2}$ [10], whereas photoautotroph-based biofuel facilities will face incident radiations of about 2000 μmol photons. $s^{-1}.m^{-2}$ at noon in locations such as Colorado [95]. This means that the growth and areal productivities of photoautotrophic microorganisms are photoinhibited in outdoors conditions unlike the idealized conditions that may exist at the lab scale. Whether through genetic engineering or the use of light diffusers, a reduction in photoinhibition of these organisms would result in higher productivity and improved environmental and energetic performance.

2.3.4.2 Replacement of Industrial Fertilizers

Sensitivity analysis has demonstrated that the nutrient sources, sodium nitrate and monopotassium phosphate, for these organisms is causative of a large fraction of the NER and GHG emissions due to the energy consumption embedded in industrial fertilizer production. The integration of cyanobacteria and microalgae based biofuels production systems with wastewater treatment plants has long been proposed as a means to reduce the environmental impact of biofuels production [30, 37, 96]. Lab and pilot scale experiments growing photosynthetic-based biofuel microorganisms in wastewater [97-129], and in sludge centrate [37, 103] have been successfully conducted. By combining photosynthetic biorefineries with wastewater facilities, the combined system could reduce the capital and operation costs required by energy expensive biological nutrient removal processes and could contribute to meet the water quality criteria required to release treated wastewater to the environment [37]. Although the displacement of fertilizers by sludge centrate and treated wastewater will reduce the carbon footprint of PSBR systems, the availability of these resources may limit expected biofuel production in the U.S.

2.3.4.3 Optimized bioprocess technologies will maximize the benefits in PSBR systems

Optimization of bioprocesses, including mixing of cultures and energy conversion technologies, are a third strategy to minimize the energy requirements for the biomass growth and maximize biofuel extraction and energy production. Optimization of sparge mixing, by maximizing microalgae biomass has been researched at air flow rates per volume of reactors ranging from 0.2 m^3 to 1.2 m^3 of air per minute per cubic meter (VVM) [82]. Although previous efforts are reported for cyanobacteria growth in photobioreactors [6, 10, 84], no such research has been reported for co-optimization of biomass and biofuel productivities of *Synechocystis* sp. PCC6803 under outdoor conditions [130].

Optimization of the growth system and optimization of process engineering variables using LCAs such as what has been presented in this study can seek to improve the metrics of sustainability for these biofuel production systems.

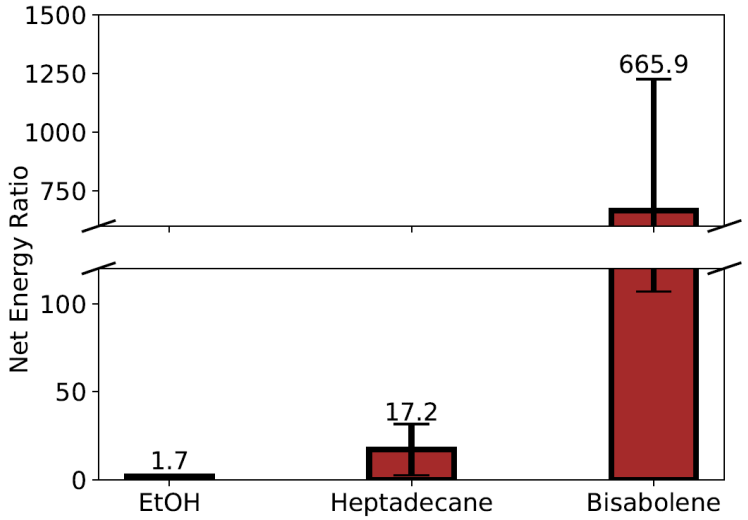

(a)

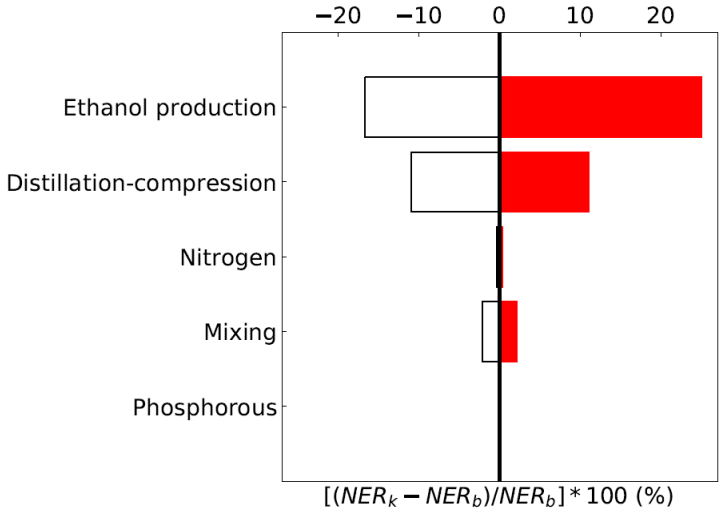

(b)

Figure 2.4 Net Energy Ratios (NER), in terms of Energy Consumed per Energy Produced, of cyanobacteria-based biofuels (a) and sensitivity analysis of the LCA based on ethanol on a percentage basis (b). The error bars represent the uncertainty of the LCA results by varying from low to high input values in the system. NER_k stands for the Net Energy Ratio response of the system due to input variation for each process by +/- 20%. NER_b stands for the Net Energy Ratio baseline input values summarized in Table 2.1.

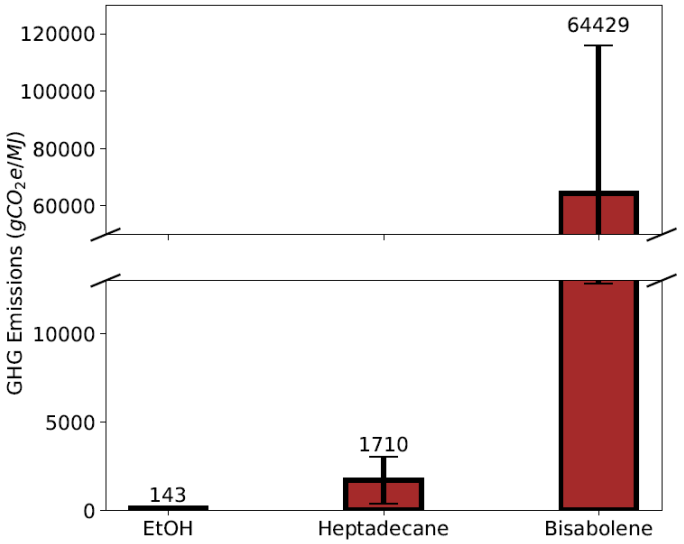

(a)

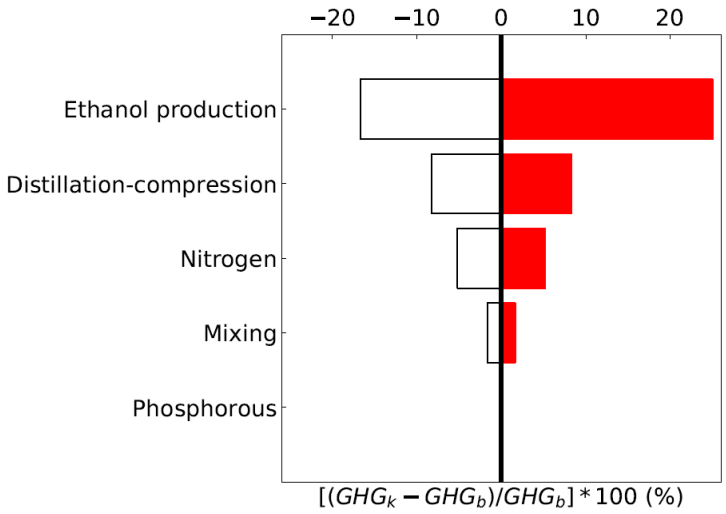

(b)

Figure 2.5 GHG emissions in equivalent carbon dioxide per energy produced of cyanobacteria-based biofuels (a) and sensitivity analysis of the LCA based on ethanol on a percentage basis (b). The error bars represent the uncertainty of the LCA results by varying from low to high input values in the system. GHG_k stands for the Greenhouse Gas emissions response of the system due to input variation for each process by +/- 20%. GHG_b stands for the Greenhouse Gas emissions baseline input values summarized in Table 2.1.

2.4 Conclusions

This study presented the results of an LCA for a set of genetically engineered cyanobacteria-based biofuel production systems. Growth and process engineering parameters from the literature were used to populate a model of the cyanobacteria growth, extraction and conversion stages. Results demonstrate that *Synechocystis* sp. PCC6803 producing bisabolene and heptadecane have higher lifecycle environmental costs than the exemplar cyanobacteria-based ethanol production systems. Sensitivity analysis was used to understand the primary drivers of the environmental costs, and to understand the organism and process engineering pathways that can improve the environmental impacts of these biofuels. Potential means to improve the lifecycle energy consumption and GHG emissions of these biofuels included: increasing biomass productivities by mitigating photoinhibition, increasing biofuel yields by increasing the carbon partitioning into bisabolene and heptadecane, minimizing resource inputs through optimization of mixing and energy conversion processes, and minimizing industrial fertilizer consumption by engineering wastewater tolerance and improve nitrogen uptake in *Synechocystis* sp. PCC6803. This study provided an important baseline of the state of the field for these cyanobacteria-based biofuels. Through further multidisciplinary development of these systems, their cost-effectiveness and sustainability can be improved so as to meet long-term objectives for biofuel productivity and environmental benefits.

2.5 Answer to Research Question 1.1

This section of the research effort has allowed us to address Research Question 1.1, which is restated and answered in section 3.5 of this dissertation.

CHAPTER 3: A Geographical Assessment of Vegetation Carbon Stocks and Greenhouse Gas Emissions on Potential Microalgae-based Biofuel Facilities in The United States[2]

3.1 Introduction

The cultivation of microalgae-based biofuel feedstocks have various advantages compared to conventional biofuels feedstocks including higher solar efficiency, high production rates, and utilization of low quality land [131]. However, the conversion of undeveloped or low-quality land to microalgae cultivation has the potential to be a disadvantage relative to conventional biofuels due to the environmental cost associated with land use change. For conventional biofuels, direct land use changes (DLUC) are a relatively minor component of the biofuels' life cycle greenhouse gas (GHG) emissions because conventional biofuels are often cultivated on preexisting dedicated croplands [132]. For example, the DLUC effects of switching from feed corn cultivation to ethanol corn cultivation are very small. In comparison, microalgae cultivation facilities are typically assumed to require the conversion of marginal agricultural, range, or undisturbed land, for which DLUC must be quantified to understand the impact on the life cycle emissions of the biofuel product.

A variety of research efforts have quantified the productivity potential and life cycle environmental impacts of microalgae biofuels. The results of these assessments are found to be highly sensitive to the siting of the modeled facility. Researchers have subsequently considered geographically-specific inputs to these LCAs including meteorological data, land types and availability, carbon dioxide (CO_2) accessibility, and more. The results of these efforts have been an evaluation of the localized life cycle impacts of microalgae-based biofuel facilities in the U.S.

[2] **This chapter is adapted from a published refereed journal article:** Arita, Carlos Quiroz, Özge Yilmaz, Semin Barlak, Kimberly B. Catton, Jason C. Quinn, and Thomas H. Bradley. "A geographical assessment of vegetation carbon stocks and greenhouse gas emissions on potential microalgae-based biofuel facilities in the United States." Bioresource technology 221 (2016): 270-275.

[7, 22, 27, 28, 78, 91, 93, 133-135]. Sustainability results currently in the literature show algal based systems to have great potential. Combining land and CO_2 availability microalgae has the capability to produce 44 billion gallon per year in the U.S. [136]. The water footprint of microalgae biofuels when optimally sited is comparable to that of other biofuels 80-291 $m^3.GJ^{-1}$ [133, 137-141]. The environmental impact of algal systems as assessed through net energy ratios and net GHG emissions of microalgae of well-developed facilities are favorable relative to petroleum-derived and biofuels ranging between -0.74-0.93 MJ consumed·(MJ produced)$^{-1}$; and between -95.7 to 534 $gCO_2eq.MJ^{-1}$ [18-21, 23, 24, 26, 27, 90-93, 135, 142-146]. None of the cited studies have taken into consideration the DLUC associated with the construction of the biofuel facilities. Canter et al. (2014) investigated the emissions associated with the actual construction of the facility but do not consider emissions associated with the disruption of the soil [147]. Ignoring DLUC in these analyses represents a discrepancy in boundary assumptions between microalgae life cycle assessments (LCAs) and the state of the art for conventional biofuels.

In general, DLUC has been shown to be a significant contributor to world-wide GHG emissions through the transport of CO_2 to the atmosphere from carbon stocks stored in soil and above ground biomass (AGB). Currently approximately 30% of anthropogenic carbon emissions are generated by deforestation and forest degradation [148]. Although DLUC is considered negligible in evaluating the environmental impacts of many 1st generation biofuels, for some particularly land-disruptive applications, DLUC has been demonstrated to have a significant effect on lifecycle emissions. For an example, gasoline and diesel produced from Canadian oil sand crude is estimated to result in 18% to 21% higher GHG emissions than U.S. conventional crudes, with the differences due primarily to DLUC [149]. Recent remote sensing research has

resulted in the development of datasets that can broadly represent the AGB and soil organic carbon (SOC) for not only forested, but also for the shrubland, and scrubland that are expected to be utilized for microalgae-based biofuel production facilities [136, 150]. There is a need to integrate available carbon stock data with microalgae based LCA to have a more holistic understanding of the environmental impact associated with biofuels derived from microalgae.

This study integrates AGB and SOC datasets with microalgae biofuels LCAs into a geographical assessment of the effect of DLUC on the life cycle GHG emissions of microalgae biofuels. The results and quantified sensitivities of this assessment allow insight into the relative importance of DLUC in assessing the sustainability of microalgae based biofuels facilities. Geographically resolved results can be used to quantitatively exclude environmentally-disadvantageous lands from consideration for microalgae biofuels cultivation. These methods and results represent the next level of fidelity in the critical assessment of microalgae biofuels on the metrics of environmental impact and will support long-term investment planning.

3.2 Materials and Methods

To evaluate the life cycle GHG emissions from microalgae-based biofuel facilities, inclusive of DLUC, carbon fluxes from microalgae cultivation and industrial processes must be taken into account [29], along with the carbon associated with disturbed AGB and Soil SOC release due to facility construction activities. The modeling workflow, illustrated in Figure 3.1, integrates the equivalent CO_2 emissions from these disturbances by applying the Intergovernmental Panel on Climate Change (IPCC) method simulated spatially across the U.S. By adding the effects of DLUC to the results of microalgae biofuels LCAs in literature, we can develop a more comprehensive assessment of the net GHG emissions of potential microalgae-based biofuel facilities in the U.S.

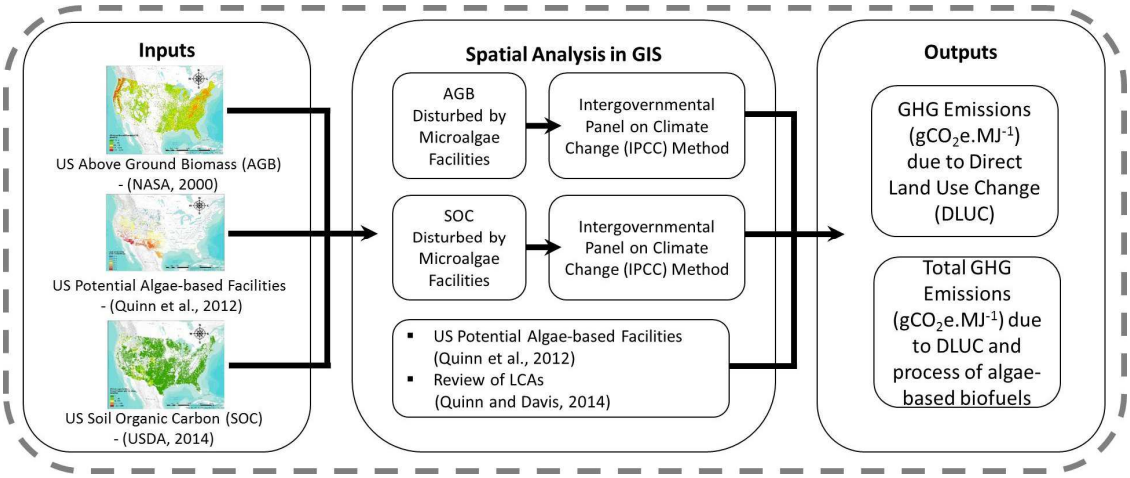

Figure 3.1 System boundaries and analysis flowchart for calculation of GHG emissions ($gCO_2eq.MJ^{-1}$) due to DLUC based on GIS model of microalgae-based biofuel facilities in the U.S.

3.2.1 Spatial Inputs to Life Cycle Assessment and Direct Land Use Change Modeling

The AGB dataset is derived from the Oak Ridge National Laboratory Distributed Active Archive Center (ORNL DAAC) for biogeochemical dynamics, National Aeronautics and Space Administration (NASA) [150]. The AGB, which is comprised of the dried matter of living organisms above ground [151], was utilized to obtain the land cover carbon, which is measured as tonnes of dried matter per hectare. The AGB maps of the U.S. and the potential microalgae-based biofuel facilities areas processed in our research is included in the Appendix B for three scenarios described below.

The potential locations for microalgae-based biofuel facilities and their lipid productivities are derived from previous research on siting of microalgae biofuels facilities as reported in Quinn et al. (2013). Only facilities of more than 400 contiguous hectares are considered. Three scenarios of land use constraints, each with progressively lower restrictions on sitting, for locating microalgae biofuels facilities are considered wherein the facilities are only located on 1) barren land with slope of less than 1%, 2) barren land with slope of less than 2%, and 3) forest or pasture or barren areas with slopes of less than 5% (see Appendix B). The projection used for

this geographical assessment is the North America Albers Equal Area Conic and the datum is the North American 1983.

To take into account the carbon disturbance in the soil due to the potential change in the land use, the total SOC estimated by the U.S. Department of Agriculture (USDA) in the total soil profile at 30 meters resolution has been incorporated in the carbon stocks balance of this assessment. These SOC maps are included in the Appendix B. By utilizing minimum microalgae facilities sizes of 400 Ha, the carbon stocks liberated by facility construction can be well represented using AGB and SOC datasets at resolutions of 240 m and 30 m, respectively.

3.2.2 Spatial Analysis of Direct Land Use Change and Related Emissions

With these inputs, we use geographical information systems (GIS) tools to synthesize the spatial GHG emissions and environmental impacts of microalgae-based biofuels production across the US. This assessment incorporates the methods of the *Good Practice Guidance for Land use, Land-use Change and Forestry* of the Intergovernmental Panel on Climate Change (IPCC, 2014). Map-algebra was applied to calculate the carbon stocks from the attribute values of the AGB and the microalgae-based biofuel facilities:

$$L_{OL} = A_d * B_w * (1 - f_{BL}) * CF + SOC \quad \text{Eq. 1}$$

L_{OL} represents the annual losses of carbon (tonnes of carbon per year); A_d is the vegetation areas affected by disturbance (hectares per year); B_W is the average biomass stock of ground cover areas (tonnes of dried matter per hectare); f_{BL} is the fraction of biomass left to decay in the environment (transferred to dead organic matter); and CF is the carbon fraction of dry matter (tonnes of carbon per ton of dried matter) [152]. The variable f_{BL} was assumed to be zero in this research as would be characteristic of an industrial facility, and CF is assumed to be 50% as recommended by the IPCC. SOC is derived from the USDA database as detailed in section 2.1.

The value of A_d was obtained from the geographical assessment of microalgae biofuel potential included in the Appendix B.

The computed losses of carbon (L_{OL}) are converted to the equivalent CO_2 emissions by the ratio of molecular weights of CO_2 (MW_{CO2}) and carbon (MW_C) [151]. The CO_2eq produced due to land disturbance is amortized over the microalgae facilities' lifetime (T), which is estimated to be 10 years, providing an annual equivalent CO_2 balance for the disturbed areas (tonnes of equivalent CO_2 per year) (IPCC, 2014):

$$CO_2eq = \frac{L_{OL} * \left(\frac{MW_{CO2}}{MW_C} \right) - C_{FFG}}{T} \quad \text{Eq. 2}$$

For comparison to an undisturbed condition, the CO_2 equivalent balance must take into account the annual increase in carbon stocks associated with accumulating AGB:

$$C_{FFG} = T * G_W * (1+R) * CF \quad \text{Eq. 3}$$

Where C_{FFG} is the annual increase in carbon stocks due to biomass increment (tonnes of carbon per year); T is the lifetime in years of the microalgae facilities, assumed to be 10 years in our research; G_W is the average annual AGB increment (tonnes of dried matter per hectare per year), 0.4 for barren areas and 0.8 for forest or pastures areas as derived from the IPCC guidelines; and R is the "root-to-shoot" ratio (ratios of belowground to aboveground biomass), 2.83 was assigned for barren areas and 0.48 for forest-pastures-barren areas as per IPCC guidelines.

3.2.3 Total GHG emissions

The results from the life cycle modeling, AGB and SOC, are combined for a total greenhouse impact quantified through the metric of CO_2eq. The GHG emissions due to DLUC are normalized by the functional unit of energy produced from microalgae-based biofuels. The

energy production as a function of US geography is obtained from previous work pertaining to barren land areas in the U.S. [136].

3.3 Results and Discussion

The results of this research are presented in three forms. First, this study quantifies the carbon that is disturbed through construction of microalgae-based biofuel facilities including both AGB and SOC. Second, by considering life cycle emissions to include both fuel production and DLUC emissions, we find that in many of the locations that are proposed for siting of algae based biofuel facilitates, the environmental benefits of microalgae based feedstock are negated due to liberation of carbon stocks. We present examples at a state level and highlight microalgae cultivation locations that should be excluded from potential production studies due to DLUC emissions. Finally, by considering a variety of LCAs from the literature, we find that the liberation of carbon stocks is not a negligible component of microalgae biofuels LCAs. Inclusion of carbon stocks in LCA reduces the net GHG benefit of microalgae by between 3-85% for the most cited microalgae biofuels LCAs.

3.3.1 AGB and SOC disturbed by microalgae-based biofuel facilities

Using the metrics of AGB and SOC, the modeling results demonstrate that the barren land areas that have been selected in some of the previous microalgae cultivation research by Quinn et al. (2013) are consistent with low values of AGB and SOC. Studies by Venteris et al. (2013) and Wigmosta et al. (2011) that consider forested, or pasture lands as suitable for microalgae production will disturb AGB and SOC at higher rates per unit of land area. Using the methods of this study for the baseline scenarios, 1 tonne per hectare of AGB and SOC corresponds to 0.18 AGB plus 0.37 SOC for a total of 0.55 tonnes of CO_2eq per year, per hectare, equivalent to 5% of the life cycle GHG emissions savings associated with microalgae production over the 10 year

life of the facility. We use these values of 1 tonne per hectare of AGB and SOC as the limits under which DLUC can be considered negligible.

When considering the construction of microalgae cultivation facilities (>400 Ha facility size) on barren lands with slopes of less than 2% as in Quinn et al. (2013), 95.4 % of these facilities are located at sites with less than one tonnes AGB per hectare. The mean AGB across the US under this land use scenario is 4.9 tonnes per hectare, the maximum is 1,500 tonnes per hectare. Considering SOC under the same land use limitations, 78% of the proposed microalgae cultivation land area has less than 1 one tonnes per hectare of SOC. Under this land use scenario, the mean SOC at the proposed microalgae cultivation facilities is 8.6 tonnes per hectare. If forested, pasture, and barren lands are considered available to build potential microalgae-based biofuel facilities, then only 64.1% of this land area has AGB of less than 1 tonne of biomass per hectare, and 88% of these areas have SOC of less than 1 tonne per hectare.

In summary, the majority of the land area available for microalgae cultivation under the land use scenarios proposed in previous research (Barren) has negligible quantities of SOC and AGB. Under the baseline land use limitation scenario (>400 ha facility size, US-wide cultivation on barren lands with slopes of less than 2%), between 5% and 22% of area under microalgae cultivation has greater than negligible GHG emissions due to DLUC. The fraction of the cultivation area with non-negligible DLUC GHG emissions increases under less-restrictive land use limitation scenarios as the SOC and AGB increase (see Appendix B).

3.3.2 Carbon stocks limit the locations available for sustainable microalgae-based biofuel cultivation

By ignoring the contribution of disturbed carbon stocks and DLUC in microalgae-based biofuel LCAs, previous researchers have overestimated microalgae productivity potential that

can be realized with environmental benefits. In this section, we combine the area-specific DLUC-associated GHG emissions with an area-specific lipid productivity model derived from Quinn et al. (2013), to present results in the form of energy-specific GHG emissions (in units of $gCO_2eq\ MJ^{-1}$).

From the results of this geographical assessment, we find that previously selected barren land areas for algae-facilities have DLUC-associated, functional unit-specific, GHG emissions ranging from 3 to 802 $gCO_2eq\ MJ^{-1}$. Figure B.6 presents the distribution of DLUC-associated GHG emissions as a cumulative distribution of land area in the US. More than 99% of the proposed cultivation areas under the baseline land use restriction scenario have DLUC-associated GHG emissions of less than or equal to 100 $gCO_2eq\ MJ^{-1}$. Figure 3.2 presents the functional unit-specific, GHG emissions of the 13 LCA studies that posit net GHG *benefits* for microalgae cultivation as reviewed by Quinn and Davis (2015). The GHG emissions benefits from each study can therefore be compared to the fraction of US microalgae cultivation area (under the baseline land limitation scenario) to determine the fraction of the US microalgae cultivation area where the GHG benefits of microalgae biofuels production including DLUC are less than zero. For example, consider the LCA results documented in Frank et al. (2013), wherein microalgae cultivation and fuels production was found to have a net GHG emissions benefit of 20 $gCO_2eq\ MJ^{-1}$, without consideration of DLUC. Moving vertically along the 20 $gCO_2eq\ MJ^{-1}$ line to the intercept with the cumulative distribution function, we can find that on 83% of the proposed microalgae cultivation area, DLUC GHG emissions are less than the GHG emissions benefits of microalgae biofuels production. Consequently, on 17% of the proposed microalgae cultivation area, the GHG emissions benefits of microalgae biofuels production are completely negated by DLUC.

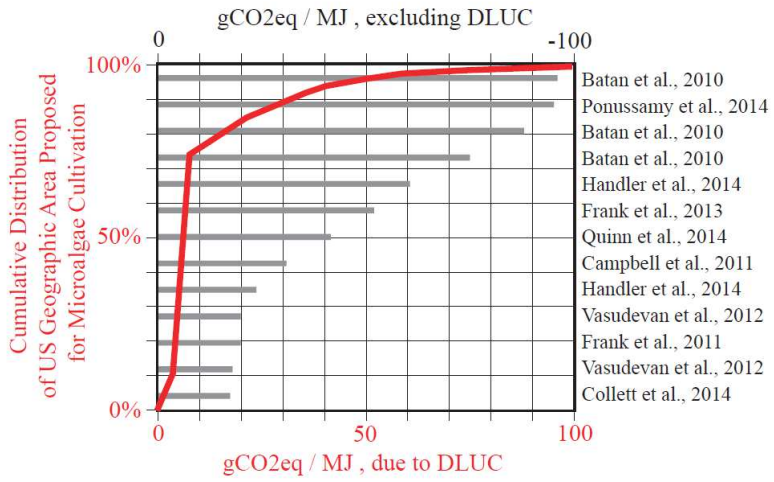

Figure 3.2 Cumulative distribution of potential US microalgae-based biofuels facilities' DLUC-inclusive GHG emissions ($gCO_2eq.MJ^{-1}$) and well-to-pump (excluding DLUC) GHG emissions benefits associated with microalgae biofuels production as represented in literature. The modeled algal biofuel scenario is based on a land restriction of barren and slop of <2%.

Using the methods of this study, we can make similar evaluations on a state-by-state level with the understanding that microalgae facility siting will perhaps be localized to states with particularly amenable climate and geography. For each case considered here, we restrict microalgae production facilities to be sited on >400 Ha sites, on barren land with slope of less than 2%. Figure B.7 presents the DLUC-associated GHG emissions from microalgae production in Arizona, where the median GHG emissions due to DLUC is 9 $gCO_2eq\ MJ^{-1}$, and Figure B.8 shows that Florida has a median DLUC-associated GHG emissions of 17 $gCO_2eq\ MJ^{-1}$. The distribution of GHG emissions for these states compared to literature are presented in Figure 3.3.

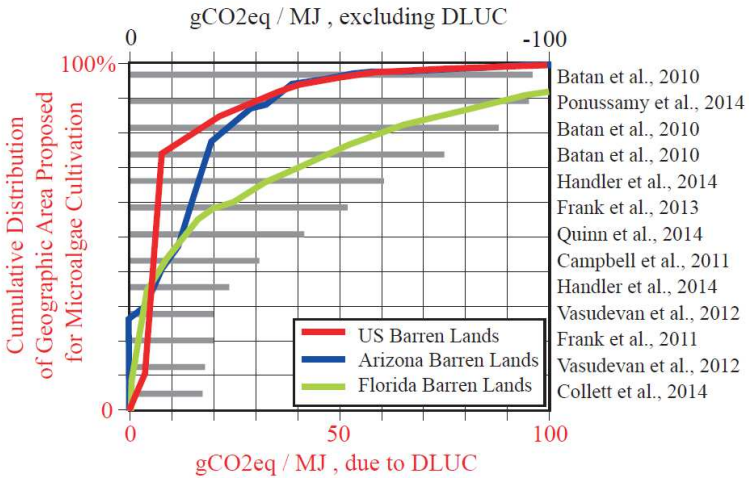

Figure 3.3 The functional unit-specific, well-to-pump GHG emissions (excluding DLUC) of the 13 LCA studies that suggest net GHG benefits for microalgae cultivation can be compared to the cumulative distribution of GHG emissions due to DLUC for the U.S, and the states of Arizona and Florida.

These results can be used to assess the tradeoff between microalgae productivity potential and DLUC-inclusive GHG emissions. Many studies of microalgae productivity potential have selected locations for production facilities where the disturbance of AGB and SOC can negate the GHG benefit from algae biofuels production (Davis et al., 2014; Venteris et al., 2013; Wigmosta et al., 2011). For example, although Venteris et al. (2013) highlighted the state of Florida as an ideal place for microalgae-based biofuel technology their models neglected the impacts of DLUC on land availability. This lead to their recommendation to allow microalgae cultivation on forested and rangelands, which would have even higher DLUC environmental impacts than presented here (see the supplemental material for other land restriction scenarios). By neglecting DLUC, previous microalgae productivity potential studies have overestimated the amount of microalgae that can be produced while maintaining a net GHG benefit.

3.3.3 Including DLUC reduces GHG benefit of microalgae biofuel

By neglecting the contribution of disturbed carbon stocks to microalgae-based biofuel life cycle GHGs, previous research has also underestimated the life cycle GHG emissions of microalgae-based biofuels that can be achieved at scale. In order to understand the effect of DLUC on the net GHGs of microalgae biofuels, we can compare the distribution of DLUC-specific GHG emissions to the GHG emissions of the microalgae biofuels production process in the context of the US Renewable Fuel Standards policy.

The US Renewable Fuel Standard requires that Advanced Biofuels achieve a 50% life cycle GHG emissions reduction relative to the life cycle GHG emissions of conventional diesel (50% of 92 $gCO_2eq\ MJ^{-1}$ equals 46 $gCO_2eq\ MJ^{-1}$) (EPA., 2016). To allow a direct comparison to the well-to-pump results that are presented in the microalgae biofuels literature, we can subtract the pump-to-wheels GHG emissions associated with biodiesel of 73.6 $gCO_2eq.MJ^{-1}$. This calculation suggests that any microalgae biofuels facility that is sited such that its DLUC-inclusive well-to-pump GHG emissions are greater than -27.6 $gCO_2eq.MJ^{-1}$, will be ineligible for Low Carbon Fuel Standard credits and its corresponding economic benefits. This comparison is presented in Figure 3.4. In this case, all of the LCAs from literature that do not meet the RFS Advanced Biofuels criteria (without DLCU) are removed from consideration. Again, we can compare the scale of the GHG emissions savings from microalgae biofuels production to the GHG emissions produced due to DLUC. For example, were Florida's barren land to be developed without consideration of its carbon stocks (leading to a statistically average DLUC contribution of 17 $gCO_2eq.MJ^{-1}$), then the net DLUC-inclusive GHG emissions of the studies of Quinn et al. (2014) and Campbell et al. (2011) would both not be able to meet the requirements

of the US Renewable Fuel Standard Advanced Biofuels as their net GHG emissions benefits are less than 27.6 $gCO_2eq.MJ^{-1}$ + 17 $gCO_2eq.MJ^{-1}$= 44.6 $gCO_2eq.MJ^{-1}$.

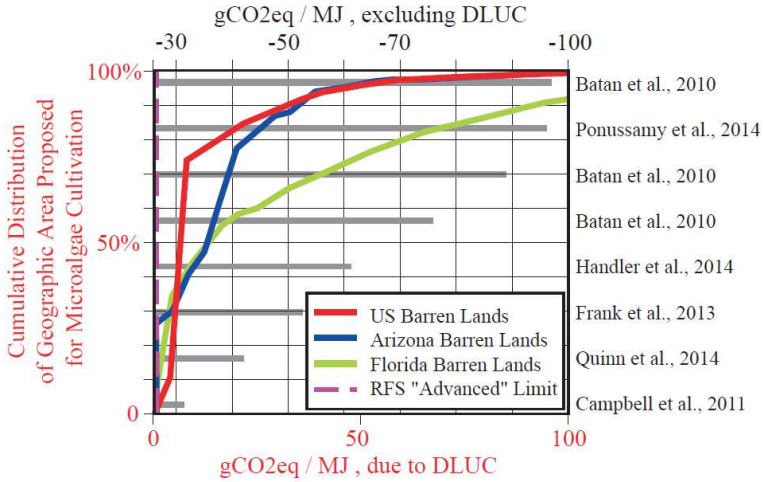

Figure 3.4 The functional unit-specific, well-to-pump GHG emissions (excluding DLUC) of the 8 LCA studies with net GHG benefits that meet the RFS Advanced Biofuels Criteria (without DLUC) for microalgae cultivation can be compared to the cumulative distribution of GHG emissions due to DLUC for the U.S, and the states of Arizona and Florida. The limit of -27.6 $gCO_2eq.MJ^{-1}$ represents the well-to-pump equivalent limit that allows microalgae based biofuels to receive Low Carbon Fuel Standard credits.

3.4 Conclusions

The GHG emissions from DLUC have been demonstrated to be a significant determinant of microalgae biofuels GHG emissions and the selection of geographical locations for the sustainable production of microalgae-based biofuels. DLUC should be considered in future microalgae-based biofuels LCA and scalability assessments.

3.5 Answer to Research Question 1.1

This section of the research effort has allowed us to address Research Question 1.1, which is restated here:

What are the baseline life cycle characteristics of a cyanobacteria-based bio-product/bio-fuel technology, in terms of sustainability goals?

Research Question 1 is associated with Hypothesis 1.1:

Cyanobacterial derived biofuels, being an emerging technology, requires further research to reduce the uncertainties in biomass productivities, mixing energy requirements, and energy conversion. DLUC due to construction of photosynthetic-derived biofuel plants in barren land areas of the U.S. plays a major role in the sustainability of this technology.

Chapter 2 and Chapter 3 have developed an LCA framework, applying the methods of ISO 14040. Key sensitivity parameters and technology gaps were identified in Chapter 2, including improved datasets and engineering of cyanobacteria, scalability and process integration, and energy and resource requirements. Cyanobacteria-derived ethanol was demonstrated to be more sustainable in terms of life cycle net energy and GHG emissions relative to other biofuels, such as bisabolane and heptadecane. Chapter 3 demonstrated that including DLUC in the LCA of photoautotrophic based biofuel facilities limits the locations available for sustainable microalgae-based biofuel cultivation. DLUC, as a result, reduces the net GHG emissions' benefit from microalgae biofuel manufacturing. The results of these studies provide support to the hypothesis that results are sensitive to uncertainties in growth and energy conversion stages, and that the details of characteristics such as DLUC can have large influence over the metrics of sustainability.

CHAPTER 4: Scalability of Combining Microalgae-based Biofuels with Wastewater Facilities: A Review[3]

4.1 Introduction

Wastewater treatment and microalgae have been linked to each other since ancient times. This connection has been extensively researched in wastewater stabilization ponds, which have been used for more than 3000 years in the world and employed in the United States since the year 1901 [103]. It is stated that in wastewater-systems, microalgae growth is governed by photosynthesis, where carbon dioxide is converted to organic compounds as the source of chemical energy. Moreover, oxygen required by aerobic bacteria, which oxidizes the organic matter, in these stabilization ponds is obtained as a by-product to contribute to the mutualism in the system (Figure 4.1). Additionally, nitrogen from wastewater is removed due to the assimilation of ammonium in algal biomass or microalgae uptakes nitrogen in the form of nitrate. As a result, regardless of the nature of the growth media, wastewater or synthetic nutrients, microalgae biomass can be estimated by taking into consideration photosynthesis energy respiration energy, and nitrogen uptake energy, as suggested by Quinn et al [153] and others.

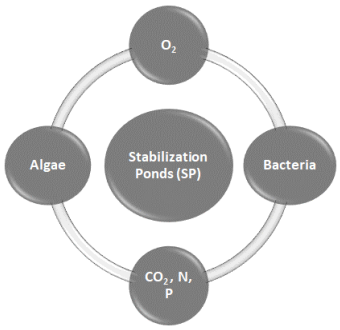

Figure 4.1 Microalgae and aerobic bacteria mutualism in wastewater stabilization ponds.

[3] **This chapter is adapted from a published refereed journal article:** Arita, Carlos E. Quiroz, Christie Peebles, and Thomas H. Bradley. "Scalability of combining microalgae-based biofuels with wastewater facilities: a review." Algal Research 9 (2015): 160-169.

Nowadays, there is an increasing interest with regards to the feasibility of growing microalgae-based biofuels by taking wastewater as the growth media and the main source of nutrients. Research has been conducted in primary and secondary treated municipal wastewater, mainly in activated sludge plants, as well as in municipal centrate, which is obtained from the sludge centrifuge [114]. Also, raw or untreated wastewater has been researched as the growth media for microalgae [106]. However, municipal centrate has been reported as the growth media with the most promising productivities in microalgae. Furthermore, microalgae strains able to grow in wastewater have been identified, from which the highest net biomass accumulation was observed in the genus of *Chlorella* when centrate was used as the growth media [108]. This genus, *Chlorella*, was reported with the highest lipid productivity in other research that used centrate as the growth media, as well (Table 4.1) [128].

Nevertheless, in the same manner that the latest technologies regarding microalgae cultivation systems have been scaled up from laboratory data [82], microalgae-based biofuels grown on wastewater may suffer the same destiny. This is because research has been barely conducted at a pilot or real scale plant in wastewater facilities. To evaluate the scalability of growing microalgae-based biofuels in wastewater, further considerations are taken into account in this research. The latest initiatives of the Environmental Protection Agency (EPA) with regards to the new regulations for nitrogen and phosphorous discharge from wastewater facilities represent an important variable in this analysis. For instance, the State of Colorado has established that existing wastewater dischargers should meet an annual median concentration of 1.0 $mg.l^{-1}$ and 15 $mg.l^{-1}$ for phosphorous and nitrogen, respectively, whereas new dischargers should accomplish concentrations of 0.7 $mg.l^{-1}$ and 7 $mg.l^{-1}$, respectively [96]. In the United States, the cost of upgrading wastewater facilities to meet nitrogen and phosphorous regulations

have ranged from about 1.5 to 138 million dollars, whereas new plants have invested from about 0.3 to 1.4 million dollars [30]. As a result, the scalability of cultivating microalgae will be assessed in depth by considering the wastewater treatment process as a whole; the presence of biological nutrient removal (BNR) operations in the process; the wastewater characteristics and flow rates at the different stages of the process; and the potential contaminants that come into the facility and that could inhibit the growth of microalgae. Last, the most suitable experimental and computational methods used to predict the growth of microalgae will be evaluated.

4.2 Microalgae-based biofuels grown in wastewater

4.2.1 Microalgae genera and strains able to grow in wastewater

Microalgae genera and their strains' ability to grow in wastewater, their growth media and the source of nutrients, has been broadly researched. In research conducted in the 70's, blue-green algae, diatoms, flagellate algae, and green algae were identified as the four groups of microalgae genera found in wastewater stabilization ponds [154]. The research claimed that 50% of the algae were green algae, 25% pigmented flagellates, 15% blue-green algae, and 10% diatoms. *Chlorella*, which is a green algae, was found to be more abundant in the Southeastern region in the United States, as well as some ponds in Africa where this algae started to disappear in the third stage by the bloom of *Spirulina*. In another case, *Scenedesmus* was the most abundant algae at Lancaster, California. Additionally, at one stabilization pond in California, *Chlamydomonas* grew at pH between 7.0 – 7.7, while *Euglena* grew when the pH ranged from 7.7 – 8.9, and *Chlorella* and *Scenedesmus* dominated in growth when the pH ranged from 8.4 – 9.8 during mid-day.

Therefore, interest concerning the feasibility of growing microalgae-based biofuels on municipal wastewater has led researchers to investigate the potential genera and strains for the

production of biofuels. Researchers claimed that microalgae genera such as *Chlorella* and *Scenedesmus* are tolerant to municipal wastewater, which removed more than 80% of ammonia, nitrate, and total phosphorous [114]. *Scenedesmus obliquus* and *Botryococcus brauniiit* were grown on secondary treated municipal wastewater for biofuels production purposes [114]; additionally, *Chlamydomonas reinhardtii* was grown in municipal centrate [107]. Moreover, in research where municipal centrate was used as the growth media, 14 algae strains from the genera of *Chlorella, Haematococcus, Scenedesmus, Chlamydomonas, and Chloroccum* were able to grow in the centrate [108]. In this investigation, the highest net biomass accumulation measured as total volatile suspended solids (TVSS) was observed with *Chlorella kessleri* followed by *Chlorella protothecoides* with values of 20143 g TVSS.l^{-1} and 1.3089 g TVSS.l^{-1}, respectively.

4.2.2 Limiting nutrients' growth-rate in wastewater for microalgae

Carbon dioxide (used as the carbon source) and light energy are harvested by microalgae cells in an autotrophic metabolism [155]. This research stated that microalgae assimilate nitrogen in different forms such as ammonium, nitrate, and urea. The nitrogen's minimum cell quota is recommended to be 0.010 gram per gram of biomass [153]. Research conducted to grow microalgae in wastewater has taken into consideration the measurement of the growth-rate limiting nutrients, such as nitrogen and phosphorous, in this media. *Desmodesmus sp*., microalgae mixed with cyanobacteria, and microalgae mixed with *Desmodesmus sp*. were cultivated in raw wastewater with concentrations of nitrogen and phosphorous at 42.3 and 35.4 mg.l^{-1}, respectively [106]. A mixture of municipal and dairy wastewater was used as the growth media for green algae in a high-rate algae pond with concentration of nitrogen and phosphorous at 51 and 2.1 mg.l^{-1}, respectively [126]. *Chlorella sp.* was cultivated in municipal raw

wastewater, primary treated wastewater, secondary treated wastewater, and centrate with nitrogen and phosphorous concentrations at 40.65 and 5.66 $mg.l^{-1}$; 38.95 and 6.86 $mg.l^{-1}$; 19.1 and 0.32 $mg.l^{-1}$; and 131.5 and 201.5 $mg.l^{-1}$, respectively [124]. Treated wastewater was used as the growth media for *Scenedesmus sp.* with concentrations of nitrogen and phosphorous at 28.85 and 3.51 $mg.l^{-1}$ [111]. *Nannochloropsis sp.* was cultivated in municipal wastewater, with concentrations of nitrogen and phosphorous at 110.2 and 5.3 $mg.l^{-1}$, which was mixed to sea water in a 1:1 ratio [105]. Lastly, different strains of microalgae such as *Hindakia sp., Chlorella sorokiniana, Auxenochlorella protothecoides,* and *Scenedesmus sp*. were grown in municipal centrate with nitrogen and phosphorous concentrations at 134 and 212 $mg.l^{-1}$ [128]. As summarized in the above values and Table 4.1, it can be observed that not only the highest nitrogen and phosphorous concentrations are reported for sludge centrate overall in the wastewater treatment process, but also the concentrations of these limiting nutrients in the centrate provided the best conditions to accomplish the highest microalgae biomass concentrations.

4.2.3 Microalgae growth and lipid productivity in wastewater

The production of lipids in microalgae cells is governed by growth temperature, pH, age of culture, microalgae strain, and nutrients such as carbon, nitrogen, and phosphorous [155]. Moreover, when the nitrogen source is depleted, the metabolism of microalgae switches from protein to lipid synthesis, which increases the lipid productivity [153].

Desmodesmus sp., microalgae mixed with cyanobacteria, and microalgae mixed with *Desmodesmus sp*. obtained biomass and lipid productivities at 13 and 1.7 $mg.l^{-1}d^{-1}$; 17 and 3.4 $mg.l^{-1}d^{-1}$; and 17 and 2.4 $mg.l^{-1}d^{-1}$, respectively, with raw municipal wastewater as the growth media [106]. Biomass and lipid productivities at 267 and 15.19 $mg.l^{-1}d^{-1}$ were obtained in

Scenedesmus sp., with treated wastewater as the growth media [111]. Furthermore, *Hindakia sp., Chlorella sorokiniana, Auxenochlorella protothecoides,* and *Scenedesmus sp*. cultivated in municipal centrate obtained biomass and lipid productivities at 275 and 77.8 $mg.l^{-1}d^{-1}$; 183.3 and 94.8 $mg.l^{-1}d^{-1}$; 268.8 and 77.7 $mg.l^{-1}d^{-1}$; and 247.5 and 74.5 $mg.l^{-1}d^{-1}$, respectively [128]. Additionally, by implementing a two-stage cultivation process, using wastewater as the growth media, the maximum biomass concentration and lipid content in microalgae was increased to 28.90% and 33.22%, respectively [129]. Among the lipid productivities observed in microalgae grown in centrate, secondary-treated wastewater, and raw wastewater, the most promising results have been obtained when the centrate was used as the source of nutrients (Table 4.1). Here it can be observed that as the maximum concentration of limiting nutrients found in sludge centrate are utilized, the highest concentration of lipids were built up in microalgae cells once nitrogen and phosphorous were depleted.

Table 4.1 Microalgae Growth and Lipid Productivity in Wastewater

Substrate	Reactor	Algae genera / species	Total Nitrogen ($mg.l^{-1}$)	Phosphorous ($mg.l^{-1}$)	Biomass productivity ($mg.l^{-1}.day^{-1}$)	Lipid productivity ($mg.l^{-1}.day^{-1}$)	Reference
Centrate	Erlenmeyer flasks and biocoil photobioreactor	*Chlamydomonas reinhardtii*	128.6	120.6	2000	505	[107]
Dairy & municipal wastewater	High rate algae pond (Batch pilot)	Green algae	51	2.1	NA	17	[126]
Dairy & municipal wastewater	High rate algae pond (semi continuous pilot)	Green algae	51	2.1	NA	24	[126]
Municipal wastewater before primary settling	NA	*Chlorella sp.*	40.65	5.66	NA	NA	[124]
Municipal wastewater after primary settling	NA	*Chlorella sp.*	38.95	6.86	NA	NA	[124]
Municipal wastewater after activated sludge tank	NA	*Chlorella sp.*	19.1	0.32	NA	NA	[124]
Municipal wastewater after sludge centrifuge: Centrate	NA	*Chlorella sp.*	131.5	201.5	NA	NA	[124]
Sea water (50%) & municipal wastewater (50%)	NA	*Nannochloropsis sp.*	110.2	5.3	NA	109	[105]
Concentrated municipal wastewater (centrate)	Laboratory	*Hindakia sp.*	134	212	275	77.8	[128]
Concentrated municipal wastewater (centrate)	Laboratory	*Chlorella sorokiniana*	134	212	183.3	94.8	[128]
Concentrated municipal wastewater (centrate)	Laboratory	*Auxenochlorella protothecoides*	134	212	268.8	77.7	[128]
Concentrated municipal wastewater (centrate)	Laboratory	*Scenedesmus sp.*	134	212	247.5	74.5	[128]
Secondary treated wastewater	Laboratory	*Chlorella sp.*	19.1	1.2	NA	NA	[99]
Treated municipal wastewater	Laboratory	*Scenedesmus sp.*	28.85	3.51	267	15.19	[111]
Municipal wastewater	Laboratory	*Desmodesmus sp.*	42.3	35.4	13	1.7	[106]

Substrate	Reactor	Algae genera / species	Total Nitrogen ($mg.l^{-1}$)	Phosphorous ($mg.l^{-1}$)	Biomass productivity ($mg.l^{-1}.day^{-1}$)	Lipid productivity ($mg.l^{-1}.day^{-1}$)	Reference
Municipal wastewater	Laboratory	*Microalgae – cyanobacteria*	42.3	35.4	17	3.4	[106]
Municipal wastewater	Laboratory	*Microalgae – Desmodesmus*	42.3	35.4	17	2.4	[106]

4.3 The role of municipal wastewater treatment facilities in microalgae growth

4.3.1 Overview of the treatment process

Biofuels' production from microalgae, which fixes carbon dioxide and uptakes nitrogen and phosphorous through the bio-treatment of wastewaters, constitutes a potential application in the short term [14]. The oxidation of organic matter and the removal of soluble nutrients from primary or secondary-treated municipal wastewater could be carried on in High Rate Algal Ponds (HRAP) [101]. In this research, organic loading rates to design HRAPs were suggested at 100–150 kg of BOD_5 (Biochemical Oxygen Demand).$ha^{-1}.d^{-1}$., 24 kg N (Nitrogen).$ha^{-1}.d^{-1}$, and 3 kg P (Phosphorous).$ha^{-1}.d^{-1}$. Productivities in HRAPs, as well as the selection of suitable microalgae strains for this application, have yet to be researched [101]. Furthermore, it has been claimed that HRAPs are the most cost-effective alternative for microalgae-based biofuels with wastewater; however, carbon dioxide addition, species control, control of grazers and parasites, biofloculation, and scalability have not been researched in depth [113].

Municipal wastewaters obtained at different stages of the wastewater treatment process of facilities have been broadly researched at a lab scale. Thus, the scalability of combining microalgae-based biofuels with wastewater requires taking into consideration the wastewater treatment process in municipal facilities to assess the best approaches to achieve success for this emerging technology. Due to the new regulations of the EPA with regards to the discharge of nitrogen and phosphorous by wastewater facilities, a typical complete-mixed activated sludge (CMAS) plant is reviewed in this research. Essentially, the CMAS process comprises the aeration tank, settling tank, solids recycle line, and the sludge wasting line (Figure 4.2).

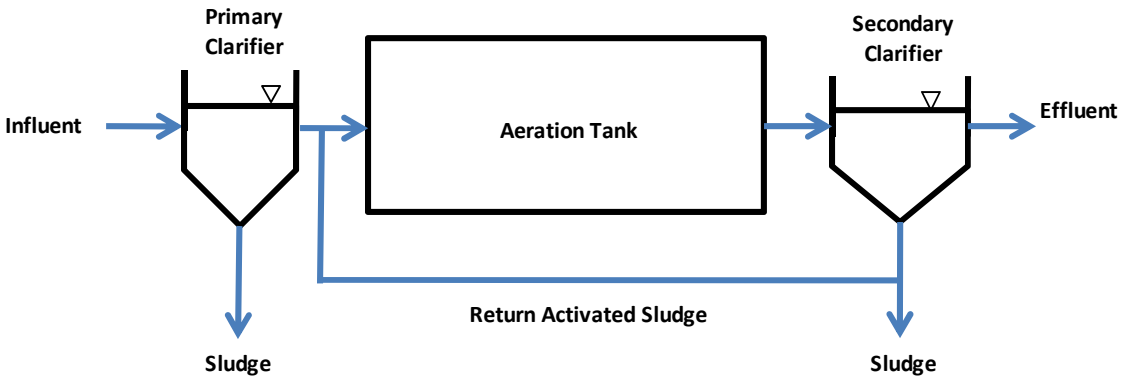

Figure 4.2 Typical complete-mix activated sludge process. Adapted from [120].

The electron donor in the wastewater, which is the organic matter measured in terms of biochemical oxygen demand (BOD), is oxidized in the aeration tank by the recycled activated sludge, which are aerobic microorganisms [156]. The author states that the oxygen required as an electron acceptor in this activated sludge process is obtained by aeration or mechanical devices. Moreover, by maintaining an extended aeration in the basin, nitrification can be achieved by the activated sludge process, which is the microbial oxidation of ammonium (NH_4^+ - N) to nitrite (NO_2^- - N) and nitrate (NO_3^- - N) [156]:

$$NH_4^+ + 1.815O_2 + 0.1304CO_2 = 0.0261C_5H_7O_2N + 0.973\ NO_3^- + 0.921H_2O + 1.973H^+ \quad \text{Eq. 1}$$

4.3.2 Biological nutrient removal (BNR) process

Facilities have been upgrading their BNR process to meet the new EPA regulations with regards to nitrogen and phosphorous discharges [30]. To accomplish these regulations further processes are taken into consideration such as denitrification and enhanced biological phosphorous removal. Denitrification is known as the reduction of NO_3^- or NO_2^- to nitrogen gas (N_2), where the NO_3^- or NO_2^- is the electron acceptor and a carbon source or the BOD in the wastewater is the electron donor [156]. On the other hand, the enhanced biological phosphorous removal is achieved in an anaerobic phase by the sequestration of phosphorous as intracellular

polyphosphate (poly P) by the biomass or sludge [156]. There are several processes for BNR, yet two of the most effective processes for both, nitrogen and phosphorous removal, are known as the Modified Bardenpho (5-stage) and the University of Cape Town (South Africa) treatment process (Table 4.2).

Table 4.2 Treatment performance and comparison of various BNR configurations [30]

Treatment Plant (State)	Treatment Process Description	Nutrient Removal Capabilities		Flow (mgd)	Average Effluent Concentration (mgl^{-1})	
		Nitrogen	Phosphorous		TN	TP
Frederick (MD)	A2/O	Good	Good	7	7.2	1
Largo (FL)	A2/O	Excellent	None	15	2.3	ND
Annapolis (MD)	Bardenpho (4-Stage)			13	7.1	0.66
Palmetto (FL)	Bardenpho (4-stage)			1.4	3.2	0.82
Medford Lakes (NJ)	Bardenpho (5-stage)			0.37	2.6	0.09
Cape Coral (FL)	Modified Bardenpho			8.5	1	0.2
Back River (MD)	MLE	Excellent	Good	180	7.6	0.19
Cambridge (MD)	MLE			8.1	3.2	0.34
Cox Creek (MD)	MLE	Good	None	15	9.7	0.89

Treatment Plant (State)	Treatment Process Description	Nutrient Removal Capabilities		Flow (mgd)	Average Effluent Concentration (mgl^{-1})	
		Nitrogen	Phosphorous		TN	TP
Freedom District (MD)	MLE			3.5	7.8	0.51
Seneca (MD)	MLE			20	6.4	0.08
Westminster (MD)	MLE-A2/O	NA	NA	5	5.3	0.79
Sod Run (MD)	Modified A2/O	NA	NA	20	9.2	0.86
Bowie (MD)	Oxidation Ditch	Excellent	Good	3.3	6.6	0.2
Cumberland (MD)	Step Feed	Moderate	None	15	7	1
Piscataway (MD)	Step Feed			30	2.7	0.09
NA	Modified UCT	Good	Excellent	NA	NA	NA

The modified Bardenpho process (Figure 4.3) consists in a first anaerobic stage for phosphorous removal, a second anoxic stage for additional denitrification of nitrate obtained from the aerobic tank, a third aerobic stage for carbon removal and nitrification, a fourth anoxic stage for denitrification, and a final aerobic stage used for the stripping of nitrogen gas [120]. In

the UCT treatment process (Figure 4.4) the activated sludge is recycled to the anoxic stage to eliminate the introduction of nitrate in the anaerobic zone; thus, it prevents the denitrification in the anaerobic tank and improves the uptake of phosphorous in such stage [120].

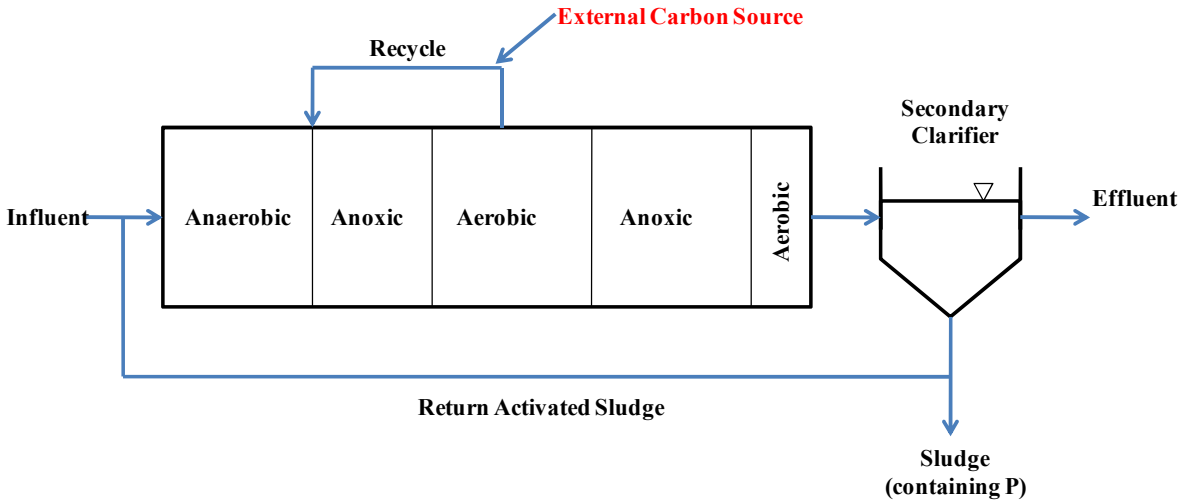

Figure 4.3 Biological nutrient removal process (BNR). Modified Bardenpho (5-stage) process Adapted from [120].

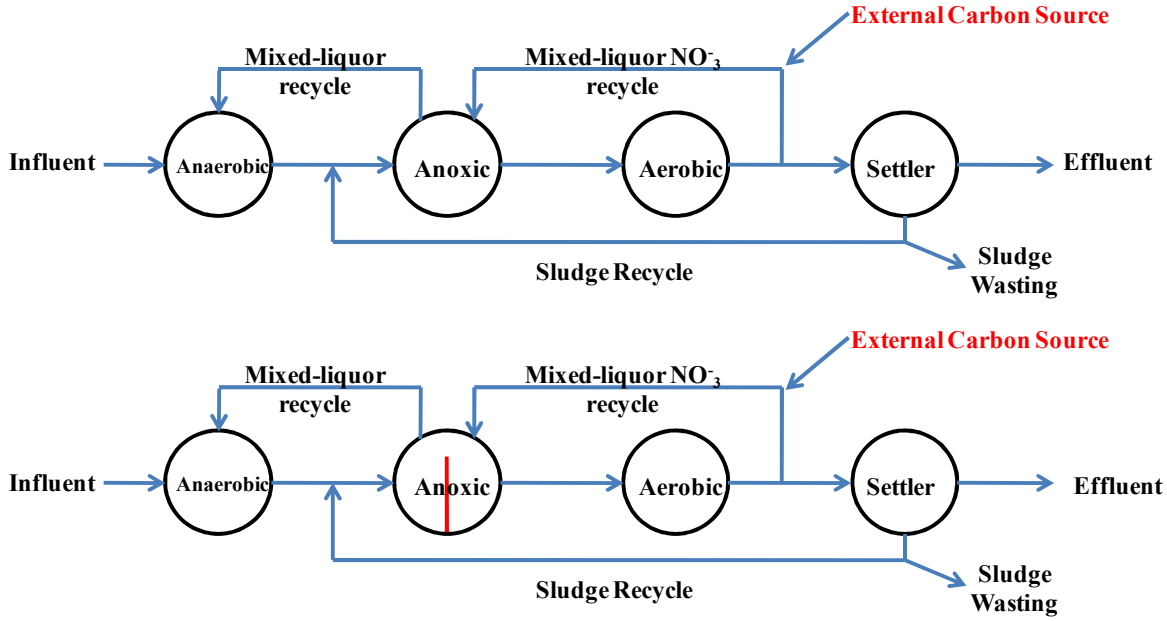

Figure 4.4 Biological nutrient removal process (BNR). University of Cape Town (UCT) Process Adapted from [156].

4.3.3 Sludge dewatering and centrate production

Dewatering is a physical operation applied to reduce the moisture of sludge to reduce the cost of trucking, ease the handling of sludge by machinery, reduce the energy required during incineration, prevent bulking in composting, reduce odors, or meet landfill requirements [120]. The most widely used techniques for dewatering stated by the author includes centrifuges, belt-filter presses, recessed-plate filter presses, drying beds, and lagoons. In the centrifuge, the sludge is fed at a constant flow rate in the rotating bowl, where the dense cake containing high concentration solids and a diluted fluid known as centrate are separated [120]. Due to the assimilation of nutrients, such as nitrogen and phosphorous in the biomass or the activated sludge, the highest concentrations of such nutrients are observed in the centrate produced by centrifugation (Table 4.1).

4.3.4 The impact of the wastewater discharge permits and their relationship with microalgae-based biofuels

Upgrading of municipal wastewater treatment facilities has led to millions of dollars in investments required to meet the new regulations with regards to nitrogen and phosphorous discharge. In a study of the EPA concerning the BNR processes and costs, the total capital costs are reported by upgraded facilities in the states of Maryland and Connecticut. Additionally, total capital costs invested by new and retrofitted small plants are also reported. For the state of Maryland, Patuxent facility built an oxidation ditch designed for 6 mgd (Mega gallons per day) for more than 2 million dollars, whereas Back River facility invested more than 138 million dollars to build a Modified Ludzack-Ettinger (MLE) Process designed at 180 mgd [30]. In the state of Connecticut, Greenwich facility incurred in more than 0.7 million dollars in MLE Process designed to treat 12 mgd, while Waterbury facility invested more than 22 million dollars

in a 4-stage Bardenpho process designed at 25 mgd [30]. Bigger facilities in terms of flow rates depicted the lower unit-capital costs (cost/mgd) for BNR removals upgrading (Table 4.3). This report developed by the EPA is the only recent cost-oriented BNR research that we are aware of, thus, we could not compare other upgrading cases of wastewater facilities located in other geographical areas.

Table 4.3 Average Unit Capital Costs for BNR Upgrades at the States of Maryland and Connecticut ($) [30]

Flow (mgd)	Cost/mgd
>0.1 - 1.0	$6,972,000
>1.0 – 10.0	$1,742,000
>10.0	$588,000

4.3.5 Potential contaminants that could inhibit the growth of microalgae

Microalgae inhibition due to inherent chemical compounds and/or constituents in wastewater, which potentially would serve as the growth media, has not been sufficiently researched. With regards to inhibition of microalgae by surfactants such as linear-alkyl-sulfonate (LAS) [120], which may be present in the wastewater, it was reported that the effect levels for microalgae ranged from 10.003 to 17.784 $mg.l^{-1}$ [157]. This research was primarily focused on the concentrations that inhibit 50% of microalgae growth relative to the control population. Inhibition of photosynthesis affected by heavy metals was researched from laboratory experiments [158]. This research established that microalgae has been demonstrated to be inhibited by Cd, Zn, Hg and Cu. For instance, the content of chlorophyll in *Chlorella sp*. was decreased by Zn and Hg, whereas the chlorophyll biosynthesis in *Euglena gracilis* was interfered by Zn, Cd or Hg. This report found disorganization of the chloroplast ultra structure in the

presence of Cd and Pb in higher plants and in the presence of several heavy metals in algae [158]. Additionally, NAD Poxidoreductase at the reducing side of PS1 in microalgae was observed to be sensitive to Hg, Zn and Cd. In general, it is claimed that heavy metals inhibit photosynthesis at physiological levels such as stomata, pigments, chloroplast structure and function, and enzymes [158]. Additionally, *Chlamydomonas reinhardtii* was reported to be inhibited at concentrations greater than 150 μM of Cd^{2+}, Cu^{2+}, Zn^{2+}, Fe^{2+}, and Co^{2+}, which was reflected in the reduction of nitrate uptake by 75% [159]. Nevertheless, the effect of cadmium at different PO_4^{-3} levels was researched in *Chlorella vulgaris* [160]. It was observed that the simultaneous increasing of Cd and decreasing of PO_4^{-3} contributed to reach a higher-degree saturated fatty acids in microalgae, concluding that this nutrient limitation and metal stress affect the lipid metabolism in a positive way [160].

4.4 Computational methods to predict the growth of microalgae in wastewater

4.4.1 Overview

Experimental and computational methods to predict the growth and productivity in microalgae-based biofuels, where wastewater is targeted as the growth media, will be critical towards the scalability of these systems for engineering and industrial purposes. Therefore, the selection of the most accurate methods are covered in this section, which are intended to be applied in further computations by considering real data from wastewater treatment facilities. The models covered in this section will take into consideration the growth kinetics limited by both light intensity and nutrients uptake, and the bioreactors mathematical models applied to the most widely used technologies such as open ponds and closed photobioreactors [14]. Moreover, the application of computational fluid dynamics (CFD) as a transcendental tool towards the scalability of microalgae bioreactors will be introduced in this section. Lastly, the most common

experimental methods used to validate the mathematical and computational models will be summarized.

4.4.2 Growth kinetics of microalgae

One of the most transcendental works in terms of growth kinetics was accomplished between 1932 and 1942, when Monod developed a simplified hyperbolic relation from the asymptotic nature of the growth dependence on substrate stated by Tessier [161]:

$$\frac{d\mu}{ds} = \frac{\mu_m - \mu}{K_s} \quad \text{Eq. 2}$$

$$\frac{\mu}{s} = \frac{\mu_m - \mu}{K_s} \quad \text{Eq. 3}$$

$$\mu = \frac{\mu_m S}{K_s + S} \quad \text{Eq. 4}$$

In this equation μ is the specific growth rate, μ_m is the maximum specific growth rate, S is the substrate, and K_s is saturation constant with dimensions of a concentration. Moreover, Tessier and Monod stated the proportionality of biomass growth and substrate utilization [161], with x being the biomass and Y the yield coefficient:

$$\frac{dx}{dt} = -Y.\frac{ds}{dt} \quad \text{Eq. 5}$$

It has been stated that the rate at which the nutrients are transported throughout the cell wall are dependent of the temperature, the light intensity, and the internal and external nutrients' concentrations [162]. Kinetics based on light intensity and nutrients uptake are the primary focus in this section. Ogbanna [163] pointed out that the saturation light required by photosynthetic growth varies upon the location and its seasonal characteristic. Moreover, Ogbonna [163] states that the incident light is attenuated by dense microalgae cultures, which contributes to low efficiencies at the surface and dark sections at the reactors' bottom. However, microalgae cells

continue growing when they move towards the dark area until the energy/intermediate products are depleted [163]. These energy/intermediate products are obtained when microalgae are exposed to the light area. The Monod growth kinetics by considering the incident light intensity (I_o) and the light saturation constant (K_L) was stated as follows [163]:

$$\mu = \frac{\mu_m . I_o}{K_L + I_o} \quad \text{Eq. 6}$$

Here, the maximum specific growth rate (μ_m) of *C. pyrenoidosa* and *S. platensis* were decreased from 0.286 and 0.083 h^{-1} to 0.0052 and 0.0034 h^{-1} when exposed to dark zones, which represents an average reduction of 97.1 % in the specific growth rate. The light saturation constants for these microalgae strains were 100 and 81.6 $\mu mol.m^{-2}.s^{-1}$, respectively, whereas the saturation light intensity (I_{max}) at which μ equals μ_m were 350 and 200 $\mu mol.m^{-2}.s^{-1}$, respectively. Furthermore, Ogbonna [163] concluded to design algal cultivation ponds at incident light intensities per volume greater than 2000 $\mu mol.m^{-3}.s^{-1}$ to avoid low cell concentrations; however, mixing should be taken into consideration since it could decrease the productivity even more. Additionally, photoinhibition has been researched in microalgae growth by considering that the specific growth rate reaches a maximum specific rate as the irradiance is increased, whereas an excess of this irradiance can inhibit photosynthesis [164]. Various models that take photoinhibition into account have been reported. One of these models is depicted as follows, where the K_I is the photoinhibition constant reported at 3,426 $\mu E.m^{-2}.s^{-1}$ for *P. tricornutum* [164]:

$$\mu = \frac{\mu_m . I_0}{K_L + I_o + \frac{I_o^{\,2}}{K_I}} \quad \text{Eq. 7}$$

One important issue to be considered is the influence of the internal nutrient storage that contributes to the uptake rates, which can overestimate the maximum quota of the limiting nutrient if not taken into account [165]. It was recommended to treat this issue by considering the maximum uptake rate of nutrients as a decreasing function of its quota. This modeling approach is known as cellular equilibrium, which is accomplishable with the Monod theory with the appropriate half saturation constant and the variation of the cell quota as a function of the external nutrient concentration [162]. This approach has already been solved by computing the nutrient uptake rate at steady state (ρ^{ss}) as a function of the substrate, maximum specific growth rate, half saturation constant for growth (K_μ), and maximum and minimum cell quota (Q_{max}/Q_{min}) [166]:

$$\rho^{ss} = \mu Q = \mu_m Q_{max} \frac{S}{K_\mu \, Q_{max}/Q_{min} + S} \qquad \text{Eq. 8}$$

From the rectangular hyperbolae on logarithm graphs the maximum short term uptake rates are obtained to solve the following equation. Where K_ρ is the half saturation constant for nutrient uptake, $K_{\mu Q}$ is the half saturation constant for steady state, ρ^{hi}_{max} is the upper limit of the maximum short term uptake rate under severe nutrient stress at low growth rate and low nutrient quotas, and ρ^{lo}_{max} is the lower limit of the maximum short term uptake rate under nutrient satiety at high growth rate and high nutrient quotas:

$$K_\rho / K_{\mu Q} = \rho^{hi}_{max} / \rho^{lo}_{max}$$
$$K_{\mu Q} = K_\rho \cdot \rho^{lo}_{max} / \rho^{hi}_{max} \qquad \text{Eq. 9}$$

When a high substrate concentration is to be modeled, equation (10) is applied, whereas equations (11) and (12) are utilized if low substrates concentrations are simulated [166]:

$$\mu_m Q_{max} = \rho^{lo}_{max} \qquad \text{Eq. 10}$$

$$\frac{\rho_{max}^{lo} S}{K_\mu \, Q_{max}/Q_{min}} = \frac{\rho_{max}^{hi} S}{K_\rho} \quad \text{Eq. 11}$$

$$K_\mu = K_\rho . \frac{\rho_{max}^{lo} S}{\rho_{max}^{hi} S} . \frac{Q_{min}}{Q_{max}} \quad \text{Eq. 12}$$

Lastly, the cellular quota (Q) and the specific growth rate (μ) can be computed by equations (13) and (14), respectively. This approach was reported to be applied for micro and major nutrients such as Fe, Mn, P and N [166]:

$$Q = Q_{max} \frac{K_\mu + S}{K_{\mu Q} + S} \quad \text{Eq. 13}$$

$$\mu = \mu_m \frac{S}{K_\mu + S} \quad \text{Eq. 14}$$

Additionally, in a study based on the effect of nitrogen and phosphorous on the growth and nutrient uptakes of *Scenedesmus sp*., it was concluded that high removal efficiencies are obtained when the nitrogen/phosphorous ratio is controlled at a range from 5:1 to 8:1 [167]. If both nutrients, nitrogen and phosphorous, are considered to be growth limiting, the Monod model should then be stated as follows [167]:

$$\mu = \mu_m \frac{S_N}{K_{s,N} + S_N} . \frac{S_P}{K_{s,P} + S_P} \quad \text{Eq. 15}$$

4.4.3 Modeling microalgae bioreactors

4.4.3.1 Challenges in modeling the scalability of microalgae grown in wastewater

The proper selection of the mathematical models to predict the growth and lipid productivities of microalgae bioreactors is a critical task towards the scalability of this technology. Additionally, nutrients availability from wastewater facilities not only in terms of concentration, but daily flows, should be considered in the application of the mathematical

models to estimate the microalgae biomass and lipids to be produced when the systems are scaled-up. The scalability of these systems will contribute not only to the engineering design of future projects associated with wastewater facilities, but also to the assessment of their environmental impacts and cost effectiveness. To accomplish these goals, issues associated to the scalability of bioreactors such as productivities decreasing due to light diffusion, mixing and dark to light cycling, and residence time distribution must be taken into account. For instance, in a research aimed to scale-up a flat plate photobioreactor, it was found that the microalgae growth was reduced by about 3.8 times in an area subjected to a diffused light, which was estimated to be 10% the intensity of the direct sunlight [11]. By considering that at noon during a summer day the incident light intensity is 2000 $\mu mol.m^{-2}.s^{-1}$, this research reported a significant increase in microalgae growth at light intensities greater than 500 $\mu mol.m^{-2}.s^{-1}$ [11]. Further experience with regards to scalability was researched in a Solix algae-growth-system (AGS) photobioreactor, where a sparge condition of 0.2 VVM (volume of air per volume of culture per minute) and a duty cycle (time on compared to time off) of 25% reduced the microalgae growth by 23% [82]. With regards to the hydrodynamics of photobioreactors, it has been stated that the scale-up of projects still need to resolve issues associated to the optimization of factors for microalgae growth such as light intensity and distribution, gas injection and mixing, and flow patterns [168]. These hydrodynamic issues will be covered in more detail in the computational fluid dynamics (CFD) section.

4.4.3.2 Scaled-up microalgae growth and neutral lipid synthesis model

This model takes into consideration that neutral lipids serve as carbon storage in an environment with limited nitrogen [169], which is obtained when this nutrient is depleted. This model was aimed to solve green microalgae systems. Packer [169] stated four assumptions for

the model development with regards to the growth rate, net carbon fixation, chlorophyll synthesis, and neutral lipid synthesis. The growth rate of non-lipid algal biomass concentration (A, equation 16) is limited by the light or the nitrogen source (equation 17), the first is being governed by the Droop cell-quota model whereas the latter is governed by Liebig's Law, where a fixed proportion of accumulated carbon ($gC.g^{-1}dw$) is maintained for the non-lipid dried weight (dw) [169].

$$\frac{dA}{dt} = \mu(A, L, H, N).A \qquad \text{Eq. 16}$$

$$\mu(A, L, H, N) = \min\left\{\mu_m.\left(1 - \frac{q}{Q(t)}\right), \frac{p(A, L, H, N)}{c}\right\} \qquad \text{Eq. 17}$$

Packer [169] reported that the carbon fixation is governed by the Poisson single-hit model of photosynthesis, where photosynthesis rate (p, equations 18 and 19) is normalized to the chlorophyll content ($gC.g^{-1}chl.d^{-1}$).

$$p(A, L, H, N) = H(t).p_m(A, L, N).\left(1 - \exp\left(\frac{-a.\phi.I(A, H)}{p_m(A, L, N)}\right)\right) \qquad \text{Eq. 18}$$

$$p_m(A, L, N) = \frac{\left(A(t).Q(t)\right)^2.p_0}{\left(A(t).Q(t)\right)^2 + q^2.\left(A(t) + L(t)\right)^2} \qquad \text{Eq. 19}$$

Also, Packer [169] stated that the chlorophyll synthesis (H, equation 20) is coupled with the nitrogen uptake (N, equations 21 and 22), where the proportion of nitrogen provided to chlorophyll synthesis is governed by the utilization to uptake ratio of carbon (c) and the nitrogen uptake is governed by the maximum nitrogen quota (Q(t), equation 23).

$$\frac{dH}{dt} = \frac{c}{p}.\mu(A, L, H, N).\rho.\upsilon(A, N) - H(t).\mu \qquad \text{Eq. 20}$$

$$\frac{dN}{dt} = -\upsilon(A, N).A(t) \qquad \text{Eq. 21}$$

$$\upsilon(A,N) = \frac{q_M - Q(t)}{q_M - q}.\left(\frac{\upsilon_m.N(t)}{N(t)+\upsilon_h}\right) \quad \text{Eq. 22}$$

$$Q(t) = \frac{A(0).Q_0 + N(0) - N(t)}{A(t)} \quad \text{Eq. 23}$$

The neutral lipid (L, equation 24) model accounts that the lipid synthesis is obtained from an excess of carbon fixation with regards to the carbon required for microalgae growth, which is obtained where the nitrogen cell quota equals the minimum nitrogen cell quota (Q=q) [169].

$$\frac{dL}{dt} = \left[p(A,L,H,N) - c.\mu(A,L,H,N)\right]A(t) \quad \text{Eq. 24}$$

Additionally, the Lambert-Beer law was used by Packer [169] to model the attenuation of light along the reactor depth as a function of the rate of light absorption by phytoplankton (I, equation 24):

$$I(A,H) = \frac{I_0}{a.H(t).A(t).z}.\left(1 - \exp\left(-a.H(t).A(t).z\right)\right) \quad \text{Eq. 25}$$

Table 4.4 depicts a list of the model parameters. It should be noticed that the minimum growth rate will be chosen from the computed light-limited growth rate and the nitrogen-limited growth rate. Furthermore, in the present research is recommended to compare additional growth-limiting factors such as photoinhibition (equation 6), cell equilibrium (equation 13), and nitrogen and phosphorous as growth-limiting nutrients (equation 14). As a result, the most critical scenario for microalgae growth can be evaluated when intended to scale-up a microalgae system associated to wastewater treatment facilities. Moreover, scaled-up coefficients that are intended to obtain more realistic microalgae growth and lipid synthesis are taken into consideration in this research such as a 23% growth reduction due to industrial sparge conditions and light duty cycle [82].

Table 4.4 Microalgae growth and lipid synthesis model parameters [169]

Parameter	Description	Units
I_o	Incident irradiance	mol photons $m^{-2}.d^{-1}$
Z	Light path	M
A	Optical cross section of chlorophyll a	$m^2.g^{-1}$chl
ϕ	Quantum efficiency	gC.(mol photons)$^{-1}$
Q	Minimum subsistence nitrogen quota	$gN.g^{-1}dw$
q_M	Maximum nitrogen quota	$gN.g^{-1}dw$
C	C subsistence quota	$gC.g^{-1}dw$
V_m	Maximum uptake rate of nitrogen	$gN.g^{-1}dw.d^{-1}$
V_h	Half-saturation coefficient	$gN.m^{-3}$
P	Maximum chlorophyll to nitrogen ratio	$gchl.g^{-1}N$
μ_m	Maximum nitrogen-limited growth rate	d^{-1}
p_o	Maximum photosynthesis rate	$gC.g^{-1}chl.d^{-1}$

4.4.3.3 Modeling and scale-up of computational fluid dynamics (CFD) for microalgae-bioreactors

CFD will play a major role in the scalability of microalgae systems where wastewater is used as the growth media. Research has already been conducted for the application of CFD to

microalgae systems, where hydrodynamics has been addressed by multiphase and turbulent models [170]. Furthermore, the importance of CFD in the mass transfer coefficient, mixing, liquid velocity, gas bubble velocity, and gas hold-up in photobioreactors was stated by Wu [170]. Additionally, Wu [170] reported previous studies where mathematical models, comprised by a three-state model and fluid mixing, were applied to predict the performance of photobioreactors at different light duty cycles and photon flux density.

When modeling photobioreactors, three important design aspects have been pointed out such as mixing, light penetration, and gas injection [168]. Bitog [168] states that mixing contributes to the light intensity distribution, CO_2 transfer, and uniform pH. Bitog [168] claimed that light penetration governs the biomass composition, growth rate, and product formation. Lastly, gas injection not only provides the CO_2 required by microalgae, but also contributes to enhance the mixing in the photobioreactor and the light duty cycle frequency. Bitog [168] claims that most microalgae bioreactors have been simulated by turbulent models. Moreover, the growth rates of some microalgae increase when subjected to a higher turbulence in the flow regimen; however, the growth decreases with further increase of the gas velocity due to cell damage [168]. Hydrodynamics studies are conducted by the application of CFD codes such as ANSYS®. The finite volume method, where control volumes are cell centered, is used by this CFD codes to solve the transport equation for mass, momentum, energy, and species [171]. The transport of a random scalar in a single phase flow, which can be named $Ø_k$, can be modeled by Fluent ANSYS® by solving the transport equation, where Γ_k and $S_{\emptyset}$ are the diffusion coefficient and source term, respectively [172].

$$\frac{\partial \rho \emptyset_k}{\partial t} + \frac{\partial}{\partial x_i}\left[\rho u_i \emptyset_k - \Gamma_k \frac{\partial \emptyset_k}{\partial x_i}\right] = S_{\emptyset} \quad k = 1, \dots, N \qquad \text{Eq. 26}$$

4.4.3.4 Validation of mathematical and computational models

Whether mathematical and/or computational models are implemented to predict the performance of photobioreactors, their accuracy must be validated by laboratory approaches. The most important parameters to be validated for scalability purposes are microalgae biomass and lipids content in a daily basis. Microalgae growth has been reported to be measured by Optical Density (OD) using an Optech model ASD19-N absorption probe connected to a fermented control hardware, where the datum was logged in a minute time scale, and by OD at 750 nm on a Hach DR5000 spectrophotometer, respectively [153]. Also, dried weight (dw) microalgae biomass has been measured simply by filtering samples in glass fiber filter paper, which was dried overnight at 100 □C [169]. Microalgae growth was also monitored in a daily basis by measuring the total volatile suspended solids (TVSS) by the APHA standard methods of the year 1995 [128]. With regards to lipids content in microalgae, this has been reported to be tested by transesterification followed by centrifugation and gas chromatography [153]. Also, neutral lipid content has been analyzed by an improved Nile red fluorescence method [169]. Lastly, total lipid analysis has been performed by centrifugation and dried by a freeze drier followed by a one-step extraction Folch method, filtering in glass fiber filter, and wash-out of water soluble components followed by a final centrifugation [128]. Other relevant analysis methods, such as nitrogen and phosphorous analysis, towards the validation of the scaled-up mathematical and computational models are additionally reported by the above authors. Furthermore, more specific details of the laboratory assays to measure microalgae biomass and lipids content can be obtained in the cited literature.

4.5 Conclusions

Despite the significant progress made in research associated to microalgae grown in wastewater, such as productivities and strains able to grow in this substrate obtained from different stages of the treatment process, most of the experiences are at a laboratory scale thus limiting the scalability of this technology. Additionally, inhibition of microalgae by potential contaminants that could be present in the wastewater such as heavy metals, surfactants, and by-products has not been sufficiently researched. This could be determinant not only in the biomass and lipid productivities but in the fate of contaminants obtained in the final product, biofuels. By evaluating the overall wastewater treatment process, previous research experience has clearly demonstrated that the most promising substrate in facilities is the centrate obtained from sludge dewatering. Also, in spite of the higher concentrations of nutrients present in raw wastewater than in secondary or biologically treated wastewater, the higher lipid productivities are obtained from the latter, which is contributed by the switched metabolism from protein to lipid synthesis upon nitrogen depletion. Consequently, mixed centrate and secondary treated wastewater at various ratios should be researched in future work towards the scalability of this technology.

Moreover, previous research has not taken into consideration the presence or absence of biological nutrient removal operations in the process, which can drastically change the characteristics of nutrients not only in the final treated effluent, but in the centrate. Additionally, since the EPA has established more rigorous nutrients-discharge permits for wastewater facilities, such as nitrogen and phosphorous, the implementation of microalgae-based biofuels facilities could not only contribute to the sustainability of wastewater facilities but to save millions of dollars to the US.

Various mathematical and computational models have been researched for ecological purposes since the early 20th century, which had the most relevant milestone with the development of the growth-kinetics Monod model in 1942. Nowadays, not only microalgae biomass models for biofuels purposes but also lipid synthesis models have been developed. Nevertheless, these models are more applicable at a laboratory scale since they have not taken into consideration the efficiency decrease in ponds and photobioreactors due to light duty cycles, mixing, and hydrodynamics of microalgae and gas sparged in the system. Consequently, we suggest that future research takes into consideration in photobioreactors modeling the minimum growth kinetics obtained from the different models available in the literature such as light-limiting, photoinhibition, cell equilibrium, nitrogen-limiting, and multiple nutrients-limiting.

The scalability of microalgae-based biofuels grown in wastewater may require to take into account additional considerations that have not been researched such as the competition for nutrients with nitrifiers, which could reduce the available levels of nitrogen for microalgae. A light-duty-cycle efficiency reduction factor, as reported by previous research, should be taken into account as well. However, scattering factors due to the presence of solids and other particles in the wastewater that could interfere in the distribution of light should also be researched in more depth. Furthermore, future work must take into account the application of computational fluid dynamics when research findings at a laboratory scale are intended to scale-up for industrial purposes towards the scalability of microalgae-based biofuels grown in substrates obtained from wastewater facilities.

4.6 Answer to Research Question 2.1

This section of the research effort has allowed us to address Research Question 2.1, which is restated and answered in section 5.5 of this dissertation.

CHAPTER 5: A Cyanobacterial Sidestream Nutrient Removal Process and its Life Cycle Implications[4]

5.1 Introduction

More than 3000 years ago, ancient civilizations utilized photoautotrophic microorganisms, including both algae and cyanobacteria strains, for wastewater treatment [37, 173]. There is modern interest in these microorganisms due to their high bioenergy productivities (10 times that of palm oil and about 131 times that of soybean [5]). The areal equivalent energy productivity of cyanobacteria is about 4 times higher than popular microalgae feedstocks [6, 174], and the cultivation of algae and cyanobacteria is not limited by the availability of high quality land [136, 175, 176]. However, the U.S. goal of producing 40 billion gallons of biofuel per year from microalgae will be limited by the availability of water and nutrients [18]. Many researchers suggested that integrating the cultivation of the photoautotrophs with wastewater treatment systems could reduce their need for water and nutrients, and could improve the economics and environmental sustainability of photosynthetic bioenergy technologies.

Wastewater treatment facilities (WWTF) in the U.S. are facing new challenges to meet the water quality criteria, controlled by state-level water regulations and the federal Environmental Protection Agency (EPA). A major consideration for these facilities is the sidestream wastewater treatment for sludge centrate due to its potent nutrient concentration resulting in potential to cause eutrophication in surface waters [30]. Several technologies have been developed for sidestream wastewater treatment including Biological Nutrient Removal (BNR) processes [31], sludge centrate recycling [38], anaerobic ammonium oxidation (Anammox) [33], adsorption

[4] **This chapter is adapted from a prepared journal article for consideration for publication:** Carlos Quiroz - Arita, John J. Sheehan, Nawa Raj Baral, Alexander Hughes, Graham Peers, Brock Hodgson, Sybil Sharvelle, Thomas H. Bradley. "A Cyanobacterial Sidestream Nutrient Removal Process and its Life Cycle Implications".

[34], ammonia stripping [38], and struvite precipitation [35, 36]. Among these processes, BNR processes such as anaerobic/anoxic/oxic (A^2/O), can reduce the total nitrogen (TN) and total phosphorous to about 2.3 and 1 $mg.l^{-1}$, respectively [30, 177]. However, these BNR technologies require a high capital cost in the range of 150 to 1,840 $\$.m^{-3}$-wastewater [37] and energy consumption of 0.09 $kwh.m^{-3}$-wastewater [38] relative to the conventional activated sludge wastewater treatment process. While struvite precipitation from sludge centrate can recover nitrogen in the form of fertilizer [35, 36], the treated effluents reported in the literature [39] with 128 ± 5 mg NH_4-$N.l^{-1}$ and 12.3 ± 6.2 mg PO_4-$P.l^{-1}$ do not meet the federal water quality criteria for nitrogen and phosphorous to discharge into surface waters.

The environmental impacts of photosynthetic biorefineries and WWTF can be reduced by integrating these technologies for the cultivation of cyanobacteria in sludge centrate and remediation of nitrogen and phosphorous from the sludge [30, 37, 96]. Several past studies [40-46] have extensively investigated the growth of photosynthetic microorganisms in wastewater. Some recent studies [37, 47, 48] have shown the potential growth of photoautotrophic microorganisms in the sludge centrate obtained from the dewatering processes of a WWTF. These studies suggest that the sludge centrate itself could be supplied as the main source of nutrients due to its high concentrations of nitrogen and phosphorous. However, ammonia, the majority of nitrogen compound present in sludge centrate has been demonstrated to inhibit the growth of cyanobacteria [49, 50]. For instance, the biomass productivity of *Synechocystis* sp. PCC6803 is inhibited at high intracellular concentrations of ammonia of 63 mg $NH_4.l^{-1}$ [51] due to damage to photosystem II[52]. These efforts suggest that photoautotrophic microorganisms, such as cyanobacteria, could potentially solve the challenges associated with the sidestream wastewater treatment system once the centrate inhibition can be mitigated or controlled.

The proposed integrated process could reduce the operating cost and energy intensity of WWTF when compared to the biological nutrient removal process. Conventional activated sludge process combined with sidestream cyanobacterial treatment could meet the standard water quality criteria and enable discharge of treated wastewater to water bodies [37]. While the environmental impacts of microalgae-based biofuel technologies have been extensively researched [19-24, 26, 27, 29, 78, 178], there is comparatively limited lifecycle assessment (LCA) of photosynthetic biorefineries based on cyanobacteria [17, 174]. These past LCA studies have focused on biofuel and bioproducts production, and none of the previous studies have investigated the synergistic benefits of combining photosynthetic biorefineries, based on *Synechocystis* sp. PCC6803, and WWTF. These synergistic benefits include improvement in the quality of water from the WWTF, energy recovery, and greenhouse gas (GHG) emissions reduction due to fossil fuels and commercial fertilizers displacements with bioenergy and co-products, respectively.

This study systematically evaluates the synergistic benefits of combining the cyanobacterial cultivation system with a municipal WWTF by using an LCA approach, supported by modelling and experimental work.

5.2 Materials and Methods

5.2.1 Goals and scope

LCA is a framework for the evaluation of the energy use, the emissions, and other environmental impacts of direct, indirect, and supply chain processes in a system [16]. The LCA model developed in this study seeks to evaluate the environmental benefits of combining cyanobacteria cultivation and nutrients remediation in photobioreactors using the sludge centrate produced by a WWTF (Drake Water Reclamation Facility (DWRF)) located in Fort Collins, CO,

USA. This WWTF is currently using a BNR process, an A^2/O process (Figure 5.1) [31, 37, 177], which was considered the base case scenario for analysis in this study.

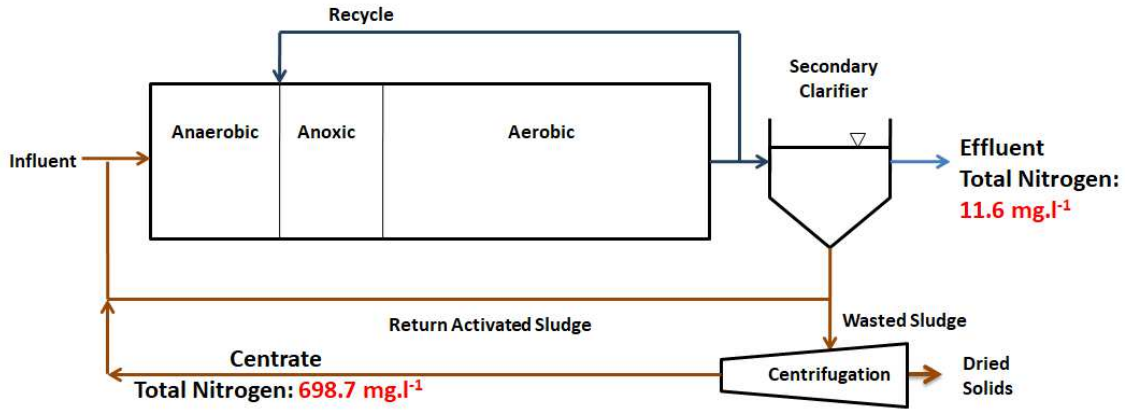

Figure 5.1 Baseline Anaerobic/anoxic/oxic (A^2/O) process. The nitrogen concentrations of the treated effluent and sludge centrate correspond to the average values of DWRF for the years 2011-2014. Figure adapted from: [37, 38, 177].

The scope of the LCA model considers the material and energy inputs, the wastewater and cyanobacterial bioprocesses, and the bioenergy and products; treated water, fertilizer, and energy (Figure 5.2). The material and energy inputs include the raw wastewater feeding an activated sludge process for carbon oxidation and the electricity consumption by the facility. *Synechocystis* sp. PCC6803 is cultivated in open raceway ponds using centrate as the source of nutrients, which is obtained from sludge dewatering process of the WWTF. The LCA model uses the displacement method to account for the credits for displacement of nutrients and energy. The primary audience for this LCA includes operators of municipal wastewater treatment facilities, scientific researchers, photosynthetic biorefinery operators, policy makers, and wastewater engineers.

5.2.2 System boundary

The boundary of the combined wastewater treatment facility, cyanobacterial cultivation, and resources recovery, including struvite precipitation and biogas electric power generation, is

illustrated in Fig. C.2. For the base case scenario, the system considers the indirect and direct electrical energy consumptions by the WWTF including the BNR process (Figure 5.1). For the combined system, the liquid centrate obtained from the sludge centrifugation serves as the source of nitrogen and phosphorous, which are required for the growth of cyanobacteria. This nutrient supplement reduces the required commercial/industrial fertilizers commonly used in photoautotrophic facilities (conventionally $NaNO_3$, KH_2PO_4).

Liquid centrate must be diluted to serve as the cyanobacteria growth media. Three centrate dilution scenarios were evaluated in this study: 3% by volume (vol%) solution of centrate, 9 vol%, and 19 vol%. Life cycle energy use and GHG emissions due to *Synechocystis* sp. PCC6803 cultivation and biomass extraction were included within the system boundary. Carbon dioxide obtained from the anaerobic digester-based generation system was recycled back to the cyanobacterial cultivation system and the credits due to the displacement of grid electricity by the electricity generation through anaerobic digester were taken into consideration in the LCA model developed for analysis in this study.

5.2.3 Functional unit

The functional unit for this LCA is the treated wastewater volume-specific rate of nitrogen uptake or removal by the system (N_r, $mgN.m^{-3}.day^{-1}$). The nitrogen removal rate is an important parameter to compare the effectiveness of wastewater treatment processes, and was recommended by the stakeholders at DWRF and city of Fort Collins utilities.

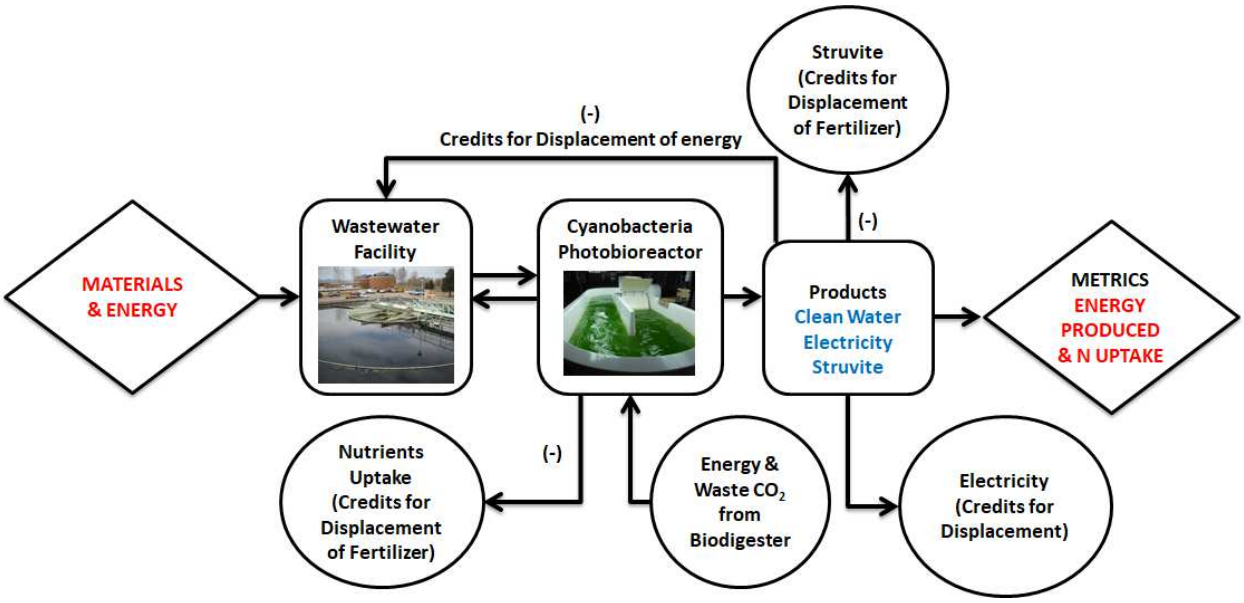

Figure 5.2 Scope of a combined cyanobacterial cultivation and nitrogen removal system.

5.2.4 Impacts assessment

Life cycle net energy and life cycle GHG emissions were used to compare the environmental impacts of the proposed combined WWTF and cyanobacteria-based sidestream treatment system to the baseline facility at DWRF (Figure 5.1). Additionally, the total inorganic nitrogen annual median value for new WWTF in the State of Colorado of 7 $mgN.l^{-1}$ [179] was used as a water discharge quality criteria.

The net energy of the system was evaluated as a difference between energy consumed ($Energy_{in}$), and energy produced ($Energy_{out}$) by the system. The energy consumed by the system includes all the life cycle energy for the processes and materials of the wastewater facility and for cyanobacteria cultivation in photobioreactors. The energy produced by the system includes electrical energy produced through anaerobic digestion and the embedded energy saved by using the struvite co-product to displace commercial fertilizers. The net energy was normalized in this study by using the volume-specific nitrogen removal rate (N_r) (Eq. 1), which was computed from the experimental work and the cyanobacteria growth model.

$$NENR = \frac{(Energy_{in} - Energy_{out})}{N_r} \quad \text{Eq. 1}$$

In addition to metrics of energy, reducing wastewater treatment facility GHG emissions is encouraged by policies such as The Colorado Climate Plan [180]. The second metric of interest, therefore, was the ratio of life cycle GHG emissions to nitrogen removal (N_r) ratio (Eq. 2). Life cycle GHG emissions ($CO_{2,\ out}$) is defined by the Intergovernmental Panel on Climate Change (IPCC) as the amount of direct and indirect (embedded) energy consumed by the system, multiplied by the emission factor based on the type of energy technology [81].

$$GHG = \frac{\left(CO_{2,\ out} - CO_{2,\ in}\right)}{N_r} \quad \text{Eq. 2}$$

To assess the impact of water quality of the system, the effluent nitrogen concentrations resulting from the cyanobacterial cultivation and nutrient uptake were computed from the experimental work and growth model. The discharge nitrogen concentrations are obtained by homogenizing this cyanobacterial cultivation effluent with the treated wastewater, as computed by mass balance in BioWin 5.2 [181]. The discharge water characteristics are compared to the regulated limits for annual median nitrogen and phosphorous concentrations established by the State of Colorado [179].

5.2.5 LCA model development

The baseline BNR DWRF, and the combined wastewater treatment facility with cyanobacteria cultivation and nitrogen removal (labelled here as the cyanobacteria-based nitrogen removal process, or CNR) were each modeled in GaBi-6, to assess and compare their environmental costs and benefits [182]. Three separate LCA models were developed of the CNR

system to assess its environmental impacts under three different centrate dilution scenarios. The coproducts of the CNR system were struvite, and the electricity generated from the anaerobic digestion of cyanobacterial biomass. The credits from these co-products were allocated by the displacement method, where struvite is assumed to be used as an alternative to commercial nitrogen fertilizer, and the electricity generated from the system is assumed to be used as a substitute for commercial grid electricity. The co-products credits were subtracted from the overall life cycle energy use and GHG emissions of the CNR systems.

5.2.6 Synechocystis sp. PCC 6803 cultivation in sludge centrate

To inform the model of cyanobacteria growth in sludge centrate, *Synechocystis* sp. PCC6803 cells were cultured in media where the level of relative concentration of standard *Synechocystis* culture media (BG-11) and wastewater centrate was set between 0-25%. All liquid media used in was filtered through a 0.2 μm filter to remove microorganisms and avoid changes in chemistry associated with autoclaving. Cultures were grown at 30°C in constant light fluxes of 150 μmol photons $m^{-2}.s^{-1}$. Growth rates of liquid cultures were monitored using cellular in vivo fluorescence with a Turner Instruments Trilogy fluorometer. All culturing took place on site at the DWRF in Fort Collins, CO, U.S.

5.2.7 Cyanobacterial Nutrient Removal Process

This LCA compares the CNR process developed in this research with the baseline BNR process used by DWRF. This section describes the proposed sidestream wastewater treatment process using cyanobacterial photobioreactors. The kinetic model used to characterize struvite precipitation from sludge centrate is also presented. The thin layer cyanobacteria growth model including centrate inhibition presented in this study was developed from the experimental work conducted at DWRF. This section also discusses a model of anaerobic co-digestion of the

activated sludge and cyanobacterial biomass. The results obtained from the experimental work and dynamic system models are inputs to the LCA model developed for analysis in this study.

5.2.8 Sidestream wastewater treatment by cyanobacterial photobioreactors

The proposed CNR process, integrated with the conventional activated sludge process, is illustrated in Figure 5.3.

To produce the cyanobacteria growth media, the treated wastewater effluent is utilized to dilute the sludge centrate in a homogenization tank. The fraction of the treated wastewater used to dilute the centrate for the three scenarios (3 vol%, 9 vol%, and 19 vol%) is 22.2%, 3.3%, and 1.5%, respectively. Struvite is recovered from the homogenized flow in a settling tank. A microfiltration unit process is removes suspended particles and organisms larger than 0.2 μm from the centrate. Centrate nitrogen and phosphorous uptake by *Synechocystis* sp. PCC6803 was performed in the photobioreactors. Cyanobacterial cultures obtained from cultivation stage are then centrifuged and the dried biomass is co-digested with activated sludge in the existing DWRF anaerobic digester unit. The nutrient-depleted growth media obtained from cyanobacterial culture centrifugation is mixed with the treated wastewater and discharged to the environment.

The system-level performance of the CNR process integrated with a conventional activated sludge process at DWRF was evaluated using a calibrated and validated BioWin process model of DWRF [183]. The conventional system includes only an aerobic zone and achieves negligible nitrogen removal due to the absence of an anoxic zone. The scenarios were compared to the baseline BNR process which consists of three stage A^2/O process with nitrification, denitrification and limited biological P removal (Figure 5.1).

The model was modified to represent an aerobic activated sludge process by removing the anaerobic and anoxic basins and removing the mixed liquor return from the baseline (Figure 5.1). The solids retention time (SRT) was reduced from 10 days for the BNR to 1.5 days for the activated sludge model considered for analysis in this study. The model included sidestream diversion of the centrate and dilution water to the CNR process based on three different dilution scenarios considered in this study. The efficiency of the CNR process was evaluated external to BioWin, which is discussed in section 2.4.3, and the resulting concentrations were returned to the BioWin model to determine the combined effluent concentration from the activated sludge and CNR processes. Using the developed models, the scenarios were run to determine the water quality impact of the activated sludge process with CNR performed at the three different dilution rates relative to the baseline BNR. Struvite precipitation is modeled using the models described in section 2.4.2. *Synechocystis* sp. PCC6803 growth curves at the cultivation stage in photobioreactors were developed from the experimental work (described in section 2.3) and the cyanobacterial growth models (described in section 2.4.3). Biogas production from cyanobacterial biomass and activated sludge are derived from the first order system co-digestion model (described in section 2.4.4).

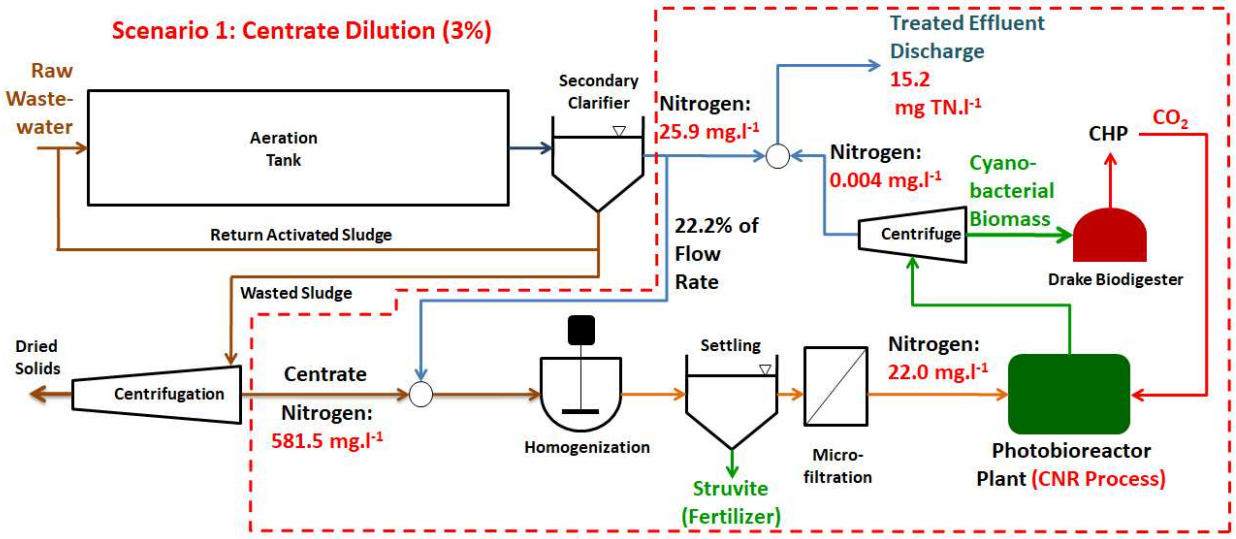

Figure 5.3 Cyanobacterial Nutrient Removal (CNR) Process. Dashed line indicates the boundary of the sidestream wastewater treatment CNR process. The sidestream wastewater treatment system utilizes the treated wastewater and the sludge centrate obtained from centrifugation of the wasted sludge, with total nitrogen (TN) concentration of 25.9 mg $N.l^{-1}$ and 581.5 mg $N.l^{-1}$, respectively. The sidestream wastewater treatment is required due to high concentration of TN in the sludge centrate.

5.2.9 Kinetics of struvite precipitation from sludge centrate

Chemical precipitation of struvite is commonly observed in wastewater systems with high concentrations of orthophosphates, NH_4-N, and Mg^{++} ions [184, 185]. Struvite precipitation is enhanced at magnesium to phosphorous ratios (Mg:P) of 1.2:1 and carbon dioxide partial pressures less than 0.35 atm [185]. Sludge centrate at DWRF is stored under anoxic conditions, where carbon dioxide partial pressures could be about 0.35 atm. Struvite precipitation is described as a first-order kinetics reaction (Eq.3) [39], where *k* is the first-order rate constant. The rate constants of struvite precipitation from the sludge centrate were obtained by solving a first-order differential equation (Eq. 3) for the time rate of change of total Nitrogen (*TN*) concentration.

$$\frac{d[TN]}{dt} = -k \cdot [TN] \qquad \text{Eq. 3}$$

5.2.10 Modelling of Synechocystis sp. PCC 6803 thin layer growth with sludge centrate inhibition

A dynamic cyanobacteria growth model including sludge centrate inhibition was developed for analysis in this study. This model incorporates ordinary differential equations (ODE) and nonlinear functions representing the effects of nitrogen quota, nitrogen uptake, chlorophyll synthesis, light absorption, photosynthesis, growth rate, and cell biomass [37, 186].

Table C.1 summarizes the required biological inputs for this model of the growth of *Synechocystis* sp. PCC6803 [84, 187, 188]. The model developed in this study is novel in that it incorporates the maximum nitrogen-limited growth rate (μ_{max}) including the measured effects of centrate inhibition. These parameters were determined from the experimental works described in section 2.3. Additionally, a competitive inhibition due to competition with nitrifiers in a wastewater environment was included in the model [156]. Competition with nitrifiers is due to the availability of an electron-acceptor, oxygen, as a result of photosynthetic activity and cultivation of cyanobacteria in a wastewater environment containing an electron-donor, nitrogen [38]. The growth inhibition of *Synechocystis* sp. PCC6803 by centrate is mathematically described by Eq. 4 [189], where all the parameters were determined experimentally and discussed under results section.

$$\mu_{IS} = \frac{\mu_{max} * S}{K+S} \cdot \left(1 - \frac{S}{K_{IS}}\right)^{n} \qquad \text{Eq. 4}$$

K_{IS} is the concentration of centrate where inhibition is observed, S is the substrate (TN) concentration, K is the concentration given one-half maximum rate, μ_{max} is maximum specific growth rate, and n is the unitless exponent defining the relationship between μ_{IS} and S.

Cyanobacterial biomass is a function of the growth rate, chlorophyll synthesis, and nitrogen (Eq. 5) [169]. The growth limiting factors in the model, nitrogen and light, are governed by the Droop cell-quota function and the Liebig's Law, respectively (Eq. 6) [169]. A fixed fraction of accumulated carbon ($gC.g^{-1}dw$) is maintained for the dried biomass. Carbon fixation is a function of the Poisson single-hit model of photosynthesis. The photosynthesis rate (Eq. 7 and 8) is normalized by the chlorophyll content ($gC.g^{-1}chl.d^{-1}$) [169]. Chlorophyll synthesis (Eq. 9) is a function of nitrogen uptake (Eq. 10 and 11) [169], which incorporates heterotrophic biomass (X_v) and nitrification (N_v) in a wastewater environment (Eq. 14) [31]. The fraction of nitrogen supplied to chlorophyll synthesis is a function of the carbon utilization to uptake ratio (c) and the nitrogen uptake is a function of the maximum nitrogen quota (Eq. 12) [169]. Light attenuation in the thin layer photobioreactor is computed by the Lambert-Beer law, which is a function of the rate of light absorption by the culture [153].

$$\frac{dA}{dt} = \mu(A,H,N)\cdot A \quad \text{Eq. 5}$$

$$\mu(A,H,N) = min\left\{\mu_{IS}\cdot\left[1-\frac{q}{Q(t)}\right], \frac{p(A,H,N)}{c}\right\} \quad \text{Eq. 6}$$

$$p(A,H,N) = H(t)\cdot p_m(A,N)\cdot\left[1-exp\left(\frac{-a\cdot\emptyset\cdot I(A,H)}{p_m(A,N)}\right)\right] \quad \text{Eq. 7}$$

$$p_m(A,N) = \frac{[A(t)\cdot Q(t)]^2\cdot P_0}{[A(t)\cdot Q(t)]^2+q^2\cdot[A(t)+L(t)]^2} \quad \text{Eq. 8}$$

$$\frac{dH}{dt} = \frac{c}{p}\cdot\ \mu(A,H,N)\cdot\rho\cdot v(A,N) - H(t)\cdot\mu(A,H,N) \quad \text{Eq. 9}$$

$$\frac{dN}{dt} = -v(A,N)\cdot A(t) \quad \text{Eq. 10}$$

$$v(A,N) = \frac{q_M - Q(t)}{q_M - q}\cdot\left[\frac{v_m\cdot(N(t)-N_v(t))}{(N(t)-N_v(t))+v_h}\right] \quad \text{Eq. 11}$$

$$Q(t) = \frac{A(0)\cdot Q_0 + N(0) - N(t)}{A(t)} \quad \text{Eq. 12}$$

$$I(A,H) = \frac{I_0}{a \cdot H(t) \cdot A(t) \cdot z} \cdot [1 - exp(-a \cdot H(t) \cdot A(t) \cdot z)] \quad \text{Eq. 13}$$

$$\frac{\Delta N_v}{\Delta t} = \frac{\Delta X_v}{\Delta t} \cdot \frac{14\ mgN}{113\ mg\ Heterotrophic\ Biomass} \quad \text{Eq. 14}$$

The dynamics of these ODEs is illustrated in Fig. C.3. Biomass growth and nitrogen depletion curves for *Synechocystis* sp. PCC6803 were computed in Matlab® for the three centrate dilution scenarios evaluated in this LCA: 3 vol%, 9 vol%, and 19 vol%. The nitrogen removal rates were compared with the baseline BNR process used by DWRF, and the output nitrogen concentrations at the stationary growth stage could be calculated.

5.2.11 Modelling of anaerobic co-digestion of activated sludge and cyanobacterial biomass

The cyanobacteria biomass from the photobioreactors are input (along with activated sludge) to the on-site anaerobic digestion system. Anaerobic digestion reduces the carbon content of input organic matter to its most reduced oxidation state [156]. Anaerobic digestion processes are carried out in three stages; hydrolysis of organic matter, acidogenesis or fermentation of organic matter into organic acids and hydrogen, and final conversion of organic acids and hydrogen into methane, known as methanogenesis [190]. Hydrolysis and methanogenesis stages can be described by a first order system of carbohydrate, lipid, and protein contents degradation as illustrated in Eq. 15 and Eq. 16 [191].

$$\frac{d[S]}{dt} = -k_{AD} \cdot [S] \quad \text{Eq. 15}$$

$$\frac{d[CH_4]}{dt} = \alpha \cdot k_{AD} \cdot [S] \quad \text{Eq. 16}$$

S is concentration of volatile solids (VS) or concentration of chemical organic demand (COD), k_{AD} is the first-order rate constant, and α is the conversion coefficient from VS or COD to the product (CH_4). Municipal sludge is reported to have carbohydrates, proteins, and lipids content of 32 wt%, 33 wt%, and 25 wt%, respectively [192]. Cyanobacteria, on the other hand, are reported to have 23.3 wt% of carbohydrates, 38.6 wt% of proteins, and 6 wt% of lipids [193]. The first order rates constants of these substrates are 0.5-2.0 d^{-1} and 0.25-0.8 d^{-1} for carbohydrates and proteins [194], respectively, and 0.7-0.76 d^{-1} for lipids [194-196].

The anaerobic digestion model was constructed in python^{TM} and validated using the daily methane production rate reported by DWRF from the existing anaerobic digester unit. The model for anaerobic digestion of cyanobacterial biomass was validated using three methane yields reported in the literature for this feedstock. The flowrates and substrate concentrations for co-digestion of sludge centrate and cyanobacterial biomass were obtained by a mass balance.

Anaerobic digestion of photoautotrophic microorganisms have been previously researched to evaluate methane yield. For instance, *Nannochloropsis salina*, a microalgae strain, could produce about 0.14 $m^3CH_4.kg\ VS^{-1}$ [197] from the lipid extracted algae biomass. Cyanobacteria strains, such as *Spirulina maxima* yields about 0.15 $m^3CH_4.kg^{-1}$ of dry biomass [198] and *Arthrospira platensis* yields about 0.20 $m^3CH_4.kg^{-1}$ of dry biomass [193].

The anaerobic digestion unit of DWRF currently produces 4,749 $m^3\ CH_4.day^{-1}$ from anaerobic digestion of the wasted activated sludge of 17,010 kg of volatile solids (VS) per day. The literature [38] reports that electrical generating efficiencies of 25 % could be achieved for electricity generation only. This study evaluated all such scenarios by considering electric power generation from biogas, electrical efficiency of 25%, obtained from co-digestion of the activated sludge and cyanobacterial biomass. Using the model proposed here, the daily methane

production rate of 4,749 m^3 CH_4.day^{-1} for the DWRF baseline BNR process was validated with a relative error of 0.08%. The electricity generation from anaerobic digester at DWRF was estimated to be 307 kW for the baseline.

5.2.12 Sensitivity Analysis of Centrate Dilution Scenarios

In experiments, the cyanobacterial biomass productivity was demonstrated to be inhibited by high concentrations of ammonia in sludge centrate (Figure 5.5). Thus, this LCA includes single point sensitivity analysis of the resource requirements and co-products characteristics for each centrate dilution scenarios considered in this study: 3 vol%, 9 vol%, and 19 vol%. The main resources required in the cultivation stage for each scenario includes sludge centrate, treated wastewater, supplemental nutrients, land, and mixing energy. These LCA inputs are summarized in Table C.2. The sensitivity analysis was performed for each scenario considering the results obtained from the cyanobacterial growth model, co-digestion model, and variability present in CNR process.

The baseline wastewater treatment facility with the BNR A^2/O process requires about 1.44 kWh of energy per m^3 of treated wastewater, as recorded by DWRF. For all the scenarios in the CNR process system, the required energy for the BNR process (0.09 kWh.m^{-3} of treated wastewater) was subtracted from the wastewater facility energy budget [38]. All the produced sludge centrate was supplied to the CNR process for all scenarios.

The nitrogen taken up by the photobioreactors was modeled at 31.3, 17.6, and 11.0 kg.day^{-1} for the three centrate dilution scenarios (3 vol%, 9 vol%, and 19 vol%), respectively. Phosphorous uptake rate for *Synechocystis* sp. PCC6803 of 0.0069 g.l^{-1}.d^{-1} [10, 84] was assumed to be constant for each scenario, since this nutrient was not researched in this study due to its lower sensitivity on GHG emissions [174]. Previous studies [83, 174] reported a mixing energy

of about 2 $W.m^{-3}$ for photobioreactors and raceway ponds. This volume-specific energy consumption was used for analysis for all the centrate dilution scenarios.

5.3 Results and Discussion

The results of analysis of the CNR process for sidestream wastewater treatment and its life cycle implications are divided into four components. First, modelling is used to describe the kinetics of struvite precipitation from centrate under anoxic conditions. Second, the cyanobacterial biomass productivities and nitrogen removal rates obtained from experimental work and computational modeling in diluted sludge centrate, are reported. Third, modeling results for the anaerobic digestion of activated sludge are presented, which was verified with the daily production of methane at the DWRF plant. The modeling results for cyanobacterial digestion, and co-digestion of activated sludge with cyanobacterial biomass are compared with the results reported in the literature. The benefits of co-digestion for the production of biogas electric power are discussed. Lastly, the life cycle implications of the integrated CNR process are compared with the baseline WWTF in terms of net energies and GHG emissions per volume-specific rate of nitrogen removed.

5.3.1 Struvite precipitation rates are increased in combined cyanobacterial cultivation and sidestream wastewater treatment

As shown in Figure 5.4, some of the nitrogen removal in the CNR process is performed by struvite precipitation. The struvite precipitation rates reported in the literature (Nelson *et al.* 2003) are 3.7 h^{-1} at pH of 8.4, 7.9 h^{-1} at pH of 8.7, and 12.3 h^{-1} at pH of 9.0. Loewenthal et al. (1994) reported that the struvite precipitation rates are increased at partial pressures of carbon dioxide less than 0.35 atm. DWRF stores sludge centrate under anoxic conditions, where high CO_2 partial pressures are expected, unlike conditions in the work performed by Nelson *et al.*

(2003) in well-mixed reactors at atmospheric pressure. Transport of sludge centrate to the homogenization tanks and settler in the CNR process abruptly reduces the CO_2 partial pressure resulting in high struvite precipitation rates. By increasing the struvite precipitation rates, there will be substantial reductions in the settling hydraulic retention times (HRT) from 14 days required under anoxic conditions to approximately 20 minutes at atmospheric pressure, assuming a precipitation rate of 3.7 h^{-1} (Figure 5.4). The reduction in HRT decreases both the capital costs and life cycle energy of the system due to lower reactor volume.

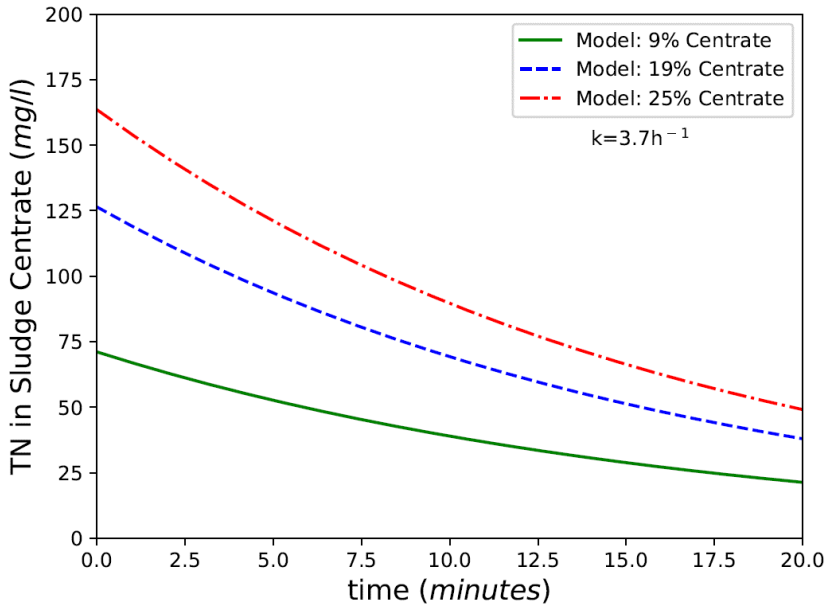

Figure 5.4 Kinetics of struvite precipitation from sludge centrate under atmospheric pressure at a precipitation rate of 3.7 h^{-1} [39].

5.3.2 Growth of Synechocystis sp. PCC 6803 including sludge centrate inhibition

In sludge centrate, nitrogen is primarily in the form of ammonia, which inhibits the growth of *Synechocystis* sp. PCC6803 at a concentration of about 49 mg NH_4-N.l^{-1} [51]. This study finds that the growth of *Synechocystis* sp. PCC6803 is completely inhibited when centrate is greater than 25 vol% (total nitrogen concentration of >163 mg TN.l^{-1}; Figure 5.5). Experimental results show that the highest value of the maximum specific growth rate of *Synechocystis* sp. PCC6803

was obtained at sludge centrate concentration of 9 vol% where TN concentration was 71mg.l^{-1} (Figure 5.5). Figure 5.5 depicts the measured and modeled range of maximum growth rates of *Synechocystis* sp. PCC6803 and the kinetic parameters for Eq. 4.

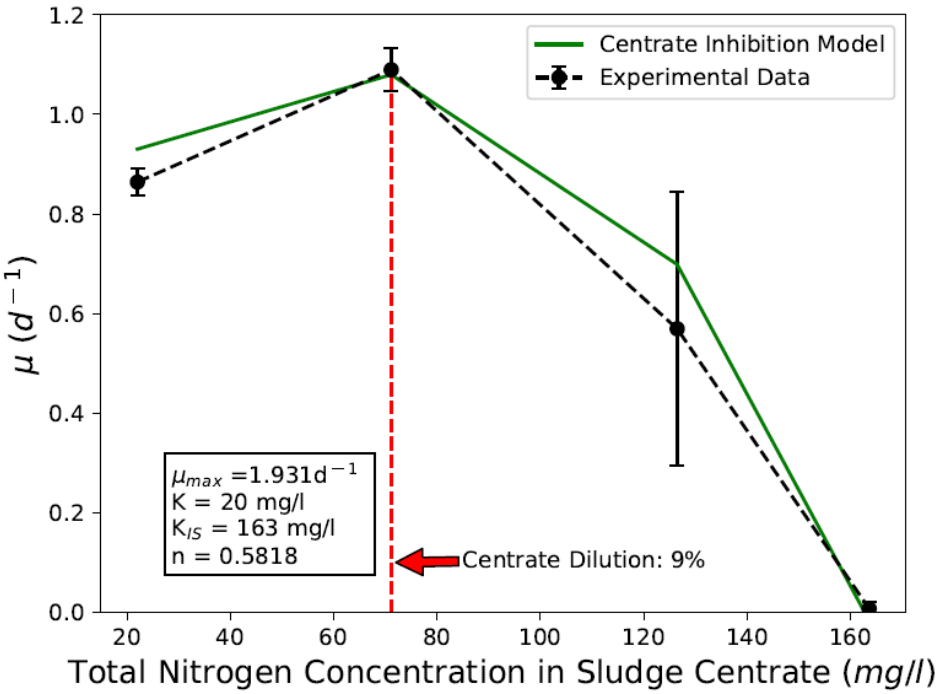

Figure 5.5 Measured and modeled maximum specific growth rates of *Synechocystis* sp. PCC6803 including sludge centrate inhibition.

Figure 5 depicts the measured and modeled dynamics of cyanobacterial biomass growth and nitrogen uptake in sludge centrate (Eq. 5-13). For comparison, Kim et al. (2010, 2011) and Quiroz-Arita et al. (2017) reported *Synechocystis* sp. PCC6803 biomass productivity in the range from 0.12 g.l^{-1}.day^{-1} to 0.76 g.l^{-1}.day^{-1} when it is grown in BG 11 media in photobioreactors at photosynthetic active radiations (PAR) of above 1,000 µmol photons m^{-2}.s^{-1}. Incorporating experimental growth rates of *Synechocystis* sp. PCC6803 with sludge centrate inhibition, this study obtained cyanobacterial biomass productivities of 0.13, 0.17, 0.15, and 0.16 g.l^{-1}.day^{-1} for centrate dilutions of 3 vol%, 9 vol%, 19 vol% (after 7 days of cultivation), and 19 vol% (after 9 days of cultivation), respectively. These results demonstrate that *Synechocystis* sp. PCC6803

biomass productivity is maximized through experiment and modelling at centrate dilutions of 9 vol%.

5.3.3 Nitrogen uptake by Synechocystis sp. PCC 6803

The modeled concentrations of TN discharged from the sidestream photobioreactors are summarized in Table 5.1. TN concentrations in Table 5.1 are presented as upper, mean, and lower concentrations corresponding to the lowest maximum specific growth rates, the mean maximum specific growth rates, and the highest maximum specific growth rates, as measured in the experiments presented in Figure 5.5.

For example, under the CNR 3 vol% centrate dilution scenario, the TN concentration of the growth media after centrifugation is 0.004 $mg.l^{-1}$ (Figure 5.6). This CNR sidestream wastewater treatment scenario meets the requirements of municipal WWTF, and the water quality criteria of the State of CO and the federal EPA. The TN concentration of the treated effluent discharged from the facility is 15.2 mg $N.l^{-1}$ (Figure 5.3, and in Appendix C). For comparison, the nitrogen concentration in the treated effluent from the conventional activated sludge process is 25.9 mg $N.l^{-1}$. These results demonstrate that the combined effluent nutrient concentration and energy requirements are notably reduced when compared to the conventional activated sludge process and the baseline BNR process, respectively.

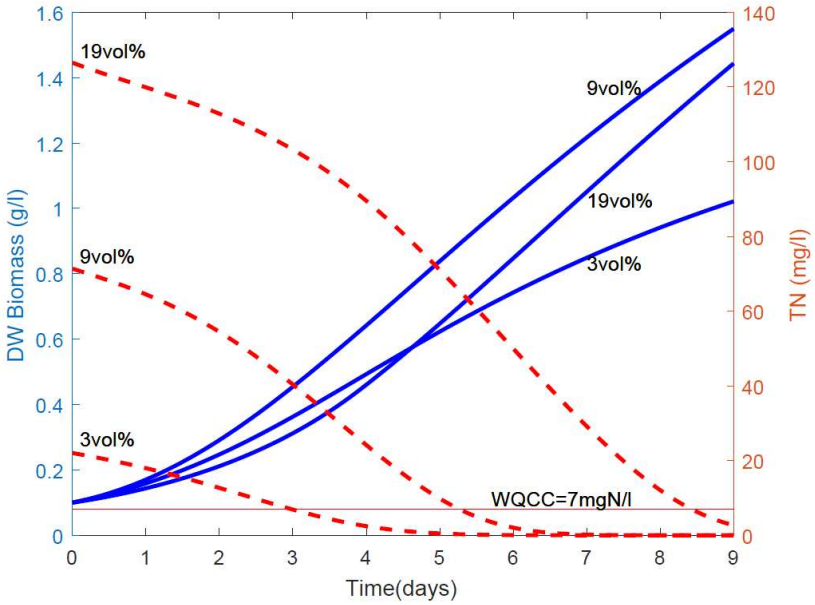

Figure 5.6 Thin layer growth modeling results for *Synechocystis* sp. PCC6803 at sludge centrate dilutions of 3 vol%, 9 vol%, and 19 vol%. The cultivation times of centrate dilutions at 3 vol% and vol9% are seven days. The cultivation time of centrate dilution at 19 vol% is nine days. DWB stands for dry weight biomass. WQCC stands for the water quality criteria for the State of CO, 7 mg $TN.l^{-1}$. DWB and TN are represented by blue straight lines and red dashed lines, respectively.

Table 5.1. Results of *Synechocystis* sp. PCC6803 thin layer growth model under the three centrate dilution scenarios

Parameter	3% Centrate (7 days of cultivation)			9% Centrate (7 days of cultivation)			19% Centrate (7 days cultivation)			19% Centrate (9 days cultivation)		
	Mean	Upper Limit	Bottom Limit	Mean	Upper Limit	Bottom Limit	Mean	Upper Limit	Bottom Limit	Mean	Upper Limit	Bottom Limit
DW biomass ($g.l^{-1}$)[a]	0.9	0.9	0.9	1.2	1.2	1.2	1.05	1.3	0.4	1.4	1.6	0.7
N_r ($mg.m^{-3}.day^{-1}$)[b]	3,100	3,100	3,100	10,200	10,200	10,200	13,900	16,700	5,600	13,800	14,000	6,900
TN effluent ($mg.l^{-1}$)[c]	0.004	0.004	0.004	0.2	0.20	0.20	29	9.7	87	2.7	0.1	64

[a] DW stands for dry weight at stationary stage

[b] N_r stands for nitrogen removal rate

[c] TN stands for total nitrogen at stationary stage

5.3.4 Co-digestion of cyanobacterial biomass with activated sludge

After centrifugation, the cyanobacteria biomass can be used as a feedstock to the existing anaerobic digester unit of a wastewater treatment facility such as DWRF.

Using the methods of section 2.4.4 and Eq. 14 and 15, the model for anaerobic digestion of cyanobacterial biomass provides a yield of 0.15 $m^3CH_4.kg^{-1}$ for *Synechocystis* sp. PCC6803, which closely represents the result for cyanobacteria obtained in previous studies [198]. Anaerobic digestion of sludge at DWRF, on the other hand, provides a yield three times greater than cyanobacteria, 0.48 $m^3CH_4.kg^{-1}$. Co-digestion of the activated sludge and cyanobacterial biomass simulated by the first order system model resulted in the increase in methane productions by 22%, 8%, and 4% for centrate dilution scenarios of 3 vol%, 9 vol%, and 19 vol%, respectively. Figure 5.7 depicts the modeling results for the 3% centrate dilution scenario.

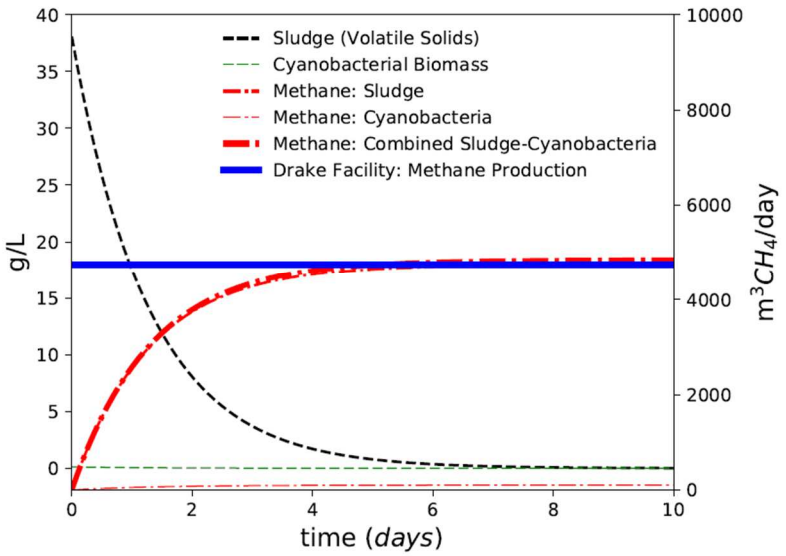

Figure 5.7 Model results for anaerobic co-digestion of activated sludge and cyanobacterial biomass for 3% centrate dilution scenario.

Methane and energy production are maximized at 3% centrate dilution. Biogas can be upgraded in the photobioreactors by carbon dioxide uptake, to close the carbon loop. For example, previous research reported CO_2 removal by *Chlorella* sp. of 23.0 ± 11.8 % [199]. By

Henry's law, we model that 0.067%, 0.012%, and 0.006% of the CO_2 produced, for centrate dilutions of 3 vol%, 9 vol%, and 19 vol%, respectively, will remain in solution (Table C.2), whereas the rest will be released to the environment. By supplying cyanobacterial biomass to the existing anaerobic digester unit of DWRF, the energy recovery of the facility can be increased without additional capital investments.

Table 5.2 Methane production and potential electrical and heat power by co-digestion of activated sludge and cyanobacterial biomass

Centrate Dilution Ratio	Product of Cyanobacteria Biomass m^3 CH_4.day^{-1}	Product of Co-digestion of Sludge and Cyanobacteria Biomass m^3 CH4.day^{-1}	Electric Power (kW)
3%	1067	5,812	376
9%	362	5,107	331
19%[a]	186	4,931	319
19%[b]	212	4,958	321
19%[c]	93	4,838	313

[a] Results obtained from the mean growth rate of *Synechocystis* sp. PCC6803

[b] Results obtained from the upper limit growth rate of *Synechocystis* sp. PCC6803

[c] Results obtained from the lower limit growth rate of *Synechocystis* sp. PCC6803

5.3.5 Life cycle Net Energy and Greenhouse Gas Emissions

As illustrated in Figure 5.8, life cycle net energy and GHG emissions can be minimized among the options modeled here at centrate dilutions of 3%. The propagated uncertainty due to experimental variability (illustrated in Table 5.1 and Figure 5.6) is negligible. These results show that the life cycle energy and GHG emissions are reduced by 8% and 17%, respectively,

relative to the baseline BNR process. The results from an LCA suggest that the centrate dilution of 3 vol% improves the water quality, and reduces the environmental impacts in terms of life cycle energy use and GHG emissions normalized by the volume-specific nitrogen removal rate.

Although the 3% scenario is most preferred using the metrics of this LCA, there are reasons to consider the costs and benefits of the other scenarios. For example, the 9 vol% scenario has the lowest net energy normalized by the treated wastewater of 1.42 kWh. m^{-3}, and the lowest land requirements of 1.39 ha (Table C.3). Further research targeting the global optimization of sustainability and techno-economic metrics will clarify the potential for tradeoffs among these options.

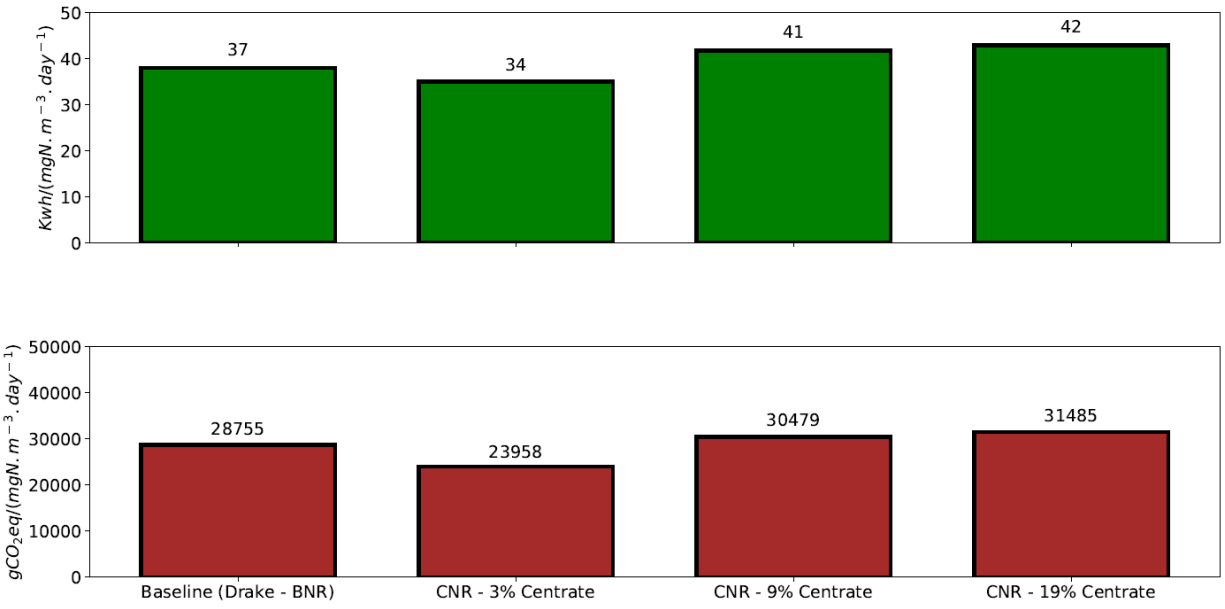

Figure 5.8 Life cycle net energies and GHG emissions of baseline wastewater treatment facility and combined system with CNR process for sidestream wastewater treatment.

5.4 Conclusions

This study presents a novel cyanobacterial nutrient removal process for sidestream wastewater treatment. Parameters associated with the cyanobacterial growth and anaerobic co-digestion models were determined experimentally. Resources recovery was investigated by

experimental and computational modeling of struvite precipitation, electric power, and combined heat and power generation. This research demonstrates that among the centrate dilution scenarios of 3 vol%, 9 vol%, and 19 vol% assessed in in this study, the system operating at 3 vol% centrate dilution was the most sustainable system in terms of nitrogen discharge concentration, net energy to nitrogen removal ratio (NENR), and the GHG emissions to nitrogen removal ratio. Next steps for this novel technology are to demonstrate scalability at pilot scale in municipal wastewater treatment facilities, and to optimize the cost, footprint, operations that would be required by integration of photobioreactors and raceways on to WWTF facilities.

5.5 Answer to Research Question 2.1

This section of the research effort has allowed us to address Research Question 2.1, which is restated here:

To what extent are the joint achievement of sustainability, scalability, and water quality goals assisted by the integration of CBR and WWTF?

Research Question 2.1 is associated with Hypothesis 2.1:

Integration of CBR and WWTF provides synergistic lifecycle benefits including the displacement of fertilizers for cyanobacteria cultivation by wastewater nutrients, reduction of energy consumption to remove nutrients from the treated wastewater, and improvement of water quality from wastewater facilities.

Chapter 4 reviewed the growth and productivity of algae and cyanobacteria grown in wastewater resources. This review suggests that sludge centrate obtained from wastewater facilities is the most promising resource to grow algae and cyanobacteria due to high concentrations of nitrogen and phosphorous. This integration has the potential to contribute to the biological nutrient removal in wastewater facilities.

Chapter 5 developed a novel integration of wastewater treatment facility and cyanobacterial cultivation, modeled and evaluated this proposed system against joint metrics for energy and carbon footprint. This chapter demonstrates that cyanobacteria is capable of growing in sludge centrate obtained from wastewater facilities, with the potential to contribute to the biological nutrient removal and wastewater remediation in wastewater treatment facilities, and to reduce WWTF life cycle energy and GHG emissions. Additional experimental validation of this process at large scale is required to enable commercialization of this technology.

The results of these studies provide support to the hypothesis that synergistic benefits are obtained, including displacement of fertilizers for cyanobacteria cultivation by wastewater nutrients, reduction of energy consumption to remove nutrients from the treated wastewater, and improvement of water quality from wastewater facilities.

CHAPTER 6: Sustainability Implications of Mixing Energy for the Industrial Scale Design of Cyanobacterial Cultivation in Open Raceway Ponds and Flat-Panel Photobioreactors[5]

6.1 Introduction

Photoautotroph-based biofuels are considered one of the most promising renewable resources to meet the global energy requirements for transportation systems [5]. Long-term research and development has resulted in demonstrations of microalgae areal oil productivities that are higher than crop-based biofuels, about 10 times that of palm oil and about 131 times that of soybean [5, 74-76]. Cyanobacteria is reported to have ~4 times the areal productivity of microalgae on an equivalent energy basis [6]. Downstream of this cultivation process, cyanobacterial biomass and bioproducts can be supplied to biorefineries producing feed, biomaterials, biosynthetic chemicals, and biofuels [77]. As such, cyanobacterial systems can be a significant contributor to more sustainable energy and production systems.

Turbulent environments are demonstrated to induce physiology responses in photoautotrophic microorganisms in open raceway ponds and photobioreactors [200-207]. Recent efforts studied the effects of turbulence dissipation rates ranging from 0 to $8.01E^{-2}$ $m^2.s^{-3}$ simulated at laboratory scale conditions (1 liter cultures) [200]. This work concluded that despite no alterations of photosynthesis activity and chlorophyll a, there is a systematic increment in the growth rates of the strain *Microcystis flos-aquae* as a function of turbulence dissipation rate and a subsequent decay in the growth rate of the strain *Anabaena flos-aquae* at high turbulence. These authors identified a maximum phosphorous uptake rate by these cyanobacteria strains at turbulence dissipation rates of $2.26E^{-2}$ $m^2.s^{-3}$, suggesting that turbulence plays an important role

[5] **This chapter is adapted from a prepared journal article for consideration for publication:** Carlos Quiroz-Arita, Kenneth F. Reardon, Pengyu Cao, Peter Chen, Jason C. Quinn, Thomas H. Bradley. "Sustainability Implications of Mixing Energy for the Industrial Scale Design of Cyanobacterial Cultivation in Open Raceway Ponds and Flat-Panel Photobioreactors".

in the biological adaptation of cyanobacteria by influencing nutrient uptake [200]. In other research, the effects of shear environments were studied for the cyanobacteria and microalgae strains *Synechocystis sp.* and *Chlamydomonas reinhardtii*, respectively, in 150 ml cultures [201]. In this study the growth rate of *Synechocystis sp.* was independent of shear stress (0 to 0.18 $N.m^{-2}$) and *Chlamydomonas reinhardtii* growth rate was linearly dependent on shear stress. These laboratory scale environments; however, are not representative of industrial scale conditions. Other impacts of turbulent mixing are cell disruption due to shear stress [208-215]. Some instances are for hybridoma cells suffering apoptosis at mixing energy inputs of $1.87E^3$ $W.m^{-3}$ [209, 216]. Other studies observed 51% lower recombinant protein production, 42% higher glucose uptake, and 50% lower lactate production cells exposed to mixing energy inputs of $6.4E^2$ $W.m^{-3}$ [209, 217]. Inhibitory effects; however, are reported at mixing energy inputs above $1E^6$ $W.m^{-3}$ and Kolmogorov microscales about less than or equal to 2.4 micrometers for mammalian cells [209]. In photobioreactors, small bubbles are reported to cause cell damage [205, 218], colliding with photoautotrophic cells and maintaining a sheared environment. The microalgae strain *Phaeodactylum tricornutum*, for instance, presented inhibition at air rates of 0.567 $m^3_{air}.min^{-1}.m^{-3}_{reactor}$, where carboxymethyl cellulose (CMC) and carboxymethyl cellulose were supplied into the medium to mitigate shear-induced damage in parallel experiments [205]. Other sparged photobioreactors cultivating *Dunaliella tertiolecta* and *D. salina* reported increments in the decay rates as a function of gas velocity, observing the highest death rates at 8.91 and 13.37 $m^3_{air}.min^{-1}.m^{-3}_{reactor}$ [218]. There is no research reported in the literature concerning the biological system response due to shear stress on cyanobacteria cells disruption, particularly on *Synechocystis sp.* PCC6803. Moreover, most of the previous research were conducted at mixing

energy inputs are 30, 100, or thousands order of magnitudes higher than is considered cost-effective for industrial cultivation systems.

Photoautotrophic biomass and biofuels productivity; therefore, are overestimated at laboratory scale experiments relative to industrial scale systems. This distinct difference in the performance of industrial systems are partially attributed to the light experienced by photoautotrophic microorganisms at outdoor conditions. For instance, the light saturation of *Synechocystis sp.* PCC6803 is reported at about 200 μmol photons.s^{-1}.m^{-2} [10, 84], whereas photoautotrophic microorganisms will face incident radiations of about 2000 μmol photons.s^{-1}.m^{-2} at noon in locations such as Colorado [11], impacting in the photo conversion efficiency. For the case of algae considering that 46% of the spectrum is in the photosynthetic active radiation (PAR) range of 400 to 700 nm, there are losses due to photon transmissions efficiency of 95%, photon utilization efficiency ranging from 10% to 30%, biomass accumulation efficiency of 50%, and biomass energy content of 21.9 kJ·g^{-1}, resulting in a total photo conversion efficiency from 2.6% (at high light) to 6.3% (at reduced light) [12]. The low photo conversion efficiency is attributed to dark and photorespiration biomass losses [62, 219, 220]. Photorespiration switches the carboxylation step in the Calvin–Benson cycle to oxygenation, dissipating photic energy and accounting for 25% reduction in the photosynthesis in C_3 plants [221]

Some previous studies have investigated the effects of mixing rates on photoautotroph biomass productivities in industrial scale systems [11, 53, 54]. Some of these efforts have identified optimum volumes of air flow rates per unit volume (VVM) of photobioreactors that might be industrially relevant for microalgae, 0.2 to 1.2 $m^3_{air}.min^{-1}.m^{-3}_{reactor}$ [11]. Many others have considered mixing energy inputs that are far outside the energy consumption that can be

considered economic, or industrially relevant, ranging from 8 to 633 $W.m^{-3}$ [53]. For raceway ponds, for instance, energy inputs from 1 to 2 $W.m^{-3}$ are utilized in the algae cultivation demonstrations performed to date [54].

There is limited research concerning the impacts of mixing energy inputs in the life cycle metrics of cyanobacterial derived biofuels [17, 174]. Previous work, for instance, consider robust modelling strategies due to the uncertainties in the mixing energy inputs. Other research evaluated the implications of mixing on growth rates and biomass productivity [11]. Maximizing microalgal and cyanobacterial biomass and bioproducts; however, provide a limited insight into the sustainability of these systems. Net Energy Ratios (NER), provide a more meaningful and exhaustive understanding of the energy efficiency and sustainable system design. To fill this research gap; therefore, we conducted (i) pilot scale experimentation cultivating *Synechocystis* sp. PCC6803 in open raceway ponds and flat-panel photobioreactors at industrially relevant mixing energy inputs and high incident radiations, (ii) evaluation of the effects of differences in mixing energy input in the growth rates and biomass productivities, and (ii) a holistic life cycle assessment modelling integrating the system response in terms of NER due to mixing energy inputs. By developing an integrated approach for laboratory experimentation and industrial-scale metrics of mixing at photo-inhibited light intensities, we obtain reliable models to quantify the sustainability of these novel biotechnology. These capabilities are required to be able to perform long-term and industrially relevant assessments of the costs, and benefits of these promising technologies, and will serve to inform the biological engineering research and development of new organisms.

6.2 Materials and Methods

To evaluate the implications of turbulent mixing in large scale open raceway ponds and flat-panel photobioreactors from laboratory experimentation, industrially relevant mixing energy inputs must be taken into account for cultivation of cyanobacteria and modelling. The workflow, illustrated in Figure 6.1, integrates *Synechocystis* sp. PCC6803 cultures scale-up and acclimation at photo-inhibited light intensities, cultivation in flat-panel photobioreactors and open raceway pond at industrially relevant mixing rates, and sustainability modelling by an LCA framework. By incorporating laboratory experiments at industrially relevant inputs, outdoor relevant light intensities and large-scale mixing rates, we developed a holistic bridge and feedback loop approach between laboratory and industrial scale experimentation.

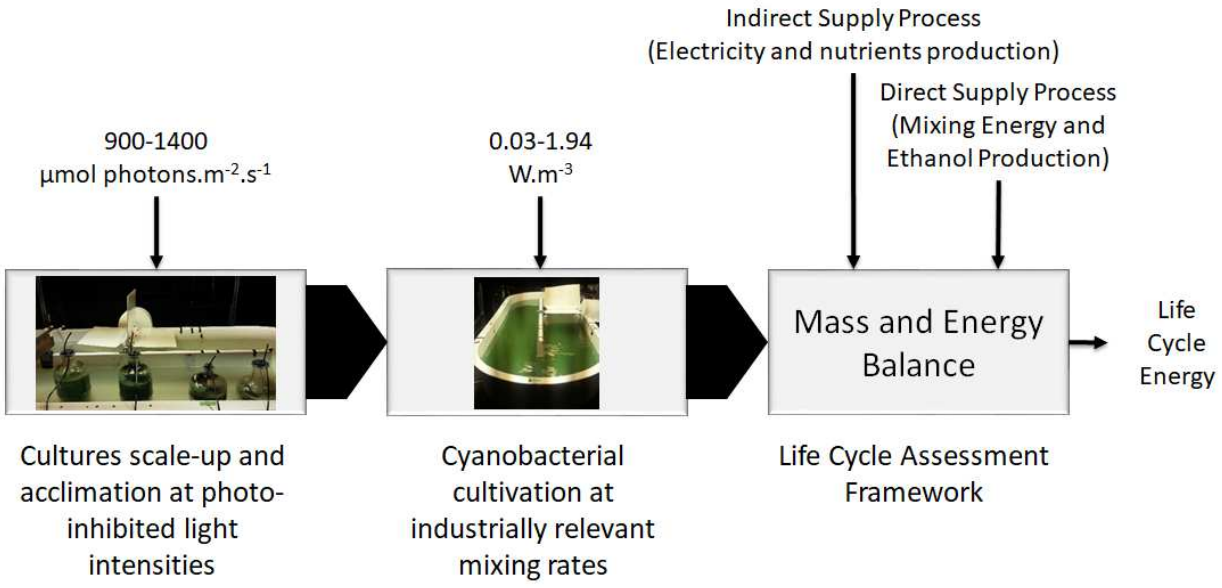

Figure 6.1 Workflow for industrial scale cyanobacterial derived biofuel assessment from bench and pilot scale experimental and model based analysis.

6.2.1 Scale-up and Acclimation of Cyanobacterial Cultures

To inform the cyanobacteria growth and the LCA models, *Synechocystis* sp. PCC6803 cells were cultured in culture media (BG-11), scaling-up and acclimating at photo-inhibited light

intensities for cultivation in 1L flat-panel photobioreactor and 700L open raceway pond, respectively. Cells were grown at 29 °C. The inoculum of 250 µL were scaled-up into 30 mL and 150 mL, grown in constant light fluxes of 60 µmol photons $m^{-2}.s^{-1}$. For acclimation in 1L flat-panel photobioreactors, 150mL cultures were inoculated into five replicates, grown in constant light fluxes of 1348 (± 84) µmol photons $m^{-2}.s^{-1}$. 10% of the acclimated cyanobacteria cultures were re-inoculated in the flat-panel photobioreactors and grown until stationary stage. For cyanobacteria cultivation in raceway ponds, the 150 mL cultures were furtherly scaled-up into 1L flasks. The 1L cultures were inoculated into 9L glass carboys, which were acclimated by using the raceway pond as a water bath at 29 °C., grown in constant light fluxes of 938 (± 46) µmol photons $m^{-2}.s^{-1}$. The 700L open raceway pond was inoculated with the 9L glass carboys cultures and grown until stationary stage.

6.2.2 Configuration for Industrially Scale Experimental Analysis of flat-Panel Photobioreactors and Open Raceway Ponds

For validation purposes of the growth and LCA models, we performed experimental work under mixing energy input variability in the flat-panel photobioreactor and open raceway pond. As illustrated in the diagram developed in Autodesk® AutoCAD® 2018, Figure 6.2, the batch process was carried out in five replicates of 1L flat-panel photobioreactors made in acrylic with surface to volume ratio of 112 $m^2 \cdot m^{-3}$. The experiments were performed at cultures depths of 20 cm. The carbon system in each flat-panel photobioreactor was normalized by scrubbing CO_2 from the supplied air with soda lime and adding 0.483 $g.day^{-1}$ of bicarbonate. Additional experiments were performed with sparged air and no addition of bicarbonate, to evaluate the mixing energies at which cultures grow limited by carbon. The cultures were grown using a high-pressure sodium (HPS) lighting system with a spectrum ranging from 400 to 700 nm at

extreme conditions, emulating a sunny day at a constant Photosynthetic Active Radiation (PAR) of 1348 (± 84) μmol photons·m^{-2}·s^{-1}. A temperature control system was provided to maintain a temperature of 32 (± 2) °C, consisting of cold plates set at the bottom of each photobioreactor and chilled water supplied through copper pipelines. In this study we aimed to resemble the light attenuation of open raceway ponds in the flat-panel photobioreactors, by providing absorptive walls (black plastic corrugated sheets) to simulate a cross section of the culture into the raceway pond. Cultures were mixed by sparged air at the bottom of the flat-panel photobioreactors at industrially relevant mixing inputs of 0.7, 0.35, and 0.17 m^3 of air per minute per cubic meter of reactor, commonly referred as VVM [11]. Additionally, experiments by an order of magnitude lower were performed, set at 0.01 VVM. The equivalent mixing energy inputs used in the flat-panel photobioreactors experiments were 1.94, 0.97, 0.47, and 0.03 $W.m^{-3}$.

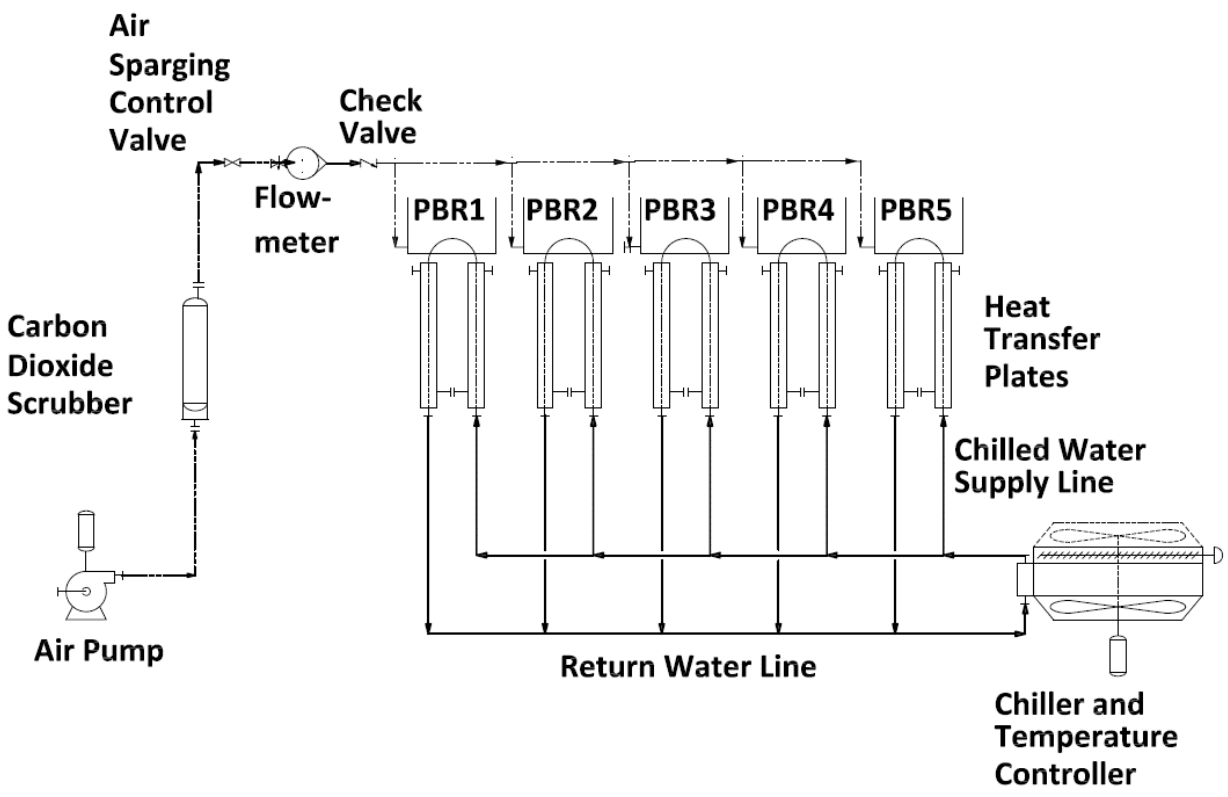

Figure 6.2 Instrumentation Diagram of Flat-panel photobioreactors system for industrial scale experimental and model based analysis.

As illustrated in the diagram developed in Autodesk® AutoCAD® 2018, Figure 6.3, the open raceway pond batch process was carried out in a 700L fiber-reinforced plastic at water depths of 20 cm. Three replicates were cultivated for statistical validity purposes. The cultures were grown using a high-pressure sodium (HPS) lighting system with a spectrum ranging from 400 to 700 nm at extreme conditions, a Photosynthetic Active Radiation (PAR) of 938 (± 46) μmol photons·m^{-2}·s^{-1}. A temperature control system was provided to maintain the cultures at 29 °C; consisting of a thermocouple, temperature controller, solenoid valve, stainless steel coil submerged into the open raceway pond, and tap water supply pipeline. The culture was mixed with a paddlewheel provided with a 90V DC Gearmotor with a rated torque of 33 in.-lb controlled by an IronHorse DC Drives. The mixing energy input used in the open raceway pond

experiments was 0.10 W.m^{-3}, an order of magnitude lower than reported in the literature for industrial systems [54].

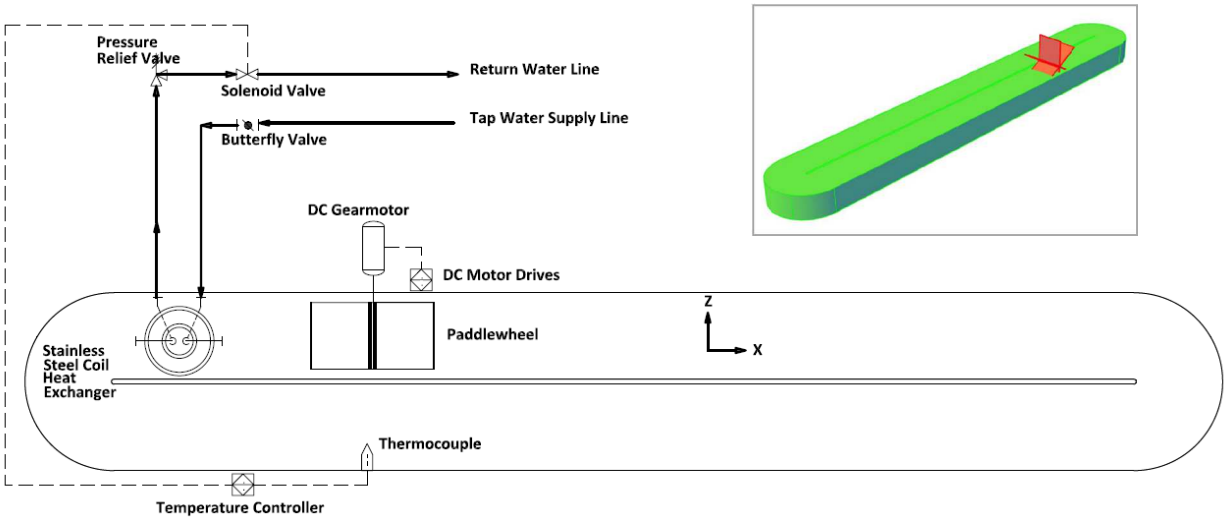

Figure 6.3 Plan View and Instrumentation Diagram of Open raceway pond system for industrial scale experimental and model based analysis. The 3D view of the Open Raceway Pond is illustrated in the upper right corner.

6.2.3 Flat-panel photobioreactors and open raceway pond monitoring

Growth rates of liquid cultures were monitored using SPECTRONIC 20 Genesys^{TM} with a frequency of eight hours. Dried weight biomass (DWB) was measured daily with 2.5 µm polypropylene prefilters dried at 60 °C and measured with high precision digital scale. The incident radiation and light attenuation were measured daily with a LI-250A Light Meter at the water surface. The maximum growth rate of *Synechocystis* sp. PCC6803 was mathematically described by Eq. 1 [222], where all the parameters were determined experimentally (Fig. D.1 and D.2) and discussed under results section.

$$\mu_{max} = \frac{ln(X_2/X_1)}{t_2 - t_1} \qquad \text{Eq. 1}$$

X_2 and X_1 are the final and initial, respectively, optical density (OD) in the exponential stage of the growth curve, t_2 and t_1 are the final and initial, respectively, time in the exponential stage of the growth curve, *and* μ_{max} is the maximum specific growth rate.

6.2.4 Life cycle Energy Implications of Mixing Energy Inputs

LCA is a framework for evaluating the energy use, emissions and impacts of direct, indirect, and supply chain processes [16]. An LCA model was developed in this study to assess the system implications of mixing energy input in cyanobacteria-based biofuel facility. This LCA considers biomass productivities from the cyanobacteria growth model described in section 2.3 and ethanol yields of *Synechocystis* sp. PCC6803. Cyanobacteria-based ethanol yields were computed from the carbon partitioning assimilated, 63%, reported in the literature for *Synechocystis* sp. PCC6803 [79]. In developing the goals and scope of this project, cyanobacteria-based ethanol production was chosen because is a near-term and commercially promising technology [17, 174], displays the highest productivities and rates of carbon partitioning [79], and could potentially meet the environmental goals as for renewable fuels in the U.S. [80].

6.2.4.1 System boundary and Functional Unit

The boundaries of the combined growth, extraction and conversion systems researched in this LCA are illustrated and summarized in Figure 6.4 [174]. The processes considered for this study start with the growth stage of the cyanobacteria, and end at the point of conversion of the bioproducts to a biofuel which can displace conventional fuels. The system includes the direct energy requirements of the facility. The water and nutrient requirements are supplied by recycled commercial water and commercial/industrial fertilizers. Carbon dioxide is assumed to be obtained from waste streams from local industrial CO_2 facilities including power plants, amine

natural gas treatment plants, and fermentation plants. The functional units for this study are the energy produced from biofuels to displace petroleum fuels, in MJ.

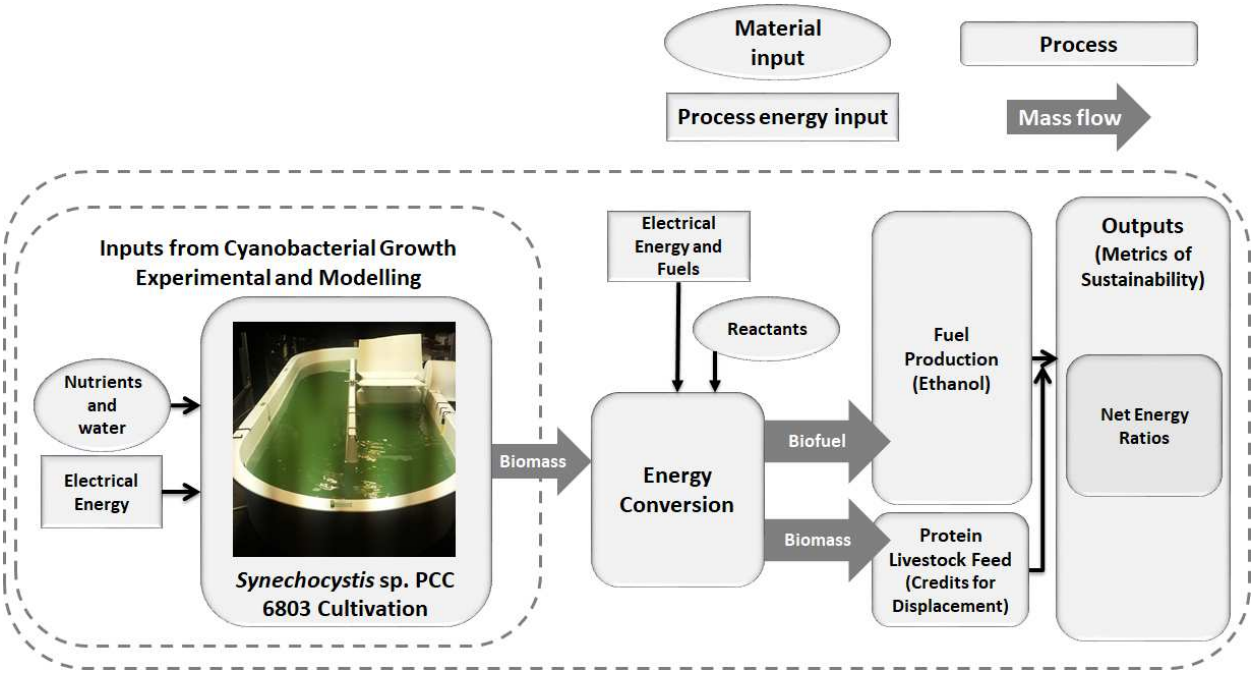

Figure 6.4 Boundaries and inputs of cyanobacterial derived biofuel LCA model. Adapted from Carlos Quiroz-Arita, John J. Sheehan, Thomas H. Bradley. Algal Research 26 (2017): 445-452.

6.2.4.2 Impacts considered

The sustainability metric and impacts considered in this study is net energy ratio (NER). The production of biofuel as an energy carrier is the primary goal of any potential biofuel technology [174]; therefore, net energy ratios (Eq. 11) was the metric of interest for this LCA.

$$NER = \frac{E_{consumed}}{E_{produced}} \quad \text{Eq. 11}$$

NER are defined in this study by normalizing the energy consumed ($E_{consumed}$) in the cyanobacteria growth, fuel extraction, and conversion processes by the energy produced ($E_{produced}$) by this system as embedded in the lower heating value of the biofuel.

6.2.4.3 LCA tools

The bioenergy system was modeled in the GaBi 6 software by constructing a model as a function of mixing energy input in the cultivation stage. GaBi is a tool that allows for the estimation of the lifecycle energy and emissions output of a process as a function of the energy, material consumed for that process [223]. The GaBi model was used to calculate the lifecycle, material consumption, and net energy use for the lifecycle of the cyanobacteria-to-biofuel process [174].

In evaluating the life cycle energy consumption of the cyanobacteria-to-biofuel process, the biomass that is not converted to fuel can be considered as a co-product. For this study, the cyanobacteria co-product credits are allocated using the displacement method. The displacement method assumes that the co-product displaces a preexisting conventional product. The displacement co-product credits represent the lifecycle energy that would be required to produce the displaced product. Co-product credits are subtracted from the overall energy of the cyanobacteria-to-biofuel process [174].

6.3 Results and Discussion

The results of this research are synthesized into three aspects. First, the biological responses of *Synechocystis* sp. PCC 6803 due to mixing energy input variation in the system are evaluated by the experimentally determined maximum growth rates and cyanobacterial biomass productivities. The significance of the response is evaluated by a one-way analysis of variance (ANOVA) and the physical processes that potentially impact this biological response are put into perspective. Second, the influence of turbulence mixing in the light experienced by either single *Synechocystis* sp. PCC 6803 cells or the bulk cyanobacterial biomass is evaluated by a well-mixed growth model validated with the experimental work in the flat-panel photobioreactors and

open raceway pond, respectively. Lastly, the implications of differences in mixing energy input in the system design and sustainability of cyanobacterial derived biofuels, particularly ethanol, are evaluated by the life energy, in terms of NER. The significance of the NER response due to mixing energy input is evaluated by a one-way ANOVA. Propagation of uncertainty in the LCA model considers the experimental error in the maximum growth rates of *Synechocystis* sp. PCC 6803, error in cyanobacterial biomass productivities, and error in biomass to ethanol conversion (0.108 to 0.280 $MJ_{Energy\ Consumed} \cdot MJ_{biofuel}^{-1}$).

6.3.1 Industrially relevant mixing energy inputs control physiological responses of *Synechocystis* sp. PCC 6803

Industrially relevant mixing energy inputs are proven to control the biological responses of *Synechocystis* sp. PCC 6803. While previous efforts evaluated the impact of mixing on microalgae growth, most of the research performed up-to-date considered uneconomic energy inputs for the industry, and the implications in the cultivation of *Synechocystis* sp. PCC 6803 in flat-panel photobioreactors and open raceway ponds are ignored. By performing experimental cultivation of this cyanobacteria strain using high incident radiations and industrially relevant mixing energy inputs, we have developed a comprehensive approach to predict the biological performance in industrial cultivation systems.

The maximum growth rates (μ_{max}) of *Synechocystis* sp. PCC 6803 and cyanobacterial biomass productivities are illustrated in Figure 6.5 and 6.6, respectively. From the experimental work performed in this research, cyanobacterial growth is demonstrated to be feasible at the lowest mixing energy inputs in flat-panel photobioreactors, 0.03 $W.m^{-3}$ and 0.47 $W.m^{-3}$, and at higher maximum growth rates and biomass productivities than observed at mixing energy inputs of 0.97 and 1.94 $W.m^{-3}$. The mixing energy input of 0.47 $W.m^{-3}$ is equivalent to an air mixing

rate of 0.17 VVM. The biological metrics at this mixing energy input were measured at 1.29 ± 0.23 d^{-1}, 0.90 ± 0.15 $g.l^{-1}$ in a residence time of 3.86 days or a productivity of 0.23 $g.l^{-1}.d^{-1}$. The significance of the biological response due to mixing energy input, particularly at mixing energy inputs of 0.47 $W.m^{-3}$, is confirmed by observing probabilistic values less than 0.05 (Figure 6.5 and 6). The 0.17 VVM evaluated in this research for *Synechocystis* sp. PCC 6803, is one third the value observed as optimal for *Nannochloropsis salina* cultivation by J.C. Quinn et al. (2012). Moreover, the mixing energy input were the biological metrics for *Synechocystis* sp. PCC 6803 are maximized in these experiments, are from 2 to 100 order of magnitudes lower than reported for various microalgae strains by Jones et al. (2017). Additionally, the mixing energy input for the cultivation of *Synechocystis* sp. PCC 6803 in open raceway pond was performed from 1 to 2 order of magnitudes lower, 0.1 $W.m^{-3}$, than reported in the industry by Sompech et al. (2012). The maximum growth rate and biomass productivity obtained from cultivation of *Synechocystis* sp. PCC 6803 in open raceway pond at 0.1 $W.m^{-3}$ are 0.76 ± 0.07 d^{-1} and 9.65 ± 1.77 $g.m^{-2}.d^{-1}$. These findings have significant implications for industrial cultivation of cyanobacteria, proven in this work to be feasible at lower mixing energy inputs than reported in the literature, potentially contributing to reduce operational costs due to energy requirements in this stage of the system.

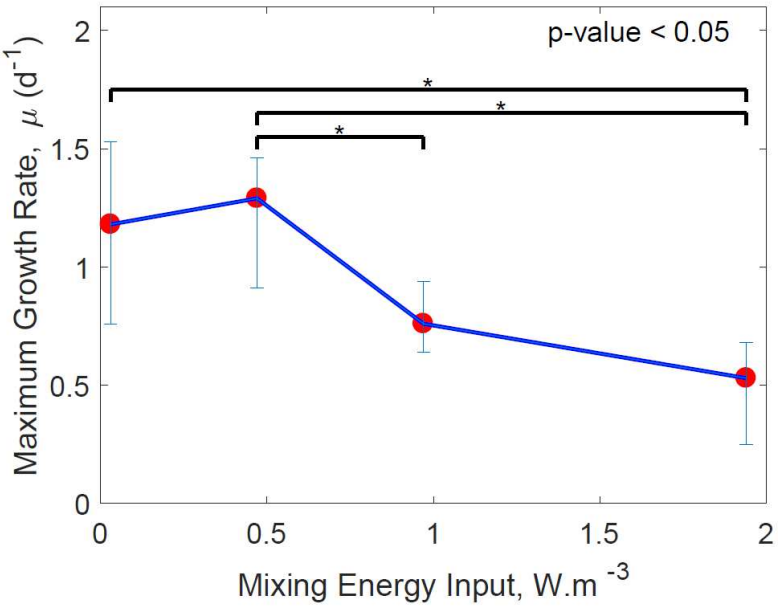

Figure 6.5. Maximum growth rate of *Synechocystis* sp. PCC 6803 in flat-panel photobioreactors. The p-value or probability value was obtained from the one-way ANOVA in Matlab®. The horizontal bars and stars link the groups that have means significantly different from each other as evaluated by the one-way ANOVA.

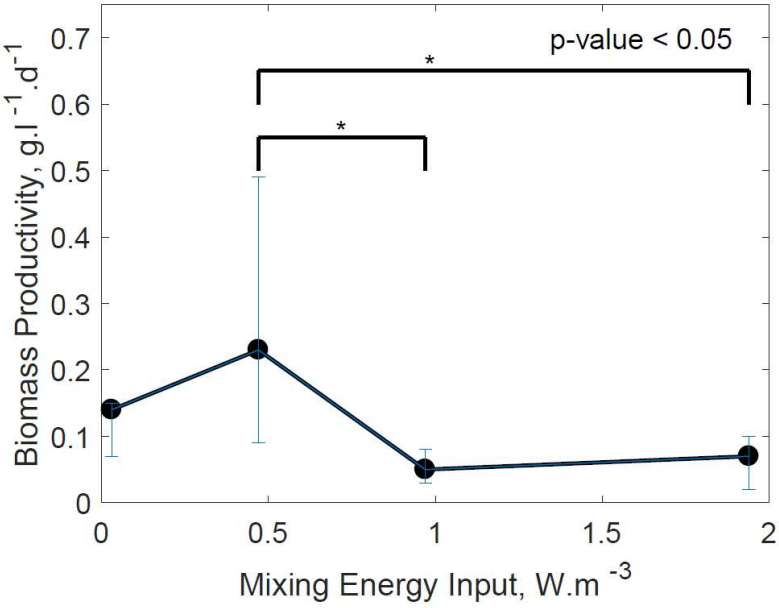

Figure 6.6 Biomass productivity of Synechocystis sp. PCC 6803 in flat-panel photobioreactors. The p-value or probability value was obtained from the one-way ANOVA in Matlab ®. The horizontal bars and stars link the groups that have means significantly different from each other as evaluated by the one-way ANOVA.

A potential driver of the biological responses observed in this work is the shear stress, constraining the growth and productivities at certain physical conditions in flat-panel photobioreactors and open raceway ponds. The mixing energy inputs were abrupt inhibition were observed in the flat photobioreactor, 0.97 and 1.94 $W.m^{-3}$; however, are yet from 100 to 200 order of magnitudes lower than the mixing energy where hybridoma cells suffered apoptosis as reported by Al□Rubeai et al. (1995) and Chalmers (2015). Comparing to the mixing energy inputs reported to by Keane et al. (2003) for mammalian cells, these are from 30 to 60 order of magnitudes higher than the values used for *Synechocystis* sp. PCC 6803. Although there is no concluding evidence of *Synechocystis* sp. PCC 6803 cells disruption due to shear stress in this research, the VVM where complete inhibition was observed, 0.70 $m^3_{air}.min^{-1}.m^{-3}_{reactor}$, is from one to two order of magnitudes lower than the air rates reported by Barbosa & Wijffels (2004) where the highest death rates were observed for *D. tertiolecta* and *D. salina*, a microalgae strain lacking of cell wall. However, the air rate where inhibition was reported for the *Phaeodactylum tricornutum* by Mirón et al. (2003) is the same order of magnitude, 0.567 $m^3_{air}.min^{-1}.m^{-3}_{reactor}$, of the air rate where inhibition is observed for *Synechocystis* sp. PCC 6803 in this research. This strain as a matter of fact, a diatom, contains a cell wall made of silica. *Synechocystis* sp. PCC 6803, on the other hand, presents a peptidoglycan layer of bacterial cell wall; therefore, cell disruption due to shear-induced damage is likely in turbulent and sheared environments such as the sparged flat-panel photobioreactor studied in this research. Nozzle size and bubbles formation at the sparger in photobioreactors has been claimed to be the cause of cell disruption [218]; therefore, the differences in the configurations used in past and present research limits the understanding of shear stress among the studies performed to date. A future direction to understand the biological responses of cyanobacteria from turbulence mixing and shear stress is

the application of Mechanomics, an emerging field that explains how external forces in the environment are sensed by cells and how they send signals to activate biological responses [208].

6.3.2 Synechocystis sp. PCC 6803 grows limited by carbon at low mixing energy inputs

The experimental results of cyanobacterial biomass productivity as a function of mixing energy inputs are illustrated in Figure 6.7, 6.8, D.3, D.4, and D.5. The one-way ANOVA results of the experimental biomass productivities are included in the Appendix D, Figure D.7, demonstrating a significant influence of mixing energy inputs as illustrated in the p-value less than 0.05. By incorporating light attenuation into the well-mixed cyanobacterial growth model of flat-panel photobioreactors, measured from the mixing energy inputs of 0.47 $W.m^{-3}$, as a function of culture depth and dry weight biomass (DWB) (Figure D.5), the model was valid for all the experiments performed at different mixing energy inputs (Figure 6.7, D.3, D.4, and D.5). by comparing experimental and computational growth performed with normalized carbon content (scrubbed CO_2 and bicarbonate addition) relative to experiments performed with sparged air (containing atmospheric CO_2), under identical mixing energy inputs, carbon was demonstrated to be the limiting nutrient for growth of *Synechocystis* sp. PCC 6803 at the lowest mixing energy input in this research, 0.03 $W.m^{-3}$ (Figure 6.7, D.3, D.4, and D.5). For this mixing energy input; for instance, if carbon is constrained to the concentrations contained in the air, 0.0011 $g.l^{-1}.min^{-1}$, this would be below the concentrations where growth is inhibited, 0.005 $g.l^{-1}$, as previously published by Kim et al. (2011).

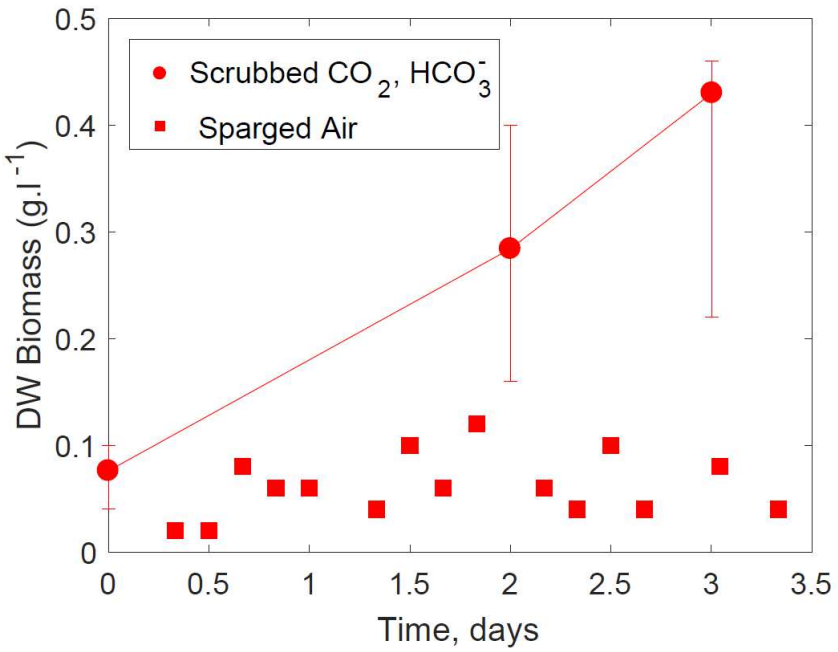

Figure 6.7 Flat-panel photobioreactor experimental growth of Synechocystis sp. PCC 6803 at mixing energy inputs of 0.01 $W.m^{-3}$. The error bars denote the upper and lower values from five experimental replicates. The cultures were cultivated at 31 ± 1 °C and 1,244 ± 47 µmol photons.s^{-1}.m^{-2}.

The biomass of *Synechocystis* sp. PCC 6803 for the open raceway pond at mixing energy input of 0.10 $W.m^{-3}$ is illustrated in Figure 6.8. The open raceway pond is operated at mixing energy inputs of 0.10 $W.m^{-3}$, an order of magnitude lower than reported by Sompech et al. (2012) was used for cultivation. Lower biomass productivities observed in the open raceway pond relative to the flat-panel photobioreactors, suggests that open raceway ponds operated in ourdoor conditions where carbon supply is not feasible growth limited by this macronutrient. To summarize, turbulent mixing more likely impact biological responses due to cell disruption induced by shear stress and constraining the carbon in the system controlled by sparged air.

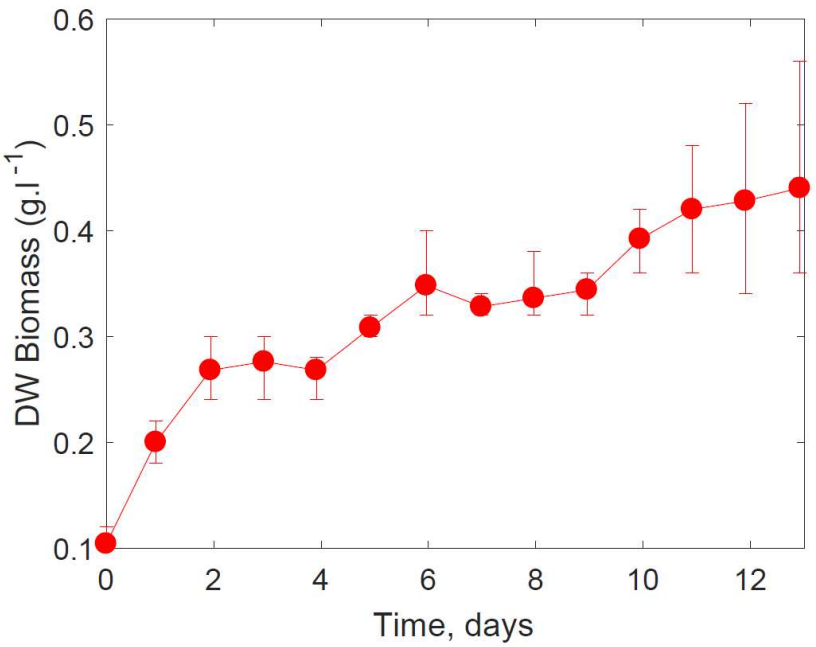

Figure 6.8 Open raceway pond experimental growth of Synechocystis sp. PCC 6803 at mixing energy inputs of 0.10 $W.m^{-3}$. The error bars denote the upper and lower values from five samples. The cultures were cultivated at 29 °C and 915 ± 79 µmol $photons.s^{-1}.m^{-2}$.

6.3.3 Low mixing energy inputs for cultivation in open raceway ponds and flat-panel photobioreactors reduce the life cycle energy of cyanobacterial biofuels

The system performance of cyanobacterial derived ethanol, as a function of mixing energy inputs in open raceway ponds and flat-panel photobioreactors, is evaluated by an LCA. By propagating the experimental uncertainty and the energy conversion, we have developed an inclusive model to evaluate the sustainability of cyanobacterial derived ethanol. These results will inform biology and engineering researchers, the industry, and policy makers to develop strategies to design new strains, bioprocesses, pathways, and incentives towards a more sustainable production of photoautotrophic biofuels.

The life cycle energy results for the open raceway pond and flat-panel photobioreactors, measured as the energy consumed that is normalized by the energy produced by the system,

NER, is illustrated as a function of mixing energy input in Figure 6.9. The one-way ANOVA results of the experimental biomass productivities are included in the Appendix D, Figure 6.9 and D.8, demonstrating a significant influence of mixing energy inputs as illustrated in the p-value less than 0.05. The response is more significant at mixing energy inputs of 0.47 $W.m^{-3}$ relative to the highest mixing energies studied. The life cycle results demonstrate that despite mixing energy inputs of 0.10 $W.m^{-3}$ used for cyanobacteria cultivation in open raceway ponds, an order magnitude lower than reported by Sompech et al. (2012), the lower cyanobacterial biomass and ethanol productivities of *Synechocystis* sp. PCC 6803 relative to the flat-panel photobioreactors make this pathway uneconomic and unsustainable as illustrated by the highest NER (Figure 6.9). The growth of *Synechocystis* sp. PCC 6803 in open raceway pond at this mixing energy input; however, was limited by carbon, unlike the experiments performed in flat-panel photobioreactors with normalized carbon content.

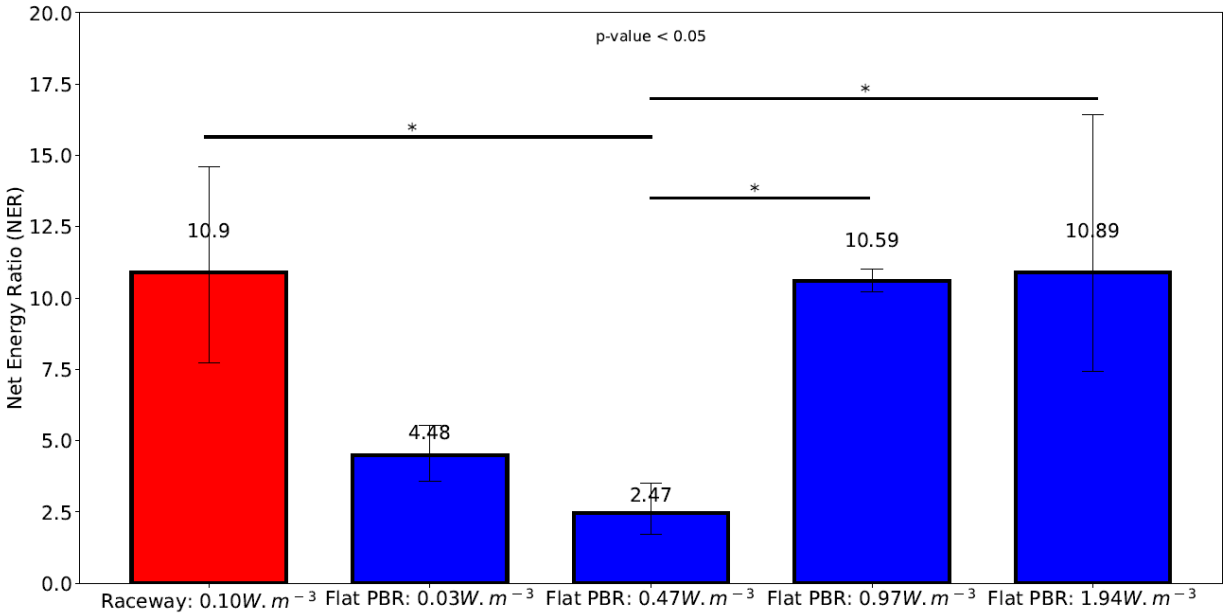

Figure 6.9 Net Energy Ratio (NER) of cyanobacterial derived ethanol with cultivation of in open raceway pond and flat-panel photobioreactor (PBR). The error bars denote the upper and lower values from the LCA model. Model uncertainty propagation is due to experimental error of cyanobacterial cultivation and biomass to energy conversion. The p-value or probability value

was obtained from the one-way ANOVA in Matlab ®. The horizontal bars and stars link the groups that have means significantly different from each other as evaluated by the one-way ANOVA.

Likewise, the highest mixing energy inputs used for flat-panel photobioreactors, 0.97 and 1.94 $W.m^{-3}$, provided low energy efficiency due to high mixing energy requirements, inhibition of *Synechocystis* sp. PCC 6803, and the resulting biomass and biofuel productivities. At 0.03 $W.m^{-3}$, the energy efficiency is significantly improved by roughly 60% relative to the highest mixing energy inputs. Moreover, at mixing energy inputs of 0.47 $W.m^{-3}$, there is a trade-off between energy requirements, and biomass and biofuel productivities of *Synechocystis* sp. PCC 6803, overcame by the latter as demonstrated by reducing the NER by 77% relative to the highest mixing energy requirements experimentation, improving energy efficiency and sustainability of the cyanobacterial derived ethanol system (Figure 6.9). This NER, 2.47 ± 0.93 $MJ_{consumed}.MJ^{-1}_{produced}$, minimized at a mixing energy input of 0.47 $W.m^{-3}$, has the same order of magnitude reported in Quiroz-Arita, Sheehan, & Bradley (2017), 1.66 $MJ_{consumed}.MJ^{-1}_{produced}$; and four to 12 times higher than the NER, 0.20-0.55 $MJ_{consumed}.MJ^{-1}_{produced}$, reported by Luo et al. (2010). However, the high NER values are in part due to photoinhibition of growth at the high light intensities used in this study; therefore, future analysis considering the outdoors daily light fluctuations will significantly improve these and other metrics of sustainability.

6.4 Conclusions

The mixing energy inputs for cultivation of *Synechocystis* sp. PCC 6803 in open-raceway ponds and flat-panel have been proven to control biological responses and life cycle metrics of sustainability in the design of cyanobacterial derived ethanol. The maximum growth rates and cyanobacterial biomass productivities were significantly impacted by differences in mixing energy inputs, demonstrated by decoupling the carbon from the mixing rate used in the flat-panel

photobioreactors experiments. The experimental work performed in this research suggests is likely that sheared environments in this turbulent flow contributed to inhibition and cell disruption at higher mixing energy inputs. Additionally, carbon was demonstrated to limit the growth at lowest sparged air rates in flat-panel photobioreactors and in open raceway ponds operated under outdoor conditions. A major contribution in this research is the driving of the life cycle energy efficiency in open raceway ponds and flat-panel photobioreactors due to differences in mixing energy input. The findings of this study; therefore, should be incorporated into future research, industry, and policies strategies for the sustainable design and operation of photoautotrophic derived biofuels and co-products systems.

6.5 Answer to Research Question 3.1

This section of the research effort has allowed us to address Research Question 3.1, which is restated here:

What are the implications of mixing rates in the life cycle metrics of flat photobioreactors and raceways ponds?

Research Question 3.1 is associated with Hypothesis 3.1:

Differences in mixing energy change metrics of growth and sustainability for photoautotrophic-derived biofuel systems.

This chapter demonstrates that there is a tradeoff between mixing energy and biomass productivity, reducing (improving) the life cycle net energy ratio of cyanobacterial biofuels at low mixing rates. Additionally, this chapter provides evidence that carbon limits the growth of cyanobacteria at low mixing energy inputs in flat-panel photobioreactors, but especially in open raceway ponds under industrially-relevant conditions. High mixing energy inputs in flat-panel photobioreactors inhibits the growth of cyanobacteria.

The results of these studies provide support to the hypothesis that differences in mixing energy inputs change metrics of growth and sustainability, improving growth and life cycle net energy ratios at low mixing energy inputs.

CHAPTER 7: Pilot scale open raceway ponds and flat-panel photobioreactors maintain well-mixed conditions under wide range of mixing energy inputs[6]

7.1 Introduction

Photoautotroph-based biofuels are considered one of the most promising renewable resources to meet the global energy requirements for transportation systems [5]. Long-term research and development has resulted in demonstrations of microalgae areal oil productivities that are higher than crop-based biofuels, about 10 times that of palm oil and about 131 times that of soybean [5, 74-76]. Cyanobacteria is reported to have ~4 times the areal productivity of microalgae on an equivalent energy basis [6]. Downstream of this cultivation process, cyanobacterial biomass and bioproducts can be supplied to biorefineries producing feed, biomaterials, biosynthetic chemicals, and biofuels [77]. As such, cyanobacterial systems can be a significant contributor to more sustainable energy and production systems.

Turbulent environments are demonstrated to induce physiological responses in photoautotrophic microorganisms in open raceway ponds and photobioreactors [200-207]. Recent efforts studied the effects of turbulence dissipation rates ranging from 0 to 0.08 $m^2.s^{-3}$ simulated at laboratory scale conditions (1 liter cultures) [200]. This work concluded that despite no alteration of photosynthesis activity on chlorophyll a, there is a systematic increase in the growth rates of the strain *Microcystis flos-aquae* as a function of the turbulent dissipation rate and a decay in the growth rate of the strain *Anabaena flos-aquae* at high turbulence. These authors identified a maximum phosphorous uptake rate by these cyanobacteria strains at turbulence dissipation rates of $2.26E^{-2}$ $m^2.s^{-3}$, suggesting that turbulence plays an important role

[6] **This chapter is adapted from a prepared journal article for consideration for publication:** Carlos Quiroz-Arita, Myra L. Blaylock, Patricia E. Gharagozloo, David Bark, Lakshmi Prasad Dasi, Thomas H. Bradley. "Pilot scale open raceway ponds and flat-panel photobioreactors maintain well-mixed conditions under wide range of mixing energy inputs".

in the biological adaptation of cyanobacteria by influencing nutrient uptake [200]. In other research, the effects of shear environments were studied for the cyanobacteria and microalgae strains *Synechocystis sp.* and *Chlamydomonas reinhardtii*, respectively, in 150 ml cultures [201]. In this study the growth rate of *Synechocystis sp.* was independent of shear stress (0 to 0.18 $N.m^{-2}$) and *Chlamydomonas reinhardtii* growth rate was linearly dependent on shear stress. These laboratory scale environments; however, are not representative of industrial scale conditions. Other impacts of turbulent mixing are cell disruption due to shear stress [208-215]. Some instances are for hybridoma cells suffering apoptosis at mixing energy inputs of $1.87E^{3}$ $W.m^{-3}$ [209, 216]. Other studies observed 51% lower recombinant protein production, 42% higher glucose uptake, and 50% lower lactate production cells exposed to mixing energy inputs of $6.4E^{2}$ $W.m^{-3}$ [209, 217]. Inhibitory effects; however, are reported at mixing energy inputs above $1E^{6}$ $W.m^{-3}$ and Kolmogorov microscales less than or equal to 2.4 micrometers for mammalian cells [209]. In photobioreactors, small bubbles are reported to cause cell damage [205, 218], colliding with photoautotrophic cells and contributing to a high shear environment. The microalgae strain *Phaeodactylum tricornutum*, for instance, presented inhibition at air rates of 0.567 $m^{3}_{air}.min^{-1}.m^{-3}_{reactor}$, where carboxymethyl cellulose (CMC) was supplied into the medium to mitigate shear-induced damage in parallel experiments [205]. Other sparged photobioreactors cultivating *Dunaliella tertiolecta* and *D. salina* reported increments in the decay rates as a function of gas velocity, observing the highest death rates at 8.91 and 13.37 $m^{3}_{air}.min^{-1}.m^{-3}_{reactor}$ [218]. There is no research reported in the literature concerning the biological system response due to shear stress on cyanobacteria cells disruption, particularly on *Synechocystis sp.* PCC6803. Moreover, most of the previous research were conducted at mixing energy inputs are 30, 100, or thousands

order of magnitudes higher than is considered cost-effective for industrial cultivation systems [53, 224].

Photoautotrophic microorganisms are cultivated in photobioreactors, the most common types being the open raceway ponds and flat panel PBR [225]. Open raceway ponds are constructed in a configuration with channels, using paddlewheel mixers that promote a low shear environment [8]. Flat-panel photobioreactors are vertically translucent flat plates, illuminated on both sides and stirred by aeration [9]. Unlike outdoor raceways and outdoor PBR, laboratory-scale experiments are most commonly grown under ideal conditions including ideal mixing rates, optimum light intensities and optimized media. Comparison of the laboratory scale literature to industrial results demonstrate that photoautotrophic biomass and biofuels productivity are overestimated at laboratory scale experiments relative to industrial scale systems. This distinct difference in the performance of industrial systems are partially attributed to the light experienced by photoautotrophic microorganisms at outdoor conditions. For instance, the light saturation of *Synechocystis sp.* PCC6803 is reported at about 200 μmol photons.s^{-1}.m^{-2} [10, 84], whereas photoautotrophic microorganisms will face incident radiations of about 2000 μmol photons.s^{-1}.m^{-2} at noon in locations such as Colorado [11] Previous studies have estimated that the total photo conversion efficiency of algae is from 2.6% (at high light) to 6.3% (at reduced light) [12]. These estimations assumed that 46% of the spectrum is in the photosynthetic active radiation (PAR) range of 400 to 700 nm, losses due to photon transmissions efficiency of 95%, photon utilization efficiency ranging from 10% to 30%, biomass accumulation efficiency of 50%, and biomass energy content of 21.9 kJ·g^{-1}. Low photo conversion efficiency in photoautotrophic microorganisms is attributed to dark and photorespiration biomass losses [62, 219, 220]. Photorespiration is well understood in plants, where carboxylation step in the Calvin–

Benson cycle is switched to oxygenation, dissipating photic energy and accounting for 25% reduction in the photosynthesis in C_3 plants [221]. Photorespiration is poorly understood in photoautotrophic microorganisms.

Some previous studies have investigated the effects of mixing rates on photoautotroph biomass productivities in industrial scale systems [11, 53, 54]. Some of these efforts have identified optimum volumes of air flow rates per unit volume (VVM) of photobioreactors that might be industrially relevant for microalgae, generally between 0.2 to 1.2 $m^3_{air}.min^{-1}.m^{-3}_{reactor}$ [11]. Many others have considered mixing energy inputs that are far outside the energy consumption that can be considered economic, or industrially relevant, ranging from 8 to 633 $W.m^{-3}$ [53, 224]. For raceway ponds, for instance, energy inputs from 1 to 2 $W.m^{-3}$ are utilized in the algae cultivation demonstrations performed to date [54]. Additionally, previous research state that mixing in industrial photobioreactors induce flashing or dark/light cycles [226-228]. For instance, by carrying experimental growth of *Chlamydomonas reinhardtii* under incident radiations fluctuating between 5 Hz and 100 Hz, growth rates were found to be linearly dependent on the light frequency. These previous efforts suggest that mixing in photobioreactors control the light regimes experienced by single cells, impacting the bulk photosynthesis and biomass productivity of photoautotrophic microorganisms. Other efforts; however, demonstrated no improvements in algal productivity at light fluctuations from 0.038 Hz to 1 Hz, modeled using a control timer to open and close a mini venetian blind device [229]. The latter frequencies ($<<$ 1 Hz), are more consistent when comparing with the circulation velocities studied for fermenters with a height to diameter ratio less than 3 ($<$ 60 seconds) and for airlift reactors with split-cylinders heights of 6.02 m. (6.5 seconds) [230].

Similarly, many studies have attempted to predict the fluid mechanics of raceway ponds and photobioreactors via Computational Fluid Dynamics (CFD) approaches [59, 60, 231]. Some raceway ponds CFD models applied to investigate velocity, heat transfer, are weakened because they use average velocities as boundary conditions [54, 71], missing the dynamics of these systems downstream of the paddlewheel. Additionally, turbulence intensities used in previous CFD applications in open raceway ponds are 3.84% [59], and default values recommended by commercial CFD codes [60, 62, 71], ranging from 5-10%. For the case of open channel flow, for instance, experimental turbulence intensities are reported at 2.8% [232]. Turbulence intensity and the impact of difference in mixing energy inputs in open raceway ponds are not fully understood. Other previous research studied particle tracking with neutrally buoyant particles in photobioreactors [73] , but the statistical and temporal nature of turbulence modeling was not considered. Previous efforts have demonstrated well mixed conditions in open raceway ponds; however, at paddlewheel speeds ranging from 15 RPM to 28 RPM [231] equivalent to mixing energy inputs estimated at 4.5 $W.m^{-3}$ to 30 $W.m^{-3}$ or two to 15 times higher than used for industrial cultivation [54, 233]. None of the previous studies have analyzed algae/cyanobacteria cell motion using modern experimental fluid mechanics, engineering signal processing, modeling, and CFD tools at industrially relevant mixing energy inputs.

Two modern methods for experimental fluid mechanics are particle image velocimetry (PIV) and Acoustic Doppler Velocimetry (ADV). PIV correlates the velocity of the fluid from the distance traveled in a short period of time by neutrally buoyant particles, captured by laser technology and high-resolution cameras [61, 63, 65-67]. Biological applications include; for instance, aquatic predator-prey interactions [234], hydrodynamics of fish in aquatic environments [64], and fluid transport by plankton aggregations [70]. ADV correlates the

velocity of the fluid from the speed of sound of an acoustic pulse [235, 236]. This technique has been widely used to understand turbulence in natural and engineered civil works including open channels [237-243]. There is previous study that utilized Acoustic Doppler Velocimetry (ADV) to describe the velocity field of raceway ponds [72]; however, ignoring the time scales and turbulence that describe the physics of these reactors. In general, turbulence of flat-panel photobioreactors and open raceway ponds are poorly understood, and today's evidence of turbulence with difference is mixing energy inputs in the light experienced by photoautotrophic microorganisms is not conclusive.

Based on this understanding of the literature we seek to understand the role of turbulent mixing on the light experience by photoautotrophic microorganisms; therefore, we conducted (i) pilot scale fluid mechanics experimentation in open raceway ponds and flat-panel photobioreactors at industrially relevant mixing energy inputs, and (ii) applied computational fluid dynamics modelling and validation. By studying turbulence as a function of mixing energy input in open raceway ponds and flat-panel photobioreactors, we aim to understand the role turbulence plays in the frequency of photoautotrophic microorganisms' motion in pilot scale systems.

7.2 Materials and Methods

To evaluate the implications of turbulent mixing on the light experienced by photoautotrophic microorganisms in pilot scale open raceway ponds and flat-panel photobioreactors, we must understand the connections between fluid mechanics and photoautotrophic microorganisms motion under differences in mixing energy inputs. The workflow, illustrated in Figure 7.1, integrates parallel but complementary experimental and computational fluid mechanics. By incorporating laboratory experiments at industrially relevant

inputs, we developed a holistic bridge and feedback loop approach between laboratory and industrial scale experimentation.

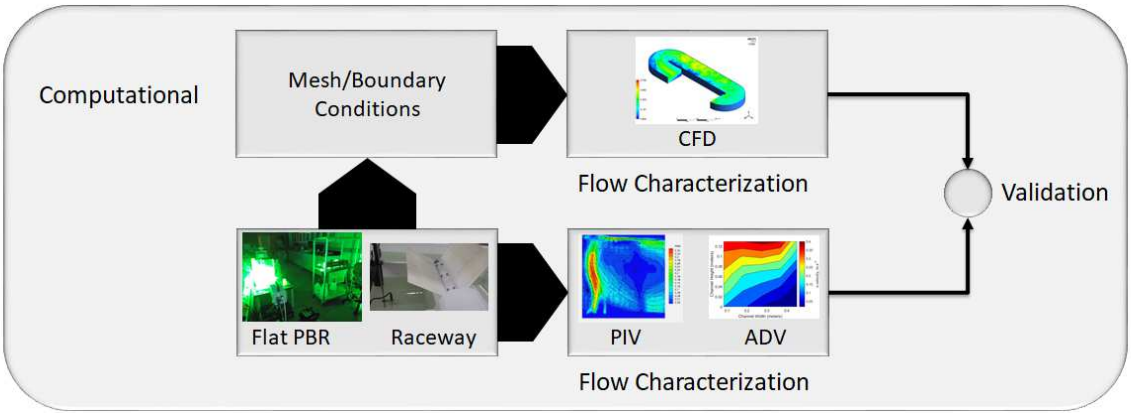

Figure 7.2 Workflow for experimental and computational fluid mechanics (top flow) and photoautotrophic growth (bottom flow) to assess the impact of mixing energy inputs.

7.2.1 Flat-Panel Photobioreactors Configuration

To validate the growth models, we performed experimental work under mixing energy input variability in the flat-panel photobioreactor and open raceway pond. As illustrated in Figure 7.2, the batch process was carried out in five replicates of 1L flat-panel photobioreactors made in acrylic with surface to volume ratio of 112 $m^2 \cdot m^{-3}$. The experiments were performed at cultures depths of 20 cm. The systems were mixed by sparged air at the bottom of the flat-panel photobioreactors at industrially relevant mixing inputs of 0.7, 0.35, and 0.17 m^3 of air per minute per cubic meter of reactor, commonly referred as VVM [11]. The equivalent mixing energy inputs used in the flat-panel photobioreactors experiments were 1.94, 0.97, and 0.47 $W.m^{-3}$.

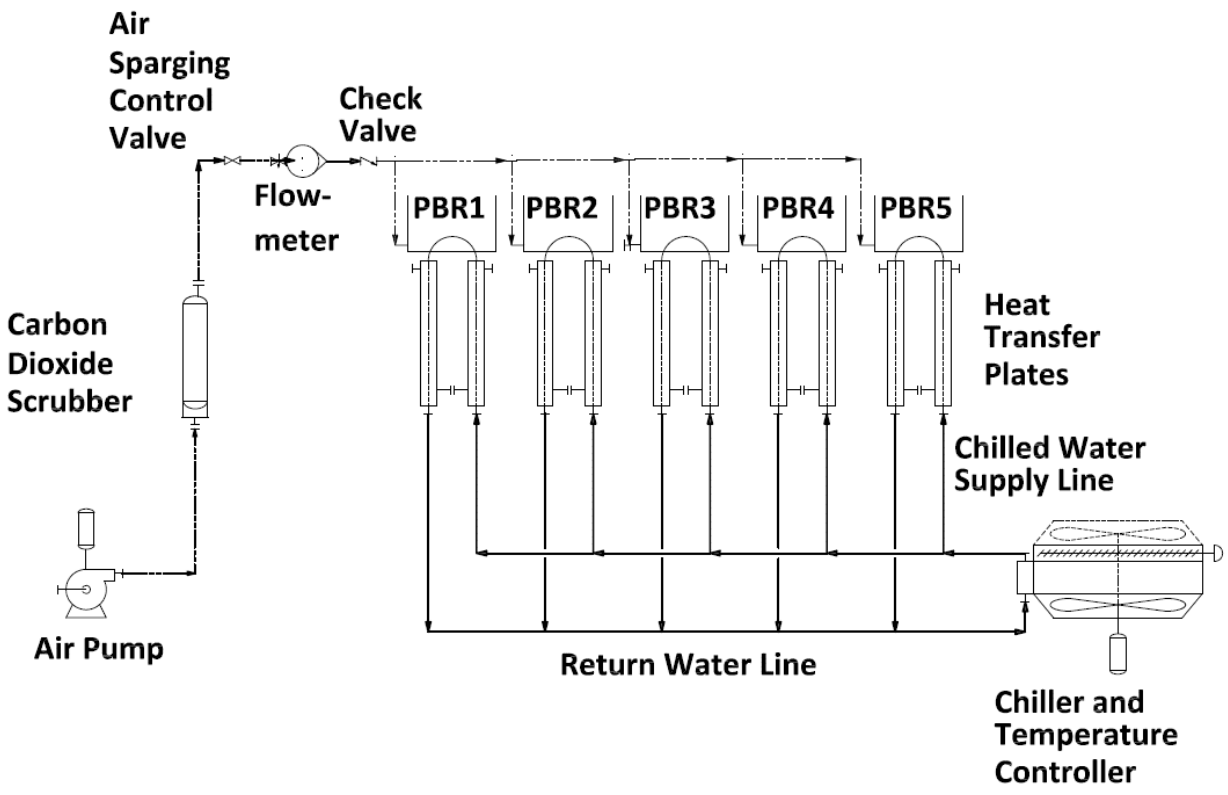

Figure 7.2 Instrumentation Diagram of Flat-panel photobioreactors system for experimental and model based analysis.

7.2.2 Open Raceway Pond Configuration

As illustrated in Figure 7.3, the open raceway pond batch process was carried out in a 700L fiber-reinforced plastic raceway at water depths of 20 cm. The system was mixed with a paddlewheel provided with a 90V DC Gearmotor with a rated torque of 33 in.-lb controlled by an IronHorse DC Drives. The mixing energy input used in the open raceway pond experiments were 2.1 $W.m^{-3}$ and 0.7 $W.m^{-3}$. Additional experiments were conducted at 0.10 $W.m^{-3}$, an order of magnitude lower than reported in the literature for industrial systems [54].

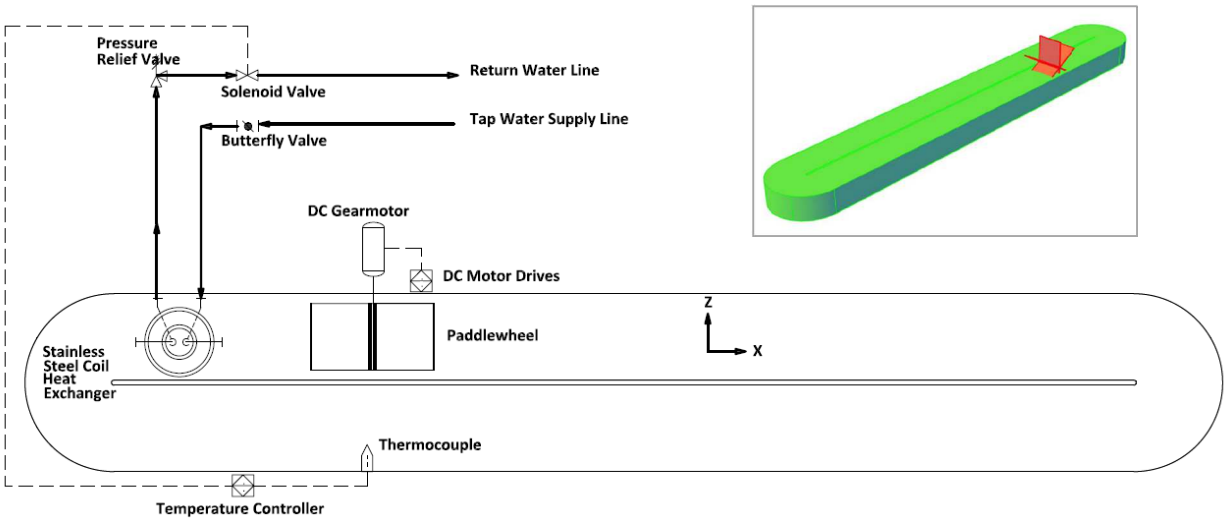

Figure 7.3 Plan View and Instrumentation Diagram of Open raceway pond system for industrial scale experimental and model based analysis. The 3D view of the Open Raceway Pond is illustrated in the upper right corner.

7.2.3 Experimental Fluid Mechanics Methods

To understand the physics of the open raceway ponds and flat-panel photobioreactors we applied a variety of fluid mechanics tools including Particle Image Velocimetry (PIV), Acoustic Doppler Velocimetry (ADV), and applied CFD.

7.2.3.1 Flat-panel photobioreactors fluid characterization by PIV

The velocity field of flat-panel photobioreactors was measured using PIV. Mixing energy inputs at 0.47 $W.m^{-3}$, 0.97 $W.m^{-3}$, and 1.94 $W.m^{-3}$ were used in this study. The study was performed with 20 mm PMMA Rhodamine-B particles, Nd:YLF Single Cavity Diode Pumped Solid State High Repetition Rate, laser with 0.2 mm thick measurement plane, double frame CMOS camera, DaVis software for processing at 1000 hz, and 32x32 double pass followed by a 12x12 single pass interrogation window.

7.2.3.2 Open raceway pond fluid characterization by ADV

The velocity field in the open raceway pond was measured using ADV. We measure fluid velocities at three different cross sections (CS); (i) downstream of the paddlewheel, (ii) at the first turn, and (iii) at the straight channel. At each cross section, we collected data in a 5X5 matrix with a Vectrino plus firmware + NORTEK. At each point, 60,000 samples at 50 Hz were collected by ADV. We performed experimentation at mixing energy inputs of 2.1 $W.m^{-3}$, 0.7 $W.m^{-3}$, and 0.1 $W.m^{-3}$ to evaluate the fluid mechanics and biological implications of reducing energy consumption by the industry.

7.2.3.3 Characterizing cell motion by CFD

To understand the frequency of photoautotrophic microorganism's motion in flat-panel photobioreactors and open raceway ponds, particle tracking is obtained from the CFD models in a Lagrangian representation of the flow. Length and time scales were computed from Kolmogorov microscales [69, 244]. The smallest length scales of motion (η) are computed by dimensional analysis as a function of the largest length scale (l) and the Reynolds number (Re) (Eq. 1), and, the smallest time scales (τ) are a function of the largest time scale (T) and the Reynolds number (Eq. 2). The viscous sub-layer in contact with a smooth wall is computed from a linear relationship between the mean velocity (U), wall shear stress (τ_w), viscosity (μ), and the distance from the wall (y) (Eq. 3) [69].

$$\eta = \frac{l}{Re^{3/4}} \quad \text{Eq. 1}$$

$$\tau = \frac{T}{Re^{1/2}} \quad \text{Eq. 2}$$

$$y = \mu \frac{U}{\tau_w} \quad \text{Eq. 3}$$

The characteristic length of the flat-panel photobioreactor and open raceway pond are 0.20 m. and 0.46 m., respectively. The Reynolds number of the flat-panel photobioreactors for

mixing energy inputs of 0.03 W.m^{-3}, 0.47 W.m^{-3}, and 0.97 W.m^{-3} are 2,913, 3,608, and 4,053, respectively. For the case of the open raceway pond, the Reynolds number at 0.1 W.m^{-3}, 0.7 W.m^{-3}, and 2.1 W.m^{-3} are 34,605, 67,840, and 93,008, respectively. The wall distance at 0.1 W.m^{-3}, 0.7 W.m^{-3}, and 2.1 W.m^{-3} are 0.0009, 0.0005, and 0.0002, respectively. The flat-panel photobioreactor and open raceway pond meshes were designed at length scales of 0.0008 m. and 0.002 m., respectively, in Trelis 16.3. CFD models were developed in ANSYS Fluent 16.1 for the flat-panel photobioreactor and open raceway pond. The inlet velocity measured from PIV and ADV, and the turbulence intensities, defined as the ratio of the velocity fluctuations (u') to the mean velocity (U) measured from the experimental data (Eq. 4) [245, 246], were used as boundary conditions for the flat-panel photobioreactor and open raceway pond.

$$I \equiv \frac{u\prime}{U} \qquad \text{Eq. 4}$$

The finite volume method was selected to guarantee conservation of mass and Direct Numerical Simulation (DNS) was applied [68, 69]. The time steps used for flat-panel photobioreactors CFD simulations were 0.02 seconds for mixing energy inputs of 0.03 W.m^{-3}, 0.47 W.m^{-3}, and 0.97 W.m^{-3}. For the case of the open raceway pond, CFD simulations were performed at 0.1 W.m^{-3}, 0.7 W.m^{-3}, and 2.1 W.m^{-3} at time steps of 0.2, 0.1, and 0.05 seconds, respectively. The CFD results were validated against experimental data and particle tracking were computed in the flat-panel photobioreactor and open raceway pond by integrating the velocity field [247]. This assumes that photoautotrophic cells are neutrally buoyant and that inertial forces are much greater than other forces these microorganisms experience such as gravity and buoyancy. The frequency of photoautotrophic cells motion was computed as the number of cycles per second with respect to the time average motion of each particle.

7.3 Results and Discussion

The results of this research are synthesized into three aspects. First, the flat-panel photobioreactor experimental fluid mechanics results are presented and the forces driving motion in these systems is discussed. Second, the open raceway pond experimental fluid mechanics results are presented, discussion is particularly focused on novel contributions to the field by understanding the turbulence intensities with differences in mixing energy input. Third, the impact of differences in mixing energy inputs in the motion of photoautotrophic microorganisms is evaluated by applying validated CFD models, based on flat-panel photobioreactors and open raceway ponds.

7.3.1 Flat-panel photobioreactor flow characterization

The velocity field of the flat-panel photobioreactor at low and high mixing energy inputs are illustrated in Figure 7.4. The mean velocity computed from PIV at mixing energy inputs of 0.47 $W.m^{-3}$, 0.97 $W.m^{-3}$ and 1.94 $W.m^{-3}$ are 0.015 $m.s^{-1}$, 0.018 $m.s^{-1}$, and 0.020 $m.s^{-1}$, respectively. For mixing energy inputs of of 0.47 $W.m^{-3}$, 0.97 $W.m^{-3}$ and 1.94 $W.m^{-3}$ the turbulence intensities are 1.4%, 1.2%, and 1.0%, respectively. Lastly, turbulent dissipation for these mixing energy inputs are $1.3E^{-5}$ $m^2.s^{-3}$, $1.7E^{-5}$ $m^2.s^{-3}$, and $1.5E^{-5}$ $m^2.s^{-3}$.

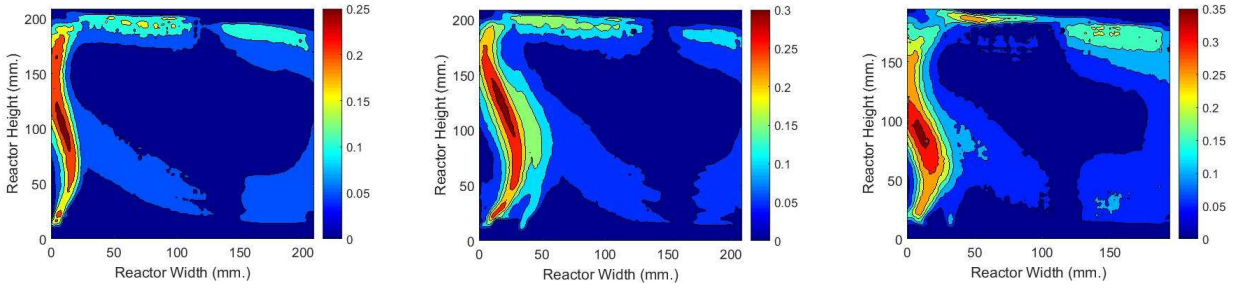

Figure 7.4 Velocity field ($m.s^{-1}$) obtained from PIV of flat-panel photobioreactor at mixing energy inputs of 0.47 $W.m^{-3}$ (left figure), 0.97 $W.m^{-3}$ (middle figure), and 1.94 $W.m^{-3}$ (right figure).

These turbulence dissipation rates are from about 100 to 600 order magnitudes lower than used by Xiao et al. (2016) where phosphorous uptake rates were maximized and growth decay was observed in different cyanobacteria strains. These results demonstrate the significant differences in the fluid environments maintained under industrially relevant mixing energy inputs relative to laboratory conditions, impacting the biological responses of photoautotrophic microorganisms.

The flow circulation in the pilot flat-panel photobioreactors is driven by the buoyancy of air bubbles supplied by the air sparger. Buoyancy only varies with bubble size and the bubble sizes are mostly dictated by the orifice size on the air sparger. Therefore, because bubble buoyancy and velocity is maintained constant, the velocity of the fluid near the air sparger is relatively constant. The flow circulation in the flat-panel photobioreactors, as a result, is theoretically constant at industrially relevant mixing energy inputs studied in our research.

7.3.2 Pilot scale open raceway pond flow characterization

By applying experimental ADV, we have a better understanding of turbulence as a function of industrially relevant mixing energy inputs in pilot open raceway ponds. The experimental velocity components (x, y, z) downstream the raceway paddle wheel are illustrated for 2.1 $W.m^{-3}$ mixing energy input as shown in Figure 7.5. The instantaneous velocity measured at each point in the cross section is illustrated in the Appendix E (Figure E2). The velocity magnitude, turbulence dissipation rates, and turbulence intensities were computed from these experimental data. Turbulence intensities, downstream the raceway paddlewheel, are illustrated in Figure 7.6.

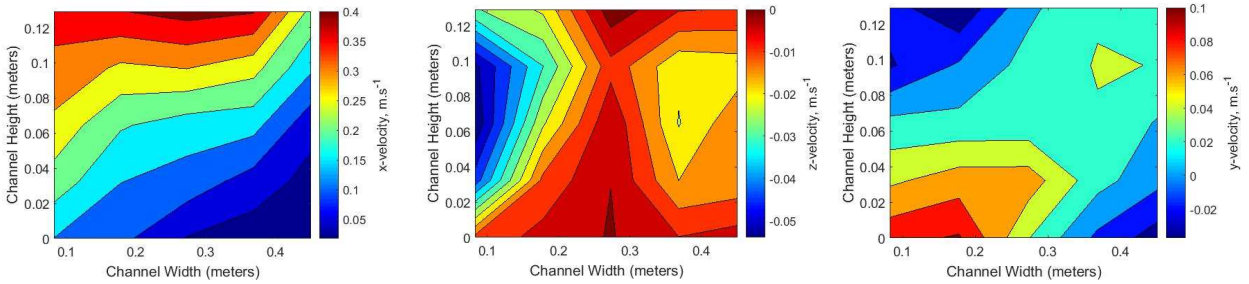

Figure 7.5 First cross section (downstream paddlewheel) velocity components ($m.s^{-1}$) of open raceway pond at mixing energy input of 2.1 $W.m^{-3}$. The left figure corresponds to the x-velocity, the middle figure corresponds to the y-velocity, and the right figure corresponds to the z-velocity.

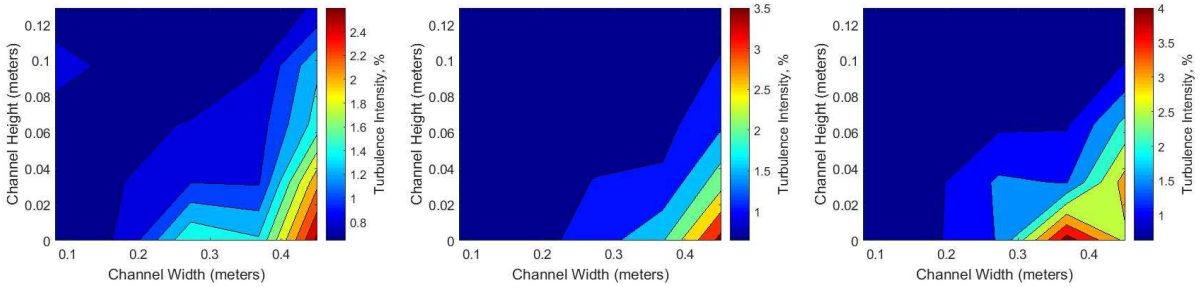

Figure 7.6 Turbulence intensities (%) of first cross section of open raceway pond at mixing energy inputs of 0.1 $W.m^{-3}$ (left figure), 0.7 $W.m^{-3}$ (middle figure) and 1.94 $W.m^{-3}$ (right figure).

Experimental velocities and turbulence intensities were used as boundary conditions of the CFD models. The velocity field of the fluid domain in the open raceway pond were computed by CFD models at mixing energy inputs 0.1 $W.m^{-3}$, 0.7 $W.m^{-3}$, and 2.1 $W.m^{-3}$ (Figure 7 and Figure E3). The velocity field of the CFD model at mixing energy inputs of 0.1 $W.m^{-3}$ is illustrated in Figure 7.7. The CFD models were validated against experimental data measured at the second and third cross section of the open raceway pond, located in the first turn and in the straight channel as illustrated in the Appendix E (Figure E1 and E5).

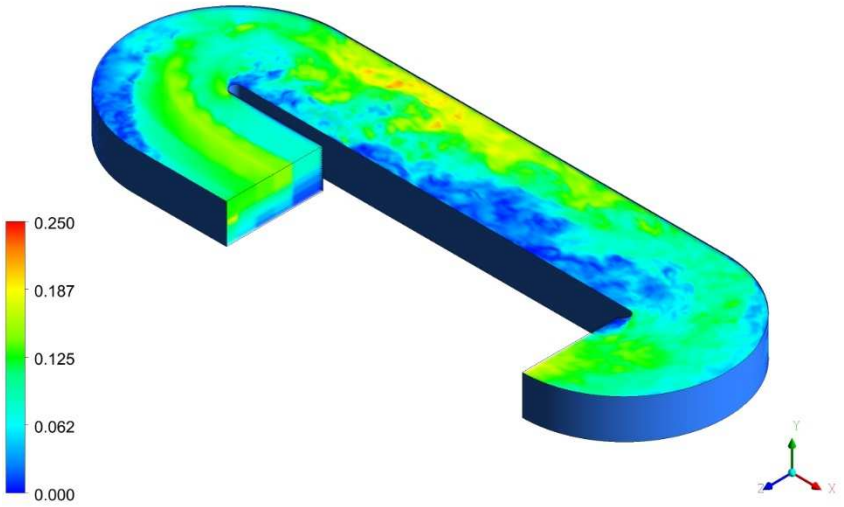

Figure 7.7. Velocify field (m.s^{-1}) from Direct Numerical Simulation based CFD model of open raceway pond at mixing energy inputs of 0.1 W.m^{-3}.

These results demonstrate that turbulence intensities have been overestimated in previous studies applying CFD to open raceway ponds. At mixing energy inputs of 0.1 W.m^{-3}, 0.7 W.m^{-3}, and 2.1 W.m^{-3} the velocity magnitudes computed from the experimental ADV data downstream the raceway paddlewheel are 0.08 m.s^{-1}, 0.15 m.s^{-1}, and 0.21 m.s^{-1}. Turbulence dissipation rates at these industrially relevant mixing energy inputs are 6.1E^{-4} m^2/s^{-3}, 2.8E^{-3} m^2/s^{-3}, and 1.1E^{-2} m^2/s^{-3}. For example, turbulence dissipation rates at mixing energy inputs of 0.1 W.m^{-3} and 0.7 W.m^{-3} were found to be 1 to 13 order of magnitudes lower than used by Xiao et al. (2016) where phosphorous uptake rates were maximized and growth decay was observed in different cyanobacteria strains. However, the turbulence dissipation rates Xiao et al. (2016) found to maximize phosphorous uptake rate in cyanobacteria strains is twice the turbulence dissipation rate computed at mixing energy inputs of 2.1 W.m^{-3}. Turbulence dissipation rates where cyanobacterial growth decay was found by Xiao et al. (2016) is seven times higher than observed

at mixing energy inputs of 2.1 $W.m^{-3}$ in our research. Turbulence intensities computed from our experimental work for the first time in a pilot open raceway pond at 0.1 $W.m^{-3}$, 0.7 $W.m^{-3}$, and 2.1 $W.m^{-3}$ are 1.02%, 1.05%, and 1.25%, respectively (Figure 9.6). Low quality data was observed in the upper left point at a mixing energy input of 0.1 $W.m^{-3}$, where a low signal-to-noise ratio below 10 was recorded with no significant implication in the average value. The turbulence intensities used by Labatut et al. (2015) are about three to four times higher than measured at industrially relevant mixing energy inputs in our research. The turbulence intensities used by Drewry et al. (2015), Pires et al. (2017), and Zhang et al. (2017) are likely four to ten times higher than found in our experimental work. Overestimated turbulence intensities, as a result, can impact the flow dynamics and turbulence in these open raceway ponds, misleading CFD results. By validating our CFD model with ADV data under different mixing energy inputs, we found that boundary conditions, including velocity profiles and turbulence intensities, were sensitive in the accuracy of the CFD models. The validation of the open raceway pond CFD model is illustrated in the Appendix E (Figure E5).

7.3.3 Frequency of cells motion are not significantly impacted due to differences in mixing energy

The frequency of photoutotrophic microornisms motion in pilot flat-panel photobioreactors and open raceway ponds are not significantly impacted due to differences in industrially relevant mixing energy inputs. Biological responses reported in previous studies due to mixing is inconclusive from laboratory experimentation. By integrating experimental and computational fluid mechanics, we have represented the physics in pilot scale environments, demonstrating the fluid dynamics in flat-panel photobioreactors and open raceway ponds have no influence in the overall light experienced by photoautotrophic microorganisms cultures. We have

demonstrated this by computing the frequency of this motion (Figure 7.8) from randomly selected particles travelling in the flat-panel photobioreactor and open raceway pond (Figure E4) Photoautotrophic microorganisms frequency of motion in flat-panel photobioreactor is driven by the buoyancy of air bubbles, in which frequencies of this motion at mixing energy inputs of 0.47 $W.m^{-3}$, 0.97 $W.m^{-3}$ and 1.94 $W.m^{-3}$ were found to be 0.036 Hz, 0.032 Hz, and 0.038 Hz, respectively. By performing an one-way analysis of variance (ANOVA) of these frequencies we found they are not significantly impacted by differences in mixing energy inputs (Figure 7.8). The frequencies of flashing lights used by Janssen, Tramper, Mur, & Wijffels (2003) and Vejrazka, Janssen, Streefland, & Wijffels (2011, 2012) are from about 13 to 300 order of magnitudes higher than observed in our experimental work at industrially relevant mixing energy inputs. Our frequencies of motion are consistent with the frequencies studied by Grobbelaar (1991) at laboratory conditions and the frequencies estimated for fermenters by M. Y. Chisti (1989). Our results demonstrate flow circulation in flat-panel photobioreactors is driven by buoyancy of air bubbles, maintained constant in this environment regardless variation in mixing energy input.

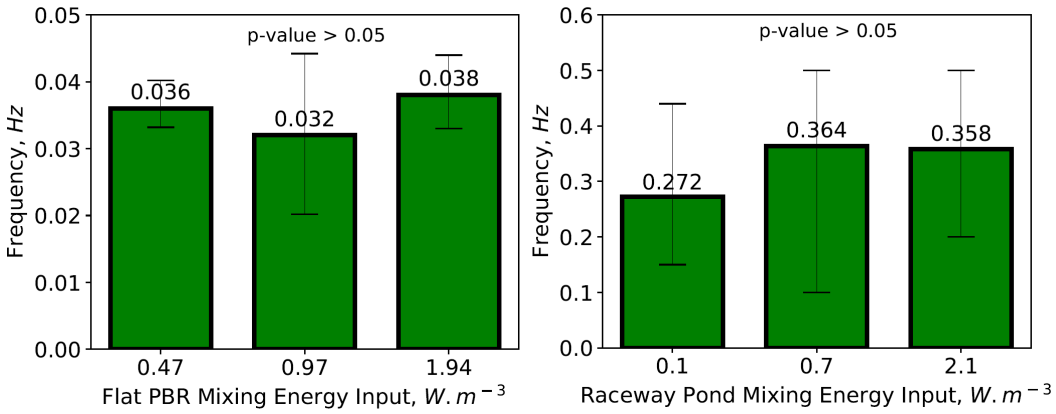

Figure 7.8 Frequency of photoautotrophic microorganism cell motion open raceway pond at mixing energy inputs of 0.1 $W.m^{-3}$ (left figure), 0.7 $W.m^{-3}$ (middle figure) and 1.94 $W.m^{-3}$ (right figure).

Frequency of photoautotrophic microorganisms motion in pilot open raceway pond are not significantly impacted at industrially relevant mixing energy inputs. Frequencies of this motions at mixing energy inputs of 0.1 $W.m^{-3}$, 0.7 $W.m^{-3}$, and 2.1 $W.m^{-3}$ are 0.272 Hz, 0.364 Hz, and 0.358 Hz. By performing an one-way ANOVA of these frequencies we found they are not significantly impacted by differences in mixing energy input (Figure 7.8). The frequencies of flashing lights used by Janssen, Tramper, Mur, & Wijffels (2003) and Vejrazka, Janssen, Streefland, & Wijffels (2011, 2012) are from about 1 to 40 order of magnitudes higher than observed in our experimental work at industrially relevant mixing energy inputs. Our frequencies of motion are consistent with the frequencies estimated for airlift reactors by M. Y. Chisti (1989). Since photoautotrophic microorganisms cells motion are not significantly impacted by mixing energy input, our research suggests well-mixed conditions at industrially relevant mixing energy inputs in pilot open raceway ponds.

Our research suggests that previous laboratory scale studies found increments in the growth rates and productivities because an increment in the photon flux supplied to the cultures at higher flashing frequencies. Moreover, differences in industrially relevant mixing energy inputs studied in our research, demonstrated that photoautotrophic microorganisms motion because buoyancy and convection have no significant difference from an statistical perspective. We demonstrated in our research, as a result, that differences in mixing energy input have no impact in the overall light experienced by bulk photoautotrophic cultures in pilot flat-panel photobioreactors and open raceway ponds.

7.4 Conclusions

Experimental and computational fluid mechanics demonstrated well-mixed conditions in pilot flat-panel photobioreactors and open raceway ponds. Our experimental and computational

work demonstrated that (i) flat-panel photobioreactors flow circulation is driven by air bubbles buoyancy, and (ii) frequency of photoautotrophic microorganisms' motion is not significantly impacted by differences in mixing energy inputs. Experimental and computational fluid mechanics and cyanobacterial growth model demonstrated well-mixed conditions in pilot flat-panel photobioreactor and open raceway ponds at industrially relevant mixing energy inputs. Meaning that the light experienced by individual cells have no impact in the light attenuation of bulk photoautotrophic cultures and productivity.

7.5 Answer to Research Question 3.2

This section of the research effort has allowed us to address Research Question 3.2, which is restated and answered in section 9.5 of this dissertation.

CHAPTER 8: A Dynamic Lumped Thermal and Well-Mixed Algal Growth Model for Pilot Scale Open Raceway Ponds[7]

8.1 Introduction

Microalgae derived biofuels are considered one of the most promising renewable resources to meet the global energy requirements for transportation systems to replace fossil fuels and reduce greenhouse gas emissions [5, 143, 248]. Long-term research and development has resulted in demonstrations of microalgae areal oil productivities that are higher than crop-based biofuels, about 10 times that of palm oil and about 131 times that of soybean [5, 74-76]. Open raceway ponds, constructed in a configuration with channels using paddlewheel mixers that promote a low shear environment [8], are considered today the most cost-effective technology for microalgae cultivation relative to other photobioreactor configurations [225, 249]. Algae biomass productivities in open raceway ponds, however, are significantly lower than those measured under laboratory conditions [250]. Laboratory-scale experiments are most commonly grown under ideal conditions including mixing rates, light saturation and optimized media, they thereby overestimate the biomass productivities achievable in outdoor conditions. There is a need for design and modelling tools to connect this gap between laboratory experimentation and industrial performance under outdoor conditions.

Differences in the performance of industrial systems relative to laboratory experimentation are partially attributed to the light and temperature experienced by photoautotrophic microorganisms at outdoor conditions. For instance, the light saturation of *Nannochloropsis oceanica* is reported at about 80 μmol photons.s^{-1}.m^{-2} at temperatures ranging

[7] **This chapter is adapted from a prepared journal article for consideration for publication:** Carlos Quiroz-Arita, Myra L. Blaylock, Patricia E. Gharagozloo, Thomas H. Bradley, Thomas Dempster, Ryan Davis, John McGowen. "A Dynamic Lumped Thermal and Well-Mixed Algal Growth Model for Pilot Scale Open Raceway Ponds".

from 25.6 °C to 29.1 °C [251], whereas these microorganisms will face incident radiations of about 2000 μmol photons.s^{-1}.m^{-2} and water temperatures up to 32 °C at noon in locations such as Arizona [233], both of these factors have the effect of reducing their photo conversion efficiency. For the case of algae, considering that 46% of the spectrum is in the photosynthetic active radiation (PAR) range of 400 to 700 nm, there are losses due to photon transmission efficiency of 95%, photon utilization efficiency ranging from 10% to 30%, biomass accumulation efficiency of 50%, and biomass energy content of 21.9 kJ·g^{-1}, resulting in a total photo conversion efficiency of between 2.6% (at high light) to 6.3% (at reduced light) [12]. Additional losses can be attributed to dark and photorespiration biomass losses [62, 219, 220]. Photorespiration switches the carboxylation step in the Calvin–Benson cycle to oxygenation, dissipating photic energy and accounting for 25% reduction in the photosynthesis in C_3 plants [221]. Photorespiration is poorly understood in microalgae under outdoors environments.

There are several ongoing efforts in the literature to predict the performance of photobioreactors through modelling. Yet, most of the literature relies on light distribution in photobioreactors based on Beer-Lambert law [55, 56, 169]. Although previous efforts measured the absorption coefficient of *Nannochloropsis sp.* in photobioreactors [56], the derived model can only be used to describe light distribution for particular validated conditions. None of the previous efforts have demonstrated the predictive capability under a wide range of environmental conditions. Models have been developed to predict future outputs based on past inputs by resolving complex systems models that may integrate physical, chemical, and biological domains [252, 253]. Advanced dynamic modelling tools can be implemented to describe the complexity of these physical and biological systems. Previous efforts have explored the application of dynamic tools to microalgae cultivation systems under the assumptions of nutrient limitation

[254, 255] and by mathematical representations of the biological responses [256]. There is limited research concerning thermal modelling in microalgae cultivation systems [257, 258], and many of these efforts fail to evaluate their predictive capability, or have only been developed and validated for specific design and operational conditions and photobioreactors [259].

None of the previous research have integrated thermal modeling and microalgae growth modeling to demonstrate their predictive capability under seasonal variability in open raceway ponds. There is a need to develop dynamic growth modelling tools to reduce mispredictions through incorporation of input weather conditions and thermal processes, and to understand the role of physical, chemical, and biological parameters in the response of the system. For this study, we will validate the developed model using thermal and growth data gathered from the ATP3 DOE experiment, in Mesa, AZ. By developing a dynamic lumped thermal and well-mixed algal growth model for pilot scale open raceway ponds, and conducting parameter estimation, in this research we can identify future efforts that may improve the modeling and therefore performance of these bioenergy systems.

8.2 Dynamic modelling, uncertainty quantification, and parameter estimation methods

To evaluate their predictive capability, a dynamic thermal model embedded into an algae growth model we must understand the physical and biological sources of uncertainty of the system. Figure 8.1 illustrates the workflow to evaluate the system, including (i) input weather conditions for Mesa, Arizona, (ii) the dynamic thermal subsystem (iii) the dynamic algal growth model and (iv) a comparison between cultivation experiments and the algae growth model. This set of models includes both biological and engineering perspectives.

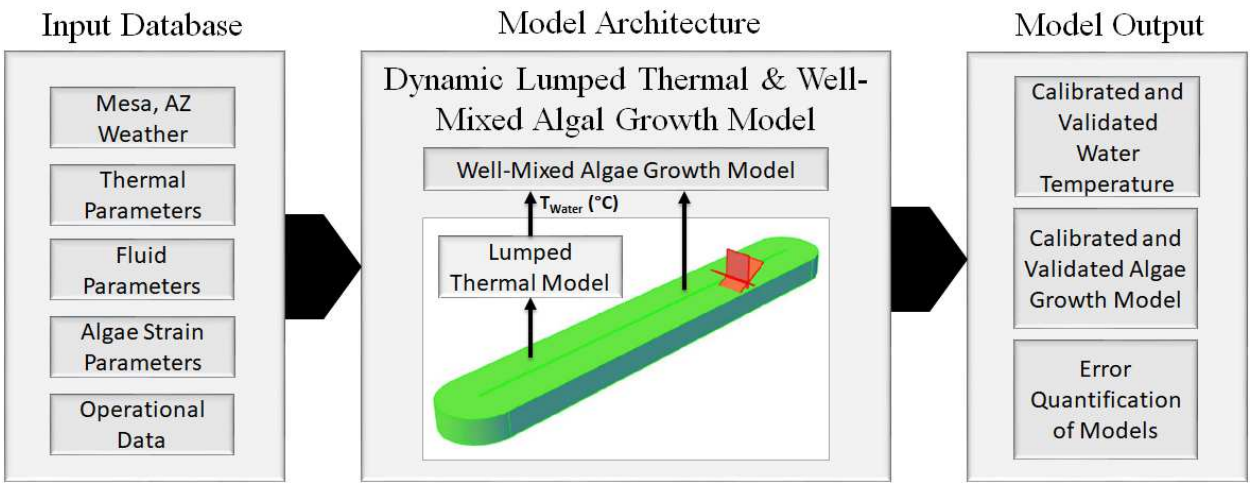

Figure 8.3 Simulation Architecture for Dynamic Thermal and Algae Growth Model.

8.2.1 Pilot Scale Open Raceway Ponds Configuration and Monitoring at ATP^3

The pilot scale open raceway ponds studied in this research are located at The Arizona Center for Algae Technology and Innovation (AzCATI), and the data used for validation and calibration was obtained during the ATP^3 Unified Field Studies. The open raceway pond experiments consist of 6 replicates, where each pond has a surface area of about 4.2 m^2, a nominal volume of 1000 liters, and the experiments were conducted at a depth of 25 cm [233]. The open raceway ponds were provided with a monitoring system that measured pH, dissolved oxygen saturation, salinity, a LiCor LI-190R quantum pyranometer (LiCor, Lincoln, NE, USA) to measure photosynthetically active radiation (PAR), and water temperature [233]. The open raceway ponds were mixed with stainless steel paddle wheel and a CO_2 sparge line for pH control linked to the YSI online pH probe [233]. The water temperature measured at ATP^3 was used for validation and calibration of the dynamic thermal model.

The experimental cultivation of microalgae in the open raceway pond was conducted at paddlewheel speeds of 10.88 RPM and a mean surface velocity of the flow of 0.107 m.s^{-1}. The open raceway ponds were inoculated with *Nannochloropsis oceanica* KA32 at concentrations of

0.05 $g.l^{-1}$ ash-free dry weight (AFDW) in salt water (35 $g.l^{-1}$) with modified f/2 media [233]. Dry weight biomass (DWB) and AFDW used for validation and calibration of the dynamic algae growth model were measured using a standardized method, including the ATP[3] Laboratory Analytical Procedure (LAP) and the gravimetric method for determination of DWB and AFDW [233, 260].

The meteorological conditions were collected at the local weather station at Arizona State University. The parameters collected by ATP[3] that were used as input data for the dynamic thermal model include air temperature (°C), relative humidity (RH, %), global light energy (W m^{-2}), and wind speed (km h^{-1}) [233]. Cultivation experiments were performed during the seasons of Fall (October to December 2013), Spring (April to May 2014), and Summer (June to July 2015). The database is available online at https://openei.org/wiki/ATP3_Data.

8.2.2 Dynamic Thermal Model

The temperature of the open raceway ponds effects the response of microalgae cultivation in terms of dark- and photo-respiration and growth. To understand the thermal parameters that drive the uncertainty of dynamic thermal modelling, we developed a lumped thermal system based on a [261] dynamic heat transfer model [252, 253]. The model adapted for the operational conditions of the pilot scale open raceway ponds takes into account considerations such as light absorption, radiation heat transfer with sky, convective heat transfer, evaporation and water control practices, and the bulk thermal capacitance of the algae media. An energy balance was carried out using a single thermal node to represent the well mixed (and thermally homogeneous reactor), and the resulting ordinary differential equation were solved numerically. This dynamic thermal model is described in the following sections.

8.2.2.1 Light Absorption

Total solar energy absorbed by (G_n) the photobioreactor media is a function of the total incident radiation (G_o), transmittance after surface reflection (τ_R), the portion of visible spectrum (estimated at 66% for wavelengths less than 900 nm), number of discretized nodes ($N = 1$), non-visible spectrum mostly infrared estimated at 34%, and transmittance after absorption at nodes above (τL) (Eq. 1) [259, 261].

$$G_n = G_o * \tau_R * \left[\frac{0.66}{N} + 0.34 * \tau L^{n-1} * (1 - \tau L)\right] \quad \text{Eq. 1}$$

Total incident radiation was obtained from the local weather station at Arizona State University. Transmittance is a function of the angle of incidence (θ_1) and angle of reflection (θ_2) (Eq. 2, Eq. 3, and Eq. 4). The angle of incidence is a function of the angular position of sun at noon with respect to plane equator (δ), latitude (φ), hour angle (ω), refractive index of water (n_1), and refractive index of air (n_2) (Eq. 5 and Eq. 6) [262].

$$\tau_R = \frac{1}{2} * \left[\frac{1-r_{parallel}}{1+r_{parallel}} + \frac{1-r_{perpendicular}}{1+r_{perpendicular}}\right] \quad \text{Eq. 2}$$

$$r_{parallel} = parallel\ reflection = \frac{tan^2(\theta_2-\theta_1)}{tan^2(\theta_2+\theta_1)} \quad \text{Eq. 3}$$

$$r_{perpendicular} = perpendicular\ reflection = \frac{sin^2(\theta_2-\theta_1)}{sin^2(\theta_2+\theta_1)} \quad \text{Eq. 4}$$

$$cos\theta_1 = sin\delta * sin\varphi + cos\delta * cos\varphi * cos\omega \quad \text{Eq. 5}$$

$$\frac{n_1}{n_2} = \frac{sin\theta_2}{sin\theta_1} \quad \text{Eq. 6}$$

Under the assumption of well-mixed conditions, a single node will represent the temperature of the growth media. The second part of equation 1, corresponds to infrared wavelength (34% of the light spectrum) which is not absorbed by chlorophyll [263] and can be neglected in the heat balance.

8.2.2.2 Radiation Heat Transfer with Sky

The sky and growth media (water) can be treated as two surfaces emitting radiation to compute the net radiative heat transfer [261]. Radiation heat transfer with sky is a function of the total emissivity of the radiating water surface (ε), the Stefan-Boltzmann constant (σ =5.67e^{-8} W.m^{-2}.K^{-4}), the temperature of the water surface (T_1), and the effective sky temperature (T_2) (Eq. 7 and Eq. 8) [253, 259, 264].

$$Q_{rad} = -\varepsilon * \sigma * \left[{T_1}^4 - {T_2}^4\right] \quad \text{Eq. 7}$$

$$hr = \varepsilon * \sigma * \left[{T_1}^2 - {T_2}^2\right] * [T_1 - T_2] \quad \text{Eq. 8}$$

The effective sky temperature (T_2, T_{sky}) is a function of the emissivity of the radiating sky surface (ε_{sky}), assumed for clear sky for the state of Arizona, which is modeled as a function of the dew point (T_{dew}), the hour of day (t), and the ambient pressure (P) (Eq. 9 and Eq. 10) [259, 264].

$${T_{sky}}^4 = \varepsilon_{sky} * Tambient^4 \quad \text{Eq. 9}$$

$$\varepsilon_{clear\ sky} = 0.711 + 0.56 * \left(\frac{T_{dew}}{100}\right) + 0.73 * \left(\frac{T_{dew}}{100}\right)^2 + 0.013 * \cos\left(\frac{2\pi t}{24}\right) + 0.00012 * (P - 100) \quad \text{Eq.10}$$

8.2.2.3 Convective Heat Transfer

Heat is also transported the fluid the local atmosphere through convective heat transfer [253, 261]. Convective heat transfer (Q_h) is modeled as the net temperature difference between the water surface temperature ($T_{surface}$) and the ambient temperature ($T_{ambient}$) times the heat transfer coefficient (h_i) (Eq. 11) [261].

$$Q_h = -h_i * \left(T_{surface} - T_{ambient}\right) \quad \text{Eq. 11}$$

The heat transfer coefficient can be estimated from the Nusselt number (N_{ux}), the thermal conductivity (k), and the characteristic length or hydraulic ratio (R_h) (Eq. 12). The Nusselt number, for turbulent flows, is a function of the Reynolds number (Re) and the Prandtl Number (Pr) (Eq. 13). The Prandtl number is a function of kinematic viscosity (ν), thermal diffusivity (α), thermal conductivity (α), fluid density (ρ), and fluid specific heat (C_p) (Eq. 14 and Eq. 15). The Reynolds number is a function of the fluid velocity (u), the characteristic length or hydraulic ratio (R_h), and the kinematic viscosity (ν) (Eq. 16). Lastly, the characteristic length or hydraulic ratio is a function of the raceway channel width (w) and height (H) (Eq. 17) [261].

$$h_i = \frac{N_{ux} * k}{R_h} \quad \text{Eq. 12}$$

$$N_{ux} = 0.0296 * Re^{4/5} * Pr^{1/3} \quad \text{Eq. 13}$$

$$P_r = \frac{\nu}{\alpha} \quad \text{Eq. 14}$$

$$\alpha = \frac{k}{\rho * C_p} \quad \text{Eq. 15}$$

$$Re = \frac{u * R_h}{\nu} \quad \text{Eq. 16}$$

$$R_h = \frac{4 * w * H}{2w + H} \quad \text{Eq. 17}$$

8.2.2.4 Conductive Heat Transfer

Heat can also be transported by conduction from the growth medium to the surrounding environment [253, 261]. Conductive heat transfer (Q_k) is modeled as the net between two nodes (T_2 and T_1) of the water bulk, assumed for this case between the water temperature and the ambient temperature, times the thermal conductivity (K) and the nodes distance (Ln), assumed to be equal to the water depth (Eq. 18) [261].

$$Q_k = -\frac{K}{Ln} * (T_2 - T_1) \quad \text{Eq. 18}$$

8.2.2.5 Evaporation and Water Control Practices

Thermal energy can be lost from the system through evaporation [261]. For the case of the open raceway ponds at ATP^3, daily evaporation was calibrated to 1.82 cm.day^{-1} due to aleatory uncertainty in modeling this parameter. To compute the thermal energy loss, the specific enthalpy due to evaporation was used in the heat balance, 2257 KJ.kg$^{-1}{}_{\text{Evaporated water}}$. Additionally, to maintain the water depth at 25 cm., the open raceway ponds are daily refilled with water. To compute the heat supplied to the system by refilling the open raceway ponds, the enthalpy of water at 40 °C, 167.53 KJ.kg$^{-1}{}_{\text{Refilled water}}$, was used based on measurements of the tap water temperature. The mass of refilled water was estimated from the water height recorded daily at ATP^3.

8.2.2.6 Capacitance, Energy Balance, and Dynamic Water Temperature Simulation

By implementing a system analogy approach, the capacitance of the fluid is defined as the capacity of the microalgae culture to storage heat (Eq. 19) [252, 253]. The heat balance (q_{th}) was computed by considering light absorption (G_n), radiation heat transfer with sky (Q_{rad}), convective heat transfer (Q_h), conductive heat transfer (Q_k), evaporation losses (E) and water addition (W), and the open raceway pond area (A) (Eq. 20). Lastly, the dynamic responses of the growth media temperature (Eq. 21) were numerically solved by the Dormand–Prince (RKDP) method in Matlab® for three seasons: Fall 2013, Spring 2014, and Summer 2015.

$$C_{th} = \rho * V * C_p \quad \text{Eq. 19}$$

$$q_{th} = A * (G_n + Q_{rad} + Q_h + Q_k - \mathrm{E} + \mathrm{W}) \quad \text{Eq. 20}$$

$$\frac{dT}{dt} = \frac{1}{C_{th}} * q_{th} \quad \text{Eq. 21}$$

8.2.3 Dynamic Algae Growth Modelling

Microalgae growth rates are responsive to their environment including temperature, radiation, and nutrient concentration. To understand the role that the environment exerts to dark- and photo-respiration responses and the growth of microalgae, we upgraded a microalgae growth model developed by Sandia National Laboratories [62, 220, 256, 265] by incorporating dark- and photo-respiration [62, 219, 220] and dynamic thermal modelling [252, 253]. The inputs to the dynamic model are the water temperature, incident radiation, and initial nutrient concentrations. The dynamic microalgae growth model is described in the following sections.

8.2.3.1 Temperature Function

Water temperature impacts the maximum growth rate of microalgae due to photo-respiration effects. This effect has been mathematically described by a normal or bell-shape curve (Eq. 22 and Eq. 23) [62, 220, 256, 265, 266], where algae growth rates are maximized at T_{opt}, and fall away from the maximum at higher and lower temperatures. This non-dimensional temperature function considers the real time water temperature (T), a parameter determining the shape (k = 0.009 °C^{-2}) and the optimum temperature of the algae strain ($T_{opt} = 24.05\ °C$) [220].

$$\emptyset_T = e^{-k*\left(T-T_{opt}\right)^2} \qquad T \leq T_{opt} \qquad \text{Eq. 22}$$

$$\emptyset_T = e^{-k*\left(T_{opt}-T\right)^2} \qquad T \geq T_{opt} \qquad \text{Eq. 23}$$

8.2.3.2 Light Function

Microalgae growth limitations and photoinhibition in a well-mixed layer is described by Steele's equation [62, 265, 267] (Eq. 24). This light function ($\emptyset_I$) considers the light saturation for *Nannochloropsis oceanica* ($I_s = 20\ W.m^2$) and the attenuation of light (I) in algal cultures based on Beer-Lambert Law [265] (Eq. 25). Attenuation of light is itself a function of the fraction of solar radiation absorbed at the water surface ($\beta = 0.1$), local incident radiation for the

state of Arizona (I_0), the attenuation coefficient (α), and the culture height (Δz). The attenuation coefficient is a function of attenuation due to sources other than algae ($k_b = 0.45$) and the chlorophyll-a concentration (φ_a) (Eq. 26) [62].

$$\emptyset_I = \frac{I}{I_s} * e^{-\frac{I}{I_s}+1} \quad \text{Eq. 24}$$

$$I = (1-\beta) * I_0 * e^{-\alpha*\Delta z} \quad \text{Eq. 25}$$

$$\alpha = k_b + 0.0088 * \varphi_a + 0.054 * {\varphi_a}^{2/3} \quad \text{Eq. 26}$$

8.2.3.3 Nutrients Function

The nutrient function ($\emptyset_n$) for microalgae growth can be computed from Monod Equation by considering the limiting nutrients: nitrogen (n), phosphorous (p), or carbon (c), and their half-saturation constant (k_s) (Eq. 27) [265]. Depletion of each of these nutrients can be estimated from the Redfield ratio (a_{pa}), growth rate (k_g), basal metabolism (BM), and algae biomass (a) (Eq. 28) [265]. The Redfield ratio for nitrogen, phosphorous, and carbon are 0.063, 0.0087, and 0.3583, respectively [265, 268]. Basal metabolism, growth rate and algae biomass will be described in the next sections.

$$\emptyset_n = \min\left(\frac{n}{k_{sn}+n}, \frac{p}{k_{sp}+p}, \frac{c}{k_{sc}+c}\right) \quad \text{Eq. 27}$$

$$\frac{dn}{dt} = -a_{pa}*(k_g\text{-}BM)*a \quad \text{Eq. 28}$$

8.2.3.4 Basal metabolism Function

Basal metabolism accounts for dark respiration and can be described as a first-order reaction (Eq. 29) [220, 266]. This equation has been previously described as a function of metabolic rate at a reference temperature ($BMo = 0.01\ d^{-1}$), the reference temperature for metabolism ($T_0 = 20\ °C$), the water temperature of the open raceway pond, and the effect of

temperature on metabolism ($K_{TB} = 0.15\ ℃^{-1}$), computed from experimentation conducted by previous authors at inhibiting light intensities and temperatures [219].

$$BM = BMo * e^{K_{TB}(T-T_0)} \quad \text{Eq. 29}$$

8.2.3.5 Dynamic Algae Growth Simulation

The growth rate (k_g) under outdoor conditions is obtained by multiplying the maximum growth rate (μ_{max}) of *Nannochloropsis oceanica* by the functions of growth limitation and inhibition by temperature ($\emptyset_T$), light ($\emptyset_I$), and nutrients ($\emptyset_n$) (Eq. 30) [62, 220, 256, 265]. Lastly, the ordinary differential equation of algae biomass is a function of growth rate under outdoor conditions and dark- and photo-respiration (Eq. 31). This equation is numerically solved by the Dormand–Prince (RKDP) method in Matlab® for three seasons: fall 2013, spring 2014, and summer 2015.

$$k_g = \mu_{max} * \emptyset_T * \emptyset_I * \emptyset_n \quad \text{Eq. 30}$$

$$\frac{da}{dt} = k_g(T, n, I) * a - BM * a \quad \text{Eq. 31}$$

8.2.4 Uncertainty Quantification

The predictive capability of dynamic thermal model and the algae growth model are evaluated for the season of Fall 2013. Uncertainties can be quantified by the error of the model with respect to the experimental data (Eq. 32) [269] and by comparing the cumulative distribution function (CDF, $d(F, S_n)$) of the model ($F(x)$) and the experimental data ($S_n(x)$) (Eq. 33) [270, 271]. The dynamic thermal model error was quantified by the mean absolute relative error (E. 34). The variable considered in this study is the water temperature of the dynamic thermal sub-system. The uncertainty of the algae growth model was quantified as the mean relative error of the model relative to the experimental data at the stationary stage of the algae growth curves.

$$error = model - experimental\ data \quad \text{Eq. 32}$$

$$d(F, S_n) = \int_{-\infty}^{\infty} |F(x) - S_n(x)| dx \quad \text{Eq. 33}$$

$$Mean\ Absolute\ Relative\ Error = Ave\left(Abs(Model_i - Experiment_i)\right) \quad \text{Eq. 34}$$

8.2.5 Calibration Procedure

The thermal parameters of the open raceway ponds that were calibrated are 1) capacitance, 2) shading of incident radiation, 3) convective heat transfer coefficients, and 4) radiation heat transfer coefficient to the sky. Additionally, because aleatory uncertainty in the measurement of evaporation and water addition to maintain constant water depths in the open raceway ponds, these parameters were calibrated. Lastly, because dark-respiration and photo-respiration in outdoor cultivation systems is poorly understood, the involved parameter were calibrated in the algae growth model. The parameters were calibrated using the data from the season of fall 2013, including the parameter determining the shape of temperature function (k = 0.009 °C^{-2}), attenuation coefficient (α) as a function of algal biomass, and effect of temperature on metabolism ($K_{TB} = 0.15\ ℃^{-1}$). The parameters were simultaneously calibrated by minimizing the error of the model with respect to the experimental data based on the cost function (Eq. 35) by the pattern search Latin Hypercube optimization method with a parameter tolerance of 1e^{-6} in Matlab®. The calibrated parameters were consequently used for validation of the model for the seasons of Spring 2014 and Summer 2015, respectively [269-271]. The propagated uncertainty in the overall system [270] includes the uncertainty inputs from the validated dynamic thermal model, and the dynamic algae growth model.

$$Cost\ Function = \sum error^2 \quad \text{Eq. 35}$$

8.3 Results and Discussion

The results of this research are synthesized into three aspects. First, we present the results of the dynamic thermal model. Second, we present the results of the dynamic well-mixed algae growth model and discuss the relevance of dark- and photorespiration in the uncertainty of the results. Lastly, we propagate the uncertainty of the dynamic thermal model by embedding it into the dynamic algae growth model. The system, including the dynamic thermal model and algae growth model, is validated for the seasons of Fall 2013, Spring 2014, and Summer 2015.

8.3.1 The uncertainty of the thermal model is driven by thermal capacitance, evaporation, and heat transfer coefficients

A lumped thermal model was valid to represent pilot open raceway ponds, validating well-mixed conditions in these systems. While previous efforts have developed thermal models for other photobioreactors configurations, our thermal model is the first effort applied to pilot open raceway ponds, quantifying uncertainty, and identifying and estimating epistemic parameters. By developing a thermal model system valid under season variability, we can reduce the propagated uncertainty when embedding the model into algae growth models.

The dynamic lumped-thermal model is validated against experimental culture temperature to quantify error. Validation of the model for the season of fall 2013 is illustrated in Figure 8.2. The model clearly overestimates the water or culture temperature in the system relative to the experimental data. By calculating the error between the model and the experimental data, this is has an mean abosulute relative error of 3 °C (Figure 8.2).

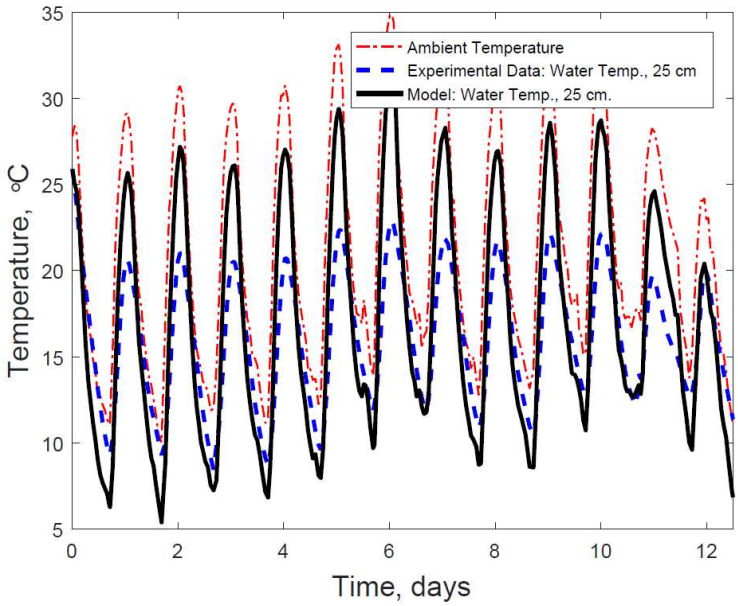

Figure 8.4 Dynamic Thermal Model Result of Open Raceway Pond for Fall 2013.

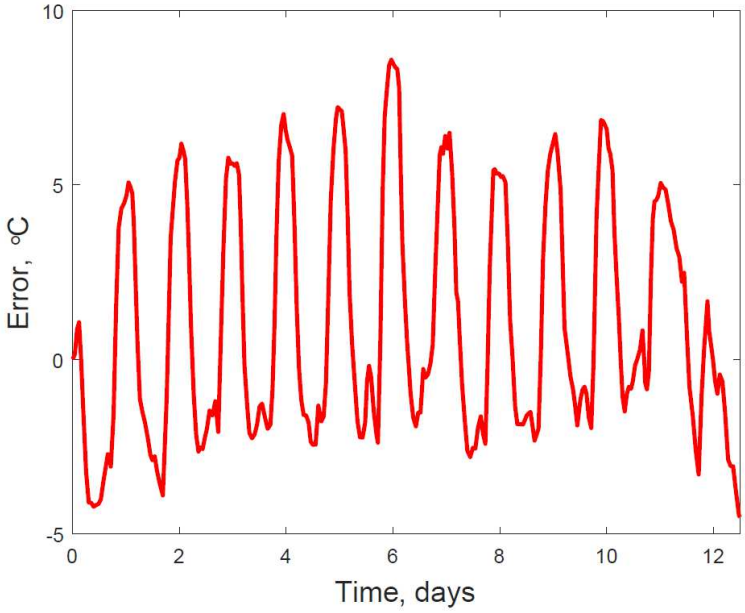

Figure 8.5 Uncertainty Quantification of Dynamic Thermal Model for Fall 2013. Error of the model relative to experimental data.

The epistemic and aleatory parameters are calibrated by the pattern search Latin Hypercube optimization method. From this parameter estimation method, thermal capacitance is

increased 4.973 times than values recommended for water by Bergman, Incropera, Frank, DeWitt, and Lavine (2006) in fundamental theory for heat transfer. Calibration of radiation shading factors in the open raceway pond was found to be negligible by this optimization method. Convective heat transfer coefficient due to paddlewheel mixing was reduced by a factor of 0.829, and convective heat transfer coefficient due to wind was reduced by a factor of 1.842e-^{3}4. Radiation heat transfer coefficient with sky was reduced by a factor of 7.459e-^{4}. Aleatory parameters, evaporation and water addition, were calibrated by factors of 0.981 and 8.1329, respectively. The calibrated lumped-thermal model is demonstrated to be valid for fall 2013 (Figure 8.4), where the mean absolute relative error is 1.8 °C. The calibrated model for thermal parameters of Fall 2013, mispredicts the mean experimental culture temperatures when validating for the seasons of Spring 2014 (Figure 8.5) and Summer 2015 (Figure 8.6) with mean absolute relative error are 5.1 °C and 6.9 °C, respectively. This uncertainty quantification, calibration, and validation approach demonstrate we need a better understanding of epistemic thermal parameters under season variability and to reduce the aleatory uncertainties of evaporation and water control practices in open raceway ponds systems.

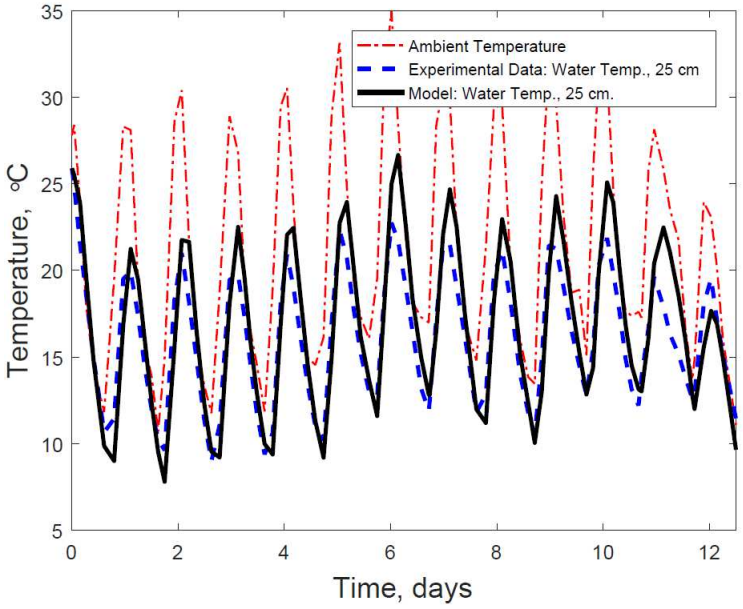

Figure 8.6 Validation of Dynamic Thermal Model for Fall 2013.

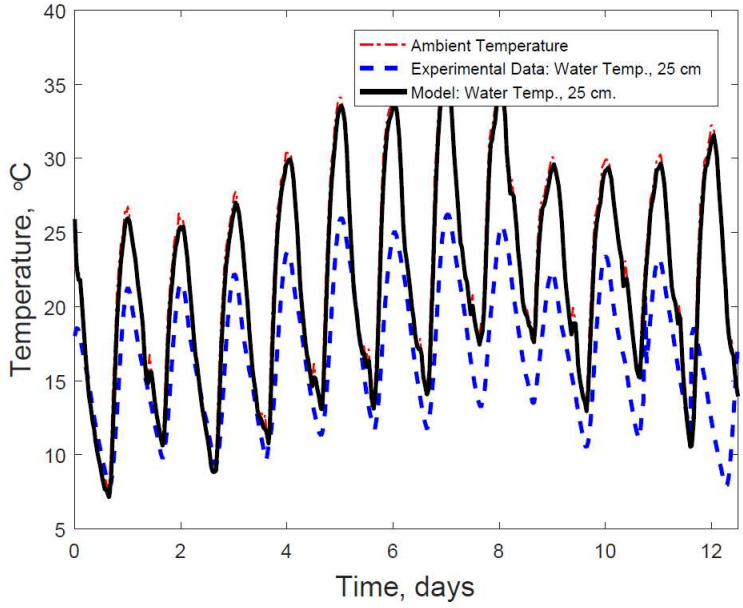

Figure 8.7 Validation of Dynamic Thermal Model for Spring 2014.

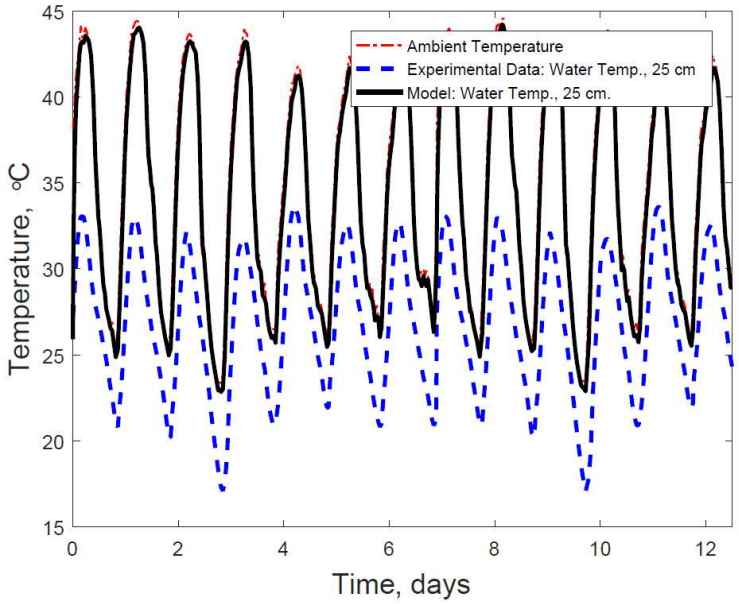

Figure 8.8 Validation of Dynamic Thermal Model for Summer 2015.

8.3.2 The uncertainty of algae growth modelling is driven by dark- and photo-respiration effects

Weather conditions impact the biological responses of microalgae in terms growth due to photo-respiration at high temperatures and radiation, and dark respiration. The functions that involve photo- and dark-respiration include the temperature function, the light function, and the basal metabolism function.

The temperature function effects due to water temperature are illustrated in Figure F.1 in the Appendix F. In here, a factor of one represents the optimal conditions for *Nannochloropsis oceanica*, 24.05 °C, a factor below one illustrates inhibition at cold temperatures and photorespiration effects at high temperatures, and a factor of zero denotes microalgae death at extreme temperatures. Incident radiation (Figure F.2a in Appendix F) control the light function effects as illustrated in Figure F.2b in the Appendix F. A factor of one represents the light saturation of *Nannochloropsis oceanica*, 20 $W.m^{-3}$. Incident radiations below this value inhibit

the growth because of light limitation, and incident radiations above this value photo-inhibits the growth because of photorespiration, denoted by factors below one. Lastly, basal metabolism loss rate due to dark respiration is illustrated in Figure F.3 in the Appendix F, where the higher growth losses are represented by the higher rates.

Well-mixed assumptions in dynamic algae growth modelling are valid for Fall 2013. The dynamic algae growth model results, dry weight biomass as a function of time, is illustrated in Figure 8.7. The mean relative error of the model (relative to the experimental data at stationary stage in the growth curve) is -35% for Fall 2013.

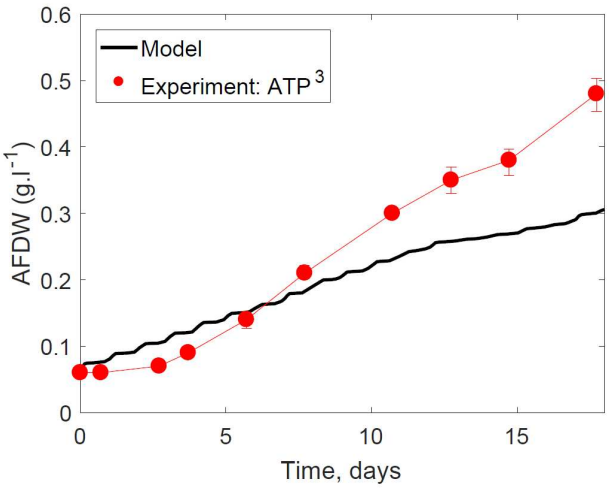

Figure 8.7 Dynamic Growth Model for Fall 2013.

By calibrating biological parameters involved in dark- and photo-respiration, the propagated uncertainty can be reduced when embedding dynamic lumped-thermal models. The calibration of parameters involved in dark- and photo-respiration include the parameter determining the shape of temperature function (k = 0.0048049 °C^{-2}), representing 0.53 times the original value a factor of 0.58083 acting as a gain for the actual attenuation coefficient (α) obtained in the model as a function of biomass; and effect of temperature on metabolism (K_{TB} =

$0.1888\ ℃^{-1}$), representing 1.23 times the original value. These estimated parameters suggest that the biomass losses due to temperature effects in photorespiration and the light attenuation computed by Beer-Lambert Law are overestimated, and that the basal metabolism or losses due to dark respiration are underestimated in these models. The calibrated dynamic algae growth model for Fall 2013, and the validation of the model for Spring 2014 and Summer 2015 are illustrated in Figure 8.8. The error of the model relative to the experimental data at stationary stage in the growth curve is 8%, 12%, and 16%, for Fall 2013, Spring 2014, and Summer 2015, respectively. The case of Summer 2015 was the only at which losses overcame growth because algae cultures more likely grew limited by nutrients as the lowest nitrogen and phosphorous concentrations were used for the experiments and modelling relative to Fall 2013 and Spring 2014. Although the calibrated parameters are valid for different seasons, a higher degree of uncertainty is observed due to variations in the environment algae experience and impact in the biological responses, including photo- and dark-respiration. The parameters calibration in this research, however, demonstrate that photorespiration, light attenuation, and dark respiration drive the uncertainty of algae growth model and the need to develop more research of this means for open raceway ponds.

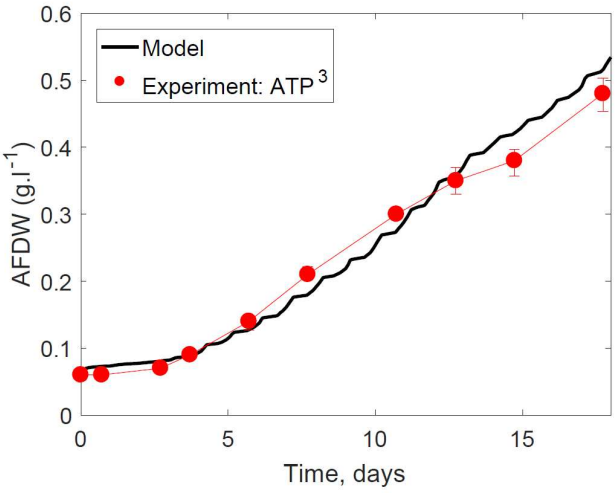
Model
Experiment: ATP 3
AFDW (g.l-1)
Time, days
0
0.1
0.2
0.3
0.4
0.5
0.6
0
5
10
15

(a)

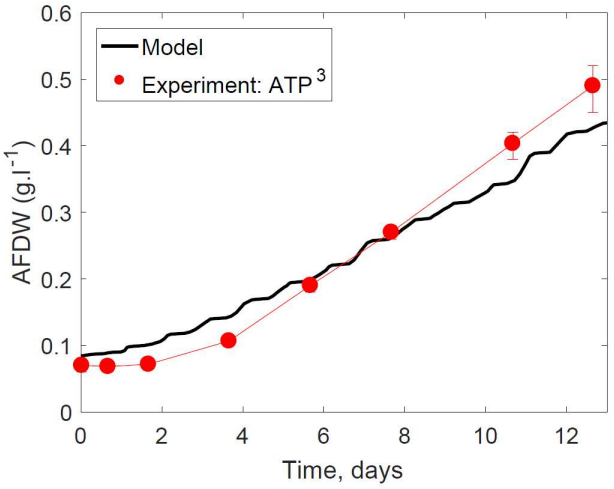
Model
Experiment: ATP 3
AFDW (g.l-1)
Time, days
0
0.1
0.2
0.3
0.4
0.5
0.6
0
2
4
6
8
10
12

(b)

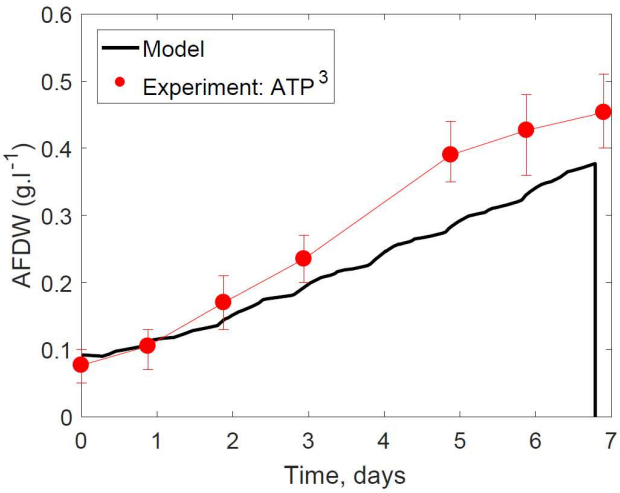

(c)

Figure 8.8 Calibration of Dynamic Algae Growth Model after Parameter Estimation for Fall 2013 (a), Validation for Spring 2014 (b), and Summer 2015 (c).

8.3.3 Propagated uncertainty in algae cultivation systems embedding thermal models increase the error for summer conditions

The error in predicting AFDW of the algae includes the error of the dynamic lumped-thermal model embedded into the dynamic algae growth model. The predictive capability of the system is illustrated for the seasons of Spring 2014, and Summer 2015 in Figure 8.9. For Summer 2015 the predicted algae AFDW error is -53%. This high error is due to the overpredicted water temperatures for summer, which result in dark- and photo-respiration effects beyond the threshold where algae is inhibited by light and temperature, reducing growth and biomass. This analysis demonstrates the importance of developing a better understanding of the error in thermal parameters as the system temperature has a high impact on the growth of the algae.

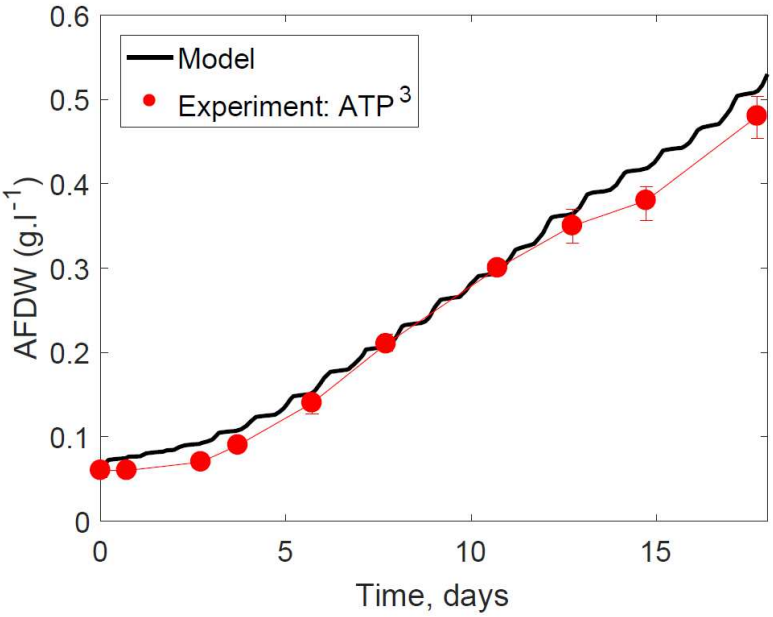
Model
Experiment: ATP 3
AFDW (g.l-1)
Time, days
0
0.1
0.2
0.3
0.4
0.5
0.6
0
5
10
15

(a)

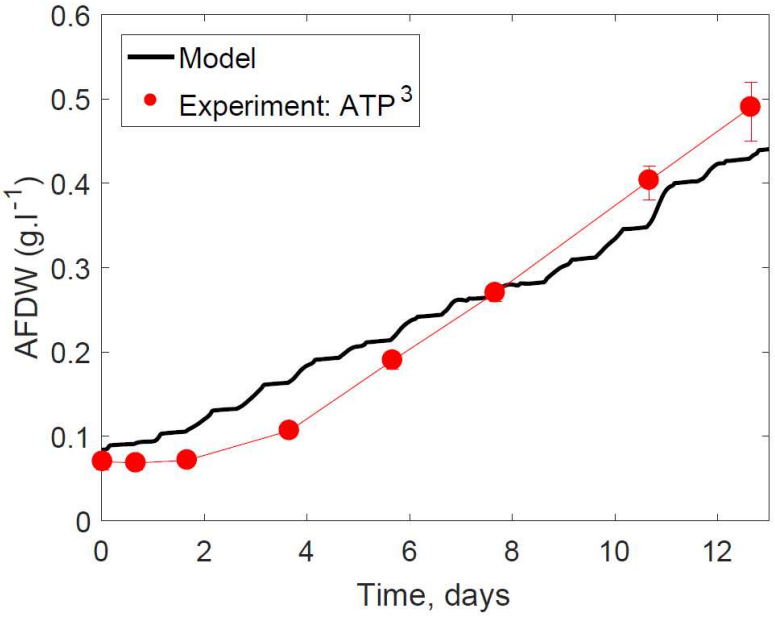
Model
Experiment: ATP 3
AFDW (g.l-1)
Time, days
0
0.1
0.2
0.3
0.4
0.5
0.6
0
2
4
6
8
10
12

(b)

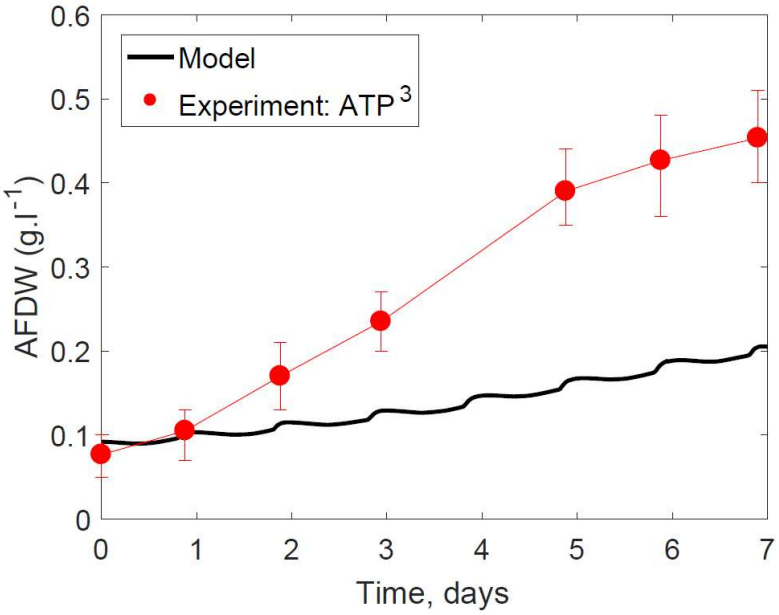

(c)

Figure 8.9 Calibration of System of Algae Growth Model Embedding Dynamic Thermal Model for Fall 2013 (a), Validation for Spring 2014 (b), and Summer 2015 (c).

8.4 Conclusions

Parameter estimation and validation of an open raceway pond cultivation system suggest that the uncertainty of integrated well-mixed thermal and algae growth models is very high. Our experimentally calibrated models demonstrate that error in the lumped-thermal model drives error in the prediction of biomass, impacting dark- and photo-respiration functions and the growth of algae.

8.5 Answer to Research Question 3.2

This section of the research effort has allowed us to address Research Question 3.2, which is restated and answered in section 9.5 of this dissertation.

CHAPTER 9: Cyanobacterial biomass productivity in pilot scale open raceway ponds and flat-panel photobioreactors is predicted by well-mixed growth modelling under a wide range of mixing energy inputs[8]

9.1 Introduction

Photoautotroph-based biofuels are considered one of the most promising renewable resources to meet the global energy requirements for transportation systems [5]. Long-term research and development has resulted in demonstrations of microalgae areal oil productivities that are higher than crop-based biofuels, about 10 times that of palm oil and about 131 times that of soybean [5, 74-76]. Cyanobacteria is reported to have ~4 times the areal productivity of microalgae on an equivalent energy basis [6]. Downstream of this cultivation process, cyanobacterial biomass and bioproducts can be supplied to biorefineries producing feed, biomaterials, biosynthetic chemicals, and biofuels [77]. As such, cyanobacterial systems can be a significant contributor to more sustainable energy and production systems.

Turbulent environments are demonstrated to induce physiological responses in photoautotrophic microorganisms in open raceway ponds and photobioreactors [200-207]. Recent efforts studied the effects of turbulence dissipation rates ranging from 0 to 0.08 $m^2.s^{-3}$ simulated at laboratory scale conditions (1 liter cultures) [200]. This work concluded that despite no alteration of photosynthesis activity on chlorophyll a, there is a systematic increase in the growth rates of the strain *Microcystis flos-aquae* as a function of the turbulent dissipation rate and a decay in the growth rate of the strain *Anabaena flos-aquae* at high turbulence. These authors identified a maximum phosphorous uptake rate by these cyanobacteria strains at

[8] **This chapter is adapted from a prepared journal article for consideration for publication:** Carlos Quiroz – Arita and Thomas H. Bradley. "Cyanobacterial biomass productivity in pilot scale open raceway ponds and flat-panel photobioreactors is predicted by well-mixed growth modelling under a wide range of mixing energy inputs".

turbulence dissipation rates of $2.26E^{-2}$ $m^2.s^{-3}$, suggesting that turbulence plays an important role in the biological adaptation of cyanobacteria by influencing nutrient uptake [200]. In other research, the effects of shear environments were studied for the cyanobacteria and microalgae strains *Synechocystis sp.* and *Chlamydomonas reinhardtii*, respectively, in 150 ml cultures [201]. In this study the growth rate of *Synechocystis sp.* was independent of shear stress (0 to 0.18 $N.m^{-2}$) and *Chlamydomonas reinhardtii* growth rate was linearly dependent on shear stress. These laboratory scale environments, however, are not representative of industrial scale conditions.

Other impacts of turbulent mixing are cell disruption due to shear stress [208-215]. Some instances are for hybridoma cells suffering apoptosis at mixing energy inputs of $1.87E^3$ $W.m^{-3}$ [209, 216]. Other studies observed 51% lower recombinant protein production, 42% higher glucose uptake, and 50% lower lactate production cells exposed to mixing energy inputs of $6.4E^2$ $W.m^{-3}$ [209, 217]. Inhibitory effects, however, are reported at mixing energy inputs above $1E^6$ $W.m^{-3}$ and Kolmogorov microscales less than or equal to 2.4 micrometers for mammalian cells [209]. In photobioreactors, small bubbles are reported to cause cell damage [205, 218], colliding with photoautotrophic cells and contributing to a high shear environment. The microalgae strain *Phaeodactylum tricornutum*, for instance, presented inhibition at air rates of 0.567 $m^3_{air}.min^{-1}.m^{-3}_{reactor}$, where carboxymethyl cellulose (CMC) was supplied into the medium to mitigate shear-induced damage in parallel experiments [205]. Other sparged photobioreactors cultivating *Dunaliella tertiolecta* and *D. salina* reported increments in the decay rates as a function of gas velocity, observing the highest death rates at 8.91 and 13.37 $m^3_{air}.min^{-1}.m^{-3}_{reactor}$ [218]. There is no research reported in the literature concerning the biological system response due to shear stress on cyanobacteria cells disruption, particularly on *Synechocystis sp.* PCC6803. Moreover, most of the previous research were conducted at mixing energy inputs are 30, 100, or thousands

order of magnitudes higher than is considered cost-effective for industrial cultivation systems [53, 224].

Photoautotrophic microorganisms are cultivated in photobioreactors, the most common types being the open raceway ponds and flat panel PBR [225]. Open raceway ponds are constructed in a configuration with channels, using paddlewheel mixers that promote a low shear environment [8]. Flat-panel photobioreactors are vertically translucent flat plates, illuminated on both sides and stirred by aeration [9]. Unlike outdoor raceways and outdoor PBR, laboratory-scale experiments are most commonly grown under ideal conditions including ideal mixing rates, optimum light intensities and optimized media. Comparison of the laboratory scale literature to industrial results demonstrate that photoautotrophic biomass and biofuels productivity are overestimated at laboratory scale experiments relative to industrial scale systems. This distinct difference in the performance of industrial systems are partially attributed to the light experienced by photoautotrophic microorganisms at outdoor conditions. For instance, the light saturation of *Synechocystis sp.* PCC6803 is reported at about 200 μmol photons.s^{-1}.m^{-2} [10, 84], whereas photoautotrophic microorganisms will face incident radiations of about 2000 μmol photons.s^{-1}.m^{-2} at noon in locations such as Colorado [11] Previous studies have estimated that the total photo conversion efficiency of algae is from 2.6% (at high light) to 6.3% (at reduced light) [12]. These estimations assumed that 46% of the spectrum is in the photosynthetic active radiation (PAR) range of 400 to 700 nm, losses due to photon transmissions efficiency of 95%, photon utilization efficiency ranging from 10% to 30%, biomass accumulation efficiency of 50%, and biomass energy content of 21.9 kJ·g^{-1}. Low photo conversion efficiency in photoautotrophic microorganisms is attributed to dark and photorespiration biomass losses [62, 219, 220]. Photorespiration is well understood in plants, where carboxylation step in the Calvin–

Benson cycle is switched to oxygenation, dissipating photic energy and accounting for 25% reduction in the photosynthesis in C_3 plants [221]. Photorespiration is poorly understood in photoautotrophic microorganisms.

Some previous studies have investigated the effects of mixing rates on photoautotroph biomass productivities in industrial scale systems [11, 53, 54]. Some of these efforts have identified optimum volumes of air flow rates per unit volume (VVM) of photobioreactors that might be industrially relevant for microalgae, generally between 0.2 to 1.2 $m^3_{air}.min^{-1}.m^{-3}_{reactor}$ [11]. Many others have considered mixing energy inputs that are far outside the energy consumption that can be considered economic, or industrially relevant, ranging from 8 to 633 $W.m^{-3}$ [53, 224]. For raceway ponds, for instance, energy inputs from 1 to 2 $W.m^{-3}$ are utilized in the algae cultivation demonstrations performed to date [54]. Additionally, previous research state that mixing in industrial photobioreactors induce flashing or dark/light cycles [226-228]. For instance, by carrying experimental growth of *Chlamydomonas reinhardtii* under incident radiations fluctuating between 5 Hz and 100 Hz, growth rates were found to be linearly dependent on the light frequency. These previous efforts suggest that mixing in photobioreactors control the light regimes experienced by single cells, impacting the bulk photosynthesis and biomass productivity of photoautotrophic microorganisms. Other efforts, however, demonstrated no improvements in algal productivity at light fluctuations from 0.038 Hz to 1 Hz, modeled using a control timer to open and close a mini venetian blind device [229]. The latter frequencies ($<<$ 1 Hz), are more consistent when comparing with the circulation velocities studied for fermenters with a height to diameter ratio less than 3 ($<$ 60 seconds) and for airlift reactors with split-cylinders heights of 6.02 m. (6.5 seconds) [230].

There are several ongoing efforts in the literature to predict the performance of photobioreactors by growth modelling. Yet, most of the literature relies on light distribution in photobioreactors based on Beer-Lambert law [55, 56, 169]. Although previous efforts measured the absorption coefficient of *Nannochloropsis sp.* in photobioreactors [56], the derived model can only be used to describe light distribution for particular validated conditions. None of the previous efforts have demonstrated the predictive capability under wide range of mixing energy input. Advanced dynamic modelling tools predict present outputs based on past inputs by resolving complex systems integrating physical, chemical, and biological domains [252, 253]. Advanced dynamic modelling tools can be implemented to describe the complexity of these physical and biological systems. Previous efforts have explored the application of dynamic tools to microalgae cultivation systems under the assumptions of nutrient limitation [254, 255] and by mathematical representations of the biological responses [256]. Lastly, previous studies have recognized photoautotrophic microorganisms plays an important role in the refraction of radiation because scattering factors and in the temperature system [57, 58, 272]. None of the previous efforts have demonstrated the predictive capability of embedding light attenuation, accounting for scattering, and growth rates as a function of photorespiration under differences in mixing energy input for photoautotrophic growth modelling.

Based on this understanding of the literature we seek to understand the role of turbulent mixing on the light experience by photoautotrophic microorganisms, therefore, we conducted cyanobacterial growth modelling and validation By studying turbulence and growth rate as a function of mixing energy input in open raceway ponds and flat-panel photobioreactors, we aim to understand the role turbulence plays in the light attenuation in cyanobacterial cultures and cyanobacterial growth in pilot scale systems.

9.2 Materials and Methods

To evaluate the implications of turbulent mixing on the light experienced by photoautotrophic microorganisms in pilot scale open raceway ponds and flat-panel photobioreactors, we must understand growth modelling under differences in mixing energy inputs. The workflow, illustrated in Figure 9.1, integrates parallel but complementary experimental and computational growth modelling. By incorporating laboratory experiments at industrially relevant inputs, outdoor relevant light intensities and large-scale mixing rates, we developed a holistic bridge and feedback loop approach between laboratory and industrial scale experimentation.

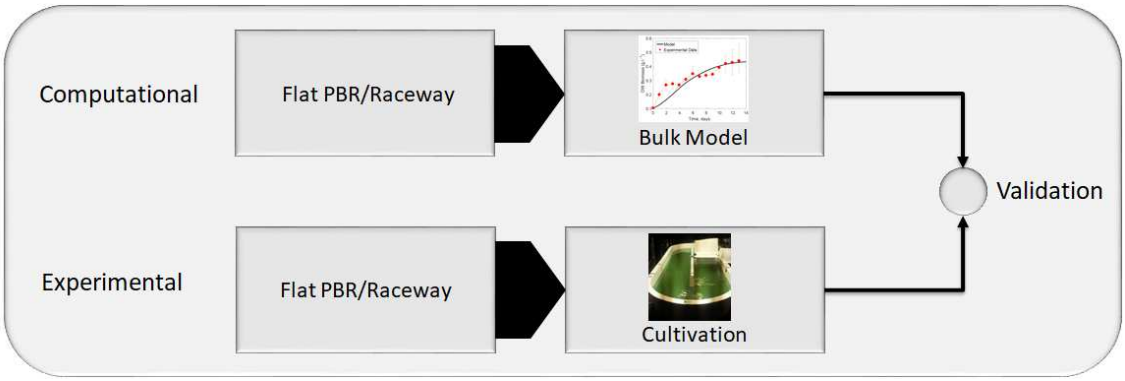

Figure 9.1 Workflow for experimental and computational photoautotrophic growth to assess the impact of mixing energy inputs.

9.2.1 Flat-Panel Photobioreactors Cultivation Methods

To validate the growth models, we performed experimental work under mixing energy input variability in the flat-panel photobioreactor and open raceway pond. As illustrated in Figure 9.2, the batch process was carried out in five replicates of 1L flat-panel photobioreactors made in acrylic with surface to volume ratio of 112 $m^2 \cdot m^{-3}$. The experiments were performed at cultures depths of 20 cm. The carbon system in each flat-panel photobioreactor was normalized by scrubbing CO_2 from the supplied air with soda lime and adding 0.483 $g.day^{-1}$ of bicarbonate.

Additional experiments were performed with sparged air and no addition of bicarbonate, to evaluate the mixing energies at which cultures grow limited by carbon. The cultures were grown using a high-pressure sodium (HPS) lighting system with a spectrum ranging from 400 to 700 nm at extreme conditions, emulating a sunny day at a constant Photosynthetic Active Radiation (PAR) of 1348 (± 84) μmol photons·m^{-2}·s^{-1}. A temperature control system was provided to maintain a temperature of 32 (± 2) °C, consisting of cold plates set at the bottom of each photobioreactor and chilled water supplied through copper pipelines. In this study we aimed to resemble the light attenuation of open raceway ponds in the flat-panel photobioreactors, by providing absorptive walls (black plastic corrugated sheets) to simulate a cross section of the culture into the raceway pond. Cultures were mixed by sparged air at the bottom of the flat-panel photobioreactors at industrially relevant mixing inputs of 0.7, 0.35, and 0.17 m^3 of air per minute per cubic meter of reactor, commonly referred as VVM [11]. Because these VVM are demonstrated to reduce the life cycle energy efficiency in photoautotrophic systems [273], we conducted additional experiments at 0.01 VVM. The equivalent mixing energy inputs used in the flat-panel photobioreactors experiments were 1.94, 0.97, 0.47, and 0.03 $W.m^{-3}$.

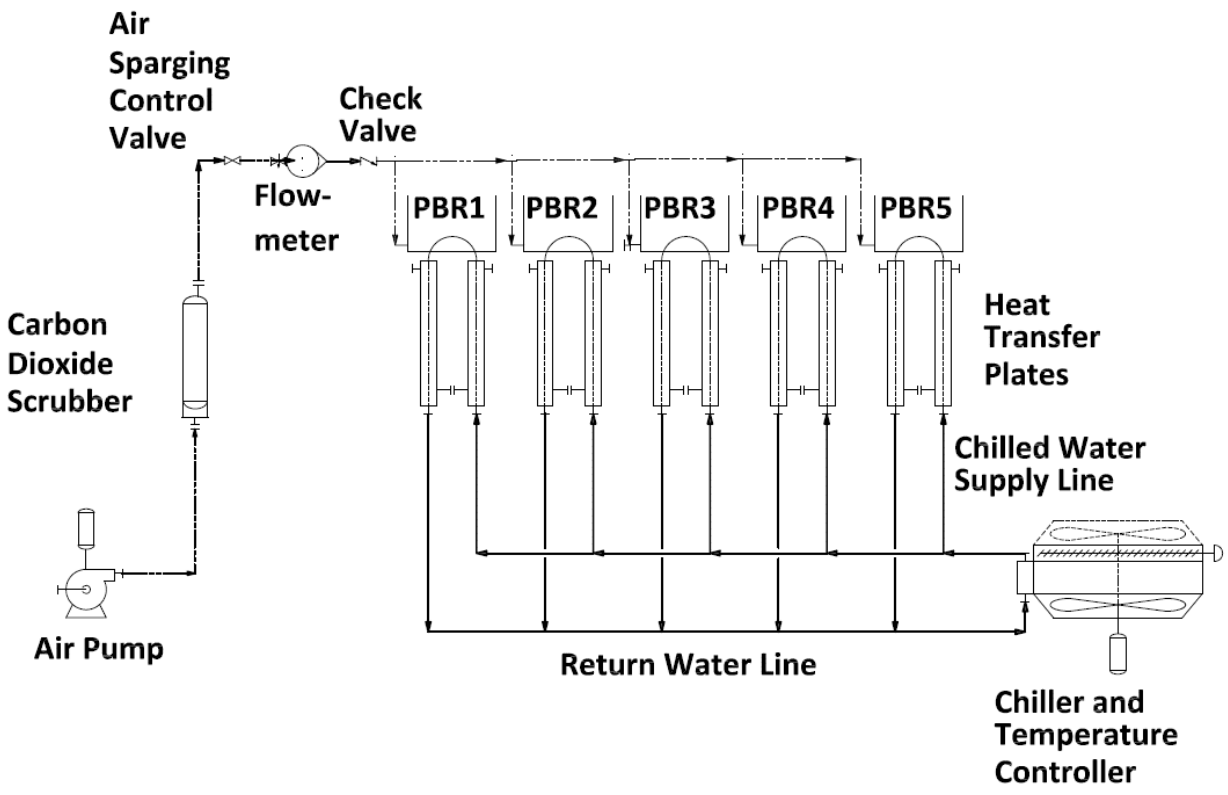

Figure 9.2 Instrumentation Diagram of Flat-panel photobioreactors system for experimental and model based analysis.

9.2.2 Open Raceway Pond Cultivation Methods

As illustrated in Figure 9.3, the open raceway pond batch process was carried out in a 700L fiber-reinforced plastic raceway at water depths of 20 cm. The cultures were grown in replicates of three using a high-pressure sodium (HPS) lighting system with a spectrum ranging from 400 to 700 nm at a Photosynthetic Active Radiation (PAR) of 938 (± 46) μmol photons·m^{-2}·s^{-1}. A temperature control system was provided to maintain the cultures at 29 °C, consisting of a thermocouple, temperature controller, solenoid valve, stainless steel coil submerged into the open raceway pond, and tap water supply pipeline. The culture was mixed with a paddlewheel provided with a 90V DC Gearmotor with a rated torque of 33 in.-lb controlled by an IronHorse DC Drives. The mixing energy input used in the open raceway pond

experiments was 0.10 $W.m^{-3}$, an order of magnitude lower than reported in the literature for industrial systems [54].

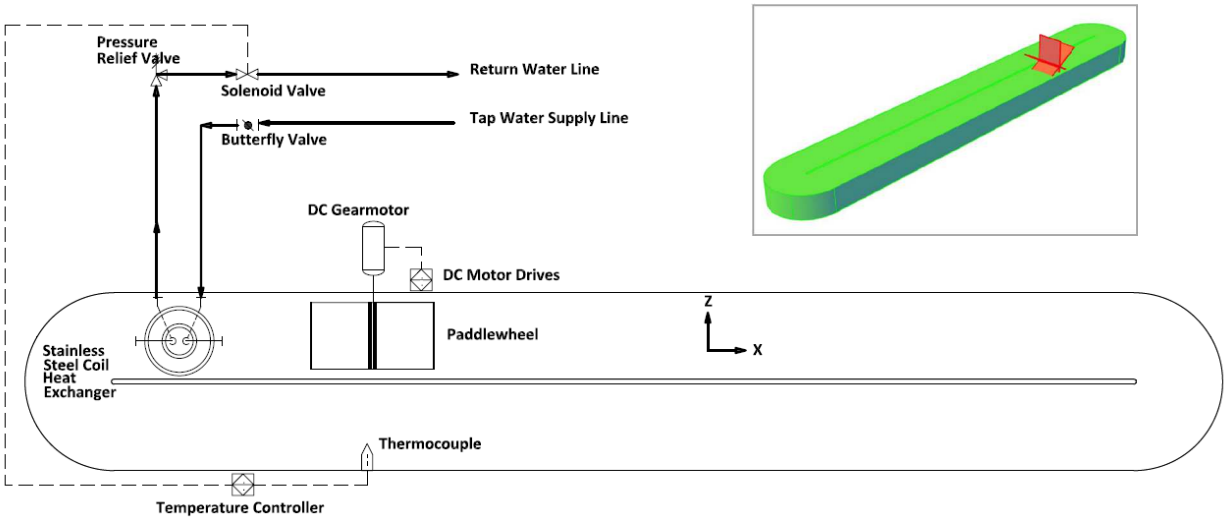

Figure 9.3 Plan View and Instrumentation Diagram of Open raceway pond system for industrial scale experimental and model based analysis. The 3D view of the Open Raceway Pond is illustrated in the upper right corner.

Growth rates of liquid cultures were monitored using SPECTRONIC 20 Genesys™ with a sampling period of eight hours. Dried weight biomass (DWB) was measured daily with 2.5 µm polypropylene prefilters dried at 60 °C and measured with high precision digital scale. The incident radiation and light attenuation were measured daily with a LI-250A Light Meter at the water surface, as well as water depths at 5 cm, 10 cm, 15 cm, and 20 cm.

9.2.3 Predictive capability of well-mixed growth models

9.2.3.1 Scale-up and Acclimation of Cyanobacterial Cultures

To inform the cyanobacteria growth and the LCA models, *Synechocystis* sp. PCC6803 cells were cultured in culture media (BG-11), scaling-up and acclimating at photo-inhibited light intensities for cultivation in 1L flat-panel photobioreactor and 700L open raceway pond, respectively. Cells were grown at 29 °C. The inoculum of 250 µL were scaled-up into 30 mL and

150 mL, grown in constant light fluxes of 60 μmol photons $m^{-2}.s^{-1}$. For acclimation in 1L flat-panel photobioreactors, 150mL cultures were inoculated into five replicates, grown in constant light fluxes of 1348 (± 84) μmol photons $m^{-2}.s^{-1}$. 10% of the acclimated cyanobacteria cultures were re-inoculated in the flat-panel photobioreactors and grown until stationary stage. For cyanobacteria cultivation in raceway ponds, the 150 mL cultures were further scaled-up into 1L flasks. The 1L cultures were inoculated into 9L glass carboys, which were acclimated by using the raceway pond as a water bath at 29 °C., grown in constant light fluxes of 938 (± 46) μmol photons $m^{-2}.s^{-1}$. The 700L open raceway pond was inoculated with the 9L glass carboys cultures and grown until stationary stage.

9.2.3.2 Well-mixed Growth Modelling and Validation

To assess the influence of turbulent mixing in the light experienced by cyanobacterial cells in photobioreactors, a well-mixed dynamic cyanobacterial growth model as a function of mixing energy input and experimentally determined light attenuation was developed for analysis in this study. This model incorporates ordinary differential equations (ODE) and nonlinear function embodying nitrogen quote, nitrogen uptake, chlorophyll synthesis, light absorption, photosynthesis, growth rate, and biomass [37, 169]. Table G.3 in the Appendix G summarizes the required biological inputs for *Synechocystis* sp. PCC6803 [10, 84, 187].

The model developed in this study is novel in that it incorporates the maximum growth rate (μ_m) with photo-inhibition and the light attenuation in *Synechocystis* sp. PCC6803 as a function of dry weight biomass and culture height. These parameters were determined from the experimental works described in section 2.2. The maximum growth rate of *Synechocystis* sp. PCC6803 was mathematically described by Eq. 5 [222], where all the parameters were determined experimentally (Figure G.1 and G.2) and discussed under results section.

$$\mu_{max} = \frac{ln(X_2/X_1)}{t_2 - t_1}$$ Eq. 5

X_2 and X_1 are the final and initial, respectively, optical density (OD) in the exponential stage of the growth curve, t_2 and t_1 are the final and initial, respectively, time in the exponential stage of the growth curve, *and* μ_{max} is the maximum specific growth rate.

Cyanobacterial biomass is a function of the growth rate, chlorophyll synthesis, and nitrogen (Eq. 6) [169]. The growth limiting factors in the model, nitrogen and light, are governed by the Droop cell-quota function and the Liebig's Law, respectively (Eq. 7) [169]. The cyanobacterial decay rate (*b*) used in the growth modelling is 0.06 d^{-1} [274]. A fixed fraction of accumulated carbon ($gC.g^{-1}dw$) is maintained for the dried biomass. Carbon fixation is a function of the Poisson single-hit model of photosynthesis. The photosynthesis rate (Eq. 8 and 9) is normalized by the chlorophyll content ($gC.g^{-1}chl.d^{-1}$) [169]. Chlorophyll synthesis (Eq. 10) is a function of nitrogen uptake (Eq. 11 and 12) [169]. The fraction of nitrogen supplied to chlorophyll synthesis is a function of the carbon utilization to uptake ratio (c) and the nitrogen uptake is a function of the maximum nitrogen quota (Eq. 13) [169]. Light attenuation in photobioreactor cultures is commonly computed by the Lambert-Beer law (Eq. 14), which is a function of the rate of light absorption by the culture [56]. In this study, however, Light attenuation (*I*) was experimentally determined as illustrated in the Appendix G (Figure G.4 and G.5) for one mixing energy input, 0.47 $W.m^{-3}$, and applied to all the growth models with mixing energy variation. Lastly, to evaluate the experimental work conducted under carbon limiting conditions, the Monod equation [161] and the uptake rate of total inorganic carbon (TIC) were incorporated into the system (Eq. 7 and 15). The carbon uptake rates for *Synechocystis* sp. PCC6803 used in this model are 0.059 $gC.l^{-1}.d^{-1}$, 0.380 $gC.l^{-1}.d^{-1}$, and 0.389 $gC.l^{-1}.d^{-1}$, for times in growth curve of 0-3 days, 3-9 days, and 9-12 days, respectively [84]. The carbon concentration at which growth is limited is 0.005 $gC.l^{-1}$ [84].

For the case of the flat-panel photobioreactors, the source of carbon was either bicarbonate or CO_2 in the sparged air. For the case of the open raceway ponds, there are two sources of carbon in the system, alkalinity measured by the city of Fort Collins as an average of 37.1 $mg.l^{-1}$ in the tap water used for cultivation, and the atmospheric carbon dioxide estimated by Henry's Law at $1.633e^{-4}$ $gC.l^{-1}$. These sources of carbon were calibrated for the raceway pond cyanobacterial growth model minimizing the sum squared error by the nonlinear least square method and a Levenberg-Marquardt algorithm. The estimated parameters were 0.25032 $gC.l^{-1}$ of total inorganic carbon and 0.0007585 $gC.l^{-1}$ in equilibrium with atmosphere. The estimated parameters are likely in this open system where tap water was daily supplied to compensate evaporation losses. Additionally, water in equilibrium with atmosphere is described as H_2CO_3* in equilibrium with CO_2 (gas phase) at certain concentrations and additional dissociation at high pH into HCO_3^- (pH greater than 6) and CO_3^{2-} (pH greater than 10) [275].

$$\frac{dA}{dt} = \mu(A,H,N)\cdot A \quad \text{Eq. 6}$$

$$\mu(A,H,N) = min\left\{\mu_{max}\cdot\left[1-\frac{q}{Q(t)}\right], \frac{p(A,H,NO}{c}, \mu_{max}\cdot\left[\frac{TIC}{K_C+TIC}\right]\right\} - b \quad \text{Eq. 7}$$

$$p(A,H,N) = H(t)\cdot p_m(A,N)\cdot\left[1-exp\left(\frac{-a\cdot\emptyset\cdot I(A,H)}{p_m(A,N)}\right)\right] \quad \text{Eq. 8}$$

$$p_m(A,N) = \frac{[A(t)\cdot Q(t)]^2\cdot P_0}{[A(t)\cdot Q(t)]^2+q^2\cdot[A(t)+L(t)]^2} \quad \text{Eq. 9}$$

$$\frac{dH}{dt} = \frac{c}{p}\cdot\ \mu(A,H,N)\cdot\rho\cdot v(A,N) - H(t)\cdot\mu(A,H,N) \quad \text{Eq. 10}$$

$$\frac{dN}{dt} = -v(A,N)\cdot A(t) \quad \text{Eq. 11}$$

$$v(A,N) = \frac{q_M-Q(t)}{q_M-q}\cdot\left[\frac{v_m\cdot N(t)}{N(t)+v_h}\right] \quad \text{Eq. 12}$$

$$Q(t) = \frac{A(0)\cdot Q_0+N(0)-N(t)}{A(t)} \quad \text{Eq. 13}$$

$$I(A,H) = \frac{I_0}{a\cdot H(t)\cdot A(t)\cdot z}\cdot[1-exp(-a\cdot H(t)\cdot A(t)\cdot z)] \quad \text{Eq. 14}$$

$$\frac{dTIC}{dt} = -k_{Carbon\ Uptake\ Rate} \quad \text{Eq. 15}$$

The biomass growth curve model for *Synechocystis* sp. PCC6803, validated with experimental work, were computed in Matlab ® for the four mixing energy inputs evaluated for the flat-panel photobioreactor: 1.94, 0.97, 0.47, and 0.03 $W.m^{-3}$, and for the mixing energy input evaluated for the open raceway pond, 0.10 $W.m^{-3}$. Details of the model and validation are presented in the Appendix G (Figure G.3).

9.3 Results and Discussion

The results of this research are synthesized into two aspects. First, the influence of turbulence mixing in the light experienced by either single *Synechocystis* sp. PCC 6803 cells or the bulk cyanobacterial biomass is evaluated by a well-mixed growth model validated with the experimental work in the flat-panel photobioreactors. Second, by embedding the light attenuation, measured in flat-panel photobioreactors in *Synechocystis* sp. PCC 6803 cultures, into the well-mixed growth model based on the open raceway pond, we demonstrated light attenuation is not impacted regardless the mixing energy input and reactor configuration.

9.3.1 The predictive capability of well-mixed growth model is demonstrated under mixing energy input variability

Our contribution suggests that mixing has no impact in the light regimes experienced by individual cells of *Synechocystis* sp. PCC 6803 in flat-photobioreactors and open raceway ponds. By constructing a well-mixed cyanobacterial growth model as a function of mixing energy input and experimentally determined light attenuation, the model is proven to be valid regardless the input energy used for flat-panel photobioreactors and open raceway pond. Our research, as a result, demonstrates that well mixed conditions are maintained for flat-panel photobioreactors and open raceway ponds at industrially relevant mixing energy inputs,

predicting the biomass productivity of *Synechocystis* sp. PCC 6803 by considering the uncertainty of the experimental results.

The well-mixed cyanobacterial growth model of *Synechocystis* sp. PCC 6803 validated for the flat-panel photobioreactor at mixing energy inputs of 0.03 $W.m^{-3}$ is illustrated in Figure 9.4. The validation of this model for mixing energy inputs of 0.47, 0.97 and 1.94 $W.m^{-3}$ in flat-panel photobioreactors are included in the Figures 9.5, 9.6, and 9.7. The one-way ANOVA results of the experimental biomass productivities are included in the Appendix G, Figure G.7, demonstrating a significant influence of mixing energy inputs as illustrated in the p-value less than 0.05. By incorporating light attenuation into the well-mixed cyanobacterial growth model of flat-panel photobioreactors, measured from the mixing energy inputs of 0.47 $W.m^{-3}$, as a function of culture depth and dry weight biomass (DWB) (Figure G.5), the model was valid for all the experiments performed at different mixing energy inputs (Figure 9.4, 9.5, 9.6, and 9.7). The DWB and biomass productivities predicted error of the model relative to the average experimental results for a mixing energy input of 0.03 $W.m^{-3}$ were -0.05 $g.l^{-1}$ and -0.019 $g.l^{-1}.d^{-1}$, respectively. For a mixing energy input of 0.47 $W.m^{-3}$ the errors were -0.22 $g.l^{-1}$ and -0.053 $g.l^{-1}.d^{-1}$. For a mixing energy input of 0.97 $W.m^{-3}$ the errors were -0.44 $g.l^{-1}$ and -0.108 $g.l^{-1}.d^{-1}$, the largest observed due to experimental inconsistencies, suggesting that cyanobacterial cultures crashed during this particular experiment. Lastly, for a mixing energy input of 1.94 $W.m^{-3}$ the errors were -0.08 $g.l^{-1}$ and -0.013 $g.l^{-1}.d^{-1}$. These results suggest that flat-panel photobioreactors operated at industrially relevant mixing energy inputs, ranging from 0.03 to 1.94 $W.m^{-3}$, maintain well-mixed conditions as their performance were accurately predicted by a well-mixed cyanobacterial growth model incorporating light attenuation in *Synechocystis* sp. PCC 6803 cultures. Additionally, by comparing experimental and computational growth performed with

normalized carbon content (scrubbed CO_2 and bicarbonate addition) relative to experiments performed with sparged air (containing atmospheric CO_2), under identical mixing energy inputs, carbon was demonstrated to be the limiting nutrient for growth of *Synechocystis* sp. PCC 6803 at the lowest mixing energy input in this research, 0.03 $W.m^{-3}$ (Figure 9.4, 9.5, 9.6, and 9.7). For this mixing energy input, for instance, if carbon is constrained to the concentrations contained in the air, 0.0011 $g.l^{-1}.min^{-1}$, this would be below the concentrations where growth is inhibited, 0.005 $g.l^{-1}$, as previously published by Kim et al. (2011).

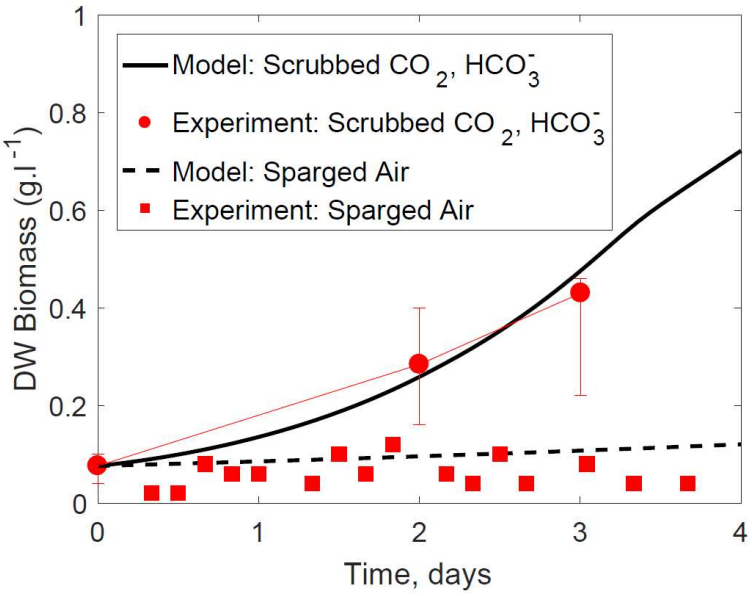

Figure 9.4 Well-mixed cyanobacterial growth model in flat-panel photobioreactor validated with experimental growth of *Synechocystis* sp. PCC 6803 at mixing energy inputs of 0.01 $W.m^{-3}$. The error bars denote the upper and lower values from five experimental replicates. The cultures were cultivated at 31 ± 1 °C and 1,244 ± 47 µmol photons.$s^{-1}.m^{-2}$.

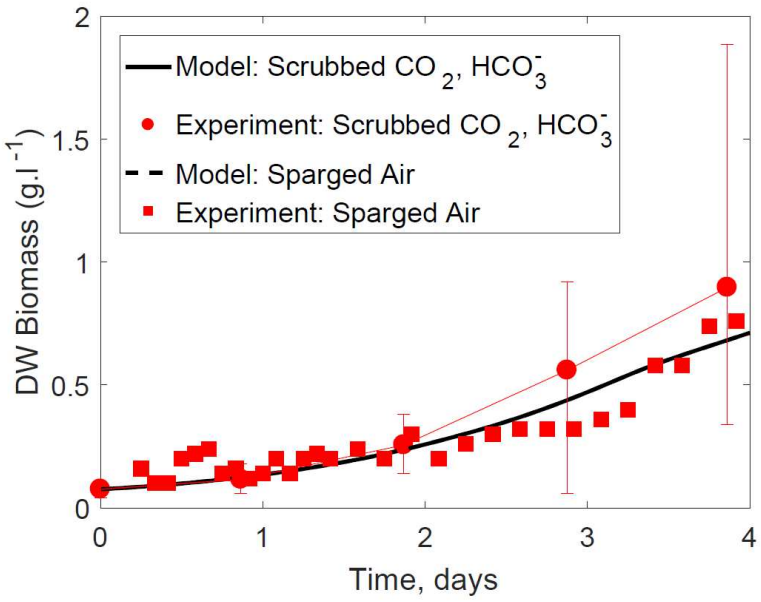

Figure 9.5 Well-mixed cyanobacterial growth model in flat-panel photobioreactor validated with experimental growth of *Synechocystis* sp. PCC 6803 at mixing energy inputs of 0.47 $W.m^{-3}$. The error bars denote the upper and lower values from five experimental replicates. The cultures were cultivated at 33 ± 1 °C and 1,385 ± 25 µmol photons.s^{-1}.m^{-2}.

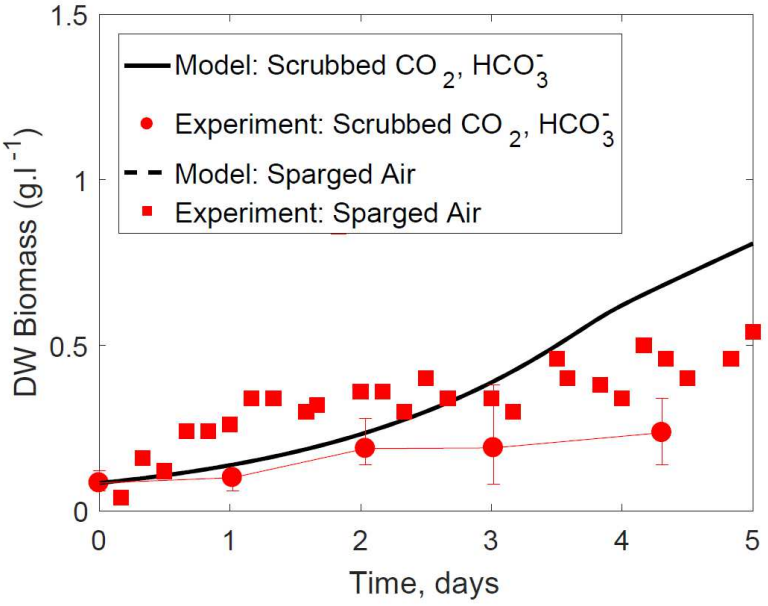

Figure 9.6 Well-mixed cyanobacterial growth model in flat-panel photobioreactor validated with experimental growth of *Synechocystis* sp. PCC 6803 at mixing energy inputs of 0.97 $W.m^{-3}$. The error bars denote the upper and lower values from five experimental replicates. The cultures were cultivated at 30 ± 1 °C and 1,323 ± 9 µmol photons.s^{-1}.m^{-2}.

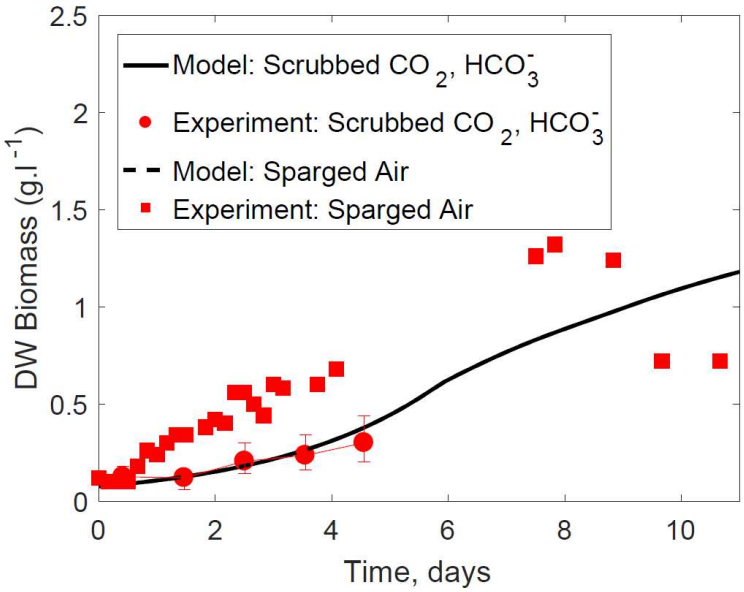

Figure 7. Well-mixed cyanobacterial growth model in flat-panel photobioreactor validated with experimental growth of *Synechocystis* sp. PCC 6803 at mixing energy inputs of 1.94 W.m^{-3}. The error bars denote the upper and lower values from five experimental replicates. The cultures were cultivated at 34 ± 1 °C and 1,440 ± 65 µmol photons.s^{-1}.m^{-2}.

9.3.2 Light attenuation in Synechocystis sp. PCC 6803 cultures is not impacted by mixing energy inputs and reactor configuration

The well-mixed cyanobacterial growth model of *Synechocystis* sp. PCC 6803 calibrated for the open raceway pond at mixing energy input of 0.10 W.m^{-3} is illustrated in Figure 9.8. By performing experimental cultivation of cyanobacterial in flat-panel photobioreactors, providing absorptive walls to constrain an incident radiation normal to the water surface, the cross section into an open raceway pond should be emulated given well-mixed conditions are maintained in both systems. Therefore, the light attenuation in the flat-panel photobioreactor configured in this research, as a function of depth and dry weight biomass at 0.47 W.m^{-3}, should resemble the light pattern of any well-mixed culture of *Synechocystis* sp. PCC 6803. From the computational growth, the light pattern measured in the flat-panel photobioreactor embedded into the growth model predicted the biomass productivity of *Synechocystis* sp. PCC 6803 performed in the open

raceway pond. These results suggest open raceway ponds at mixing energy inputs of 0.10 $W.m^{-3}$, maintain well-mixed conditions regardless that an order of magnitude lower than reported by Sompech et al. (2012) was used for cultivation. Additionally, the predictive capability of the growth model under either nitrogen or carbon limitation, demonstrated with the flat-panel photobioreactors experimental work, provides more evidence that open raceway ponds operated in ourdoor conditions where carbon supply is not feasible growth limited by this macronutrient. The relevance of these findings supports the previous work published by Grobbelaar (1991), suggesting mixing has no implications in the culture productivity due to light regimes experienced by single photoautotrophic cells. Turbulent mixing, as a result, more likely impact biological responses due to cell disruption induced by shear stress and constraining the carbon in the system controlled by sparged air. To summarize, pilot flat-panel and open raceway ponds operated at industrially relevant mixing energy inputs maintain well-mixed conditions.

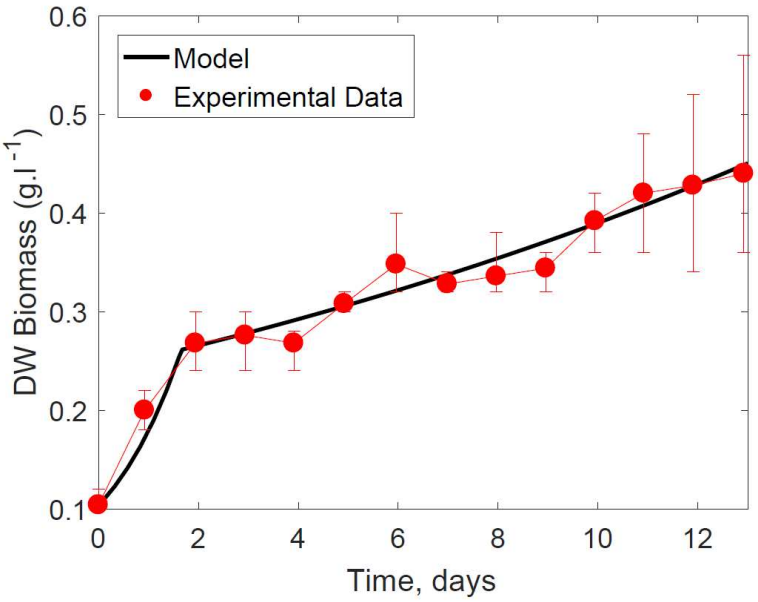

Figure 8. Well-mixed cyanobacterial growth model in open raceway pond validated with experimental growth of Synechocystis sp. PCC 6803 at mixing energy inputs of 0.10 $W.m^{-3}$. The error bars denote the upper and lower values from five experimental replicates. The cultures were cultivated at 29 °C and 915 ± 79 µmol $photons.s^{-1}.m^{-2}$.

9.4 Conclusions

In both flat-panel photobioreactors and open raceway ponds, experimental measurements of cyanobacterial growth were compared to bulk computational models of growth, at various mixing energies. That these results are indistinguishable demonstrates that the light experienced by individual cells has no measurable impact on the metrics of *Synechocystis* sp. PCC 6803 culture and productivity.

9.5 Answer to Research Question 3.2

This section of the research effort has allowed us to address Research Question 3.2, which is restated here:

> *What is the incident radiation and thermal environment experienced by single cyanobacteria cells. How is the bulk thermal system impacted by turbulent mixing?*

Research Question 3.2 is associated with Hypothesis 3.1:

> *Fluid flow and mixing in open raceway ponds is hypothesized to strongly influence algae growth. Pilot scale open raceway ponds and flat-panel photobioreactors maintain well-mixed conditions under a variety of operating conditions, and their cyanobacterial growth performance is described by well-mixed models.*

Chapter 7 demonstrates that the period of algae and cyanobacteria cell motion is not significantly changed under wide range of mixing energy input in pilot photobioreactors. This means that differences in mixing energy input have a small impact on the light experienced by photoautotrophic microorganisms in flat-panel photobioreactors and open raceway ponds. The predictive capability of CFD modeling is demonstrated and validated, providing reliable boundary conditions are given as described in this chapter from experimental fluid mechanics tools.

Chapter 8 demonstrates the predictive capability of lumped-thermal models, suggesting well mixed conditions in pilot open raceway ponds operated in outdoors conditions in Arizona. The uncertainty in the growth model results is driven by uncertainty in thermal and biological parameters, leading to low predictive capabilities from the growth models.

Chapter 9 demonstrates the predictive capability of a cyanobacterial growth model in a photo-inhibiting environment with differences in mixing energy input. By incorporating photo-inhibited maximum specific growth rate of cyanobacteria as a function of mixing energy input and scattering factors accounted in experimental light attenuation, we demonstrated well mixed conditions in pilot flat-panel photobioreactors and open raceway ponds. Additionally, we demonstrated that the accuracy of the model is driven by photorespiration, intrinsically incorporated in the photo-inhibited maximum specific growth rate of cyanobacteria growth modelling.

These results provide evidence against the hypothesis that fluid mechanics are important. When the growth characteristics of the culture can be predicted at various fluid mechanics conditions without consideration of the fluid mechanics, the results are demonstrated to be independent of the mixing conditions of the culture. The results of Chapter 7, 8, and 9 provide evidence that the fluid mechanics of the cyanobacteria culture can be characterized as well mixed for all industrially relevant mixing energies surveyed in this study for pilot scale flat-panel photobioreactors and open raceway ponds.

CHAPTER 10: Conclusions

10.1 Contributions to the Field

The overall research objectives of this study are to build a bridge and feedback loop approach to connect laboratory-scale and industrial-scale assessments of photoautotrophic based biosystems.

The primary contributions to the field from this research are presented below:

1. Developed a new assessment approach to predict the performance of industrial scale systems from laboratory experimentations for new organisms' biosynthetic products.
2. Developed first inclusive geographical assessment of microalgae facilities in the U.S. to evaluate the impact of DLUC on life cycle GHG emissions by constructing microalgae production systems in barren land areas.
3. Integrated wastewater engineering and photoautotrophic cultivation technologies to review and recommend bioprocesses that improve water quality from wastewater facilities and increase growth of photoautotrophic microorganisms.
4. Evaluation of the synergistic benefits of the integration of wastewater treatment facilities and cyanobacterial biorefineries for large scale systems for the first time using novel wastewater-specific sustainability metrics.
5. Developed first LCA integrating metrics of sustainability responses into tradeoffs between mixing energy inputs and growth.
6. Developed first flow characterization of pilot flat-panel photobioreactors and open raceway ponds by advanced experimental fluid mechanics tools under industrially relevant mixing energy inputs.

7. Performed first quantification of error of dynamic thermal models embedded into algae growth models.
8. Provided evidence of carbon limiting conditions for cyanobacteria growth at low mixing energy inputs in flat-panel photobioreactors and open raceway ponds, and demonstrated maximum specific growth rates due to photorespiration drives accuracy of photoautotrophic growth models.
9. Demonstrated well-mixed conditions in pilot scale flat-panel photobioreactors and open raceway ponds at industrially relevant mixing energy inputs by performing experimental fluid mechanics characterizations with well-mixed thermal and growth modelling.
10. Rigorous experimental development of scalable models, biological relations, and energy consumption models for life cycle energy and GHG emissions.

10.2 Summary of Answers to Research Questions

This dissertation has developed a novel approach to assess the sustainability of photoautotrophic biorefineries by an LCA, and understanding the effects of the physical environment in the growth and productivity of algae and cyanobacteria. In chapter 2, for instance, cyanobacterial-derived ethanol was demonstrated to be more sustainable in terms of life cycle net energy and GHG emissions relative to other biofuels, such as bisabolane and heptadecane. Chapter 3 demonstrated that DLUC reduces the net GHG emissions' benefit from microalgae biofuel manufacturing. The results of these studies provide support to the hypothesis that results are sensitive to uncertainties in growth and energy conversion stages, and that the details of characteristics such as DLUC can have large influence over the metrics of sustainability.

Chapters 4 and 5 demonstrates that sludge centrate obtained from wastewater facilities could be used for cultivation of algae and cyanobacteria, with the potential to contribute to the biological nutrient removal and wastewater remediation in wastewater treatment facilities. The results of these studies provide support to the hypothesis that synergistic benefits are obtained by integrating cyanobacterial cultivation and wastewater treatment, including displacement of fertilizers for cyanobacteria cultivation by wastewater nutrients, reduction of energy consumption to remove nutrients from the treated wastewater, and improvement of water quality from wastewater facilities.

Chapter 6 demonstrates that there is a tradeoff between mixing energy and biomass, reducing the life cycle energy at low mixing rates. Additionally, this chapter provides evidence that carbon limits the growth of cyanobacteria at low mixing energy inputs in flat-panel photobioreactors and open raceway ponds. High mixing energy inputs in flat-panel photobioreactors inhibits the growth of cyanobacteria. Lastly, Chapters 7, 8, and 9 demonstrate well-mixed conditions in pilot flat-panel photobioreactors and open raceway ponds where (i) algae and cyanobacteria cells motion are not significantly impacted under wide range of mixing energy input, (ii) lumped thermal models are capable to predict the temperature of the system, and (iii) well-mixed cyanobacteria growth models predict the biomass productivity, given maximum specific growth rates impacted by photo- and dark- respiration. The results of Chapter 7, 8, and 9 provide evidence that the fluid mechanics of the cyanobacteria culture can be characterized as well mixed for all industrially relevant mixing energies surveyed in this study for pilot scale flat-panel photobioreactors and open raceway ponds.

10.3 Future work

The future directions of this dissertation research will be to develop a better understanding of epistemic and aleatory thermal parameters in algal and cyanobacterial cultivation in raceways and photobioreactors. This work has demonstrated that it is very important to understand the role of thermal conditions on the performance of biological responses. We lack of holistic understanding of the impacts of physical environments in the growth and productivity of algae and cyanobacteria cultivation systems, and the sustainability implications of producing biofuels in large scale systems, that can be improved by the application of experimental and computational fluid mechanics to industrial scale photobioreactors and open raceway ponds. These efforts will feed high level LCA and technoeconomic models to evaluate sustainability and economics metrics.

My future research will endeavor to improve the predictive capability of dynamic thermal and algae/cyanobacteria growth models, incorporating rigorous experimental characterization of the physical environment and the biological effects under industrial and outdoor conditions. I will strive to understand the physical and biological connections and sources of uncertainties of photobioreactors and open raceway ponds at laboratory, pilot, and industrial scale system throughout my career. To gain a better understanding of the impact of the physical environment in the biological responses of algae and cyanobacteria, I will expand my efforts studying the flow characteristics incorporating additional variables such as fluid viscosity, photoautotrophic density, and photobioreactors and open raceway ponds scale. To understand the biological implications of the physical environment, I will explore the application of Mechanomics as part of my research interests on prediction of microalgae growth responses.

As part of my future work, I will continue integrating my civil and mechanical engineering expertise by exploring wastewater treatment remediation and bioenergy technologies. My efforts will include the integration of algae and cyanobacteria technologies into municipal wastewater treatment facilities towards biological nutrient removal processes, anaerobic digestion, and energy conversion. In the integration of these and other water and energy systems I will study resiliency through scenario modeling and uncertainty propagation. Lastly, I will seek to integrate research gaps between laboratory experimentation and industrial scale systems by incorporating bioengineering, civil and environmental engineering, and mechanical engineering experimentation and toolsets to reduce the uncertainty of sustainability assessments by techno-economic and LCA frameworks.

REFERENCES

1. Bernard, C., Les cyanobactéries et leurs toxines. Revue Francophone des Laboratoires, 2014. 2014(460): p. 53-68.
2. Rogers, M. and P.J. Keeling, *Lateral Transfer and Recompartmentalization of Calvin Cycle Enzymes of Plants and Algae.* Journal of Molecular Evolution, 2004. **58**(4): p. 367-375.
3. Keeling, P.J., *The Number, Speed, and Impact of Plastid Endosymbioses in Eukaryotic Evolution.* Annual Review of Plant Biology, 2013. **64**(1): p. 583-607.
4. Keeling, P.J., *The endosymbiotic origin, diversification and fate of plastids.* Philosophical Transactions of the Royal Society of London B: Biological Sciences, 2010. **365**(1541): p. 729-748.
5. Chisti, Y., *Biodiesel from microalgae.* Biotechnology Advances, 2007. **25**(3): p. 294-306.
6. Robertson, D., et al., *A new dawn for industrial photosynthesis.* Photosynthesis Research, 2011. **107**(3): p. 269-277.
7. Venteris, E.R., et al., *A GIS Cost Model to Assess the Availability of Freshwater, Seawater, and Saline Groundwater for Algal Biofuel Production in the United States.* Environmental Science & Technology, 2013. **47**(9): p. 4840-4849.
8. Oswald, W.J., *Large-scale algal culture systems (engineering aspects).* Micro-algal biotechnology. Cambridge University Press, Cambridge, 1988: p. 357-394.
9. Little, A., *Pilot plant studies in the production of Chlorella.* Algal Culture: From Laboratory to Pilot Plant, 1953: p. 235-273.

10. Kim, H.W., et al., *Photoautotrophic nutrient utilization and limitation during semi-continuous growth of Synechocystis sp. PCC6803.* Biotechnology and Bioengineering, 2010. **106**(4): p. 553-563.

11. Quinn, J.C., C.W. Turner, and T.H. Bradley, *Scale-Up of flat plate photobioreactors considering diffuse and direct light characteristics.* Biotechnol Bioeng, 2012. **109**(2): p. 363-70.

12. Weyer, K.M., et al., *Theoretical maximum algal oil production.* Bioenergy Research, 2010. **3**(2): p. 204-213.

13. Biller, P. and A. Ross, *Potential yields and properties of oil from the hydrothermal liquefaction of microalgae with different biochemical content.* Bioresource technology, 2011. **102**(1): p. 215-225.

14. Brennan, L. and P. Owende, *Biofuels from microalgae—a review of technologies for production, processing, and extractions of biofuels and co-products.* Renewable and sustainable energy reviews, 2010. **14**(2): p. 557-577.

15. Rosenberg, J.N., et al., *A green light for engineered algae: redirecting metabolism to fuel a biotechnology revolution.* Current opinion in Biotechnology, 2008. **19**(5): p. 430-436.

16. Rebitzer, G., et al., *Life cycle assessment: Part 1: Framework, goal and scope definition, inventory analysis, and applications.* Environment international, 2004. **30**(5): p. 701-720.

17. Luo, D., et al., *Life Cycle Energy and Greenhouse Gas Emissions for an Ethanol Production Process Based on Blue-Green Algae.* Environmental Science & Technology, 2010. **44**(22): p. 8670-8677.

18. Batan, L., et al., *Net Energy and Greenhouse Gas Emission Evaluation of Biodiesel Derived from Microalgae.* Environmental Science & Technology, 2010. **44**: p. 7975-7980.

19. Campbell, P.K., T. Beer, and D. Batten, *Life cycle assessment of biodiesel production from microalgae in ponds.* Bioresource Technology, 2011. **102**(1): p. 50-56.

20. Collet, P., et al., *Biodiesel from microalgae – Life cycle assessment and recommendations for potential improvements.* Renewable Energy, 2014. **71**(0): p. 525-533.

21. Frank, E., et al., *Life cycle comparison of hydrothermal liquefaction and lipid extraction pathways to renewable diesel from algae.* Mitigation and Adaptation Strategies for Global Change, 2013. **18**(1): p. 137-158.

22. Frank, E.D., et al., *Life-cycle analysis of algal lipid fuels with the GREET model*. 2011, Center for Transportation Research, Energy Systems Division, Argonne National Laboratory: Oak Ridge, TN.

23. Handler, R.M., et al., *Life cycle assessment of algal biofuels: Influence of feedstock cultivation systems and conversion platforms.* Algal Research, 2014. **4**(0): p. 105-115.

24. Ponnusamy, S., et al., *Life cycle assessment of biodiesel production from algal bio-crude oils extracted under subcritical water conditions.* Bioresource Technology, 2014. **170**(0): p. 454-461.

25. Quinn, J.C. and R. Davis, *The potentials and challenges of algae based biofuels: A review of the techno-economic, life cycle, and resource assessment modeling.* Bioresoruce Technology in press.

26. Quinn, J.C., et al., *Microalgae to Biofuels Lifecycle Assessment-Multiple Pathway Evaluation.* Algal Research, 2014. **4**: p. 116-122.

27. Vasudevan, V., et al., *Environmental Performance of Algal Biofuel Technology Options.* Environmental Science & Technology, 2012. **46**(4): p. 2451-2459.

28. Wigmosta, M.S., et al., *National microalgae biofuel production potential and resource demand.* Water Resources Research, 2011. **47**(3): p. W00H04.

29. Batan, L., et al., *Net Energy and Greenhouse Gas Emission Evaluation of Biodiesel Derived from Microalgae.* Environmental Science and Technology, 2010. **44**(20): p. 6.

30. EPA, *Biological Nutrient Removal Processes and Costs*. 2007, United States Environmental Protection Agency: Washington, DC 20460.

31. Rittmann, B.E. and P.L. McCarty, *Environmental biotechnology: principles and applications*. 2012: Tata McGraw-Hill Education.

32. Breidt, S., *Evaluation of cost effective approaches for nutrient removal in urban stormwater and wastewater: City of Fort Collins case study*. 2015, Colorado State University. Libraries.

33. Dapena□Mora, A., et al., *Enrichment of Anammox biomass from municipal activated sludge: experimental and modelling results.* Journal of Chemical Technology and Biotechnology, 2004. **79**(12): p. 1421-1428.

34. Sengupta, S. and A. Pandit, *Selective removal of phosphorus from wastewater combined with its recovery as a solid-phase fertilizer.* Water research, 2011. **45**(11): p. 3318-3330.

35. Forrest, A., et al., *Optimizing struvite production for phosphate recovery in WWTP.* Journal of Environmental Engineering, 2008. **134**(5): p. 395-402.

36. Wang, J., et al., *Engineered struvite precipitation: Impacts of component-ion molar ratios and pH.* Journal of Environmental Engineering, 2005. **131**(10): p. 1433-1440.

37. Arita, C.Q., C. Peebles, and T.H. Bradley, *Scalability of Combining Microalgae-based Biofuels with Wastewater Facilities: A Review.* Algal Research, 2015.

38. Metcalf and Eddy, *Wastewater engineering treatment and resource recovery*. McGraw-Hill series in civil and environmental engineering. 2015, Boston: McGraw-Hill.

39. Nelson, N.O., R.L. Mikkelsen, and D.L. Hesterberg, *Struvite precipitation in anaerobic swine lagoon liquid: effect of pH and Mg: P ratio and determination of rate constant.* Bioresource Technology, 2003. **89**(3): p. 229-236.

40. Carberry, J. and F. Henshaw, *Biokinetic parameters of a photosynthetic waste stabilization process.* Water Science and Technology, 1989. **21**(6-7): p. 647-658.

41. Craggs, R., et al., *Algal biofuels from wastewater treatment high rate algal ponds.* Water Science and Technology, 2011. **63**(4): p. 660-665.

42. Craggs, R.J., T.J. Lundquist, and J.R. Benemann, *Wastewater treatment and algal biofuel production*, in *Algae for biofuels and energy*. 2013, Springer. p. 153-163.

43. García, J., et al., *Long term diurnal variations in contaminant removal in high rate ponds treating urban wastewater.* Bioresource Technology, 2006. **97**(14): p. 1709-1715.

44. Green, F.B., et al., *Advanced integrated wastewater pond systems for nitrogen removal.* Water Science and Technology, 1996. **33**(7): p. 207-217.

45. Llorens, M., J. Saez, and A. Soler, *Primary productivity in a deep sewage stabilization lagoon.* Water Research, 1993. **27**(12): p. 1779-1785.

46. Park, J., R. Craggs, and A. Shilton, *Wastewater treatment high rate algal ponds for biofuel production.* Bioresource technology, 2011. **102**(1): p. 35-42.

47. Selvaratnam, T., et al., *Maximizing recovery of energy and nutrients from urban wastewaters.* Energy, 2016. **104**: p. 16-23.

48. Zhou, W., et al., *Local bioprospecting for high-lipid producing microalgal strains to be grown on concentrated municipal wastewater for biofuel production.* Bioresource Technology, 2011. **102**(13): p. 6909-6919.

49. Dai, G., et al., *Differential sensitivity of five cyanobacterial strains to ammonium toxicity and its inhibitory mechanism on the photosynthesis of rice-field cyanobacterium Ge–Xian–Mi (Nostoc).* Aquatic toxicology, 2008. **89**(2): p. 113-121.

50. DAI, G.Z., B.S. QIU, and K. Forchhammer, *Ammonium tolerance in the cyanobacterium Synechocystis sp. strain PCC 6803 and the role of the psbA multigene family.* Plant, cell & environment, 2014. **37**(4): p. 840-851.

51. Cai, T., et al., *Comparison of Synechocystis sp. PCC6803 and Nannochloropsis salina for lipid production using artificial seawater and nutrients from anaerobic digestion effluent.* Bioresource technology, 2013. **144**: p. 255-260.

52. Drath, M., et al., *Ammonia triggers photodamage of photosystem II in the cyanobacterium Synechocystis sp. strain PCC 6803.* Plant physiology, 2008. **147**(1): p. 206-215.

53. Jones, S.M.J., T.M. Louw, and S.T.L. Harrison, *Energy consumption due to mixing and mass transfer in a wave photobioreactor.* Algal Research, 2017. **24**(Part A): p. 317-324.

54. Sompech, K., Y. Chisti, and T. Srinophakun, *Design of raceway ponds for producing microalgae.* Biofuels, 2012. **3**(4): p. 387-397.

55. Naderi, G., H. Znad, and M.O. Tade, *Investigating and modelling of light intensity distribution inside algal photobioreactor.* Chemical Engineering and Processing: Process Intensification, 2017.

56. Quinn, J., L. De Winter, and T. Bradley, *Microalgae bulk growth model with application to industrial scale systems.* Bioresource technology, 2011. **102**(8): p. 5083-5092.

57. Incropera, F. and W. Houf, *A Three-flux method for predicting radiative transfer in aqueous suspensions.* J. Heat Transfer, 1979. **101**: p. 496-501.

58. Incropera, F., T. Craig, and W. Houf, *Radiation transfer in absorbing-scattering liquids—II. Comparisons of measurements with predictions.* Journal of Quantitative Spectroscopy and Radiative Transfer, 1984. **31**(2): p. 139-147.

59. Labatut, R.A., et al., *Modeling hydrodynamics and path/residence time of aquaculture-like particles in a mixed-cell raceway (MCR) using 3D computational fluid dynamics (CFD).* Aquacultural Engineering, 2015. **67**(Supplement C): p. 39-52.

60. Pires, J.C.M., M.C.M. Alvim-Ferraz, and F.G. Martins, *Photobioreactor design for microalgae production through computational fluid dynamics: A review.* Renewable and Sustainable Energy Reviews, 2017. **79**(Supplement C): p. 248-254.

61. Adhikari, D. and E. Longmire, *Visual hull method for tomographic PIV measurement of flow around moving objects.* Experiments in fluids, 2012. **53**(4): p. 943-964.

62. Drewry, J.L., et al., *A computational fluid dynamics model of algal growth: development and validation.* Transactions of the ASABE, 2015. **58**(2): p. 203-213.

63. Foeth, E., et al., *Time resolved PIV and flow visualization of 3D sheet cavitation.* Experiments in Fluids, 2006. **40**(4): p. 503-513.

64. Gemmell, B.J., D. Adhikari, and E.K. Longmire, *Volumetric quantification of fluid flow reveals fish's use of hydrodynamic stealth to capture evasive prey.* Journal of The Royal Society Interface, 2014. **11**(90): p. 20130880.

65. Jeon, Y.J. and H.J. Sung, *PIV measurement of flow around an arbitrarily moving body.* Experiments in fluids, 2011. **50**(4): p. 787-798.

66. Khalitov, D. and E. Longmire, *Simultaneous two-phase PIV by two-parameter phase discrimination.* Experiments in fluids, 2002. **32**(2): p. 252-268.

67. Kiger, K. and C. Pan, *PIV technique for the simultaneous measurement of dilute two-phase flows.* Journal of fluids engineering, 2000. **122**(4): p. 811-818.

68. Moin, P. and K. Mahesh, *Direct numerical simulation: a tool in turbulence research.* Annual review of fluid mechanics, 1998. **30**(1): p. 539-578.

69. Versteeg, H.K. and W. Malalasekera, *An introduction to computational fluid dynamics: the finite volume method*. 2007: Pearson Education.

70. Wilhelmus, M.M. and J.O. Dabiri, *Observations of large-scale fluid transport by laser-guided plankton aggregations.* Physics of Fluids, 2014. **26**(10): p. 101302.

71. Zhang, J.-Y., et al., *Investigation of light transfer procedure and photobiological hydrogen production of microalgae in photobioreactors at different locations of China.* International Journal of Hydrogen Energy, 2017. **42**(31): p. 19709-19722.

72. Chiaramonti, D., et al., *Review of energy balance in raceway ponds for microalgae cultivation: Re-thinking a traditional system is possible.* Applied Energy, 2013. **102**(Supplement C): p. 101-111.

73. Fernandes, B.D., et al., *Development of a novel user-friendly platform to couple light regime characterization with particle tracking - cells' light history determination during phototrophic cultivations.* Algal Research, 2017. **24**(Part A): p. 276-283.

74. Brune, D., T. Lundquist, and J. Benemann, *Microalgal biomass for greenhouse gas reductions: potential for replacement of fossil fuels and animal feeds.* Journal of Environmental Engineering, 2009. **135**(11): p. 1136-1144.

75. Lardon, L., et al., *Life-cycle assessment of biodiesel production from microalgae.* Environmental science & technology, 2009. **43**(17): p. 6475-6481.

76. Rodolfi, L., et al., *Microalgae for oil: Strain selection, induction of lipid synthesis and outdoor mass cultivation in a low□cost photobioreactor.* Biotechnology and bioengineering, 2009. **102**(1): p. 100-112.

77. Wijffels, R.H., O. Kruse, and K.J. Hellingwerf, *Potential of industrial biotechnology with cyanobacteria and eukaryotic microalgae.* Current opinion in biotechnology, 2013. **24**(3): p. 405-413.

78. Quinn, J.C. and R. Davis, *The potentials and challenges of algae based biofuels: A review of the techno-economic, life cycle, and resource assessment modeling.* Bioresource Technology, 2015. **184**: p. 444-452.

79. Angermayr, S.A., A. Gorchs Rovira, and K.J. Hellingwerf, *Metabolic engineering of cyanobacteria for the synthesis of commodity products.* Trends in Biotechnology, 2015. **33**(6): p. 352-361.

80. EPA, *Renewable Fuel Standard Program, U.S. Environmental Protection Agency, Vol. 2016.* 2016, Environmental Protection Agency: Washington DC, United States.

81. IPCC, *Guidelines for National Greenhouse Gas Inventories, Vol. 2, Energy*. 2006, National Greenhouse Gas Inventories Programme, IGES: Japan.

82. Quinn, J.C., et al., *Nannochloropsis production metrics in a scalable outdoor photobioreactor for commercial applications.* Bioresour Technol, 2012. **117**: p. 164-71.

83. Posten, C. and C. Walter, *Microalgal biotechnology potential and production*. 2012, Berlin: Walter de Gruyter.

84. Kim, H.W., et al., *Nutrient acquisition and limitation for the photoautotrophic growth of Synechocystis sp. PCC6803 as a renewable biomass source.* Biotechnology and Bioengineering, 2011. **108**(2): p. 277-285.

85. Davies, F.K., et al., *Engineering Limonene and Bisabolene Production in Wild Type and a Glycogen-Deficient Mutant of Synechococcus sp. PCC 7002.* Frontiers in Bioengineering and Biotechnology, 2014. **2**: p. 21.

86. Wang, W., X. Liu, and X. Lu, *Engineering cyanobacteria to improve photosynthetic production of alka(e)nes.* Biotechnology for Biofuels, 2013. **6**: p. 69-69.

87. Argonne and DOE. *Greenhouse Gases, Regulated Emissions, and Energy Use in Transportation (GREET) Model*. 2014; Available from: https://greet.es.anl.gov/greet/index.htm.

88. Wang, X., D.R. Ort, and J.S. Yuan, *Photosynthetic terpene hydrocarbon production for fuels and chemicals.* Plant Biotechnology Journal, 2015. **13**(2): p. 137-146.

89. Gatrell, S., et al., *Nonruminant Nutrition Symposium: Potential of defatted microalgae from the biofuel industry as an ingredient to replace corn and soybean meal in swine and poultry diets.* Journal of animal science, 2014. **92**(4): p. 1306-1314.

90. Passell, H., et al., *Algae biodiesel life cycle assessment using current commercial data.* Journal of Environmental Management, 2013. **129**(0): p. 103-111.

91. Sills, D.L., et al., *Quantitative Uncertainty Analysis of Life Cycle Assessment for Algal Biofuel Production.* Environmental Science & Technology, 2013. **47**(2): p. 687-694.

92. Grierson, S., V. Strezov, and J. Bengtsson, *Life cycle assessment of a microalgae biomass cultivation, bio-oil extraction and pyrolysis processing regime.* Algal Research, 2013. **2**(3): p. 299-311.

93. Brentner, L.B., M.J. Eckelman, and J.B. Zimmerman, *Combinatorial Life Cycle Assessment to Inform Process Design of Industrial Production of Algal Biodiesel.* Environmental Science & Technology, 2011. **45**(16): p. 7060-7067.

94. Sadrameli, S., W. Seames, and M. Mann, *Prediction of higher heating values for saturated fatty acids from their physical properties.* Fuel, 2008. **87**(10): p. 1776-1780.

95. Quinn, J.C., et al., *Nannochloropsis production metrics in a scalable outdoor photobioreactor for commercial applications.* Bioresource Technology, 2012. **117**: p. 164-171.

96. EPA. *States Nutrient Criteria Plans*. 2014 02/17/2014 02/26/2014]; Available from: http://www2.epa.gov/nutrient-policy-data/states-nutrient-criteria-plans.

97. Bernstein, H.C., et al., *Direct measurement and characterization of active photosynthesis zones inside wastewater remediating and biofuel producing microalgal biofilms.* Bioresource Technology, 2014.

98. Chen, W.T., et al., *Hydrothermal liquefaction of mixed-culture algal biomass from wastewater treatment system into bio-crude oil.* Bioresour Technol, 2014. **152**: p. 130-9.

99. Cho, S., et al., *Reuse of effluent water from a municipal wastewater treatment plant in microalgae cultivation for biofuel production.* Bioresour Technol, 2011. **102**(18): p. 8639-45.

100. Christenson, L. and R. Sims, *Production and harvesting of microalgae for wastewater treatment, biofuels, and bioproducts.* Biotechnol Adv, 2011. **29**(6): p. 686-702.

101. Craggs, R.J., et al., *Algal biofuels from wastewater treatment high rate algal ponds.* Water Sci Technol, 2011. **63**(4): p. 660-5.

102. Dickinson, K.E., C.G. Whitney, and P.J. McGinn, *Nutrient remediation rates in municipal wastewater and their effect on biochemical composition of the microalga Scenedesmus sp. AMDD.* Algal Research, 2013. **2**(2): p. 127-134.

103. EPA, *Design Manual. Municipal Wastewater Stabilization Ponds*, in *EPA-625/1-83-015*, U.S.E.P. Agency, Editor. 1983: Cincinnati, OH 45268.

104. Ghosh, S. and N.G. Love, *Application of rbcL based molecular diversity analysis to algae in wastewater treatment plants.* Bioresour Technol, 2011. **102**(3): p. 3619-22.

105. Jiang, L., et al., *Biomass and lipid production of marine microalgae using municipal wastewater and high concentration of CO2.* Applied Energy, 2011. **88**(10): p. 3336-3341.

106. Komolafe, O., et al., *Biodiesel production from indigenous microalgae grown in wastewater.* Bioresour Technol, 2014. **154**: p. 297-304.

107. Kong, Q.X., et al., *Culture of microalgae Chlamydomonas reinhardtii in wastewater for biomass feedstock production.* Appl Biochem Biotechnol, 2010. **160**(1): p. 9-18.

108. Li, Y., et al., *Integration of algae cultivation as biodiesel production feedstock with municipal wastewater treatment: strains screening and significance evaluation of environmental factors.* Bioresour Technol, 2011. **102**(23): p. 10861-7.

109. Lizzul, A.M., et al., *Combined remediation and lipid production using Chlorella sorokiniana grown on wastewater and exhaust gases.* Bioresour Technol, 2014. **151**: p. 12-8.

110. Markou, G., D. Vandamme, and K. Muylaert, *Using natural zeolite for ammonia sorption from wastewater and as nitrogen releaser for the cultivation of Arthrospira platensis.* Bioresour Technol, 2014. **155C**: p. 373-378.

111. McGinn, P.J., et al., *Assessment of the bioenergy and bioremediation potentials of the microalga Scenedesmus sp. AMDD cultivated in municipal wastewater effluent in batch and continuous mode.* Algal Research, 2012. **1**(2): p. 155-165.

112. Osundeko, O. and J.K. Pittman, *Implications of sludge liquor addition for wastewater-based open pond cultivation of microalgae for biofuel generation and pollutant remediation.* Bioresour Technol, 2014. **152**: p. 355-63.

113. Park, J.B., R.J. Craggs, and A.N. Shilton, *Wastewater treatment high rate algal ponds for biofuel production.* Bioresour Technol, 2011. **102**(1): p. 35-42.

114. Pittman, J.K., A.P. Dean, and O. Osundeko, *The potential of sustainable algal biofuel production using wastewater resources.* Bioresour Technol, 2011. **102**(1): p. 17-25.

115. Rawat, I., et al., *Dual role of microalgae: Phycoremediation of domestic wastewater and biomass production for sustainable biofuels production.* Applied Energy, 2011. **88**(10): p. 3411-3424.

116. Selvaratnam, T., et al., *Evaluation of a thermo-tolerant acidophilic alga, Galdieria sulphuraria, for nutrient removal from urban wastewaters.* Bioresource Technology, 2014.

117. Shi, J., B. Podola, and M. Melkonian, *Application of a prototype-scale Twin-Layer photobioreactor for effective N and P removal from different process stages of municipal wastewater by immobilized microalgae.* Bioresour Technol, 2014. **154**: p. 260-6.

118. Sturm, B.S.M. and S.L. Lamer, *An energy evaluation of coupling nutrient removal from wastewater with algal biomass production.* Applied Energy, 2011. **88**(10): p. 3499-3506.

119. Su, Y., A. Mennerich, and B. Urban, *Synergistic cooperation between wastewater-born algae and activated sludge for wastewater treatment: influence of algae and sludge inoculation ratios.* Bioresour Technol, 2012. **105**: p. 67-73.

120. Tchobanoglous, G., *Wastewater engineering treatment and reuse*. McGraw-Hill series in civil and environmental engineering, ed. G. Tchobanoglous, F.L. Burton, and H.D. Stensel. 2003, Boston: McGraw-Hill.

121. Tchobanoglous, G., et al., *Wastewater Engineering: Treatment and Reuse*. 2003: McGraw-Hill Education.

122. Udom, I., et al., *Harvesting microalgae grown on wastewater.* Bioresour Technol, 2013. **139**: p. 101-6.

123. Wang, B. and C.Q. Lan, *Biomass production and nitrogen and phosphorus removal by the green alga Neochloris oleoabundans in simulated wastewater and secondary municipal wastewater effluent.* Bioresour Technol, 2011. **102**(10): p. 5639-44.

124. Wang, L., et al., *Cultivation of green algae Chlorella sp. in different wastewaters from municipal wastewater treatment plant.* Appl Biochem Biotechnol, 2010. **162**(4): p. 1174-86.

125. Wang, M., et al., *Kinetics of nutrient removal and expression of extracellular polymeric substances of the microalgae, Chlorella sp. and Micractinium sp., in wastewater treatment.* Bioresour Technol, 2014. **154**: p. 131-7.

126. Woertz, I., et al., *Algae Grown on Dairy and Municipal Wastewater for Simultaneous Nutrient Removal and Lipid Production for Biofuel Feedstock.* Journal of Environmental Engineering, 2009: p. 8.

127. Zhang, T.Y., et al., *Isolation and heterotrophic cultivation of mixotrophic microalgae strains for domestic wastewater treatment and lipid production under dark condition.* Bioresour Technol, 2013. **149**: p. 586-9.

128. Zhou, W., et al., *Local bioprospecting for high-lipid producing microalgal strains to be grown on concentrated municipal wastewater for biofuel production.* Bioresour Technol, 2011. **102**(13): p. 6909-19.

129. Zhou, W., et al., *A hetero-photoautotrophic two-stage cultivation process to improve wastewater nutrient removal and enhance algal lipid accumulation.* Bioresour Technol, 2012. **110**: p. 448-55.

130. Weissman, J.C., R.P. Goebel, and J.R. Benemann, *Photobioreactor design: mixing, carbon utilization, and oxygen accumulation.* Biotechnology and bioengineering, 1988. **31**(4): p. 336-344.

131. Wijffels, R.H. and M.J. Barbosa, *An Outlook on Microalgal Biofuels.* Science, 2010. **329**(5993): p. 796-799.

132. Kendall, A. and B. Chang, *Estimating life cycle greenhouse gas emissions from corn–ethanol: a critical review of current U.S. practices.* Journal of Cleaner Production, 2009. **17**(13): p. 1175-1182.

133. Batan, L., J.C. Quinn, and T.H. Bradley, *Analysis of water footprint of a photobioreactor microalgae biofuel production system from blue, green and lifecycle perspectives.* Algal Research, 2013. **2**(3): p. 196-203.

134. Quinn, J.C., et al., *Microalgae to biofuels lifecycle assessment — Multiple pathway evaluation.* Algal Research, 2013.

135. Woertz, I.C., et al., *Life Cycle GHG Emissions from Microalgal Biodiesel – A CA-GREET Model.* Environmental Science & Technology, 2014. **48**(11): p. 6060-6068.

136. Quinn, J.C., et al., *Geographical Assessment of Microalgae Biofuels Potential Incorporating Resource Availability.* BioEnergy Research, 2013. **6**(2): p. 591-600.

137. Dominguez-Faus, R., et al., *The water footprint of biofuels: A drink or drive issue?* Environmental Science & Technology, 2009. **43**(9): p. 3005-3010.

138. King, C.W. and M.E. Webber, *Water intensity of transportation.* Environmental Science & Technology, 2008. **42**(21): p. 7866-7872.

139. Mekonnen, M.M. and A.Y. Hoekstra, *The green, blue and grey water footprint of crops and derived crop products.* Hydrology and Earth System Sciences, 2011. **15**(5): p. 1577-1600.

140. Wu, M., et al., *Consumptive water use in the production of ethanonl and petroleum gasoline*. 2009, Argonne National Laboratory (ANL).

141. Yang, J., et al., *Life-cycle analysis on biodiesel production from microalgae: water footprint and nutrients balance.* Bioresource technology, 2011. **102**(1): p. 159-165.

142. Adesanya, V.O., et al., *Life cycle assessment on microalgal biodiesel production using a hybrid cultivation system.* Bioresource Technology, 2014. **163**(0): p. 343-355.

143. Azadi, P., et al., *The carbon footprint and non-renewable energy demand of algae-derived biodiesel.* Applied Energy, 2014. **113**: p. 1632-1644.

144. Liu, X., et al., *Pilot-scale data provide enhanced estimates of the life cycle energy and emissions profile of algae biofuels produced via hydrothermal liquefaction.* Bioresource Technology, 2013. **148**(0): p. 163-171.

145. Shirvani, T., et al., *Life cycle energy and greenhouse gas analysis for algae-derived biodiesel.* Energy & Environmental Science, 2011. **4**(10): p. 3773-3778.

146. Soh, L., et al., *Evaluating microalgal integrated biorefinery schemes: Empirical controlled growth studies and life cycle assessment.* Bioresource Technology, 2014. **151**(0): p. 19-27.

147. Canter, C.E., et al., *Infrastructure associated emissions for renewable diesel production from microalgae.* Algal Research, 2014. **5**: p. 195-203.

148. Goetz, S.J., et al., *Mapping and monitoring carbon stocks with satellite observations: a comparison of methods.* Carbon Balance Manag, 2009. **4**: p. 2.

149. Cai, H., et al., *Well-to-Wheels Greenhouse Gas Emissions of Canadian Oil Sands Products: Implications for U.S. Petroleum Fuels.* Environmental Science & Technology, 2015.

150. Kellndorfer, J., et al., *NACP Aboveground Biomass and Carbon Baseline Data (NBCD 2000)*. 2012, Data set. Available on-line [http://daac.ornl.gov] from ORNL DAAC, Oak Ridge, Tennessee, U.S.A.http://dx.doi.org/10.3334/ORNLDAAC/1081: U.S.A., 2000.

151. Mitchard, E. *A step by step guide to making maps of vegetation carbon stocks*. 2013 04/25/2013 01/31/2014].

152. IPCC. *Good Practice Guidance for Land Use,Land-Use Change and Forestry*. 2014 01/31/2014].

153. Quinn, J., L. de Winter, and T. Bradley, *Microalgae bulk growth model with application to industrial scale systems.* Bioresour Technol, 2011. **102**(8): p. 5083-92.

154. Palmer, C.M., *Algae and Water Pollution*. 1977, United States Environmental Protection Agency: Cincinnati, OH 45268.

155. Perez-Garcia, O., et al., *Heterotrophic cultures of microalgae: metabolism and potential products.* Water Res, 2011. **45**(1): p. 11-36.

156. Rittmann, B.E. and P.L. McCarty, *Environmental biotechnology principles and applications*. McGraw-Hill series in water resources and environmental engineering, ed. P.L. McCarty. 2001, Boston: McGraw-Hill.

157. LEWIS, M.A., *Chronic toxicities of surfactants and detergent builders to algae: A review and risk assessment.* ECOTOXICOLOGY AND ENVIRONMENTAL SAFETY, 1990. **20**: p. 17.

158. CLIJSTERS, I. and F.V. ASSCHE, *Inhibition of photosynthesis by heavy metals.* Photosynthesis Research, 1985. **7**: p. 10.

159. Devriese, M., et al., *Effect of heavy metals on nitrate assimilation in the eukaryotic microalga Chlamydomonas reinhardtii.* Plant Physiology and Biochemistry, 2001. **39**: p. 6.

160. Chia, M.A., et al., *Lipid composition of Chlorella vulgaris (Trebouxiophyceae) as a function of different cadmium and phosphate concentrations.* Aquat Toxicol, 2013. **128-129**: p. 171-82.

161. Droop, M.R., *25 Years of Algal Growth Kinetics: A Personal View.* Botanica Marina, 1983. **XXVI**: p. 14.

162. DiToro, D.M., *Applicability of cellular equilibrium and monod theory to phytoplankton growth kinetics.* Ecological Modeling, 1980. **8**: p. 18.

163. Ogbonna, J.C., H. Yada, and H. Tanaka, *Effect of Cell Movement by Random Mixing between the Surface and Bottom of Photobioreactors on Algal Productivity.* Journal of Fermentation and Bioengineering, 1995. **79**(2): p. 6.

164. Grima, E.M., et al., *Photobioreactors: light regime, mass transfer, and scaleup.* Journal of Biotechnology, 1999. **70**: p. 17.

165. Klausmeier, C.A., E. Litchman, and S.A. Levin, *Phytoplankton growth and stoichiometry under multiple nutrient limitation.* Limnology and Oceanography, 2004. **49**(4): p. 8.

166. Morel, F.M.M., <*Kinetics of nutrient uptake and growth in phytoplankton.* Phycology, 1987. **23**: p. 14.

167. Xin, L., et al., *Effects of different nitrogen and phosphorus concentrations on the growth, nutrient uptake, and lipid accumulation of a freshwater microalga Scenedesmus sp.* Bioresour Technol, 2010. **101**(14): p. 5494-500.

168. Bitog, J.P., et al., *Application of computational fluid dynamics for modeling and designing photobioreactors for microalgae production: A review.* Computers and Electronics in Agriculture, 2011. **76**(2): p. 131-147.

169. Packer, A., et al., *Growth and neutral lipid synthesis in green microalgae: a mathematical model.* Bioresour Technol, 2011. **102**(1): p. 111-7.

170. Wu, B., *Advances in the use of CFD to characterize, design and optimize bioenergy systems.* Computers and Electronics in Agriculture, 2013. **93**: p. 195-208.

171. ANSYS, I., *ANSYS CFX Introduction*. 2011: Canonsburg, PA.

172. ANSYS, I., *ANSYS FLUENT User's Guide*. 2011: Canonsburg, PA.

173. EPA, D.M., *Onsite Wastewater Treatment and Disposal Systems.* USEPA, Oct, 1980.

174. Quiroz-Arita, C., J.J. Sheehan, and T.H. Bradley, *Life cycle net energy and greenhouse gas emissions of photosynthetic cyanobacterial biorefineries: Challenges for industrial production of biofuels.* Algal Research, 2017.

175. Wigmosta, M.S., et al., *National microalgae biofuel production potential and resource demand.* Water Resources Research, 2011. **47**(3).

176. Arita, C.Q., et al., *A geographical assessment of vegetation carbon stocks and greenhouse gas emissions on potential microalgae-based biofuel facilities in the United States.* Bioresource technology, 2016. **221**: p. 270-275.

177. You, S., et al., *Nitrification efficiency and nitrifying bacteria abundance in combined AS-RBC and A2O systems.* Water Research, 2003. **37**(10): p. 2281-2290.

178. Fang, L.L., et al., *Life cycle assessment as development and decision support tool for wastewater resource recovery technology.* Water research, 2016. **88**: p. 538-549.

179. Colorado Department of Public Health and Environment, C.E., *Regulation #85: Nutrients Management Control Regulation 5 CCR 1002-85*, in *Water Quality Control Comission*. 2012: CO, U.S.

180. Colorado, S.o., *Colorado Climate Plan: State Level Policies and Strategies to Mitigate and Adapt*. 2015: CO, U.S.

181. EnviroSim. *BioWin. Retrieved from https://envirosim.com/products/biowin.* 2017; Available from: https://envirosim.com/products/biowin.

182. thinkstep, *GaBi*, in *Sustainability Software*. 2018, Retrieved from https://www.thinkstep.com/software: Germany.

183. Lincoln H. Mueller, J., *Analysis of Nutrient Removal at The Drake Water Reclamation Facility*. 2016, Colorado State University. Libraries.

184. Speece, R.E., *Anaerobic biotechnology and odor/corrosion control for municipalities and industries*. 2008, Archae Press.

185. Loewenthal, R., U. Kornmüller, and E. Van Heerden, *Modelling struvite precipitation in anaerobic treatment systems.* Water Science and Technology, 1994. **30**(12): p. 107-116.

186. Packer, A., et al., *Growth and neutral lipid synthesis in green microalgae: a mathematical model.* Bioresource technology, 2011. **102**(1): p. 111-117.

187. Formighieri, C., *Solar-to-fuel Conversion in Algae and Cyanobacteria*. 2015: Springer.

188. Kim, H.W., et al., *Photoautotrophic nutrient utilization and limitation during semi□continuous growth of Synechocystis sp. PCC6803.* Biotechnology and bioengineering, 2010. **106**(4): p. 553-563.

189. Luong, J., *Generalization of Monod kinetics for analysis of growth data with substrate inhibition.* Biotechnology and Bioengineering, 1987. **29**(2): p. 242-248.

190. Lawrence, A.W. and P.L. McCarty, *Kinetics of methane fermentation in anaerobic treatment.* Journal (Water Pollution Control Federation), 1969: p. R1-R17.

191. Vavilin, V., et al., *Hydrolysis kinetics in anaerobic degradation of particulate organic material: an overview.* Waste management, 2008. **28**(6): p. 939-951.

192. O'Rourke, J.T., *Kinetics of anaerobic treatment at reduced temperatures*. 1968.

193. Markou, G., I. Angelidaki, and D. Georgakakis, *Carbohydrate-enriched cyanobacterial biomass as feedstock for bio-methane production through anaerobic digestion.* Fuel, 2013. **111**: p. 872-879.

194. Garcia-Heras, J., *Reactor sizing, process kinetics and modelling of anaerobic digestion of complex wastes.* Biomethanization of the organic fraction of municipal solid wastes, 2003: p. 31-43.

195. Masse, L., et al., *Neutral fat hydrolysis and long□chain fatty acid oxidation during anaerobic digestion of slaughterhouse wastewater.* Biotechnology and bioengineering, 2002. **79**(1): p. 43-52.

196. Shimizu, T., K. Kudo, and Y. Nasu, *Anaerobic waste□activated sludge digestion–a bioconversion mechanism and kinetic model.* Biotechnology and Bioengineering, 1993. **41**(11): p. 1082-1091.

197. Quinn, J.C., et al., *Microalgae to biofuels: Life cycle impacts of methane production of anaerobically digested lipid extracted algae.* Bioresource technology, 2014. **171**: p. 37-43.

198. Varel, V., T. Chen, and A. Hashimoto, *Thermophilic and mesophilic methane production from anaerobic degradation of the cyanobacterium Spirulina maxima.* Resources, conservation and recycling, 1988. **1**(1): p. 19-26.

199. Lebrero, R., et al., *Biogas upgrading from vinasse digesters: a comparison between an anoxic biotrickling filter and an algal□bacterial photobioreactor.* Journal of Chemical Technology and Biotechnology, 2016. **91**(9): p. 2488-2495.

200. Xiao, Y., et al., *Effect of Small-Scale Turbulence on the Physiology and Morphology of Two Bloom-Forming Cyanobacteria.* PloS one, 2016. **11**(12): p. e0168925.

201. Fadlallah, H., et al. *Effects of Shear Stress on the Growth Rate of Micro-Organisms in Agitated Reactors*. in *ASME 2016 Fluids Engineering Division Summer Meeting collocated with the ASME 2016 Heat Transfer Summer Conference and the ASME 2016 14th International Conference on Nanochannels, Microchannels, and Minichannels*. 2016. American Society of Mechanical Engineers.

202. Kumar, K., et al., *Development of suitable photobioreactors for CO 2 sequestration addressing global warming using green algae and cyanobacteria.* Bioresource technology, 2011. **102**(8): p. 4945-4953.

203. Moisander, P.H., et al., *Small□scale shear effects on heterocystous cyanobacteria.* Limnology and Oceanography, 2002. **47**(1): p. 108-119.

204. Havens, K.E., et al., *N: P ratios, light limitation, and cyanobacterial dominance in a subtropical lake impacted by non-point source nutrient pollution.* Environmental Pollution, 2003. **122**(3): p. 379-390.

205. Mirón, A.S., et al., *Shear stress tolerance and biochemical characterization of Phaeodactylum tricornutum in quasi steady-state continuous culture in outdoor photobioreactors.* Biochemical Engineering Journal, 2003. **16**(3): p. 287-297.

206. Michels, M.H., et al., *Effects of shear stress on the microalgae Chaetoceros muelleri.* Bioprocess and biosystems engineering, 2010. **33**(8): p. 921-927.

207. Nguyen, M.A. and A.L. Hoang, *A review on microalgae and cyanobacteria in biofuel production*. 2016, USTH.

208. Wang, J., et al., *Mechanomics: an emerging field between biology and biomechanics.* Protein & cell, 2014. **5**(7): p. 518-531.

209. Chalmers, J.J., *Mixing, aeration and cell damage, 30+ years later: what we learned, how it affected the cell culture industry and what we would like to know more about.* Current Opinion in Chemical Engineering, 2015. **10**: p. 94-102.

210. Sieck, J.B., et al., *Development of a scale-down model of hydrodynamic stress to study the performance of an industrial CHO cell line under simulated production scale bioreactor conditions.* Journal of biotechnology, 2013. **164**(1): p. 41-49.

211. Han, R.B. and Y.J. Yuan, *Oxidative Burst in Suspension Culture of Taxus cuspidataInduced by a Laminar Shear Stress in Short□Term.* Biotechnology progress, 2004. **20**(2): p. 507-513.

212. Yi, W., et al., *Proteomic profiling of human bone marrow mesenchymal stem cells under shear stress.* Molecular and cellular biochemistry, 2010. **341**(1-2): p. 9-16.

213. Sieck, J.B., et al., *Adaptation for survival: Phenotype and transcriptome response of CHO cells to elevated stress induced by agitation and sparging.* Journal of biotechnology, 2014. **189**: p. 94-103.

214. Kunnen, S.J., et al., *Comprehensive transcriptome analysis of fluid shear stress altered gene expression in renal epithelial cells.* Journal of cellular physiology, 2017.

215. Richardson, G.M., J. Lannigan, and I.G. Macara, *Does FACS perturb gene expression?* Cytometry Part A, 2015. **87**(2): p. 166-175.

216. Al□Rubeai, M., et al., *Death mechanisms of animal cells in conditions of intensive agitation.* Biotechnology and bioengineering, 1995. **45**(6): p. 463-472.

217. Keane, J.T., D. Ryan, and P.P. Gray, *Effect of shear stress on expression of a recombinant protein by Chinese hamster ovary cells.* Biotechnology and bioengineering, 2003. **81**(2): p. 211-220.

218. Barbosa, M.J. and R.H. Wijffels, *Overcoming shear stress of microalgae cultures in sparged photobioreactors.* Biotechnology and bioengineering, 2004. **85**(1): p. 78-85.

219. Edmundson, S.J. and M.H. Huesemann, *The dark side of algae cultivation: Characterizing night biomass loss in three photosynthetic algae, Chlorella sorokiniana, Nannochloropsis salina and Picochlorum sp.* Algal Research, 2015. **12**: p. 470-476.

220. Gharagozloo, P.E., et al., *Analysis and modeling of Nannochloropsis growth in lab, greenhouse, and raceway experiments.* Journal of applied phycology, 2014. **26**(6): p. 2303-2314.

221. Sharkey, T.D., *Estimating the rate of photorespiration in leaves.* Physiologia Plantarum, 1988. **73**(1): p. 147-152.

222. Shuler, M.L. and F. Kargi, *Bioprocess Engineering: Basic Concepts*. 2002: Prentice Hall.

223. thinkstep. *Sustainability Consulting and Software* 2018 02/17/2014 01/23/2018]; Available from: https://www.thinkstep.com/about.

224. Sánchez Mirón, A., et al., *Bubble□column and airlift photobioreactors for algal culture.* AIChE Journal, 2000. **46**(9): p. 1872-1887.

225. *Microalgal Biotechnology: Potential and Production*, C. Posten and C. Walter, Editors. 2013, DE GRUYTER: Germany.

226. Janssen, M., et al., *Enclosed outdoor photobioreactors: Light regime, photosynthetic efficiency, scale□up, and future prospects.* Biotechnology and bioengineering, 2003. **81**(2): p. 193-210.

227. Vejrazka, C., et al., *Photosynthetic efficiency of Chlamydomonas reinhardtii in flashing light.* Biotechnology and bioengineering, 2011. **108**(12): p. 2905-2913.

228. Vejrazka, C., et al., *Photosynthetic efficiency of Chlamydomonas reinhardtii in attenuated, flashing light.* Biotechnology and bioengineering, 2012. **109**(10): p. 2567-2574.

229. Grobbelaar, J.U., *The influence of light/dark cycles in mixed algal cultures on their productivity.* Bioresource technology, 1991. **38**(2-3): p. 189-194.

230. Chisti, M.Y., *Airlift bioreactors*. 1989: Elsevier Applied Science.

231. Ali, H., et al., *Numerical prediction of algae cell mixing feature in raceway ponds using particle tracing methods.* Biotechnology and bioengineering, 2015. **112**(2): p. 297-307.

232. Nezu, I. and W. Rodi, *Open-channel flow measurements with a laser Doppler anemometer.* Journal of Hydraulic Engineering, 1986. **112**(5): p. 335-355.

233. McGowen, J., et al., *The Algae Testbed Public-Private Partnership (ATP3) framework; establishment of a national network of testbed sites to support sustainable algae production.* Algal Research, 2017. **25**: p. 168-177.

234. Adhikari, D. and E.K. Longmire, *Infrared tomographic PIV and 3D motion tracking system applied to aquatic predator–prey interaction.* Measurement Science and Technology, 2012. **24**(2): p. 024011.

235. Lohrmann, A., R. Cabrera, and N.C. Kraus. *Acoustic-Doppler velocimeter (ADV) for laboratory use*. in *Fundamentals and advancements in hydraulic measurements and experimentation*. 1994. ASCE.

236. Kraus, N.C., A. Lohrmann, and R. Cabrera, *New acoustic meter for measuring 3D laboratory flows.* Journal of Hydraulic Engineering, 1994. **120**(3): p. 406-412.

237. Parsheh, M., F. Sotiropoulos, and F. Porté-Agel, *Estimation of power spectra of acoustic-Doppler velocimetry data contaminated with intermittent spikes.* Journal of Hydraulic Engineering, 2010. **136**(6): p. 368-378.

238. Rusello, P.J. and E.A. Cowen. *Turbulent dissipation estimates from pulse coherent doppler instruments*. in *Current, Waves and Turbulence Measurements (CWTM), 2011 IEEE/OES 10th*. 2011. IEEE.

239. Doroudian, B., D. Hurther, and U. Lemmin, *Discussion of "turbulence measurements with acoustic doppler velocimeters" by Carlos M. García, Mariano I. Cantero, Yarko Niño, and Marcelo H. García.* Journal of Hydraulic Engineering, 2007. **133**(11): p. 1286-1289.

240. García, C.M., et al., *Closure to "Turbulence Measurements with Acoustic Doppler Velocimeters" by Carlos M. García, Mariano I. Cantero, Yarko Niño, and Marcelo H. García.* Journal of Hydraulic Engineering, 2007. **133**(11): p. 1289-1292.

241. Blanckaert, K. and U. Lemmin, *Means of noise reduction in acoustic turbulence measurements.* Journal of hydraulic Research, 2006. **44**(1): p. 3-17.

242. Hurther, D. and U. Lemmin, *A correction method for turbulence measurements with a 3D acoustic Doppler velocity profiler.* Journal of Atmospheric and Oceanic Technology, 2001. **18**(3): p. 446-458.

243. Nikora, V.I. and D.G. Goring, *ADV measurements of turbulence: Can we improve their interpretation?* Journal of Hydraulic Engineering, 1998. **124**(6): p. 630-634.

244. Tennekes, H. and J.L. Lumley, *A first course in turbulence*. 1972: MIT press.

245. Schlichting, H. and K. Gersten, *Boundary-layer theory*. 2016: Springer.

246. Russo, F. and N.T. Basse, *Scaling of turbulence intensity for low-speed flow in smooth pipes.* Flow Measurement and Instrumentation, 2016. **52**: p. 101-114.

247. Yunus, A.C. and J.M. Cimbala, *Fluid mechanics fundamentals and applications*. International Edition, McGraw Hill Publication. 2010.

248. Demirbas, M.F., *Biofuels from algae for sustainable development.* Applied Energy, 2011. **88**(10): p. 3473-3480.

249. Jonker, J. and A. Faaij, *Techno-economic assessment of micro-algae as feedstock for renewable bio-energy production.* Applied Energy, 2013. **102**: p. 461-475.

250. Rawat, I., et al., *Biodiesel from microalgae: a critical evaluation from laboratory to large scale production.* Applied energy, 2013. **103**: p. 444-467.

251. Sandnes, J., et al., *Combined influence of light and temperature on growth rates of Nannochloropsis oceanica: linking cellular responses to large-scale biomass production.* Journal of Applied Phycology, 2005. **17**(6): p. 515-525.

252. Ogata, K., *System dynamics*. Vol. 3. 1998: Prentice Hall New Jersey.

253. Palm, W.J., *Modeling, analysis, and control of dynamic systems*. 1983: Wiley New York.

254. Geider, R., H. MacIntyre, and T. Kana, *Dynamic model of phytoplankton growth and acclimation: responses of the balanced growth rate and the chlorophyll a: carbon ratio to light, nutrient-limitation and temperature.* Marine Ecology Progress Series, 1997: p. 187-200.

255. Wirtz, K.W. and M. Pahlow, *Dynamic chlorophyll and nitrogen: carbon regulation in algae optimizes instantaneous growth rate.* Marine Ecology Progress Series, 2010. **402**: p. 81-96.

256. James, S.C. and V. Boriah, *Modeling algae growth in an open-channel raceway.* Journal of Computational Biology, 2010. **17**(7): p. 895-906.

257. Li, S., et al., *Thermal modeling of greenhouse aquaculture raceway systems.* Aquacultural engineering, 2009. **41**(1): p. 1-13.

258. Shang, H., et al., *A dynamic thermal model for heating microalgae incubator ponds using off-gas.* Chemical Engineering Science, 2010. **65**(16): p. 4591-4597.

259. Weyer-Geigel, K.M., *Heat-balance model and thermal analysis of an algae growth system for biofuel*. 2008, Colorado State University.

260. Zhu, C. and Y. Lee, *Determination of biomass dry weight of marine microalgae.* Journal of applied phycology, 1997. **9**(2): p. 189-194.

261. Bergman, T.L., et al., *Fundamentals of heat and mass transfer*. 2011: John Wiley & Sons.

262. Duffie, J.A. and W.A. Beckman, *Solar engineering of thermal processes*. 2013: John Wiley & Sons.

263. Stramski, D., *Refractive index of planktonic cells as a measure of cellular carbon and chlorophyll a content.* Deep Sea Research Part I: Oceanographic Research Papers, 1999. **46**(2): p. 335-351.

264. Martin, M. and P. Berdahl, *Characteristics of infrared sky radiation in the United States.* Solar energy, 1984. **33**(3-4): p. 321-336.

265. Chapra, S., *Surface water quality modeling, Series in Water Resources and Environmental Engineering*. 1997, McGraw-Hill, New York, USA.

266. Cerco, C.F. and T.M. Cole, *Three-Dimensional Eutrophication Model of Chesapeake Bay. Volume 1: Main Report*. 1994, ARMY ENGINEER WATERWAYS EXPERIMENT STATION VICKSBURG MS ENVIRONMENTAL LAB.

267. Di Toro, D.M., D.J. O'CONNOR, and R.V. Thomann, *A dynamic model of the phytoplankton population in the Sacramento—San Joaquin Delta*. 1971, ACS Publications.

268. Geider, R.J. and J. La Roche, *Redfield revisited: variability of C [ratio] N [ratio] P in marine microalgae and its biochemical basis.* European Journal of Phycology, 2002. **37**(1): p. 1-17.

269. Oberkampf, W.L., T.G. Trucano, and C. Hirsch, *Verification, validation, and predictive capability in computational engineering and physics.* Applied Mechanics Reviews, 2004. **57**(5): p. 345-384.

270. Roy, C.J. and W.L. Oberkampf, *A comprehensive framework for verification, validation, and uncertainty quantification in scientific computing.* Computer methods in applied mechanics and engineering, 2011. **200**(25-28): p. 2131-2144.

271. Ferson, S., W.L. Oberkampf, and L. Ginzburg, *Model validation and predictive capability for the thermal challenge problem.* Computer Methods in Applied Mechanics and Engineering, 2008. **197**(29-32): p. 2408-2430.

272. Morita, M., Y. Watanabe, and H. Saiki, *Evaluation of photobioreactor heat balance for predicting changes in culture medium temperature due to light irradiation.* Biotechnology and bioengineering, 2001. **74**(6): p. 466-475.

273. Quiroz-Arita, C., J.J. Sheehan, and T.H. Bradley, *Life cycle net energy and greenhouse gas emissions of photosynthetic cyanobacterial biorefineries: Challenges for industrial production of biofuels.* Algal Research, 2017. **26**: p. 445-452.

274. Jewell, W.J. and P.L. McCarty, *Aerobic decomposition of algae.* Environmental Science & Technology, 1971. **5**(10): p. 1023-1031.

275. Edzwald, J.K., *Water Quality and Treatment A Handbook on Drinking Water*. 2010: McGrawHill.

276. Smith, P., *Land use change and soil organic carbon dynamics.* Nutrient Cycling in Agroecosystems, 2007. **81**(2): p. 169-178.

277. Soil-Survey-Staff. *Gridded Soil Survey Geographic (gSSURGO) Database for Alabama*. United States Department of Agriculture, Natural Resources Conservation Service [07/15/2014]; Available from: http://datagateway.nrcs.usda.gov/.

278. Soil-Survey-Staff. *Gridded Soil Survey Geographic (gSSURGO) Database for Arkansas*. United States Department of Agriculture, Natural Resources Conservation Service [07/15/2014]; Available from: http://datagateway.nrcs.usda.gov/.

279. Soil-Survey-Staff. *Gridded Soil Survey Geographic (gSSURGO) Database for Arizona*. United States Department of Agriculture, Natural Resources Conservation Service [07/15/2014]; Available from: http://datagateway.nrcs.usda.gov/.

280. Soil-Survey-Staff. *Gridded Soil Survey Geographic (gSSURGO) Database for California*. United States Department of Agriculture, Natural Resources Conservation Service [07/15/2014]; Available from: http://datagateway.nrcs.usda.gov/.

281. Soil-Survey-Staff. *Gridded Soil Survey Geographic (gSSURGO) Database for Colorado*. United States Department of Agriculture, Natural Resources Conservation Service [07/15/2014]; Available from: http://datagateway.nrcs.usda.gov/.

282. Soil-Survey-Staff. *Gridded Soil Survey Geographic (gSSURGO) Database for Connecticut*. United States Department of Agriculture, Natural Resources Conservation Service [07/15/2014]; Available from: http://datagateway.nrcs.usda.gov/.

283. Soil-Survey-Staff. *Gridded Soil Survey Geographic (gSSURGO) Database for Delaware*. United States Department of Agriculture, Natural Resources Conservation Service [07/15/2014]; Available from: http://datagateway.nrcs.usda.gov/.

284. Soil-Survey-Staff. *Gridded Soil Survey Geographic (gSSURGO) Database for Florida*. United States Department of Agriculture, Natural Resources Conservation Service [07/15/2014]; Available from: http://datagateway.nrcs.usda.gov/.

285. Soil-Survey-Staff. *Gridded Soil Survey Geographic (gSSURGO) Database for Georgia*. United States Department of Agriculture, Natural Resources Conservation Service [07/15/2014]; Available from: http://datagateway.nrcs.usda.gov/.

286. Soil-Survey-Staff. *Gridded Soil Survey Geographic (gSSURGO) Database for Iowa*. United States Department of Agriculture, Natural Resources Conservation Service [07/15/2014]; Available from: http://datagateway.nrcs.usda.gov/.

287. Soil-Survey-Staff. *Gridded Soil Survey Geographic (gSSURGO) Database for Idaho*. United States Department of Agriculture, Natural Resources Conservation Service [07/15/2014]; Available from: http://datagateway.nrcs.usda.gov/.

288. Soil-Survey-Staff. *Gridded Soil Survey Geographic (gSSURGO) Database for Illinois*. United States Department of Agriculture, Natural Resources Conservation Service [07/15/2014]; Available from: http://datagateway.nrcs.usda.gov/.

289. Soil-Survey-Staff. *Gridded Soil Survey Geographic (gSSURGO) Database for Indiana*. United States Department of Agriculture, Natural Resources Conservation Service [07/15/2014]; Available from: http://datagateway.nrcs.usda.gov/.

290. Soil-Survey-Staff. *Gridded Soil Survey Geographic (gSSURGO) Database for Kansas*. United States Department of Agriculture, Natural Resources Conservation Service [07/15/2014]; Available from: http://datagateway.nrcs.usda.gov/.

291. Soil-Survey-Staff. *Gridded Soil Survey Geographic (gSSURGO) Database for Kentucky*. United States Department of Agriculture, Natural Resources Conservation Service [07/15/2014]; Available from: http://datagateway.nrcs.usda.gov/.

292. Soil-Survey-Staff. *Gridded Soil Survey Geographic (gSSURGO) Database for Louisiana*. United States Department of Agriculture, Natural Resources Conservation Service [07/15/2014]; Available from: http://datagateway.nrcs.usda.gov/.

293. Soil-Survey-Staff. *Gridded Soil Survey Geographic (gSSURGO) Database for Massachusetts*. United States Department of Agriculture, Natural Resources Conservation Service [07/15/2014]; Available from: http://datagateway.nrcs.usda.gov/.

294. Soil-Survey-Staff. *Gridded Soil Survey Geographic (gSSURGO) Database for Maryland*. United States Department of Agriculture, Natural Resources Conservation Service [07/15/2014]; Available from: http://datagateway.nrcs.usda.gov/.

295. Soil-Survey-Staff. *Gridded Soil Survey Geographic (gSSURGO) Database for Maine*. United States Department of Agriculture, Natural Resources Conservation Service [07/15/2014]; Available from: http://datagateway.nrcs.usda.gov/.

296. Soil-Survey-Staff. *Gridded Soil Survey Geographic (gSSURGO) Database for Michigan*. United States Department of Agriculture, Natural Resources Conservation Service [07/15/2014]; Available from: http://datagateway.nrcs.usda.gov/.

297. Soil-Survey-Staff. *Gridded Soil Survey Geographic (gSSURGO) Database for Minnesota*. United States Department of Agriculture, Natural Resources Conservation Service [07/15/2014]; Available from: http://datagateway.nrcs.usda.gov/.

298. Soil-Survey-Staff. *Gridded Soil Survey Geographic (gSSURGO) Database for Missouri*. United States Department of Agriculture, Natural Resources Conservation Service [07/15/2014]; Available from: http://datagateway.nrcs.usda.gov/.

299. Soil-Survey-Staff. *Gridded Soil Survey Geographic (gSSURGO) Database for Mississippi*. United States Department of Agriculture, Natural Resources Conservation Service [07/15/2014]; Available from: http://datagateway.nrcs.usda.gov/.

300. Soil-Survey-Staff. *Gridded Soil Survey Geographic (gSSURGO) Database for Montana*. United States Department of Agriculture, Natural Resources Conservation Service [07/15/2014]; Available from: http://datagateway.nrcs.usda.gov/.

301. Soil-Survey-Staff. *Gridded Soil Survey Geographic (gSSURGO) Database for North Carolina*. United States Department of Agriculture, Natural Resources Conservation Service [07/15/2014]; Available from: http://datagateway.nrcs.usda.gov/.

302. Soil-Survey-Staff. *Gridded Soil Survey Geographic (gSSURGO) Database for North Dakota*. United States Department of Agriculture, Natural Resources Conservation Service [07/15/2014]; Available from: http://datagateway.nrcs.usda.gov/.

303. Soil-Survey-Staff. *Gridded Soil Survey Geographic (gSSURGO) Database for Nebraska*. United States Department of Agriculture, Natural Resources Conservation Service [07/15/2014]; Available from: http://datagateway.nrcs.usda.gov/.

304. Soil-Survey-Staff. *Gridded Soil Survey Geographic (gSSURGO) Database for New Hampshire*. United States Department of Agriculture, Natural Resources Conservation Service [07/15/2014]; Available from: http://datagateway.nrcs.usda.gov/.

305. Soil-Survey-Staff. *Gridded Soil Survey Geographic (gSSURGO) Database for New Jersey*. United States Department of Agriculture, Natural Resources Conservation Service [07/15/2014]; Available from: http://datagateway.nrcs.usda.gov/.

306. Soil-Survey-Staff. *Gridded Soil Survey Geographic (gSSURGO) Database for New Mexico*. United States Department of Agriculture, Natural Resources Conservation Service [07/15/2014]; Available from: http://datagateway.nrcs.usda.gov/.

307. Soil-Survey-Staff. *Gridded Soil Survey Geographic (gSSURGO) Database for Nevada*. United States Department of Agriculture, Natural Resources Conservation Service [07/15/2014]; Available from: http://datagateway.nrcs.usda.gov/.

308. Soil-Survey-Staff. *Gridded Soil Survey Geographic (gSSURGO) Database for New York*. United States Department of Agriculture, Natural Resources Conservation Service [07/15/2014]; Available from: http://datagateway.nrcs.usda.gov/.

309. Soil-Survey-Staff. *Gridded Soil Survey Geographic (gSSURGO) Database for Ohio*. United States Department of Agriculture, Natural Resources Conservation Service [07/15/2014]; Available from: http://datagateway.nrcs.usda.gov/.

310. Soil-Survey-Staff. *Gridded Soil Survey Geographic (gSSURGO) Database for Oklahoma*. United States Department of Agriculture, Natural Resources Conservation Service [07/15/2014]; Available from: http://datagateway.nrcs.usda.gov/.

311. Soil-Survey-Staff. *Gridded Soil Survey Geographic (gSSURGO) Database for Oregon*. United States Department of Agriculture, Natural Resources Conservation Service [07/15/2014]; Available from: http://datagateway.nrcs.usda.gov/.

312. Soil-Survey-Staff. *Gridded Soil Survey Geographic (gSSURGO) Database for Pennsylvania*. United States Department of Agriculture, Natural Resources Conservation Service [07/15/2014]; Available from: http://datagateway.nrcs.usda.gov/.

313. Soil-Survey-Staff. *Gridded Soil Survey Geographic (gSSURGO) Database for Rhode Island*. United States Department of Agriculture, Natural Resources Conservation Service [07/15/2014]; Available from: http://datagateway.nrcs.usda.gov/.

314. Soil-Survey-Staff. *Gridded Soil Survey Geographic (gSSURGO) Database for South Carolina*. United States Department of Agriculture, Natural Resources Conservation Service [07/15/2014]; Available from: http://datagateway.nrcs.usda.gov/.

315. Soil-Survey-Staff. *Gridded Soil Survey Geographic (gSSURGO) Database for South Dakota*. United States Department of Agriculture, Natural Resources Conservation Service [07/15/2014]; Available from: http://datagateway.nrcs.usda.gov/.

316. Soil-Survey-Staff. *Gridded Soil Survey Geographic (gSSURGO) Database for Tennessee*. United States Department of Agriculture, Natural Resources Conservation Service [07/15/2014]; Available from: http://datagateway.nrcs.usda.gov/.

317. Soil-Survey-Staff. *Gridded Soil Survey Geographic (gSSURGO) Database for Texas*. United States Department of Agriculture, Natural Resources Conservation Service [07/15/2014]; Available from: http://datagateway.nrcs.usda.gov/.

318. Soil-Survey-Staff. *Gridded Soil Survey Geographic (gSSURGO) Database for Utah*. United States Department of Agriculture, Natural Resources Conservation Service [07/15/2014]; Available from: http://datagateway.nrcs.usda.gov/.

319. Soil-Survey-Staff. *Gridded Soil Survey Geographic (gSSURGO) Database for Virginia*. United States Department of Agriculture, Natural Resources Conservation Service [07/15/2014]; Available from: http://datagateway.nrcs.usda.gov/.

320. Soil-Survey-Staff. *Gridded Soil Survey Geographic (gSSURGO) Database for Vermont*. United States Department of Agriculture, Natural Resources Conservation Service [07/15/2014]; Available from: http://datagateway.nrcs.usda.gov/.

321. Soil-Survey-Staff. *Gridded Soil Survey Geographic (gSSURGO) Database for Washington*. United States Department of Agriculture, Natural Resources Conservation Service [07/15/2014]; Available from: http://datagateway.nrcs.usda.gov/.

322. Soil-Survey-Staff. *Gridded Soil Survey Geographic (gSSURGO) Database for Wisconsin*. United States Department of Agriculture, Natural Resources Conservation Service [07/15/2014]; Available from: http://datagateway.nrcs.usda.gov/.

323. Soil-Survey-Staff. *Gridded Soil Survey Geographic (gSSURGO) Database for West Virginia*. United States Department of Agriculture, Natural Resources Conservation Service [07/15/2014]; Available from: http://datagateway.nrcs.usda.gov/.

324. Soil-Survey-Staff. *Gridded Soil Survey Geographic (gSSURGO) Database for Wyoming*. United States Department of Agriculture, Natural Resources Conservation Service [07/15/2014]; Available from: http://datagateway.nrcs.usda.gov/.

APPENDIX A: Cyanobacterial Growth in Baseline LCA

The genetically engineered cyanobacteria, *Synechocystis* sp. PCC6803, that are the subject of this study, are cultivated in enclosed photobioreactors to protect them from contamination and to enable the collection of the biofuel from the photobioreactor media and headspace. The batch bioprocess is carried out in flat photobioreactors providing a total culture volume of 126,000 m^3. For validation purposes of the growth stage subsystem of this LCA, we performed experimental work in a bench scale flat photobioreactor with surface to volume ratio of 112 $m^2.m^{-3}$. Cultures were mixed by sparged air at the bottom of the photobioreactor at 0.5 m^3 of air per minute per cubic meter (VVM) (+/- 0.3). Photobioreactors were inoculated with *Synechocystis* sp. PCC6803 cells at 0.107 $g.l^{-1}$ (+/- 0.061). The cultures were grown using a high-pressure sodium (HPS) lighting system with a spectrum ranging from 400 to 700 nm at extreme conditions, sunny day at noon or a Photosynthetic Active Radiation (PAR) over 1,600 µmol $Photons.m^{-2}.s^{-1}$. Cyanobacterium biomass was harvested upon quasi-steady state conditions, reaching a productivity of 0.128 $g.l^{-1}.d^{-1}$ (+/- 0.033) (Figure A.1).

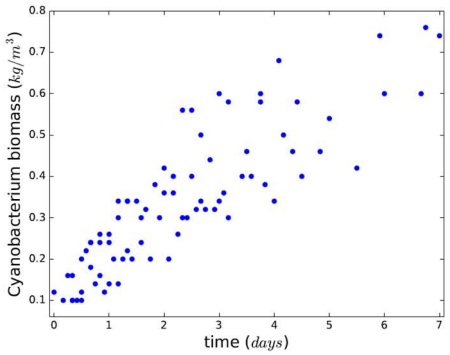

Figure A.1 Dry weight biomass results of *Synechocystis* sp. PCC6803 grown in a bench scale flat photobioreactor.

APPENDIX B: Geographical Assessment of DLUC in Microalgae Facilities

1 Life cycle assessment (LCA) of Microalgae-based facilities systems

Our Geographical Information System (GIS) model, where the impact of vegetation carbon stocks on the GHG emissions avoided by microalgae facilities due to photosynthesis and fossil fuels displacements is assessed, has integrated previous efforts concerning scaled-up growth models of Solix Biosystems photobioreactors, Life Cycle Assessments (LCA) in a "strain-to-pump" baseline scenario, and geographical selection of potential microalgae facilities as illustrated in Figures B.1 and B.2.

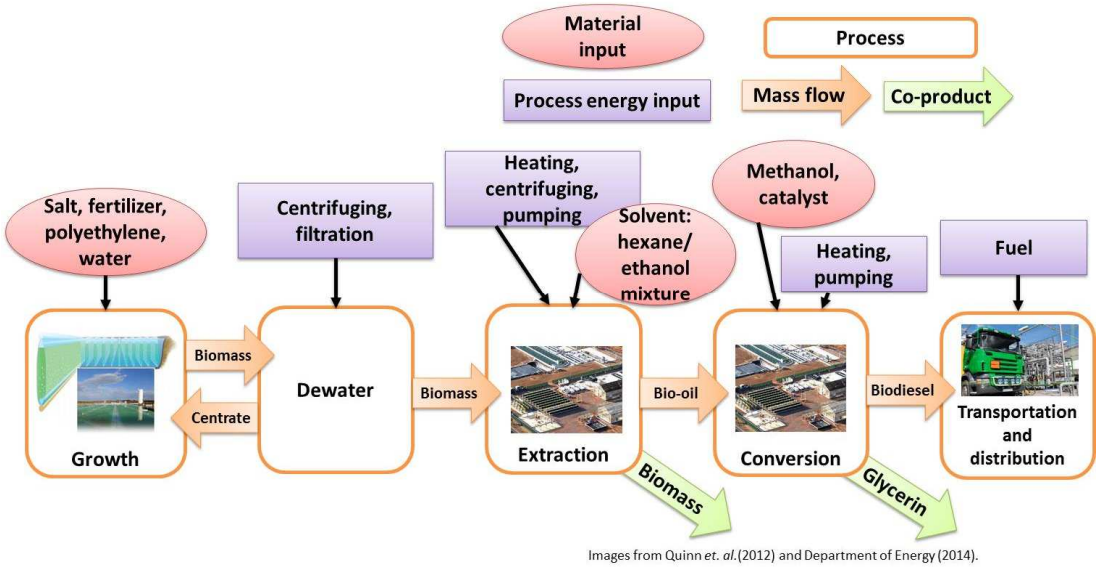

Figure B.1 Microalgae-based biofuel facilities Systems (Adapted from Batan *et. al.*, 2010).

These previous efforts have contributed to determine scalability metrics to produce the 40 billion gallons of microalgae-based biofuels in the U.S. (Table B.1), life cycle water footprints in ten different locations in the U.S. (Table B.2), net energy ratios (NER) of microalgae facilities by taking into consideration the energy consumption for each feedstock processing stage (Tables B.3), and the greenhouse gas (GHG) emissions (Table B.4) evaluated under three energy source scenarios including the U.S. electricity mix, the northeast electricity mix, and the California State

electricity mix (Table S4). Detailed information of these models incorporated in our GIS model can be obtained from Batan *et. al.[29, 133]* and Quinn *et. al.[136, 153]*. From these previous models, a unit value of GHG avoided by microalgae production of 2.262 tonnes of CO_2eq per m^3 of oil extracted was obtained and further utilized in our GIS model.

Table B.1 Scalability Metrics Derived from Microalgae to Biofuels Process Model [29]

Scalability Metrics	Value	Resources' availability in the US (%)
Land required	1.09 x 107 acres	16% of Colorado area (0.45% of US)
CO_2 consumption	8.17 x 1011 $kg.a^{-1}$	32% of from US power generation
Natural gas consumption	1.39 x 1011 $kWh.a^{-1}$	2% of US production
Electricity consumption	2.77 x 1011 $kWh.a^{-1}$	7% of US production
Water consumption	1.34 x 1012 $gal.a^{-1}$	27% of Colorado river annual flow
Nitrogen consumption	4.71 x 1010 $kg.a^{-1}$	1900% of US urea production
Algae biodiesel production	40 x 109 $gal.a^{-1}$	18% of US transportation energy sector 7500% of North American production

Scalability Metrics	Value	Resources' availability in the US (%)
Glycerin coproduct production	2.1 x 1010 $kg.a^{-1}$	11% of protein required for NOAA US aquaculture production outlook for 2025
Algae extract coproduct production	6.3 x 108 $kg.a^{-1}$	

Table B.2 Lifecycle water footprint, coproduct credits and net lifecycle water footprint for the 10 US sites evaluated for four fuel pathways. All values are presented in $m^3 \cdot GJ^{-1}$. Negative values appear between parentheses [133]

		Coproduct credits				Lifecycle water footprint
		Energy allocation		Displacement allocation		With coproduct
Locations		Min.	Max.	Min.	Max.	credits
Tempe, AZ	26–46	1.0	3.7	5.9	327	(282)–44
Hayfield Pump Plant, CA	44–79	1.0	3.7	5.9	328	(249)–75
John Martin, CO	30–53	1.0	3.7	5.9	327	(274)–49
Yellowtail, MT	24–44	1.0	3.7	5.9	333	(291)–43

Locations		Coproduct credits				Lifecycle water footprint
		Energy allocation		Displacement allocation		With coproduct credits
		Min.	Max.	Min.	Max.	
North Platte, NE	21–41	1.0	3.7	5.9	327	(291)–40
Boulder City, NV	46–83	1.0	3.7	5.8	325	(241)–80
State University, NM	34–60	1.0	3.7	6.0	333	(274)–56
Grand Falls, TX	33–58	1.0	3.7	6.0	332	(274)–54
Fish Springs, UT	29–50	1.0	3.6	5.8	322	(272)–47
Farson, WY	25–44	1.0	3.6	5.8	324	(282)–43

Table B.3 Net Energy Ratio (NER) in MJ/MJ of Conventional Diesel, Soybean Biodiesel, and Microalgae Biodiesel Processes [29]

Stage	Conventional Diesel	Soybean Biodiesel	Microalgae Biodiesel
Crude oil recovery	0.05		
Growth		0.32	0.73
Dewater			0.17

Stage	Conventional Diesel	Soybean Biodiesel	Microalgae Biodiesel
Oil extraction		0.46	0.21
Fuel conversion	0.13	0.17	0.17
Feedstock input		1.50	0.43
Transportation and distribution	$1.8X10^{-7}$	0.01	0.01
Coproducts credits		(0.83)	(0.79)
Total NER*	**0.19**	**1.64**	**0.93**

*NER is established as MJ consumed·(MJ produced)$^{-1}$

Table B.4 Net GHG Emissions of Conventional Diesel, Soybean Biodiesel, and Microalgae Biodiesel Processes [29]

GHG Emission	Conventional Diesel	Soybean Biodiesel	Microalgae Biodiesel
CO_2 ($g.MJ^{-1}$)	14.69	-72.73	-59.49
CH^4 ($g.MJ^{-1}$)	2.48	0.42	0.74
N^2O ($g.MJ^{-1}$)	0.07	0.58	-16.54
Net "strain to pump" GHG ($gCO_2eq \cdot MJ^{-1}$)	**17.24**	**-71.73**	**-75.29**

Table B.5 Analysis of Net GHG per source of Electricity with a LCA boundary of "strain-to-pump" for the baseline scenario [29]

GHG Emission	Conventional Diesel U.S. Electricity Mix	Soybean Biodiesel U.S. Electricity Mix	Microalgae Biodiesel California State Electricity Mix	Microalgae Biodiesel Northeast Electricity Mix	Microalgae Biodiesel U.S. Electricity Mix
CO_2 ($g.MJ^{-1}$)	14.69	-72.73	-80.36	-72.34	-59.49
CH^4 ($g.MJ^{-1}$)	2.48	0.42	0.45	0.45	0.74
N^2O ($g.MJ^{-1}$)	0.07	0.58	-16.56	-16.54	-16.54
Net GHG ($gCO_2eq \cdot MJ^{-1}$)	**17.24**	**-71.73**	**-96.47**	**-88.43**	**-75.29**

GHG emissions researched in LCA of Open Raceway Ponds (ORP) and Photobioreactors (PBR) have a broad range; therefore, increasing the uncertainty concerning the environmental benefits or impacts of this technology as illustrated in Table B.6. In our research, as a result, we have taken into account this wide range of GHG emissions per unit of produced energy as a baseline; then, we can evaluate the uncertainty as for the impact of carbon stocks on these emissions researched under different technologies and performances. By considering the broad range of GHG emissions as illustrated in Table B.6 and the contributions due to carbon stocks we researched, the raw data of the final GHG emissions we have obtained in our research is depicted in Table B.7.

Table B.6 Summary of LCA of Open Raceway Ponds (ORP) and Photobioreactors (PBR) [18-21, 23, 24, 26, 27, 29, 90-93, 135, 142-146]

Author	Year	Technology*	Productivity $g.m^{-2}.d^{-1}$	Lipid Percent	GHG $gCO_2.MJ^{-1}$
Ponnusamy *et. al.* (2014)	2014	ORP		24%	-95.7
Batan *et. al.* (2010)	2010	PBR	25	50%	-75.29
Handler *et. al.* (2014)	2014	ORP	25	25%	-60.8
Frank *et. al.* (2013)	2013	ORP	25	25%	-52
Quinn *et. al.* (2014)	2014	ORP	50	25%	-41.7
Campbell *et. al.* (2011)	2011	ORP	30		-31
Handler *et. al.* (2014)	2014	ORP	12	10%	-23.7
Vasudevan *et. al.* (2012)	2012	ORP	20	25%	-20
Frank *et. al.* (2011)	2011	ORP	25	25%	-19.90
Vasudevan *et. al.* (2012)	2012	ORP	20	25%	-18
Collet *et. al.* (2014)	2014	ORP	20	46%	-17.4
Azadi *et. al.* (2014)	2014	ORP	21.9	30%	13
Woertz *et. al.* (2014)	2014	ORP	20	30%	24.05
Liu *et. al.* (2013)	2013				33
Sills *et. al.* (2013)	2013	PBR/ORP	25		34

Author	Year	Technology*	Productivity $g.m^{-2}.d^{-1}$	Lipid Percent	GHG $gCO_2.MJ^{-1}$
Azadi *et. al.* (2014)	2014	ORP	21.9	30%	37
Shirvani *et. al.* (2011)	2011	ORP	18.6	30%	47.8
Adesanya *et. al.* (2014)	2014	PBR/ORP		40%	51
Soh *et. al.* (2014)	2014			9%	64
Brentner *et. al.* (2011)	2011	PBR	68	25%	80.5
Passell *et. al.* (2013)	2013		25	50%	107
Sills *et. al.* (2013)	2013		25		184
Vasudevan *et. al.* (2012)	2012	ORP	20	25%	205
Grierson *et. al.* (2013)	2013	PBR			230
Brentner *et. al.* (2011)	2011	ORP	48	25%	534

Table B.7 Raw data of GHG emissions per unit of energy produced histograms by considering the impact of carbon stocks. Adapted from: [18-21, 23, 24, 26, 27, 29, 90-93, 135, 142-146]

U.S. Electricity Mix (Batan *et. al.*, 2010)		Campbell *et. al.* (2011)		Frank *et. al.* (2011)		Shirvani *et. al.* (2011)		Brentner *et. al.* (2011)	
Bins	Count	Bins	Count	Bins	Count	Bins	Count	Bins	Count
-61.62	25	-17.62	25	-6.62	25	61.38	25	94.38	25
-36.86	7	7.14	7	18.14	7	86.14	7	119.14	7
-12.1	0	31.9	0	42.9	0	110.9	0	143.9	0

U.S. Electricity Mix (Batan *et. al.*, 2010)		Campbell *et. al.* (2011)		Frank *et. al.* (2011)		Shirvani *et. al.* (2011)		Brentner *et. al.* (2011)	
Bins	Count	Bins	Count	Bins	Count	Bins	Count	Bins	Count
12.66	1	56.66	1	67.66	1	135.66	1	168.66	1
37.42	16	81.42	16	92.42	16	160.42	16	193.42	16
62.18	6	106.18	6	117.18	6	185.18	6	218.18	6
86.94	2	130.94	2	141.94	2	209.94	2	242.94	2
111.7	1	155.7	1	166.7	1	234.7	1	267.7	1
136.46	1	180.46	1	191.46	1	259.46	1	292.46	1
161.22	0	205.22	0	216.22	0	284.22	0	317.22	0
185.98	0	229.98	0	240.98	0	308.98	0	341.98	0
210.74	0	254.74	0	265.74	0	333.74	0	366.74	0
235.5	1	279.5	1	290.5	1	358.5	1	391.5	1
260.26	0	304.26	0	315.26	0	383.26	0	416.26	0
285.02	0	329.02	0	340.02	0	408.02	0	441.02	0
309.78	0	353.78	0	364.78	0	432.78	0	465.78	0
334.54	0	378.54	0	389.54	0	457.54	0	490.54	0
359.3	0	403.3	0	414.3	0	482.3	0	515.3	0
384.06	0	428.06	0	439.06	0	507.06	0	540.06	0
408.82	0	452.82	0	463.82	0	531.82	0	564.82	0
433.58	0	477.58	0	488.58	0	556.58	0	589.58	0
458.34	0	502.34	0	513.34	0	581.34	0	614.34	0

U.S. Electricity Mix (Batan *et. al.*, 2010)		Campbell *et. al.* (2011)		Frank *et. al.* (2011)		Shirvani *et. al.* (2011)		Brentner *et. al.* (2011)	
Bins	Count	Bins	Count	Bins	Count	Bins	Count	Bins	Count
483.1	0	527.1	0	538.1	0	606.1	0	639.1	0
507.86	0	551.86	0	562.86	0	630.86	0	663.86	0
532.62	0	576.62	0	587.62	0	655.62	0	688.62	0
557.38	0	601.38	0	612.38	0	680.38	0	713.38	0
582.14	0	626.14	0	637.14	0	705.14	0	738.14	0
606.9	0	650.9	0	661.9	0	729.9	0	762.9	0
631.66	0	675.66	0	686.66	0	754.66	0	787.66	0
656.42	0	700.42	0	711.42	0	779.42	0	812.42	0
681.18	0	725.18	0	736.18	0	804.18	0	837.18	0
705.94	0	749.94	0	760.94	0	828.94	0	861.94	0
730.7	0	774.7	0	785.7	0	853.7	0	886.7	0
755.46	0	799.46	0	810.46	0	878.46	0	911.46	0
780.22	0	824.22	0	835.22	0	903.22	0	936.22	0
804.98	0	848.98	0	859.98	0	927.98	0	960.98	0
829.74	0	873.74	0	884.74	0	952.74	0	985.74	0
854.5	0	898.5	0	909.5	0	977.5	0	1010.5	0
879.26	0	923.26	0	934.26	0	1002.26	0	1035.26	0
904.02	0	948.02	0	959.02	0	1027.02	0	1060.02	0
928.78	0	972.78	0	983.78	0	1051.78	0	1084.78	0

U.S. Electricity Mix (Batan *et. al.*, 2010)		Campbell *et. al.* (2011)		Frank *et. al.* (2011)		Shirvani *et. al.* (2011)		Brentner *et. al.* (2011)	
Bins	Count	Bins	Count	Bins	Count	Bins	Count	Bins	Count
953.54	0	997.54	0	1008.54	0	1076.54	0	1109.54	0
978.3	0	1022.3	0	1033.3	0	1101.3	0	1134.3	0
1003.06	0	1047.06	0	1058.06	0	1126.06	0	1159.06	0
1027.82	0	1071.82	0	1082.82	0	1150.82	0	1183.82	0
1052.58	0	1096.58	0	1107.58	0	1175.58	0	1208.58	0
1077.34	0	1121.34	0	1132.34	0	1200.34	0	1233.34	0
1102.1	0	1146.1	0	1157.1	0	1225.1	0	1258.1	0
1126.86	0	1170.86	0	1181.86	0	1249.86	0	1282.86	0
1151.62	1	1195.62	1	1206.62	1	1274.62	1	1307.62	1

2 Geographical distribution of lipid productivities of microalgae-based biofuel facilities

Our research has taken into consideration the various efforts that have quantified productivity potential of microalgae considering geographically specific meteorological data, land availability, and carbon dioxide (CO_2) accessibility, and evaluated the life cycle GHG emissions of microalgae-based biofuel facilities in the United States (U.S.) [134] [136] [29] [78] [27, 93] [91] [135]. Potential areas of microalgae-based biofuel facilities at minimum farm sizes of 400 Ha and their lipid productivities were obtained from the research reported by Quinn *et. al.* [136]. The three land cover scenarios reported by Quinn *et. al.* [136] were taken into consideration in this research to model carbon stocks. These scenarios are barren areas with slopes of less than

1% and less than 2%, respectively, and forest or pasture or barren areas with slopes of less than 5%. These lipid productivities maps, illustrated in Figure B.2, were utilized in our research to asses above and below ground carbon stocks.

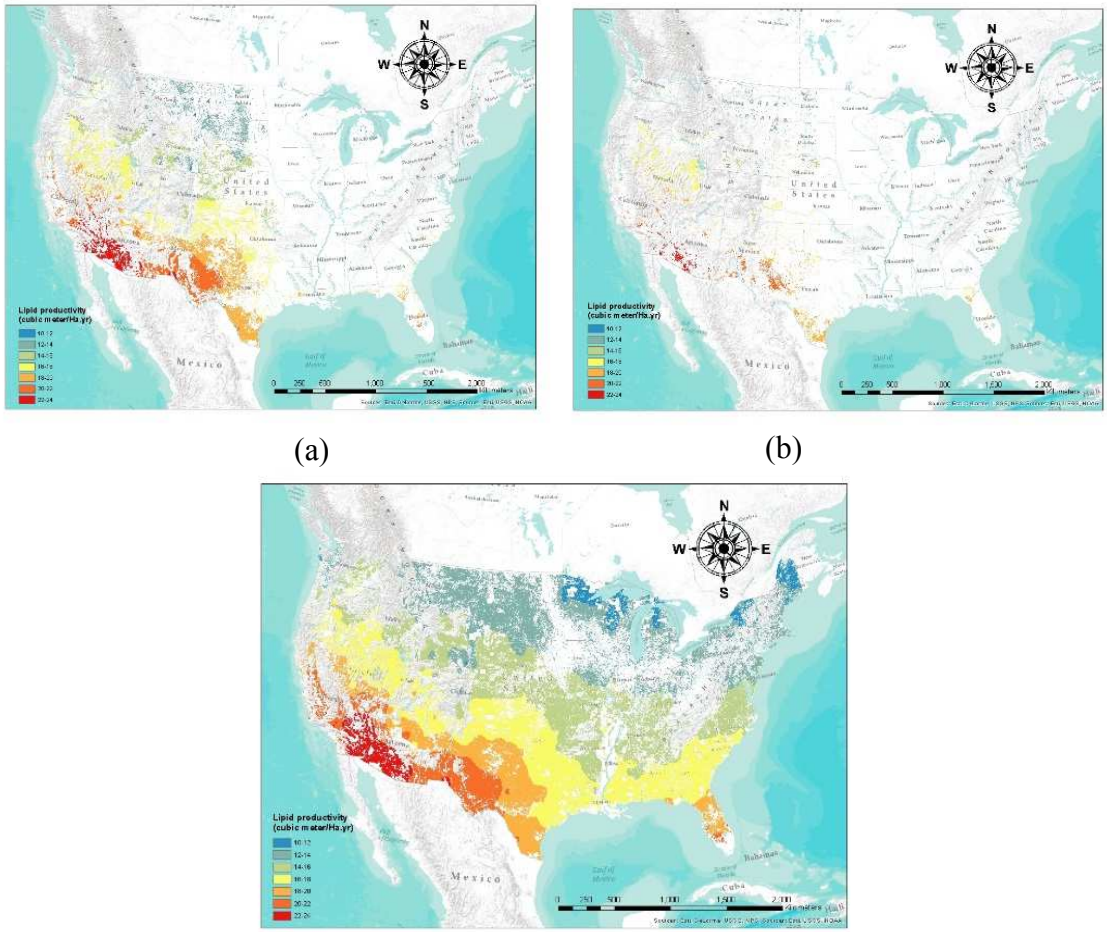

(a) (b)

(c)

Figure B.2 (a) Baseline: Lipid productivity potential of algae facilities located on barren lands with slopes of less than 2% (b) Lipid productivity potential of algae facilities located on barren lands with slopes of less than 1% (c) Lipid productivity potential of algae facilities located on forest-pastures-barren lands with slopes of less than 5% [136].

3 Above and below ground carbon

Above Ground Biomass (AGB) dataset was obtained from the Oak Ridge National Laboratory Distributed Active Archive Center (ORNL DAAC) for biogeochemical dynamics of the National Aeronautics and Space Administration (NASA) [150]. The AGB, which is

comprised of the dried matter of living organisms above ground [151], was utilized to obtain the land cover carbon, which is measured as tonnes of dried matter per hectare. The AGB maps on the U.S. and the potential microalgae-based biofuel facilities areas processed in our research are illustrated in Figures B.3 and B.4, respectively, for the three scenarios described in the section 2 of this supplementary material. Additionally, the areal distribution of the AGB for the three scenarios of our research is presented in Table B.7. When the U.S. AGB map was limited to the potential areas for microalgae-based biofuel facilities on barren lands with slopes of less than 2% and less than 1% (Figure B.2), it was observed that in the research conducted by Quinn *et. al.* [136] 95.4 % and 95.0% of these facilities were located at sites with AGB values equal or less than one ton per hectare. The remainder of the areas, 4.6% in barren lands with slopes of less than 2%, were located at AGB values ranging from 1 to 3,440 tonnes per hectare, whereas the maximum U.S. AGB is 4,101 tonnes per hectare (Figure B.3). If forest-pasture-barren lands are also included to build potential micro-algae based biofuel facilities, 35.89% of these areas would be installed on sites with AGB ranged from 1 to 3,440 tonnes.Ha^{-1} (Table B.7).

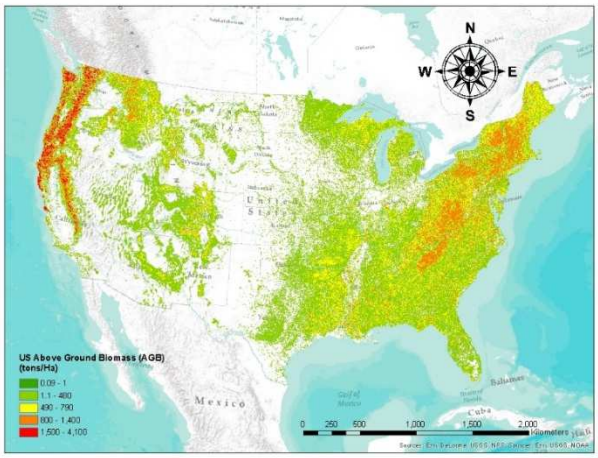

Figure B.3 United States above-ground biomass (AGB) map [150].

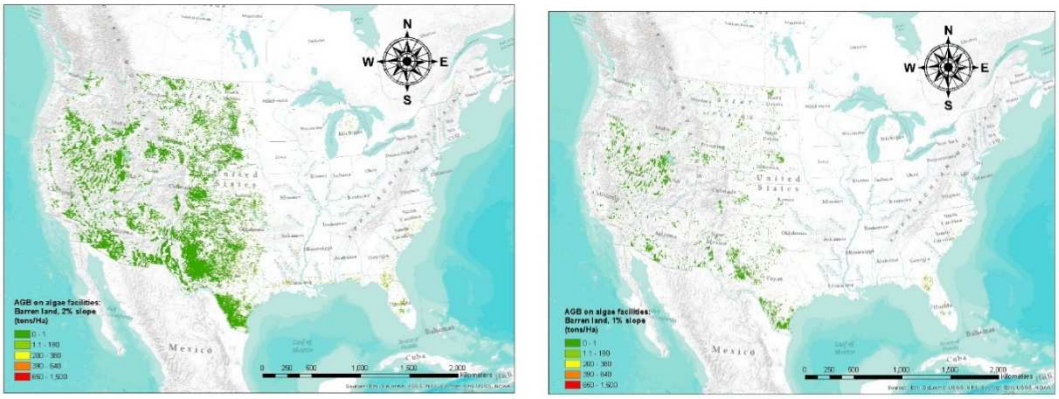

(a) (b)

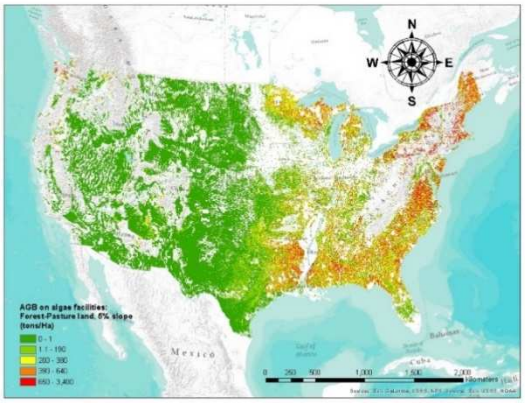

(c)

Figure B.3 Above-ground biomass (AGB) on potential microalgae-based biofuel facilities areas (a) Baseline: barren lands, less than 2% slopes (b) barren lands, less than 1% slopes (c) forest-pastures-barren lands, less than 5% slopes.

Table B.7 AGB on potential microalgae-based biofuels facilities areas

AGB (tonnes.Ha^{-1})	Land Area (%)		
	Barren land, 2% slope (baseline)	Barren land, 1% slope	Forest-pasture-barren land, 5% slope
0 – 1	95.40	95.00	64.11
1 – 190	3.60	3.60	15.52
190 – 380	0.60	0.90	8.14
380 – 640	0.30	0.40	8.70
640 –3440*	0.10	0.10	3.52

AGB (tonnes.Ha^{-1})	Land Area (%)		
	Barren land, 2% slope (baseline)	Barren land, 1% slope	Forest-pasture-barren land, 5% slope

*Barren lands at 1% and 2% slopes have a maximum of 1500 tonnesHa^{-1}.

Although most of the previously selected areas for potential microalgae-based biofuel facilities depict SOC values lower than 1-tonnes.Ha^{-1} (Table B.8), this carbon source is an important component in the carbon stocks balance [276].The contribution of the disturbed SOC by facilities in terms of biomass range from 0 to 1,100 tonnes.Ha^{-1} for barren lands with slopes of less than 2% and forest-pasture-barren lands, whereas barren lands with less than 1% of slope reach a maximum value of 360 tonnes.Ha^{-1} (Figure B.5).

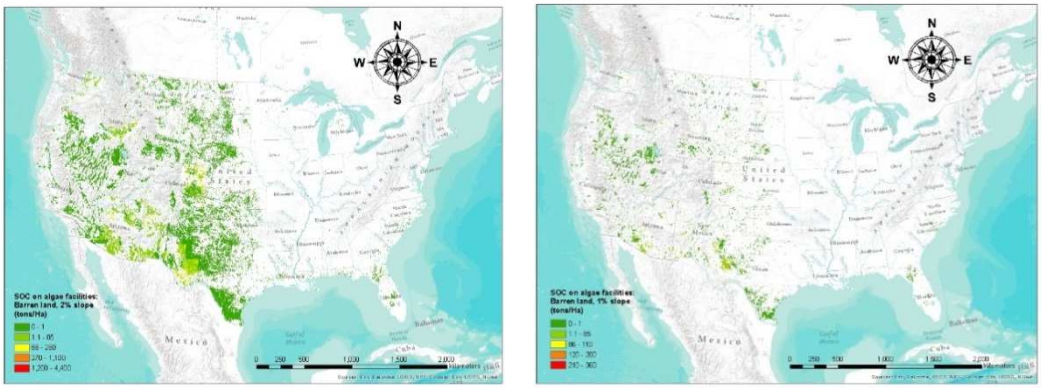

(a) (b)

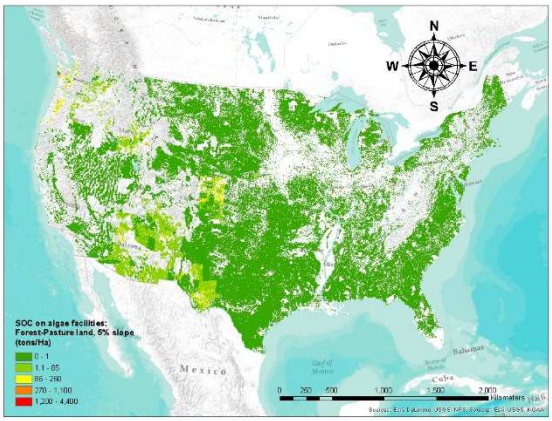

(c)

Figure B.4 Soil Organic Carbon (SOC) on potential microalgae-based biofuels facilities areas (a) Baseline: barren lands, less than 2% slopes (b) barren lands, less than 1% slopes (c) forest-pastures-barren lands, less than 5% slopes [277-324].

Table B.8 SOC on potential microalgae-based biofuels facilities areas

SOC ($tonnes.Ha^{-1}$)	Land Area (%)		
	Barren land, 2% slope (baseline)	Barren land, 1% slope	Forest-pasture-barren land, 5% slope
0 – 1	78.48	83.47	88.70
1 – 85	18.97	14.89	9.81
85 – 1100*	2.60	1.60	1.50

*Barren lands at 1% have a maximum of 360 $tonnes.Ha^{-1}$.

4 Geographical distribution of potential microalgae-based biofuels facilities GHG emissions due to direct land use change

From the results of this geographical assessment, we find that previously selected barren land areas for algae-facilities have DLUC-associated, functional unit-specific, GHG emissions ranging from 3 to 802 $gCO_2eq\ MJ^{-1}$. Figure 2 presents the distribution of DLUC-associated GHG emissions as a cumulative distribution of land area in the US. More than 99% of the proposed cultivation areas under the baseline land use restriction scenario have DLUC-

associated GHG emissions of less than or equal to 100 $gCO_2eq\ MJ^{-1}$. Figure 4 presents the DLUC-associated GHG emissions from microalgae production in Arizona, where the median GHG emissions due to DLUC is 9 $gCO_2eq\ MJ^{-1}$, and Figure 5 shows that Florida has a median DLUC-associated GHG emissions of 17 $gCO_2eq\ MJ^{-1}$.

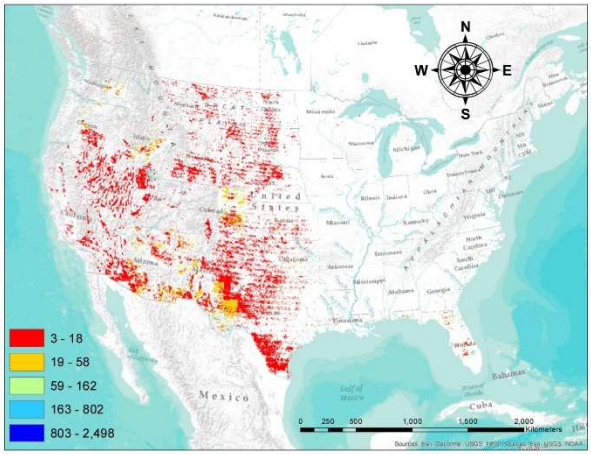

Figure B.5 Geographical distribution of potential US microalgae-based biofuels facilities' DLUC-inclusive GHG emissions ($gCO_2eq.MJ^{-1}$).

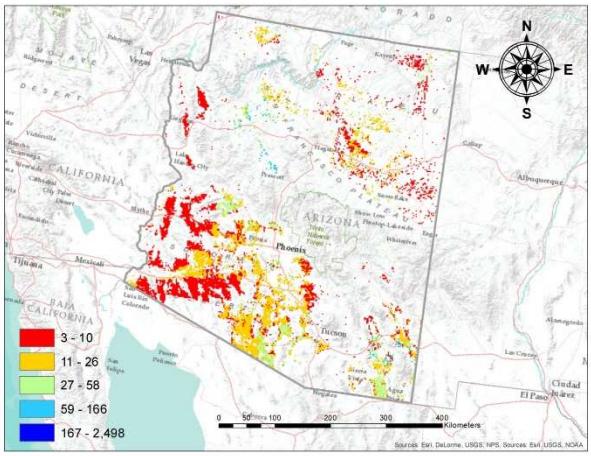

Figure B.6 Geographical distribution of potential microalgae-based biofuels facilities GHG emissions due to DLUC ($gCO_2eq.MJ^{-1}$), for the state of Arizona, US.

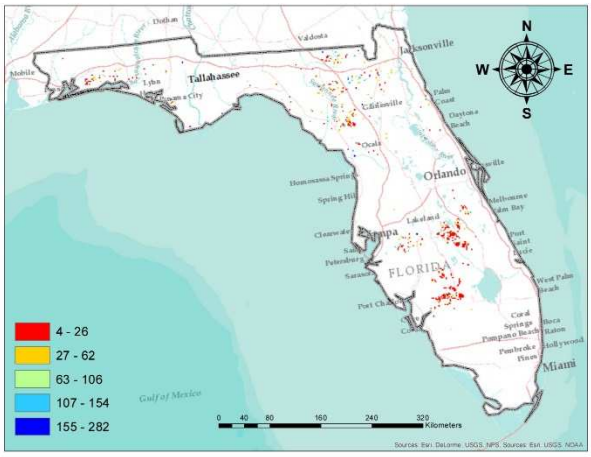

Figure B.7 Geographical distribution of potential microalgae-based biofuels facilities GHG emissions due to DLUC ($gCO_2eq.MJ^{-1}$), for the state of Florida, US.

APPENDIX C: Combined Wastewater Treatment Facility and Cyanobacterial Biorefinery

1 Baseline Biological Nutrient Removal Process and Scenarios Combining an Activated Sludge Process with Cyanobacterial Nutrient Removal

The LCA model developed in this study seeks to evaluate the synergistic environmental benefits of combining cyanobacteria cultivation and nutrients remediation in photobioreactors using the sludge centrate produced by a wastewater treatment facility (Drake Water Reclamation Facility (DWRF)) located in Fort Collins, CO, USA. For the base case scenario, the system considers the indirect and direct electrical energy consumptions by the wastewater treatment facility including the Biological Nutrient Removal (BNR) process. This waste water treatment facility is currently using a BNR process, an Anaerobic/Anoxic/Oxic (A^2/O) process as illustrated in Figure C.1 (Arita et al. 2015, Rittmann and McCarty 2012, You et al. 2003).

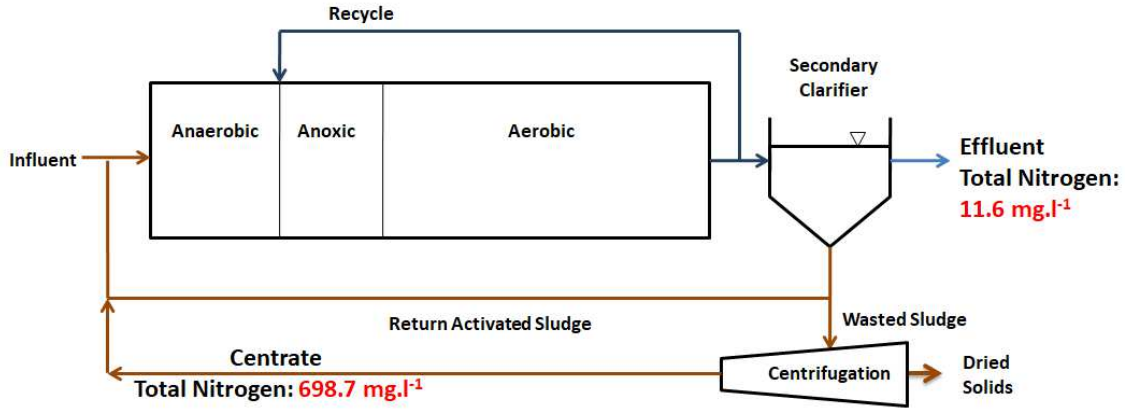

Figure C.1 Anaerobic/anoxic/oxic (A^2/O) process. The nitrogen concentrations of the treated effluent and sludge centrate correspond to the average values of DWRF for the years 2011-2014. Figure adapted from: [37, 38, 177].

The boundary of the combined wastewater treatment facility, cyanobacterial cultivation, and resources recovery, including struvite precipitation and biogas electric power generation, is illustrated in Figure C.2. For the combined system, the liquid centrate obtained from the sludge

centrifugation serves as the sources of nitrogen and phosphorous, which are required for the growth of cyanobacteria. This nutrient supplement reduces the required commercial/industrial fertilizers commonly used in photoautotrophic facilities (conventionally $NaNO_3$, KH_2PO_4).

Three centrate dilution scenarios were evaluated in this study: 3 vol%, 9 vol%, and 19 vol%. Life cycle energy use and GHG emissions due to Synechocystis sp. PCC6803 cultivation and biomass extraction were included within the system boundary. Carbon dioxide obtained from the anaerobic digester-based generation system was recycled back to the cyanobacterial cultivation system and the credits due to the displacement of grid electricity by the electricity generation through anaerobic digester were taken into consideration in the LCA model developed for analysis in this study.

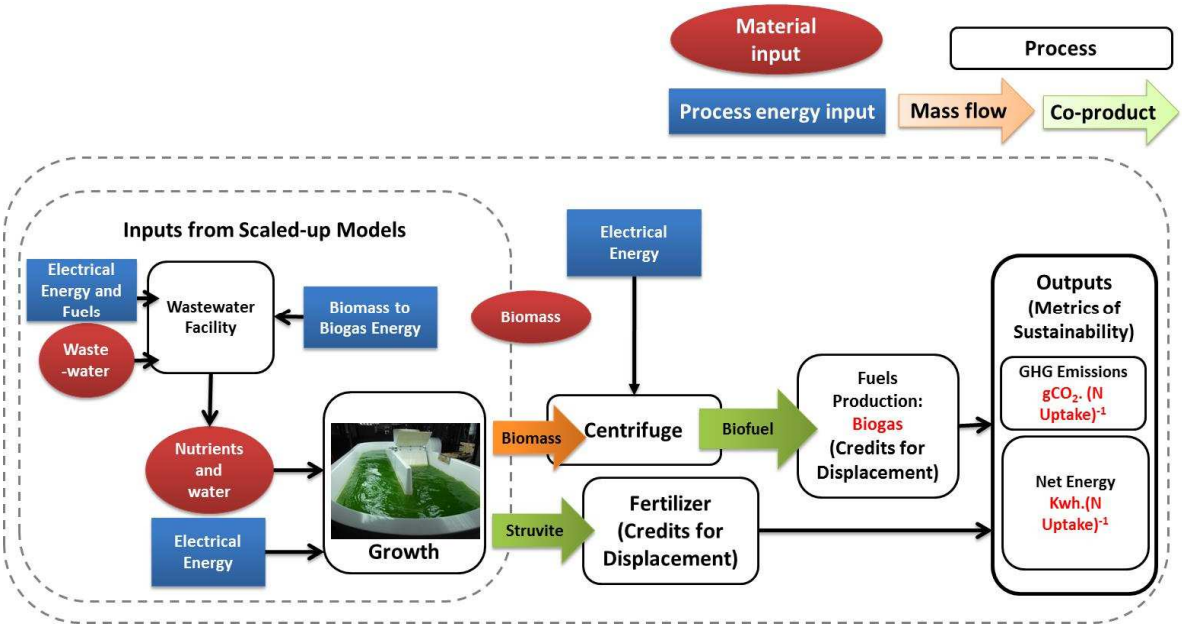

Figure C.2 Boundaries of Cyanobacterial Nutrient Removal (CNR) Process for Sidestream Wastewater Treatment.

2 Cyanobacterial Growth Model

A dynamic cyanobacterial growth model with sludge centrate inhibition was developed for analysis in this study. This model incorporates ordinary differential equations and nonlinear

function embodying nitrogen quote, nitrogen uptake, chlorophyll synthesis, light absorption, photosynthesis, growth rate, and biomass (Arita et al. 2015, Packer et al. 2011a).

Table C.1 summarizes the required biological inputs for Synechocystis sp. PCC6803(Formighieri 2015, Kim et al. 2010a, Kim et al. 2011). The novelty of the model developed in this study is the incorporation of the maximum nitrogen-limited growth rate (μm) with centrate inhibition. These parameters were determined from the experimental works described in the section 2.3. Additionally, a competitive inhibition due to the potential growth of nitrifiers in a wastewater environment was embedded into the model (Rittmann and McCarty 2001). The dynamics of this second order system is illustrated in Figure C.3.

Table C.1. Biological inputs for growth model based on *Synechocystis* sp. PCC6803

Parameter	Description	Units	Value	Reference
A	Optical cross section of chlorophyll a	$m^2.g^{-1}chl$	17	[84, 188]
ϕ	Quantum efficiency	$gC.(mol\ photons)^{-1}$	1.263	[187]
Q	Minimum subsistence nitrogen quota	$gN.g^{-1}dw$	0.0197	[188]
q_M	Maximum nitrogen quota	$gN.g^{-1}dw$	0.129	[188]
C	C subsistence quota	$gC.g^{-1}dw$	0.512	[84, 188]
V_m	Maximum uptake rate of nitrogen	$gN.g^{-1}dw.d^{-1}$	0.156	[84]
V_h	Half-saturation coefficient	$gN.m^{-3}$	39.2	[84]

Parameter	Description	Units	Value	Reference
P	Maximum chlorophyll to nitrogen ratio	$gchl.g^{-1}N$	0.116	[84]
p_o	Maximum photosynthesis rate	$gC.g^{-1}chl.d^{-1}$	47.87	[84]

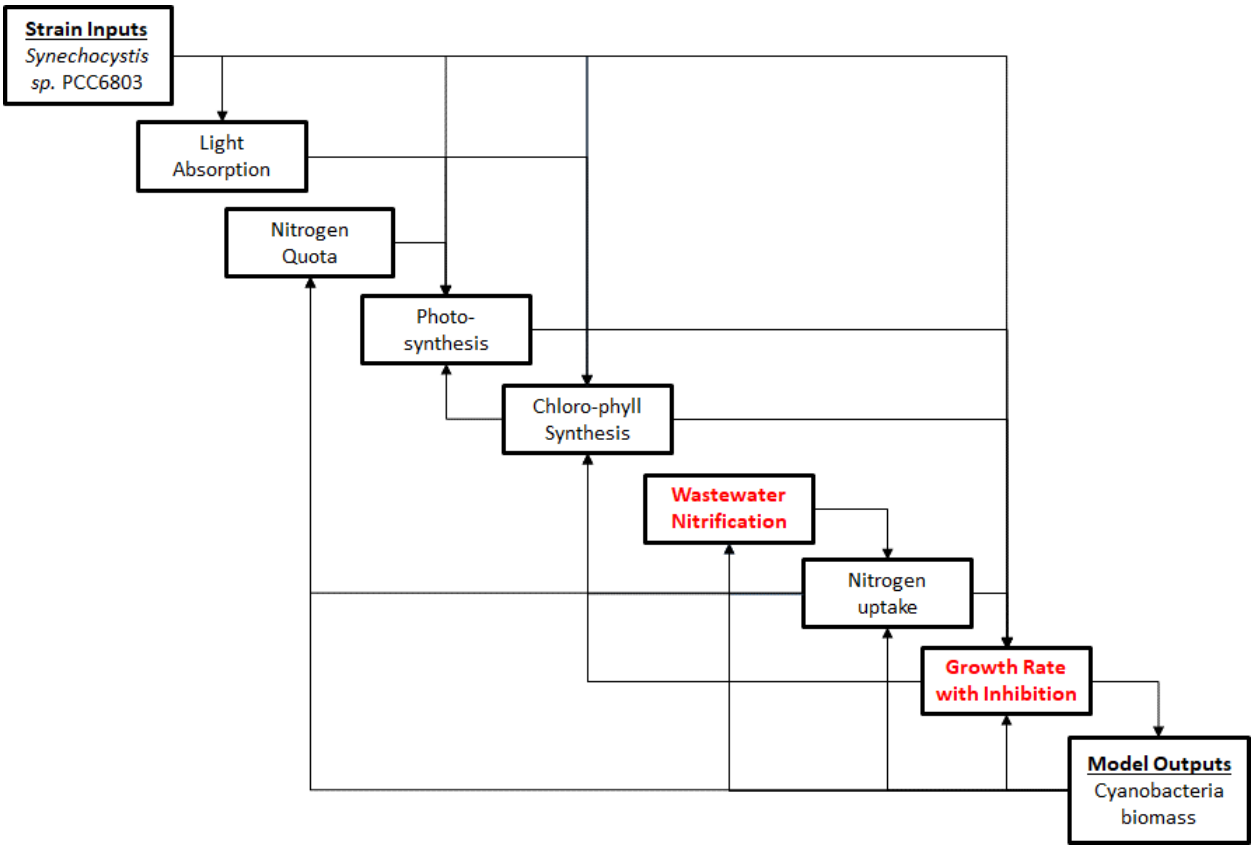

Figure C.3. Dynamic Thin Layer Cyanobacterial Growth Model with Centrate Inhibition and Competive Inhibition by Nitrifiers in Wastewater Environments.

3 LCA of Baseline Wastewater Facility and Cyanobacterial Nutrient Removal Process

The major LCA inputs and outputs of the activated sludge and CNR processes are summarized in Table C.2. The inputs include the wastewater and sludge centrate flowrates, nutrient requirements for cultivation of cyanobacteria, electricity and heat requirements for the activated sludge process and open raceway ponds. The main outputs include cyanobacterial

biomass, biogas production from co-digestion of the activated sludge and cyanobacterial biomass, and electricity and heat generation from biogas.

Table C.2. Inputs for LCA scenarios

Metric	Units	3 vol% Centrate Dilution	9 vol% Centrate Dilution	19 vol% Centrate Dilution
Drake Water Reclamation Facility flowrate	$L.d^{-1}$	44,327,172	44,327,172	44,327,172
Sludge-centrate flowrate	$L.d^{-1}$	264,979	264,979	264,979
Required flowrate by open raceway ponds	$L.d^{-1}$	10,107,050	1,741,289	870,645
Treated wastewater requirements for centrate dilution	%	22.2	3.3	1.4
Nitrogen requirements	$kg.d^{-1}$	31.33	17.59	11.97
Phosphorous requirements	$kg.d^{-1}$	69.74	12.01	6.0
Cyanobacterial biomass	$kg.d^{-1}$	7116.25	2414.784	1240.26
CO_2 available from biogas	$kg.d^{-1}$	9,080.14	8,823.18	8,778.05
CO_2 requirements for photosynthesis	$kg.d^{-1}$	14,857.36	2,559.70	1,279.85
CO_2 in liquid solution from Henrys Law	$kg.day^{-1}$	6.05	1.04	0.52
Electrical power from biogas combustion	$KWh.d^{-1}$	7657.4	7440.7	7402.7
Heatfrom biogas	$MJ.d^{-1}$	110,258	107,138	106,590
Electricity requirements by wastewater facility*	$KWh.d^{-1}$	60,285	60,285	60,285
Electricity requirements for mixing/cooling	$KWh.d^{-1}$	609	105	52
Heating requirements for cultivation	$MJ.d^{-1}$	511,215	88,074	44,037

*The electricity requirements of the wastewater facility with BNR process is 64,274 $KWh.day^{-1}$

The performance of the CNR process integrated with an activated sludge of DWRF was evaluated by using a calibrated and validated BioWin process model [183]. The scenarios were compared to the baseline BNR process which is three stage A^2/O process with nitrification, denitrification and limited biological P removal. The model for the activated sludge process was modified by removing the anaerobic and anoxic basins and the mixed liquor return (Figure C.1). The focus of the BioWin simulations was to estimate the effluent nutrient concentrations with and without the sidestream CNR. The effluent TN value for BNR and AS processes are 14.91 mg-N.l^{-1} and 25.89 mg-N.l^{-1}, respectively, correlating to a removal rate of 53% and 19%, respectively (Table C.3). Based on the three dilution scenarios evaluated by implementing CNR and removing the centrate return, a notable improvment to the combined effluent TN concentrations are obtained. The TN concentration would be reduced to 15.24, 18.94, and 19.37 mgN/L for the 3 vol%, 9 vol%, and 19 vol% centrate dilution scenarios, respectively (Table C.3). For all of the scenarios, the overall improvment to the combined effluent TN concentrations is estimated with the implementation of CNR with the 3 vol% scenarioresulting in the most efficient removal process achieving a TN removal rate of 52%. The BioWin results suggest that by removing the centrate return and based on the bench scale CNR, the combined effluent nutrient concentration and energy requirements are notably reduced when compared to the baseline BNR process.

The results from an LCA suggest that the centrate dilution of 3 vol% improves the water quality, and reduces the environmental impacts in terms of life cycle energy use and GHG emissions normalized by the nitrogen removal rate. Operational and capital costs; however, are minimized at 9 vol% scenario. For instance, the 3 vol% has the lowest NENR and GHG emissions of 37.95 kwh/(mgN.m^{-3}.day^{-1}) and 28,755 gCO_2-eq/(mgN.m^{-3}.day^{-1}), respectively. The

9 vol% scenario, on the other hand, has the lowest net energy normalized by the treated wastewater of 1.42 kwh. m^{-3}, and the lowest land requirements of 1.39 ha (Table C.3). The uncertainty of the biological experimental results of the 19 vol% scenario makes the 3 and 9 vol% more reliable alternatives for the CNR process.

Table C.3. Summary of metrics of sustainability for centrate dilutions scenarios

Metric	Drake Facility	3 vol% Centrate Dilution	9 vol% Centrate Dilution	19 vol% Centrate Dilution
CNR Effluent Total Nitrogen ($mg.l^{-1}$)	-	0.004	0.2	2.7
Combined Effluent Total Nitrogen ($mg.l^{-1}$)	14.9[a] (25.9[b])	15.24	18.94	19.37
NENR ($kwh/(mgN.m^{-3}.day^{-1})$)	37.95	34.95	41.73	42.82
GHG emissions (gCO_2-eq/($mgN.m^{-3}.day^{-1}$))	28,755	23,958	30,479	31,485
Net Energy Facility (kwh. m^{-3})	1.45	1.54	1.42	1.41
GHG emissions (gCO_2-eq. m^{-3})	1,095.64	1,053.01	1,040.27	1,038.68
Mixed Effluent and Centrate ($m^3.day^{-1}$)	-	10,107	1,741	871
Land (ha)*	-	39.09	1.39	0.42

* Available area at DWRF is 45 ha.

[a] BNR process DWRF

[b] Activated Sludge process

APPENDIX D: Cyanobacteria Growth Under Wide Range of Mixing Energy Inputs

1 Cyanobacterial Growth

The maximum growth rates of Synechocystis sp. PCC6803 were determined experimentally from Fig. D.1 and D.2. The biomass growth curve model for *Synechocystis* sp. PCC6803 for the four mixing energy inputs evaluated for the flat-panel photobioreactor: 1.94, 0.97, 0.47, and 0.03 $W.m^{-3}$, are illustrated in Figures 7, D.3, D.4 and D.5. The experimental results for the flat-panel photobioreactors and the open raceway pond are summarized in Tables D.1 and D.2.

Table D.1. Summary of experimental growth of *Synechocystis* sp. PCC6803 in flat-panel photobioreactors

Metric	VVM			
	0.7	0.35	0.17	0.01
μ (d^{-1})	0.53 (±0.17)	0.76 (±0.15)	1.29 (±0.23)	1.18 (±0.28)
DW Biomass ($g.l^{-1}$)	0.30 (±0.03)	0.24 (±0.02)	0.90 (±0.15)	0.43 (±0.03)
Productivity ($g.l^{-1}.d^{-1}$)	0.07	0.05	0.23	0.14
Water Temp (□C)	34 (±1)	30 (±1)	31 (±1)	33 (±1)
PAR ($\mu molphotons.m^{-2}.s^{-1}$)	1440 (±65)	1,323 (±9)	1,244 (±47)	1,385 (±25)

Table D.2. Summary of experimental growth of *Synechocystis* sp. PCC6803 in open raceway pond

Metric	0.1 $W.m^{-3}$		
	Replicate 1	Replicate 2	Replicate 3
μ (d^{-1})	0.68 (± 0.12)	0.82 (± 0.08)	0.81 (± 0.09)
DW Biomass ($g.l^{-1}$)	0.45 (± 0.04)	0.39 (± 0.02)	-
Productivity ($g.l^{-1}d^{-1}$)	0.06	0.04	-
Productivity ($g.m^{-2}d^{-1}$)	11.4	7.9	-
Water Temp (□C)	29	29	29
PAR ($\mu molphotons.m^{-2}.s^{-1}$)	990 (± 116)	914.8 (± 79.1)	907.8 (± 79.3)

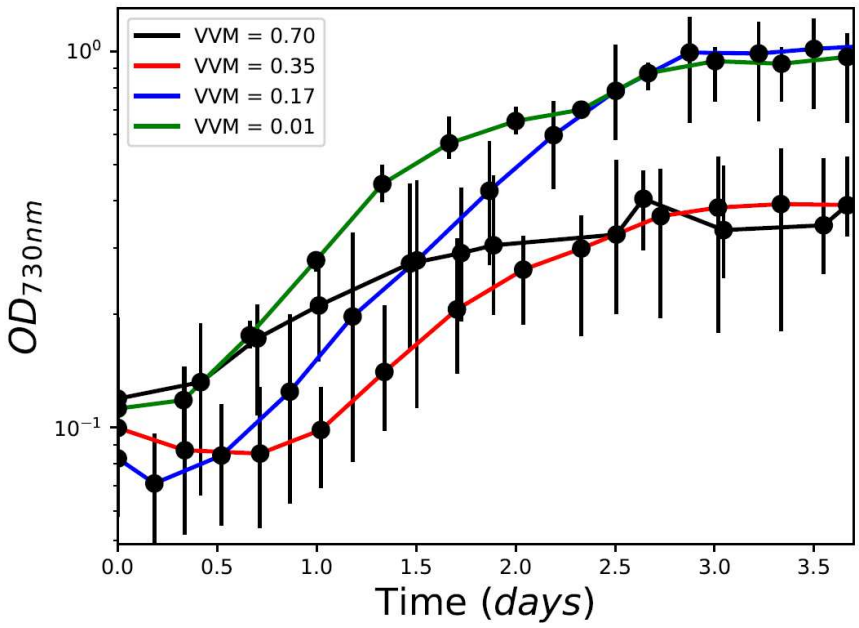

Figure D.9. Optical density of *Synechocystis* sp. PCC 6803growth in flat-panel photobioreactors. The error bars denote the upper and lower values from five experimental replicates

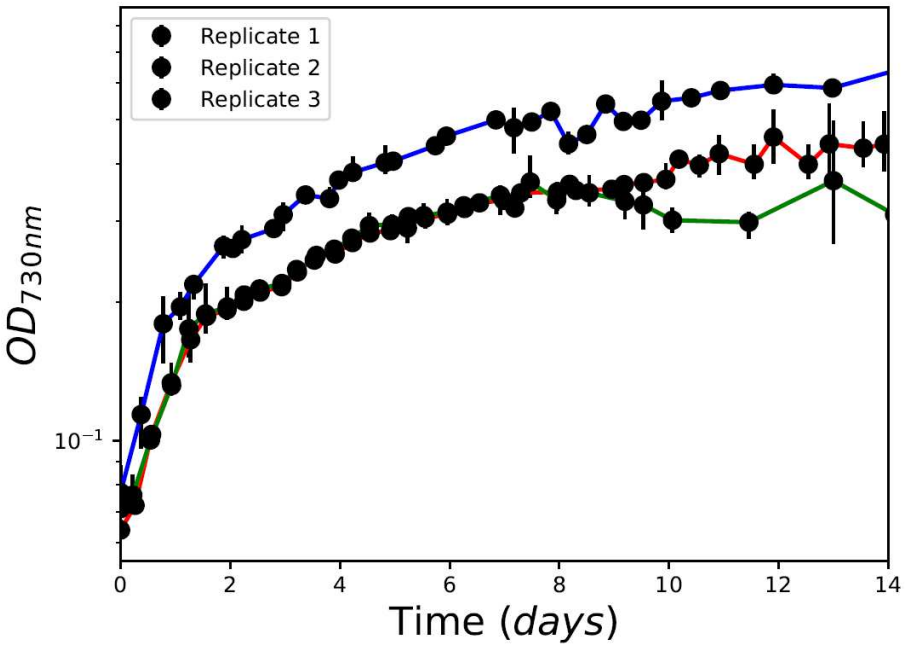

Figure D.10. Optical density of Synechocystis sp. PCC 6803 grown in open raceway pond. The error bars denote the upper and lower values from five experimental samples

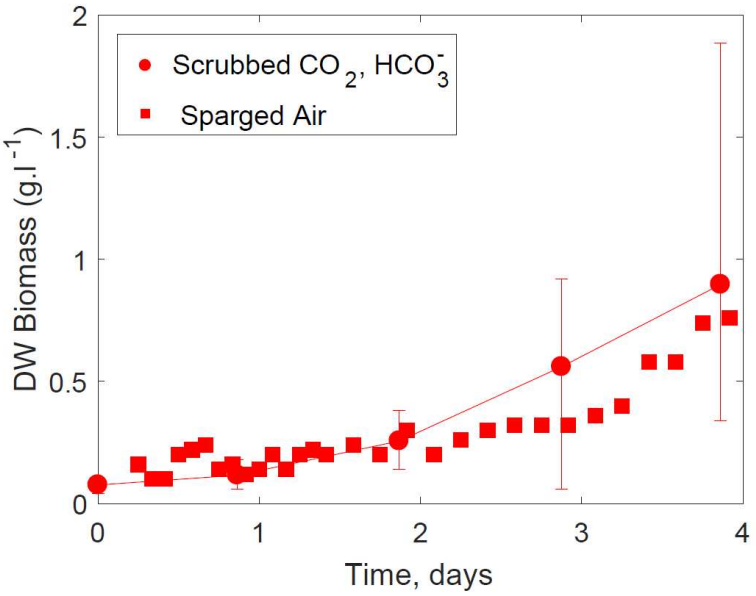

Figure D.3 Flat-panel photobioreactor experimental growth of *Synechocystis* sp. PCC 6803 at mixing energy inputs of 0.47 W.m^{-3}. The error bars denote the upper and lower values from five experimental replicates. The cultures were cultivated at 33 ± 1 °C and 1,385 ± 25 µmol photons.s^{-1}.m^{-2}.

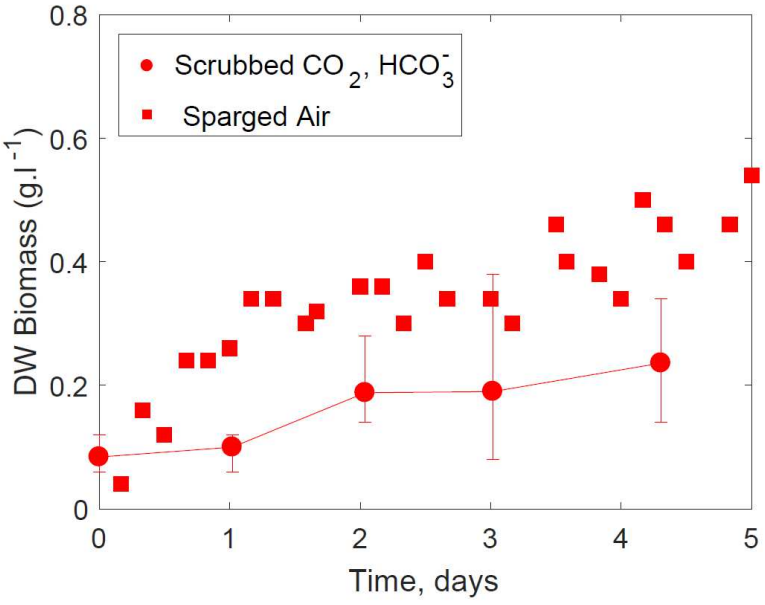

Figure D.4 Flat-panel photobioreactor experimental growth of *Synechocystis* sp. PCC 6803 at mixing energy inputs of 0.97 W.m^{-3}. The error bars denote the upper and lower values from five experimental replicates. The cultures were cultivated at 30 ± 1 °C and 1,323 ± 9 µmol photons.s^{-1}.m^{-2}.

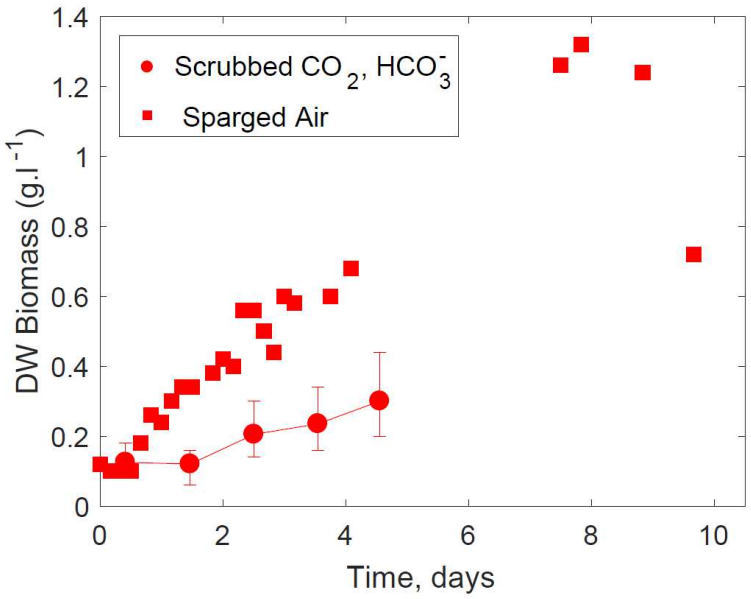

Figure D.5 Well-mixed cyanobacterial growth model in flat-panel photobioreactor validated with experimental growth of Synechocystis sp. PCC 6803 at mixing energy inputs of 1.94 W.m-3. The error bars denote the upper and lower values from five experimental replicates. The cultures were cultivated at 34 ± 1 °C and 1,440 ± 65 µmol photons.s^{-1}.m^{-2}.

2 Statistical analysis of experimental growth and metrics of sustainability

The significance of the growth rates, biomass productivities, and Net Energy Ratios (NER) response is evaluated by a one-way analysis of variance (ANOVA), and illustrated at Figures D.6, D.7, and D.8. The on-way ANOVA demonstrate a significant influence of mixing energy inputs as illustrated in the p-value less than 0.05.

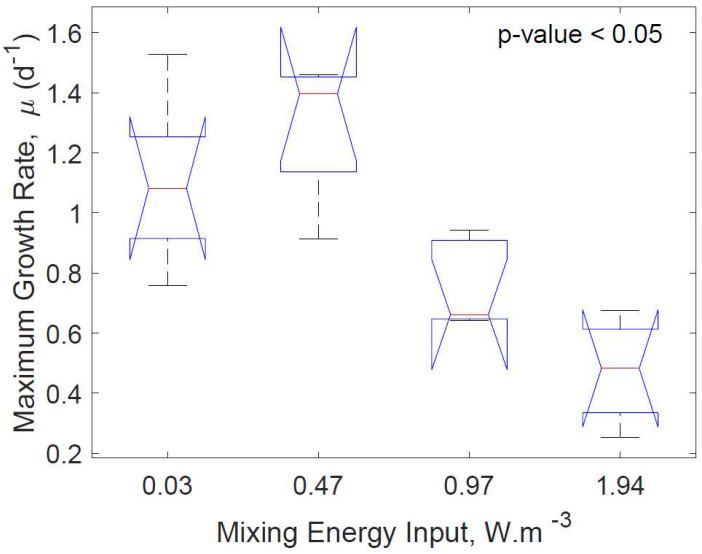

Figure D.6. Maximum growth rate of Synechocystis sp. PCC 6803 in flat-panel photobioreactors. The central mark is the median and the edges of the box are the 25th and 75th percentiles (1st and 3rd quantiles). The whiskers extend to the most extreme data points that are not considered outliers. The outliers are plotted individually. The outliers are plotted individually. The p-value or probability value was obtained from the one-way ANOVA in Matlab®.

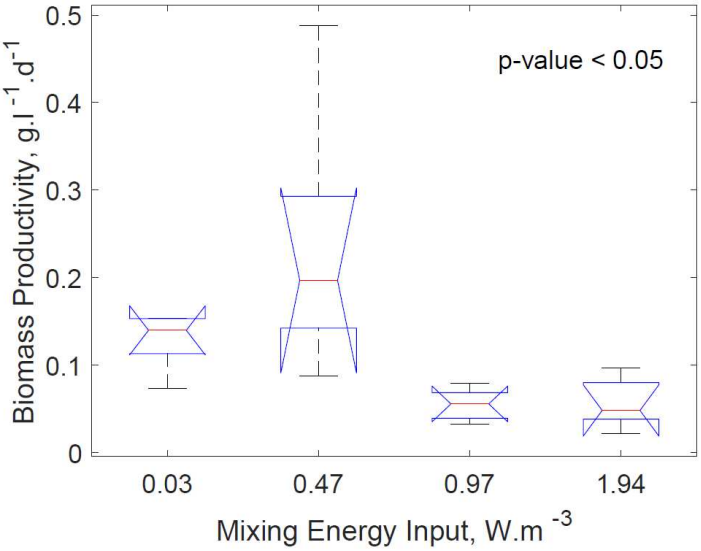

Figure D.7. Cyanobacterial biomass productivity of *Synechocystis* sp. PCC 6803 in flat-panel photobioreactors. The central mark is the median and the edges of the box are the 25th and 75th percentiles (1st and 3rd quantiles). The whiskers extend to the most extreme data points that are not considered outliers. The outliers are plotted individually. The p-value or probability value was obtained from the one-way ANOVA in Matlab®.

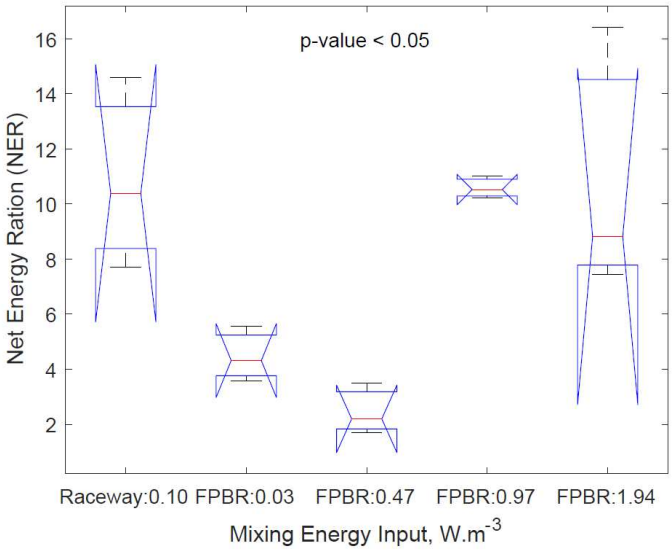

Figure D.8. Net Energy Ratio (NER) of cyanobacterial derived ethanol with cultivation of in open raceway pond and flat-panel photobioreactor (PBR). The central mark is the median and the edges of the box are the 25th and 75th percentiles (1st and 3rd quantiles). The whiskers extend to the most extreme data points that are not considered outliers. The outliers are plotted individually. The p-value or probability value was obtained from the one-way ANOVA in Matlab®.

APPENDIX E: Applied CFD of Flat-panel Photobioreactors and Open Raceway Ponds

1 Computational Fluid Dynamics of Open Raceway Pond

To understand the frequency of photoautotrophic microorganism's motion in flat-panel photobioreactors and open raceway ponds, particle tracking are obtained from the CFD models in a Lagrangian representation of the flow. The finite volume method was selected to guarantee conservation of mass and Direct Numerical Simulation (DNS) was applied to obtain precise details of turbulence [68, 69], influencing the motion of photoautotrophic microorganisms. the velocity field of the fluid domain in the open raceway pond were computed by CFD models at mixing energy inputs 0.1 $W.m^{-3}$, 0.7 $W.m^{-3}$, and 2.1 $W.m^{-3}$ (Figure 7.7 and Figure E3). The velocity field of the CFD model at mixing energy inputs of 0.1 $W.m^{-3}$ is illustrated in Figure 7.7. The CFD models were validated against experimental data measured at the second and third cross section of the open raceway pond, located in the first turn and in the straight channel as illustrated in the Supplementary material (Figure E1 and E5). By integrating experimental and computational fluid mechanics, we have represented the physics in pilot scale environments, demonstrating the fluid dynamics in flat-panel photobioreactors and open raceway ponds have no influence in the overall light experienced by photoautotrophic microorganisms cultures. We have demonstrated this by computing the frequency of this motion (Figure 8) from randomly selected particles travelling in the flat-panel photobioreactor and open raceway pond (Figure E4).

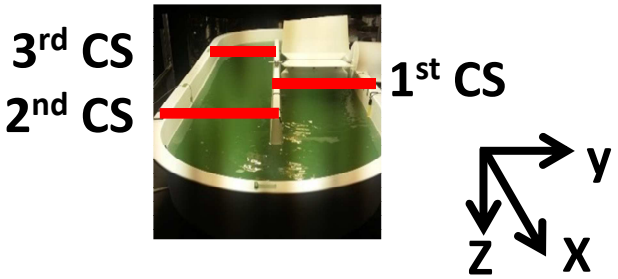

Figure E1. Open raceway pond Coordinates. The x-velocity follows the flow direction downstream the paddlewheel. The y-velocity points towards the vertical wall of the raceway pond. The z-velocity point towards the bottom of the raceway pond. The firs cross section (CS) is located downstream the paddlewheel. The second CS is located in the first turn of the channel. The third CS is located in the straight channel behind the paddlewheel.

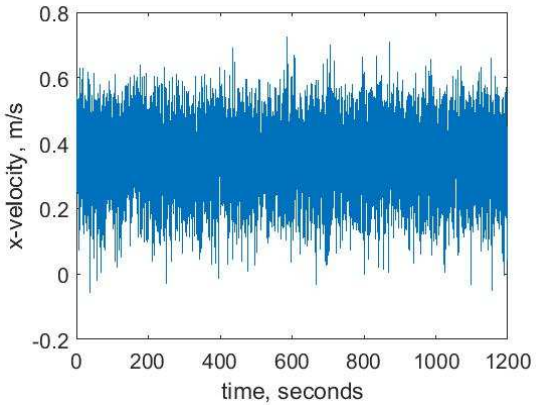

Figure E2. Example of instantaneous velocity measured in open raceway pond by ADV.

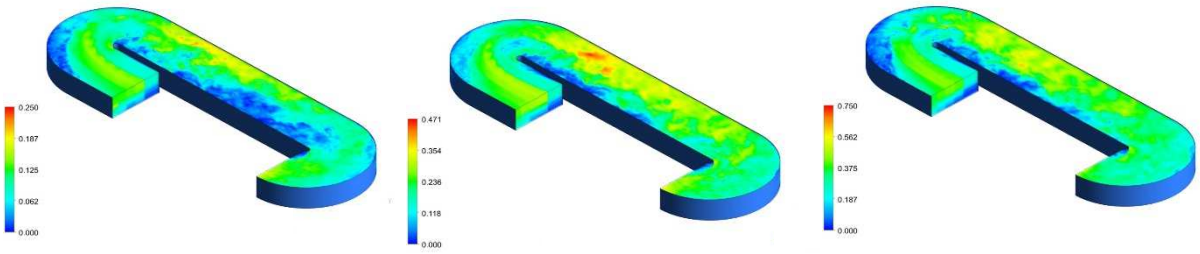

Figure E3. DNS based CFD model of open raceway pond at mixing energy inputs of 0.1 $W.m^{-3}$ (left figure), 0.7 $W.m^{-3}$ (middle figure) and 1.94 $W.m^{-3}$ (right figure).

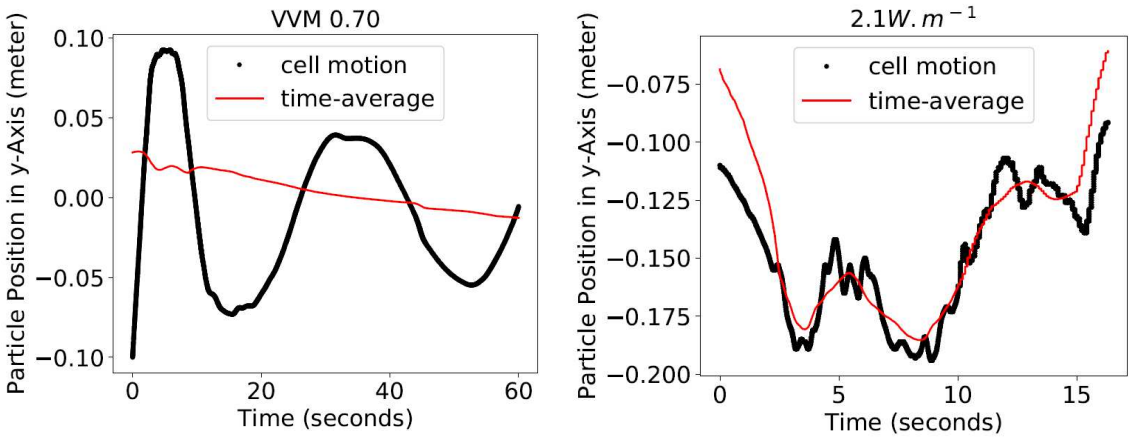

Figure E4. Photoautotrophic microorganism cell motion open raceway pond at flat-panel photobioreactor (left figure) and open raceway pond (right figure).

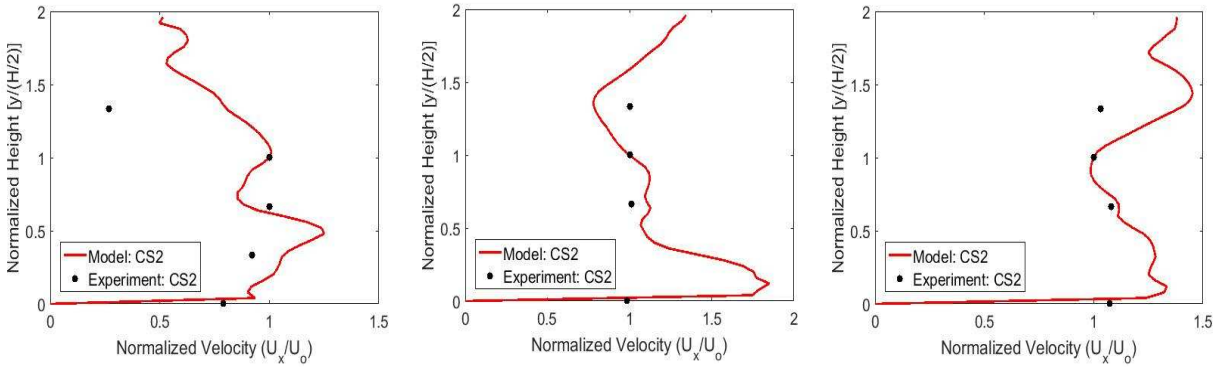

Figure E5. Validation of DNS based CFD model of open raceway pond at mixing energy inputs of 0.1 W.m^{-3} (left figure), 0.7 W.m^{-3} (middle figure) and 1.94 W.m^{-3} (right figure).

APPENDIX F: Temperature Function, Light Function, and Basal Metabolism

Weather conditions impact the biological responses of microalgae in terms growth due to photo-respiration at high temperatures and radiation, and dark respiration. The functions that involve photo- and dark-respiration include the temperature function, the light function, and the basal metabolism function. The temperature function effects due to water temperature is illustrated in Figure F.1. In here, a factor of one represents the optimal conditions for *Nannochloropsis oceanica*, 24.05 °C, a factor below one illustrates inhibition at cold temperatures and photorespiration effects at high temperatures, and a factor of zero denotes microalgae death at extreme temperatures. Incident radiation (Figure F.2a) control the light function effects as illustrated in Figure F.2b. A factor of one represents the light saturation of *Nannochloropsis oceanica*, 20 $W.m^{-3}$. Incident radiations below this value inhibit the growth because light limitation and incident radiations above this value photo-inhibits the growth because photorespiration, denoted by factors below one. Lastly, basal metabolism loss rate due to dark respiration is illustrated in Figure F.3, where the higher growth losses are represented by the higher rates.

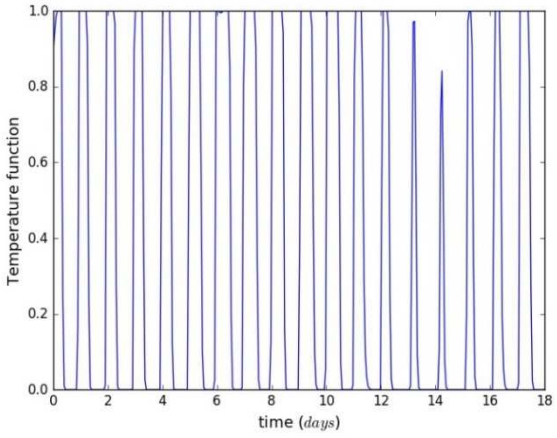

Figure F.1 Temperature function for Fall 2013.

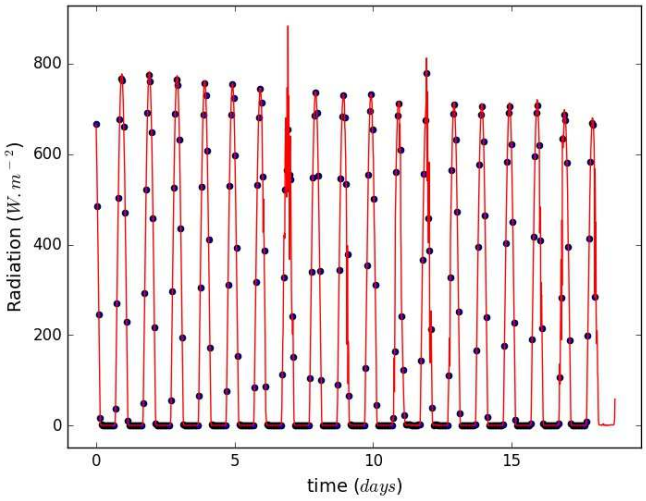

(a)

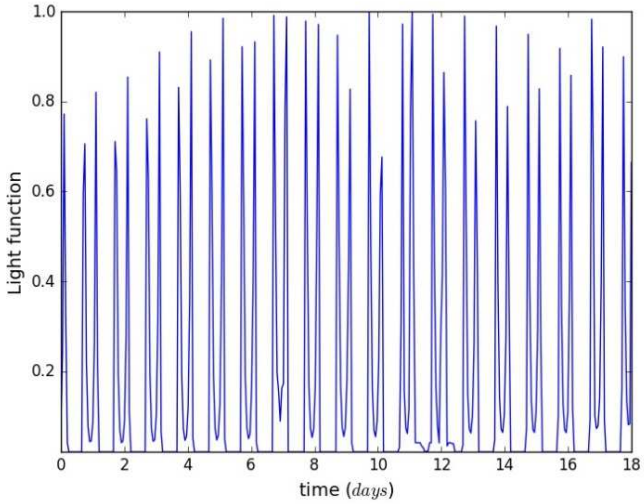

(b)

Figure F.2 Incident Radiation (a) and light function (b) for Fall 2013.

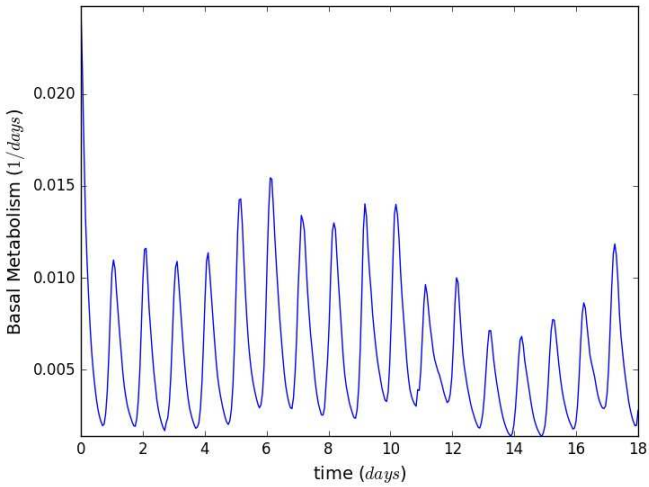

Figure F.3. Basal metabolism Response for Fall 2013.

APPENDIX G: Well-mixed Cyanobacterial Growth Model Parameters

1 Well-mixed Cyanobacterial Growth Modelling

To assess the influence of turbulence mixing in the light experienced by cyanobacterial cells in photobioreactors, a well-mixed dynamic cyanobacterial growth model as a function of mixing energy input and experimentally determined light attenuation was developed for analysis in this study. This model incorporates ordinary differential equations (ODE) and nonlinear function embodying nitrogen quote, nitrogen uptake, chlorophyll synthesis, light absorption, photosynthesis, growth rate, and biomass [37, 169]. Table G.1 summarizes the required biological inputs for *Synechocystis* sp. PCC6803 [10, 84, 187].

The model developed in this study is novel in that it incorporates the maximum growth rate (μm) with photo-inhibition and light attenuation in Synechocystis sp. PCC6803 as a function of optical density and depth. These parameters were determined from the experimental works described in section 2.2. The maximum growth rates of Synechocystis sp. PCC6803 were determined experimentally from Figure G.1 and G.2. The biomass growth curve model for *Synechocystis* sp. PCC6803, validated with experimental work, were computed in Matlab ® for the four mixing energy inputs evaluated for the flat-panel photobioreactor: 1.94, 0.97, 0.47, and 0.03 $W.m^{-3}$, and for the mixing energy input evaluated for the open raceway pond, 0.10 $W.m^{-3}$. The dynamics of the model is synthesized in Figure G.3. Light attenuation in photobioreactor cultures is commonly computed by the Lambert-Beer law, which is a function of the rate of light absorption by the culture [56]. In this study; however, Light attenuation (I) was experimentally determined as illustrated in Figure G.4 and G.5.

Table G.1 Summary of experimental growth of *Synechocystis* sp. PCC6803 in flat-panel photobioreactors

Metric	VVM			
	0.7	0.35	0.17	0.01
μ (d^{-1})	0.53 (±0.17)	0.76 (±0.15)	1.29 (±0.23)	1.18 (±0.28)
DW Biomass ($g.l^{-1}$)	0.30 (±0.03)	0.24 (±0.02)	0.90 (±0.15)	0.43 (±0.03)
Productivity ($g.l^{-1}.d^{-1}$)	0.07	0.05	0.23	0.14
Water Temp (□C)	34 (±1)	30 (±1)	31 (±1)	33 (±1)
PAR ($\mu molphotons.m^{-2}.s^{-1}$)	1440 (±65)	1,323 (±9)	1,244 (±47)	1,385 (±25)

Table G.2 Summary of experimental growth of *Synechocystis* sp. PCC6803 in open raceway pond

Metric	0.1 $W.m^{-3}$		
	Replicate 1	Replicate 2	Replicate 3
μ (d^{-1})	0.68 (± 0.12)	0.82 (± 0.08)	0.81 (± 0.09)
DW Biomass ($g.l^{-1}$)	0.45 (± 0.04)	0.39 (± 0.02)	-
Productivity ($g.l^{-1}d^{-1}$)	0.06	0.04	-

Metric	0.1 W.m^{-3}		
	Replicate 1	Replicate 2	Replicate 3
Productivity (g.m^{-2}d^{-1})	11.4	7.9	-
Water Temp (□C)	29	29	29
PAR (µmolphotons.m^{-2}.s^{-1})	990 (± 116)	914.8 (± 79.1)	907.8 (± 79.3)

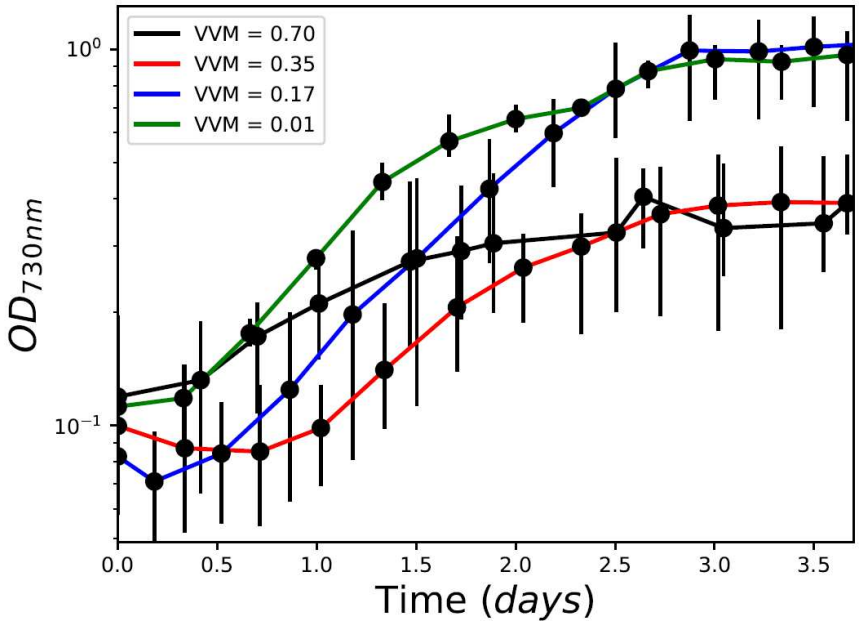

Figure G.11 Optical density of *Synechocystis* sp. PCC 6803growth in flat-panel photobioreactors. The error bars denote the upper and lower values from five experimental replicates.

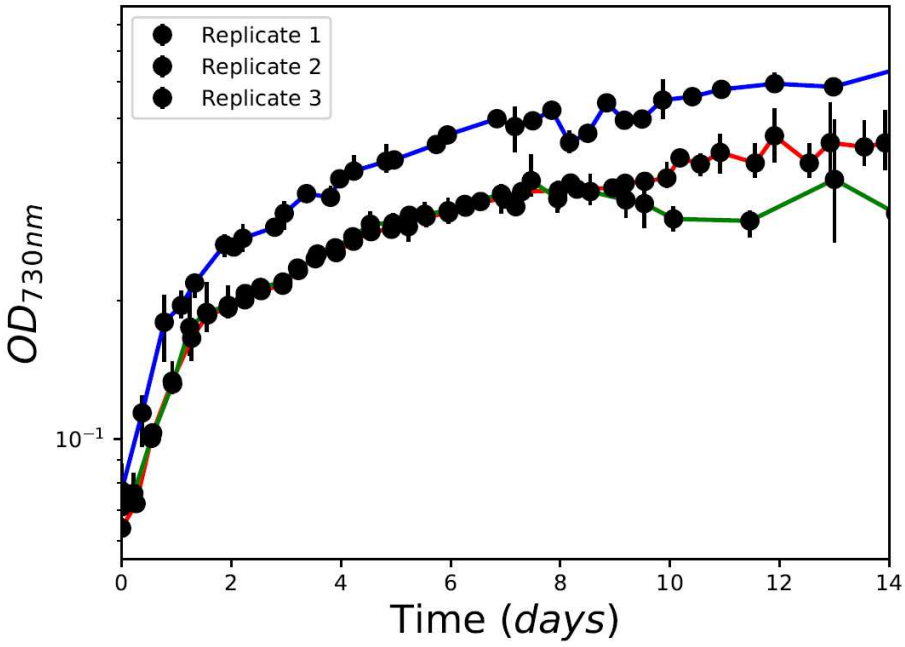

Figure G.12 Optical density of *Synechocystis* sp. PCC 6803 grown in open raceway pond. The error bars denote the upper and lower values from five experimental samples.

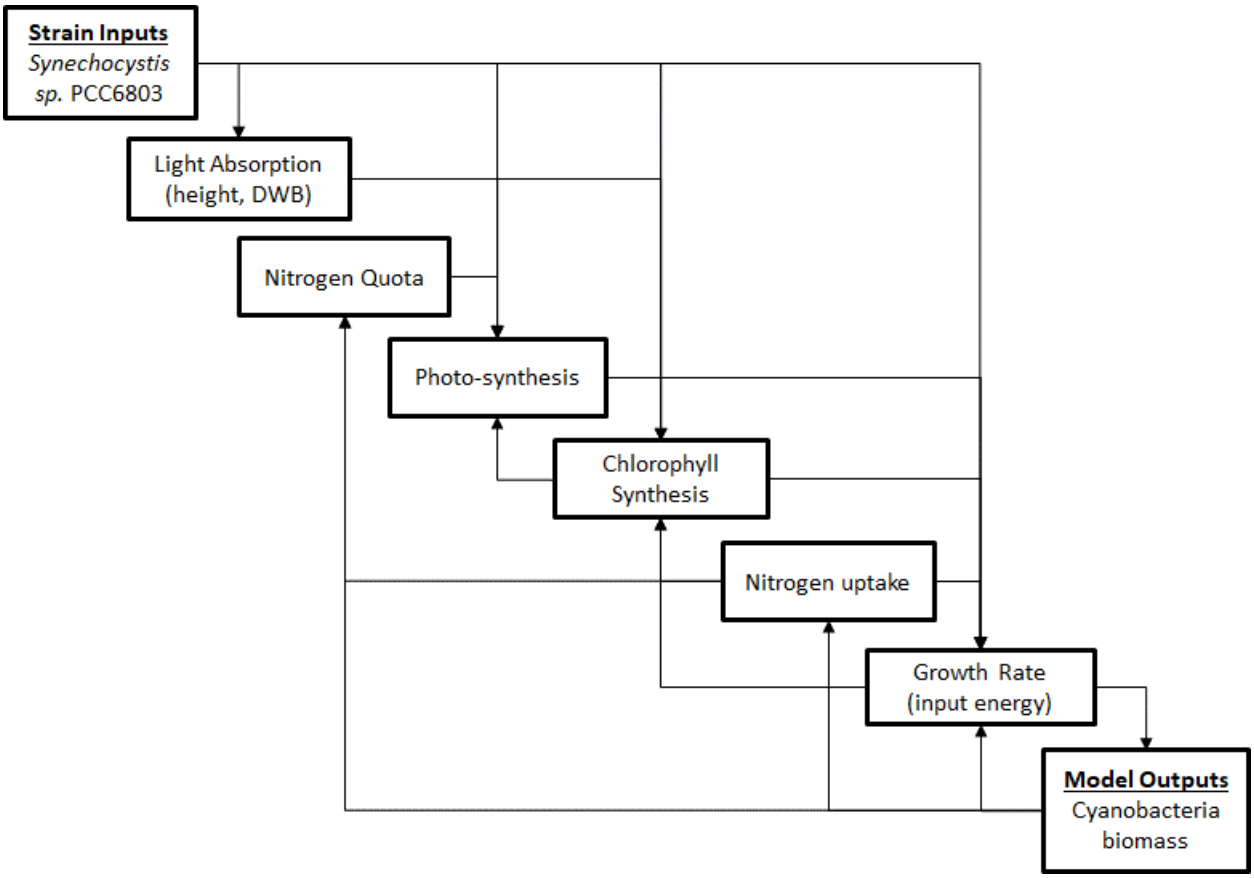

Figure G.13 Illustration of well-mixed cyanobacterial growth model based on *Synechocystis* sp. PCC 6803.

Table G.3 Biological inputs for growth model based on *Synechocystis* sp. PCC6803

Parameter	Description	Units	Value	Reference
A	Optical cross section of chlorophyll a	$m^2.g^{-1}chl$	17	[10, 84]
ϕ	Quantum efficiency	$gC.(mol\ photons)^{-1}$	1.263	[187]
Q	Minimum subsistence nitrogen quota	$gN.g^{-1}dw$	0.0197	[10]
q_M	Maximum nitrogen quota	$gN.g^{-1}dw$	0.129	[10]

Parameter	Description	Units	Value	Reference
C	C subsistence quota	$gC.g^{-1}dw$	0.512	[10, 84]
V_m	Maximum uptake rate of nitrogen	$gN.g^{-1}dw.d^{-1}$	0.156	[84]
V_h	Half-saturation coefficient	$gN.m^{-3}$	39.2	[84]
P	Maximum chlorophyll to nitrogen ratio	$gchl.g^{-1}N$	0.116	[84]
p_o	Maximum photosynthesis rate	$gC.g^{-1}chl.d^{-1}$	47.87	[84]

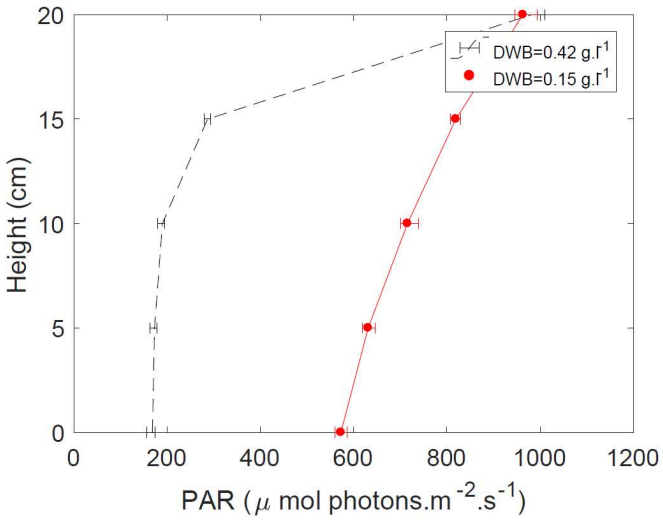

Figure G.14 Light attenuation in *Synechocystis* sp. PCC 6803 cultures in open raceway ponds as a function of depth and dry weight biomass.

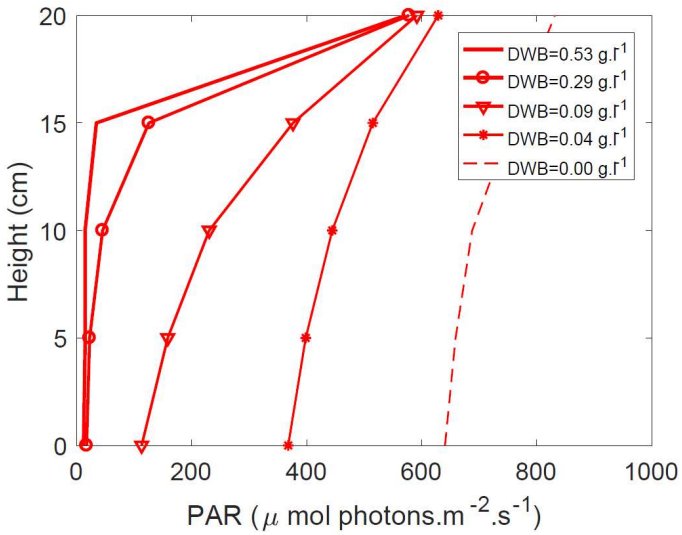

Figure G.15 Light attenuation in *Synechocystis* sp. PCC 6803 cultures in flat-panel photobioreactors as a function of depth and dry weight biomass.

2 Validation of computational growth of Synechocystis sp. PCC 6803 in flat-panel photobioreactors

The well-mixed cyanobacterial growth model of Synechocystis sp. PCC 6803 validated for the flat-panel photobioreactor at mixing energy inputs of 0.03, 0.97 and 1.94 $W.m^{-3}$ are included in the Figures 5, 6, and 7. The significance of the growth rates and biomass productivities is evaluated by a one-way analysis of variance (ANOVA), and illustrated at Figures G.6 and G.7. The on-way ANOVA demonstrate a significant influence of mixing energy inputs as illustrated in the p-value less than 0.05.

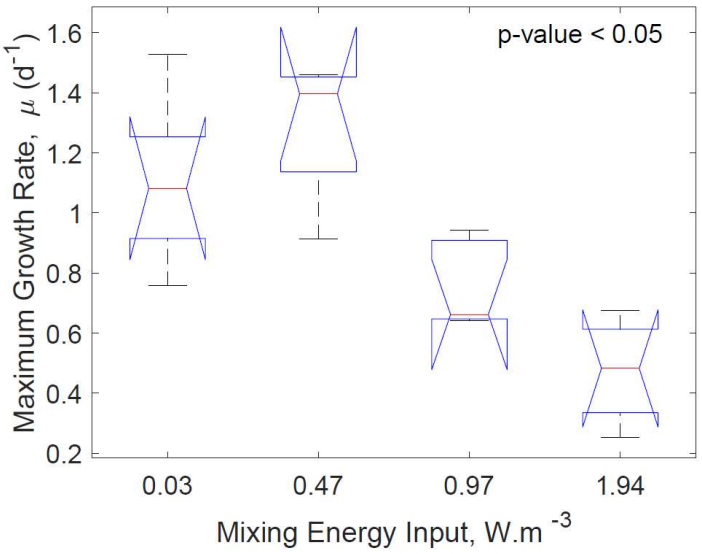

Figure G.6. Maximum growth rate of *Synechocystis* sp. PCC 6803 in flat-panel photobioreactors. The central mark is the median and the edges of the box are the 25th and 75th percentiles (1st and 3rd quantiles). The whiskers extend to the most extreme data points that are not considered outliers. The outliers are plotted individually. The outliers are plotted individually. The p-value or probability value was obtained from the one-way ANOVA in Matlab®.

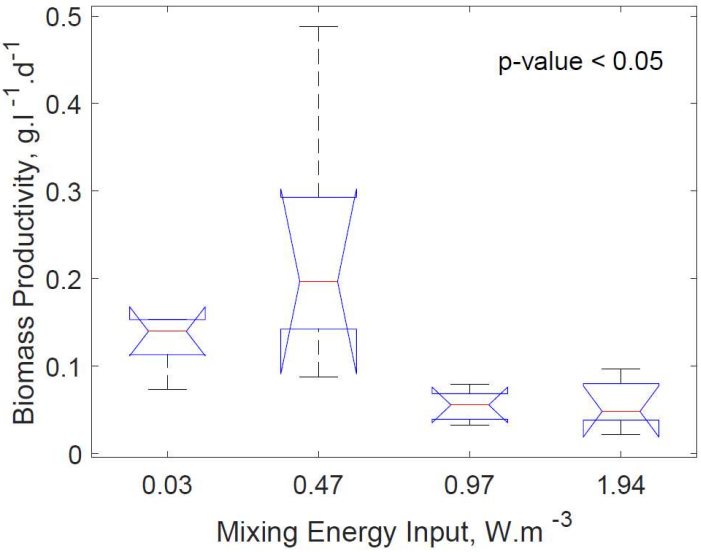

Figure G.7. Cyanobacterial biomass productivity of Synechocystis sp. PCC 6803 in flat-panel photobioreactors. The central mark is the median and the edges of the box are the 25th and 75th percentiles (1st and 3rd quantiles). The whiskers extend to the most extreme data points that are not considered outliers. The outliers are plotted individually. The p-value or probability value was obtained from the one-way ANOVA in Matlab®.